DISINTEGRATION RATE DETERMINATION BY 4π-COUNTING

Pate

DISINTEGRATION RATE DETERMINATION BY 4π-COUNTING

by

Brian David Pate, M.Sc.(Lond.)

Thesis submitted to the Faculty of Graduate Studies and Research of McGill University in partial fulfilment of the requirements for the Degree of Doctor of Philosophy.

From the Radiochemistry Laboratory,
Department of Chemistry, McGill University,
under the supervision of Dr. Leo Yaffe.

McGill University,
Montreal, Canada

April 1955

ACKNOWLEDGMENTS

It is a pleasure for the author to acknowledge his indebtedness to the following persons and institutions:

The National Research Council of Canada, for financial assistance in the form of a Studentship during the academic session 1954-1955, and grants-in-aid.

Atomic Energy of Canada Ltd. for grants-in-aid, and the loan of equipment.

McGill University Chemistry Department for Demonstratorships during the academic sessions 1953-1954 and 1954-1955.

Drs. R. E. Bell and G. T. Ewan of the Physics Department, and Profs. J. D. Jackson and R. T. Sharp of the Mathematics Department, McGill University, for helpful discussion and advice both during the experimental work and during the preparation of this thesis.

Finally it is especially a pleasure to acknowledge the constant encouragement and invaluable direction the author has received from Professor Leo Yaffe, during the two years in which this research work was carried out.

TABLE OF CONTENTS

	Page
A) INTRODUCTION	1
1) PREFACE	1
2) ABSOLUTE DISINTEGRATION RATE DETERMINATION	4
(a) Energy Emission Methods	5
(i) Calorimetry	5
(ii) Ionization Measurements	8
(b) Particle Counting Methods	11
(i) Coincidence Counting	30
(ii) Low Geometry Counting	34
(iii) Gas Counting	38
(iv) Scintillation Counting	40
3) 4π-COUNTING	41
(a) History	41
(b) Advantages of a 4π-counting Geometry	42
B) COUNTER RESPONSE PROBABILITY	47
1) INTRODUCTION	47
(a) Gas Multiplication and Electron-Collection Efficiency.	49
(b) Counter "Geometry"	52
(c) Resolution Losses	52
2) COUNTING APPARATUS	53
3) EXPERIMENTAL TECHNIQUES, RESULTS AND DISCUSSION	58
(a) Gas Multiplication	61
(i) High Voltage Characteristics of the Counter	61
(ii) Response Probability as a Function of Source Position	77
(iii) Effect of Variation of Gold Thickness of Source Mount Films	81
(iv) Effect of Purity of Counting Gas	82

Page

(b) Counter Geometry 88

(c) Response Probability at Higher Counting Rates 91

4) CONCLUSIONS 93

C) THE FABRICATION AND CALIBRATION OF VERY THIN FILMS: ABSORPTION OF RADIATION BY THE SOURCE MOUNT 95

1) INTRODUCTION 95

2) THE FABRICATION AND THICKNESS CALIBRATION OF VERY THIN FILMS 96

(a) Introduction 96

(b) Procedures 98

(i) Film Production 98
(ii) Measurement of Film Superficial Density 101
(iii) Gold Coating 109

3) CORRECTION FOR SOURCE-MOUNT ABSORPTION 116

(a) Introduction 116

(b) Experimental Procedure and Results 120

(i) Single Film Source Mount Characteristics 121
(ii)Sandwich Characteristics 121

(c) Discussion 124

(i) The Sandwich Procedure 124
(ii) The Absorption Curve Procedure 124

D) SELF-ABSORPTION 131

1) INTRODUCTION 131

2) EXPERIMENTAL TECHNIQUES AND RESULTS 147

(a) Source Preparation 147

(b) Estimation of Self-Absorption 164

3) DISCUSSION 168

Page

E) ABSORPTION AND SCATTERING OF BETA-RADIATION IN A COUNTER GEOMETRY OF 4π STERADIANS 174

1) INTRODUCTION 174

(a) Absorption of Beta-Radiation 175

(b) Backscattering of Beta-Radiation 179

(c) Coincidences in a 4π-Counter 182

2) EXPERIMENTAL TECHNIQUES AND RESULTS 184

3) DISCUSSION 206

(a) The Phenomena of Coincident Discharges 206

(i) Gas Backscattering 216
(ii) Wall Backscattering 218

(b) Absorption and Scattering of Beta-Radiation by the Source-Mounting Film 220

(c) Sandwich Procedure for Correcting for Source-Mount Absorption Losses 240

F) SUMMARY AND CONTRIBUTIONS TO KNOWLEDGE 245

BIBLIOGRAPHY 248

APPENDIX A

1) Circuit Diagram of AEP 1448 Amplifier 255

2) Circuit Diagram of AEP 1509 Coincidence Unit 256

APPENDIX B

Results of International Intercomparison of Standards 257

APPENDIX C

Papers published during the course of this research work 258

A. INTRODUCTION

1) PREFACE

The type of radiation observed to be emitted in a nuclear transition is related to the lifetime of the initial state, from which the transition occurs. Both are dependent on the change of angular momentum and parity, and on the energy available, from the transition between the initial and final states.

Thus neutron and proton emission is generally associated with the decay of highly excited nuclear states with lifetimes less than 10^{-18} seconds. The emission of α- and β-particles, and electron-capture, is observed during the decay of the ground states or low-lying isomeric states of nuclides with an unstable nuclear n:p ratio. The decay of such states is characterized by lifetimes with respect to α-emission of 10^{-6} seconds to 10^{17} years. Lifetimes with respect to β-emission may be as short as 10^{-3} seconds, but are generally between a few seconds and about 10^{12} to 10^{15} years.

There are exceptions to this general picture since α-emission is also found to be associated with the decay of very highly excited states, and of the ground states of very unstable species such as He^5 and Li^5.

γ-emission is observed in transitions between the excited states of a single nuclear species, the lifetimes of the decaying states being generally of the order of or greater than 10^{-14} seconds. States of which the lifetimes are so long, due to a large change in angular momentum being involved, as to be observable experimentally, are termed nuclear isomers, and the γ-transitions from these states isomeric transitions.

Consequently from the above, it is true to say that the nuclear species customarily encountered in nuclear chemical work, being of a half-life greater than a few seconds, will decay by α- or β-emission, by electron-capture, or by isomeric transition. γ-radiation will also be observed from short lived excited states, when these are fed by an α- or β-transition.

Further, much of the counting work to be performed involves β^--radiation. This is due to the fact that two of the principal types of nuclear reactions studied by radiochemical techniques, namely radiative capture of neutrons, and the low-energy fission reaction, lead to neutron-excessive nuclides, which decay by emission of negative electrons. Hence in this thesis we shall be interested mainly in the determination of β^--disintegration-rates.

For most purposes in Nuclear Physics and many in Nuclear Chemistry, the measurement of the disintegration-rates of samples of radioactive material relative to a suitable standard, or the comparison of two or more such disintegration-rates with an uncalibrated measuring system, supplies the required analytical data. Such would be the case, for example, in all tracer work involving only one radioactive species, and where sample preparation and mounting can be performed in a standardized way. In these circumstances relative activity measurements are possible with care to within a few percent.

Frequently, however, the best experimental method for a given purpose involves determination of disintegration-rates in an absolute way. This is the case, for example, in nuclear physics and nuclear

chemistry experimental work such as the determination of fluxes of neutrons, protons, deuterons, or α-particles by the activation method, the determination of cross-sections or absolute yields of nuclear reactions, and the investigation of the distribution of mass and charge among the products of a spallation or fission reaction. It is also the case when tracer methods are used, in which a comparison of the disintegration-rates of two or more differing nuclear species is required, or in a tracer application involving a single species when the samples for assay can not be mounted identically.

An accurate knowledge of the disintegration-rate of radioactive material for therapeutic use is also important, and much of the effort expended on improving the accuracy of absolute counting methods has been concerned with standardization of these materials. The nuclides most commonly met with under these circumstances are Na^{24}, Co^{60}, I^{131}, Au^{198} and P^{32}.

Disintegration-rate determinations to a precision of ± 20 percent present little difficulty. Determinations to ± 2 percent are much more difficult, and most of the experimental work has, up until quite recently, been reported with an error limit of at least this magnitude.

Certain problems in radiochemistry, however, will benefit from an analytical method of greater precision. As an example we may quote the investigation of the fine structure in the mass-yield curve from a fission-reaction, where significant effects may be observed as the small difference between two larger quantities, such as the yields of β-decay chains of neighbouring mass numbers. Clearly the precision to which the difference may be measured is markedly dependent on the

precision with which the chain yields themselves are known, and hence on the precision of the original disintegration-rate determinations.

This thesis will describe experimental work aimed at improving the accuracy attainable with the most promising and widely applicable method of disintegration-rate determination, namely 4π-counting. It will be shown that determinations are now possible to better than $\pm$ 0.5 percent for nuclides emitting β-radiation of moderate or high energy, and preliminary results presented from experimental work on self-absorption phenomena indicate that a comparable accuracy will shortly be possible with α-emitters and low-energy β-emitters also.

In this section we shall briefly describe and compare the various methods of absolute disintegration-rate determination available, discuss in detail the principles of 4π-counting, and enumerate the several sources of error to which this method is subject.

2) ABSOLUTE DISINTEGRATION-RATE DETERMINATION

The methods which have been successfully used for this purpose may be divided into two main groups. Firstly, there are those methods which rely on a measurement of the rate at which energy is emitted by the radioactive material. The result is then used to calculate the rate of disintegration N_o by the relationship

$$N_o = E / \bar{e} \qquad \ldots\ldots(1)$$

where E is the observed rate of energy emission and $\bar{e}$ is the mean energy release per disintegration. The second group of methods involves counting the rate at which the products of disintegration

(electrons, α-particles, photons) leave the sample, and calculating the disintegration-rate from the number of particles produced per disintegration.

(a) Energy Emission Methods

The methods of this group have two inherent disadvantages. Firstly, they lack sensitivity relative to particle counting methods, which restricts their application to relatively large amounts of radioactive material. (Particle counting methods, while not directly applicable to sources above a limiting strength, can be used in conjunction with suitable aliquoting and dilution of the sample.) Secondly, they require an accurate knowledge of the mean energy dissipation per disintegration, which implies a knowledge of the relevant decay scheme and particularly data for α-energies or β-energy distributions to an accuracy at least as great as that required for the final disintegration-rate value.

Two principal methods have been used to measure the rate of energy emission from radioactive materials - calorimetry and ionization measurements.

(i) Calorimetry

Calorimetric methods were among the first to be applied in measurements of the phenomenon of radioactivity, the rate of emission of heat by radium being measured by Curie and Laborde (35) and Rutherford and Barnes (119). They have continued to find employment up to the present day, owing to the peculiar advantages of the method - the accuracy attainable is independent of the thickness or physical state

of the sample, and the method is free from the radiation scattering or absorption problems of particle counting. An accuracy as high as ± 1 percent at the millicurie level can be obtained in the best forms of calorimeter.

Myers (105) has extensively reviewed the various types of calorimeter that have been used in the past half-century. All are designed so as to ensure that the type of radiation, whose energy is being measured, is absorbed as completely as possible, while any accompanying radiation should exert only a small disturbing influence. Thus calorimeters for the relatively soft α- and β-radiation are generally constructed with thin walls to permit the escape of nuclear gamma radiation, while calorimeters for gamma-radiation must rely on absorption of photons in a massive block inside the calorimeter, with the source outside so arranged that heating effects from α- or β-radiations do not interfere. Hence gamma-calorimeters will have a large heat capacity, which will reduce sensitivity in all but the isothermal type of design. However a successful gamma-calorimeter has been designed (27).

The earliest types of calorimeter were of the twin differential microcalorimeter type (35, 119) in which differences in pressure between two air chambers, one heated by the sample, were measured. Later a null type instrument was employed, in which the heating effect of the sample in one half was balanced against that of an electrical feed in the other. A twin adiabatic microcalorimeter designed for the measurement of alpha energies, capable of measuring 1 calorie per hour or 10 mC.

of α-activity, both to a precision of ± 1 percent, has recently been described (77).

Most of the modern designs have, however, been of single chamber, adiabatic or isothermal design, in which the system is separately calibrated by an electrical feed experiment. The most successful design appears to be the constant pressure liquid nitrogen system in which the volume of nitrogen gas produced in a given period by the heating effect of the sample is used as a measure of the amount of heat dissipated. This system was used by Stout and Jones (139) to measure the α-energy dissipation from plutonium metal, and hence the half-life of Pu^{239}. It was later adapted by Cannon and Jenks (26, 27) for use with β- and γ-emitters, their design being capable of measuring heat inputs as low as 7×10^{-6} cals/sec or 1 Mev beta-activity at the 5 mC level, both to an accuracy of 1 percent.

It is seen from equation (1) that a knowledge of the mean disintegration energy dissipation $\bar{e}$ allows a calculation of N_o from the observed energy emission, but equally well if the disintegration-rate N_o is known from some other measurement, then calorimetry can be used for an independent measurement of α- and γ-energies or mean energies of beta-spectra. This constitutes a valuable check on values obtained from eg. beta-spectrometric observations, and indeed much of the literature on calorimetry is concerned with this aspect of the subject (27, 77, 79, 105, 139, 152).

Although the use of very low temperatures to reduce specific heats of construction materials (132) and magnetic methods below $1^{\circ}K$

(105) should in theory allow an extension of the sensitivity to measure heat inputs of 10^{-8} to 10^{-10} cals/hour, practical designs of calorimeter for use with radioactive materials do not yet appear to be capable of this type of performance. Background effects (27), due mainly to heat flow into the calorimeter from the surroundings, place a limit to the sensitivity of about 1 mC for determinations accurate to ± 1 percent with α- and β-emitters (77).

(ii) Ionization Measurements

This method, like the calorimetric method, is of long standing in the study of radioactivity. It was used by Eve in 1906 and later by Moseley and Robinson (103) to measure the β- and γ-radiation energy of members of the radium decay series. Recent work in the application of ionization measurements specifically to the determination of disintegration rates has been reported in articles by Gray (63), Perry (111) and Marinelli (96). The U.S. National Bureau of Standards currently uses β-ionization chambers (130) and γ-ionization chambers (130, 134) as secondary standardization instruments.

As was described above, a measurement of total β- or γ-radiation energy dissipation can be used either to calculate from a mean particle or photon energy the sample disintegration-rate, or vice-versa. Much of the work in which ionization chambers have appeared has been performed with the latter end in view. This is due to the need in radiological work to know the amount of energy dissipated in body-tissues by radiations from radioactive materials applied diagnostically or therapeutically.

Gray has discussed the theory of the method (61, 62, 63) and

described most elegant experimental methods for its application (63). The theory treats the ionization chamber as an approximation to an infinitesimal cavity in a solid medium at any point of which electronic energy is being dissipated at a mean rate E_M per unit mass per second. Then the mean ionization produced per unit mass of gas in the infinitesimal cavity situated at that point is

$$J_M = E_M / \overline{P_M W} \qquad .....(2)$$

where P is the ratio of the mass-stopping power of the solid relative to the gas, and W is the mean energy expended in the creation of a pair of ions in the gas.

If the solid is under γ-irradiation in such a way that the generation and dissipation of energy due to electron-interactions at the point considered are equal, then

$$E_M = N \sum \phi_s h\nu_s (\sigma_a + \tau)_s \qquad .....(3)$$

where N is the total γ-flux, ϕ_s is the fraction of photons with energy $h\nu_s$, σ_a is the Compton scattering cross-section and τ is the photo-electric cross-section. (We shall neglect pair-production.) Hence in this case the ionization in a chamber due to a source of disintegration rate R at distance r is

$$J_M = R \frac{1}{\overline{P_M W}} \cdot \frac{e^{-\mu t}}{4\pi r^2} \cdot \sum \phi_s h\nu_s (\sigma_a + \tau)_s \qquad .....(4)$$

where μ is the absorption coefficient and t the thickness of the ionization-chamber wall.

In the case of a β-emitter, if this is uniformly distributed throughout the hypothetical solid, such that the disintegration rate

per unit mass of solid is Q, then

$$E_M = Q\overline{E}_\beta \qquad .....(5)$$

and hence $$J_M = Q.\overline{E_\beta} \,/\, \overline{P_M W} \qquad .....(6)$$

where $\overline{E_\beta}$ is the mean β-energy.

Hence if the various constants of these equations are known, observed J_M values may be related to the required disintegration rates. Alternatively a comparison technique may be used (63) employing a radium source of known strength as a standard. The errors arising under these circumstances are from the uncertainty in the value for the ionization produced at a given distance from a standard radium source, and in the value of W. They total about ± 4 percent.

Experimentally, the designsof chamber which have been successfully used are numerous. They are generally cylindrical with the central collecting electrode connected to a suitable electrometer system, and operated under conditions of "saturation ion-collection" (see below). For measurement of relatively intense gamma sources, the source is external to the chamber (63) while weaker sources are frequently placed inside the chamber (130). Gray's method of mounting internal sources of β-radiation is particularly noteworthy. The material is diluted with a solution of gelatin of such concentration that the mixture is fluid at 30°C but solidifies on cooling to room temperature. It is thus cast as an internal coating on the ionization chamber walls of about 4 mm. thickness, and approaches the theoretical situation quite closely.

Estimates of the sensitivity attainable by ionization-chamber techniques applied to disintegration-rate determinations vary with the

design of chamber considered. For γ-emitters the limit is probably at or about 1 μC, (111, 130) determinable with an accuracy of about ± 4 percent. With β-emitters a greater sensitivity may be possible. These figures assume, of course, that the necessary data for the mean particle energy are available to the accuracy quoted, or that the system has been standardized by comparison with a method of calibration of greater accuracy (130).

(b) Particle Counting Methods

Methods in this group have the advantages of great sensitivity, since individual particles and hence individual disintegrations are detected, and specificity, since the type of radiation and its energy (characteristic of a specific nuclear transition) may also be measured. They have too, inherent disadvantages, namely liability to errors arising from absorption and scattering of radiation, and the need for complex electronic equipment.

Before discussing the several methods of disintegration-rate determination by particle counting, we shall discuss the available methods of particle detection.

Particle Detectors

Two main methods of detection of α-particles, fast electrons and γ-radiation have been employed, namely scintillation and ionization methods. The former were used in the earliest days of the study of radioactivity, when the scintillations produced on zinc sulphide screens bombarded by particles were counted by eye. The technique has recently reappeared in a modified form, the scintillations produced in a phosphor, suitable for the radiation studied, being recorded with a photoelectric

tube or photomultiplier. This field has recently been reviewed by Birks (15); however it is generally outside the scope of this thesis, and will only be alluded to occasionally in what follows in connection with the rare applications scintillation techniques have found in absolute counting work.

Ionization methods, of much wider application in this field, rely for particle detection on the ionization produced in a gas by the primary radiation itself, or in the case of γ-radiation by secondary electronic radiation.

Ionization

The theory of the energy loss of a fast electron by inelastic collisions with atomic electrons has been published by Bethe (9, 10) and others. The rate of energy loss per cm. of path length, $\frac{dE}{dx}$, by an electron of mass m and velocity v in a medium of N atoms/cm^3 of atomic number Z and ionization potential I, is of the form

$$-\frac{dE}{dx} = \frac{4\pi e^4 N}{mv^2} Z \log_e \frac{mv^2}{2I}\sqrt{\frac{e}{2}} \qquad .....(7)$$

for non-relativistic electron velocities.

The number of ions produced per unit path length as a function of particle energy goes through a maximum at particle energies of the order of 150 ev, through a minimum at about 2 Mev, and exhibits a slow rise with particle energies increasing above 2 Mev. The theory of ionization yield has been outlined by Fano (43).

The average energy expended in forming one ion-pair, W, is larger than the ionization potential I ($\sim$ 2I), since many of the collisions lead to excitation of the gas molecules without ionization, and in the case of those collisions that do lead to ionization, kinetic energy is

imparted to the products of ionization. Fast secondary electrons may in turn lead to secondary ionization, the various forms of ionization being measured in terms of S_p, and S_t, primary and total specific ionizations respectively (ions per cm. per atmosphere of gas). In ionization chambers total ionization is of interest, while primary ionization values are more important in multiplicative counters.

It follows that a particle of initial energy E makes on the average

$$n = \frac{E}{W} \qquad .....(8)$$

primary ion pairs before being brought to rest, neglecting for the moment the variation of W with energy, which differs from gas to gas and is generally small.

The primary ionization produced by an initially monoenergetic radiation is not, however, constant but exhibits a statistical fluctuation from particle to particle. This might be expected to be described by a Poisson distribution, ie. the probability of a particle producing x ion-pairs is

$$P(x) = e^{-n} \frac{n^x}{x!} \qquad .....(9)$$

Then the observed variance of n, the mean number of ion-pairs produced would be

$$V_n = n \qquad .....(10)$$

Fano (44) has shown on theoretical grounds that

$$V_n = Fn \qquad .....(11)$$

where F has a value of 0.3 for atomic H, for which the necessary data for calculation were available.

The original products of the ionization process are generally a positive singly charged gas-ion and an electron. Unless positive ions and electrons are separated they will quickly recombine to reform neutral gas molecules.

Separated electrons (ie. in a region free of positive ions) have a tendency to attach themselves to certain neutral gas-molecules to form negative ions. The probability of this happening in the time of collection of ions in a counting chamber, is generally small, except in the case of some substances containing electro-negative atoms such as oxygen or sulphur. Since electron-attachment is generally deleterious to counter operation, purification of counter gases from these substances is desirable.

Counting Chambers

The various experimental forms, and the mode of operation of ionization chambers, proportional counters, and Geiger-Müller counters have been the subject of a voluminous literature. This has been reviewed and clarified in a number of excellent texts (85, 117, 138, 146). Historically, the origin of the ionization chamber lies in the nineteenth century, where it was first used in work on the conduction of gases. Rutherford and Geiger (120) first used a proportional counter and also subsequently the Geiger-Müller counter, although this instrument owed considerable improvement to the workers after whom it is usually named (53).

The various types of particle detector are differentiated with respect to the discharge mechanism they employ, particularly by the ratio of the quantity of ionization produced by a fast particle

traversing the chamber to the quantity of charge collected at the electrode system as a result of this event.

Thus consider a cylindrical chamber with a peripheral cathode and a thin axial anode, filled with a suitable gas, whose characteristics will be discussed later. Suppose that radiation, producing (a) 10 ion pairs and (b) 100 ion pairs in the chamber per incident particle, enters the chamber. Then as an increasing potential is applied between the electrodes, the quantity of charge collected per incident particle will be found (146) to vary as shown in Figure 1.

With the potential increasing from zero, the charge collected (n) increases, reaching a value of (a) 10 and (b) 100 electronic charges at a potential V_1, when all the ionization produced in the chamber is being collected, and "saturation-ionization-chamber" behavior is observed. This persists until potential V_2 is reached, when electrons acquire enough energy between collisions with gas molecules to cause further ionization, and electron multiplication commences. Between potentials V_2 and V_3, the number of electrons produced from a single initial electron, although a function of polarization potential, is constant from event to event, and hence the charge collected is directly related to the energy dissipated in the chamber. The latter is then said to be operating as a proportional counter. At V_3 the discharge corresponding to the particles causing the largest initial ionization is causing a temporary drop in counter field over most of the anode region and above this potential, proportionality is not maintained for such particles, although it may be for particles causing less ionization. Thus the region with potentials in excess of V_3 is termed the region of

Figure 1

Charge collected per incident particle as a function of potential applied to the chamber electrodes (diagrammatic).

(a) particle produces 10 ion-pairs in chamber.

(b) particle produces 100 ion-pairs in chamber.

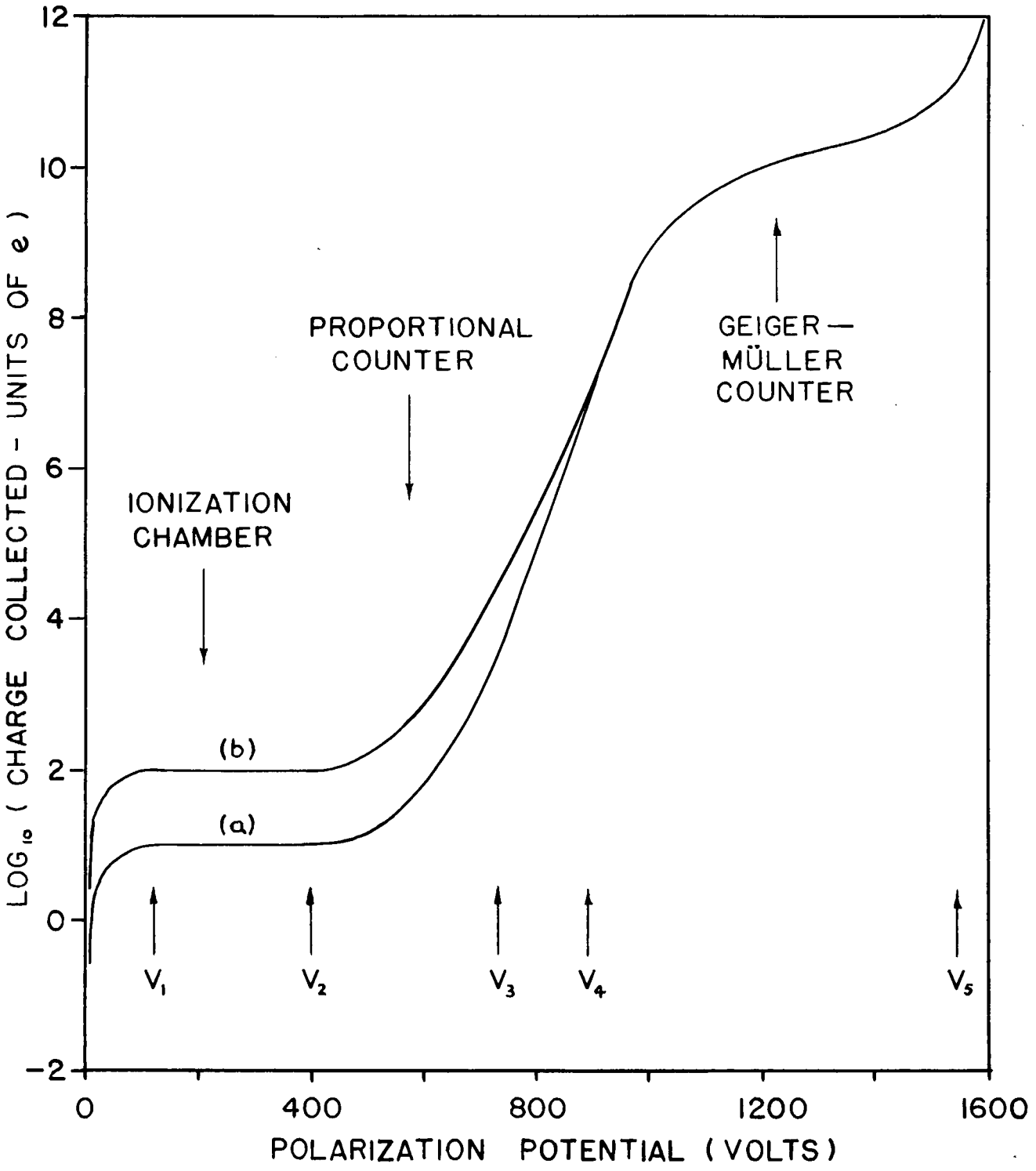
12
10
8
6
4
2
0
-2
LOG₁₀ (CHARGE COLLECTED - UNITS OF e)
PROPORTIONAL COUNTER
GEIGER — MÜLLER COUNTER
IONIZATION CHAMBER
(b)
(a)
V₁
V₂
V₃
V₄
V₅
0
400
800
1200
1600
POLARIZATION POTENTIAL (VOLTS)

limited proportionality, which persists until potential V_4, when the two curves (a) and (b) have converged to a single line. At potentials above V_4 then, the electrodes collect the same amount of charge per event regardless of the original ionization, and this behavior is characteristic of Geiger-Müller counter operation. Above V_5, the counter ceases to resolve successive events and goes into continuous discharge.

The curves of Figure 1 are not to be confused with what we shall term the High Voltage Characteristic of the chamber. This is the relationship of the counting-rate observed (with an amplifying and recording system suitable for the region of Figure 1 in which it is desired to operate) to the polarization potential, with a given number of particles entering the chamber per unit time interval. This curve is shown in Figure 2 (a), being similar for the various modes of operation outlined above except for a shift in potential scale.

At potential V_A, the events causing the largest amounts of ionization in the chamber produce an output pulse larger than the minimum size which will trigger the recorder, and begin to record. As the potential is raised, the numbers of particles registering increases, until at V_B essentially all incident particles are recorded. This counting-rate then remains more or less constant up to potential V_C, although it may increase somewhat due to various secondary processes (see below). Above V_C the pulse amplitude increases beyond the value that the amplification system can accommodate and multiple pulsing and similar effects become important. The chamber is normally operated at a potential between V_B and V_C.

Figure 2

(a) High Voltage Characteristic of a Counter (diagrammatic).

(b) Discriminator Bias Characteristic of a Counter (diagrammatic).

(a)

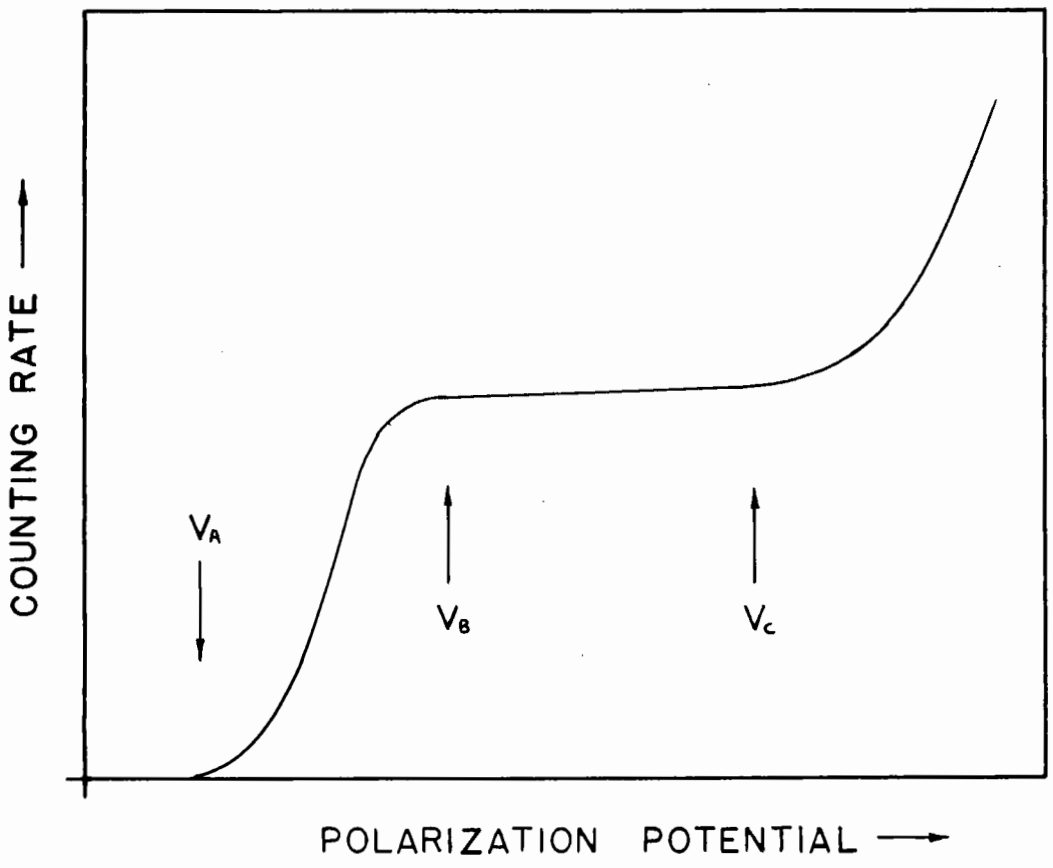
COUNTING RATE
V_A
V_B
V_C
POLARIZATION POTENTIAL

(b)

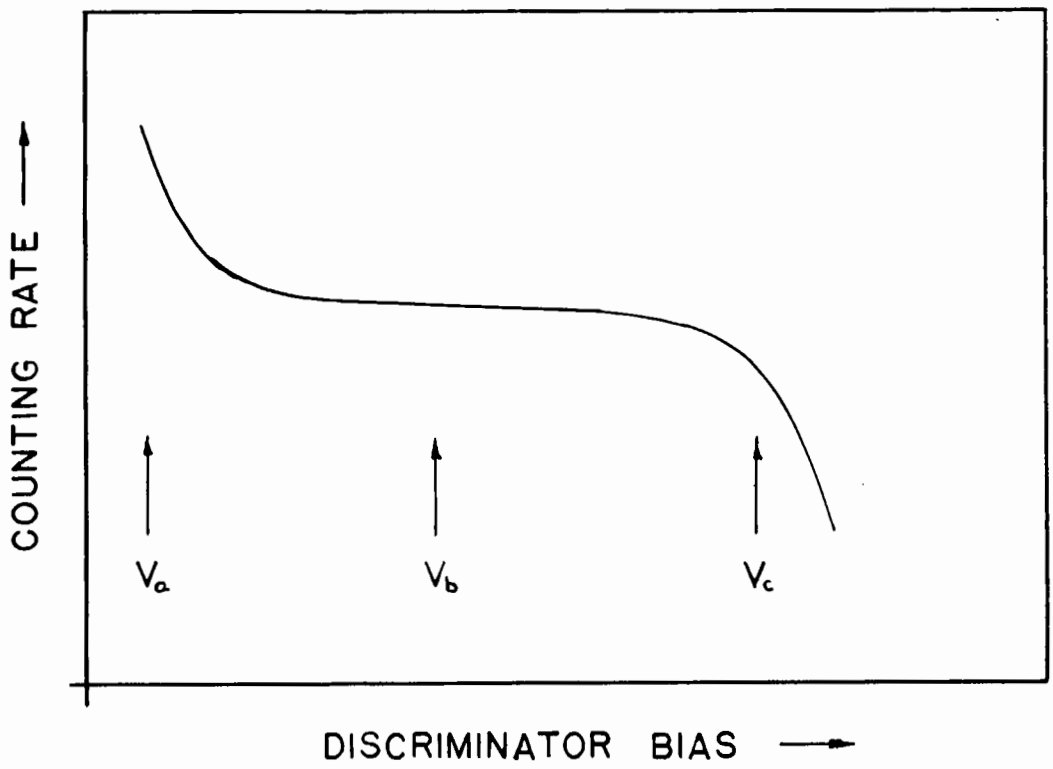
COUNTING RATE
V_a
V_b
V_c
DISCRIMINATOR BIAS

Another characteristic often given in the literature for counters of various types is the Discriminator Bias Characteristic. A representative curve is reproduced in Figure 2 (b). At low bias voltages such as V_a, any low amplitude spurious pulses will trigger the recorder and the counting rate will be higher than the rate at which particles are traversing the sensitive volume. However raising the bias voltage to eg. V_b prevents these pulses registering, and a bias-"plateau" is obtained on which the "true" counting rate is maintained over a range of bias voltage values. These plateau may or may not have a significant slope, according to the absence or presence of the agencies causing the slope on the High-Voltage plateau. At higher bias voltages such as V_c, the counting rate falls due to pulses from the observed ionizing events failing to register. The counter is normally operated on the bias-plateau in the region of voltage V_b.

We will now consider the various modes of counter operation in more detail.

Ionization Chambers

Two broad classes of ionization chambers are distinguished: ionization-current chambers, and pulse chambers. The former measure the total ionization produced in the chamber as a continuous current, the latter resolve bursts of ionization separated in time, owing their origin to the passage of individual ionizing particles through the chamber.

If an ionization chamber is polarized by the application of a suitable potential between electrodes inserted in the gas, motion of the gas ions (and electrons) will produce a current density

$$\vec{j} = \vec{j}^{+} + \vec{j}^{-} \qquad \ldots\ldots(12)$$

where $\vec{j}^{+} \quad n^{+}e\vec{w}^{+} - D^{+}e \ \vec{\text{grad}}\ n^{+}$ .....(13)

and $\vec{j}^{-} \quad n^{-}e\vec{w}^{-} - D^{-}e \ \vec{\text{grad}}\ n^{-}$ .....(14)

Here $\vec{j}^{\pm}$ represent the current densities of positive and negative charge of magnitude $|e|$, $n^{\pm}$ are the corresponding charge densities, $\vec{w}^{\pm}$ their drift velocities, and $D^{\pm}$ their coefficients of diffusion.

The drift velocity $\vec{w}$ is parallel to the applied field and the first term of (13) and (14) represents the ion current caused by application of the field. The second term represents the diffusion current due to the mean thermal agitational velocity of the gas ions (u), $\bar{u}$ being related to the diffusion coefficient D, and mean free path of the ions $\bar{l}$, by

$$D = \frac{\bar{l}\bar{u}}{3} \qquad .....(15)$$

The drift velocity $\vec{w}$ is related to the external field-strength E by

$$\vec{w} = \frac{\mu\vec{E}}{p} \qquad .....(16)$$

where p is the gas pressure and μ the ionic mobility. μ values for positive and negative gas ions are approximately equal, while that for free electrons is several orders of magnitude larger, accounting for the importance of the reduction of electron attachment in fast response counters. The high mobility of electrons can be utilized more effectively if the ionization chamber design is cylindrical with the positive electrode of small diameter at the axis of the chamber. Under these conditions the polarization field strength will be non-uniform, decreasing rapidly with increasing distance from the central electrode. Since the contribution to the current observed by each ion is proportional to the potential in which it moves (equation 16), the

electrons, which move towards the anode through the highest field strength, will make the predominating contribution to the external current, and their high mobility becomes even more significant.

As the polarization potential across an ionization chamber is increased, an increase in the current in the external circuit is observed. This however does not increase indefinitely, but reaches a constant value which remains unchanged during a further increase of potential. This condition is termed "saturation ion-collection" and the whole phenomenon is due to the effect of competition between ion collection and ion recombination. At low potentials, the ions produced by an ionizing event are only slowly separated. Hence they have a relatively large probability of recombination, and a small ion-current is observed. At larger potentials more rapid separation occurs, and eventually under saturation conditions effectly no recombination occurs, all ions formed being collected.

Hence with a situation as shown in Figure 3 with the chamber polarized by P, across a resistor R, assumed for the moment to be of high resistance, then the time constant of the circuit formed by the resistor and capacitance C of the chamber, amplifier input etc., is

$$RC >> T^{+} \text{ and } T^{-}$$

where T^{+} and T^{-} are the collection times of positive and negative ions respectively. The collection of ions at the two electrodes will alter the potential across R (by an amount small compared to the total potential across R), and the change of potential produced by ion collection as a function of time is shown in Figure 3 (b). The fast initial rise in time T^{-} is due to collection of the highly mobile electrons and the

Figure 3

(a) Ionization Chamber Circuit (diagrammatic)

(b) Charge-pulse collection with a circuit of large time-constant (diagrammatic)

(c) Charge-pulse collection with a circuit of short time-constant (diagrammatic)

(a)

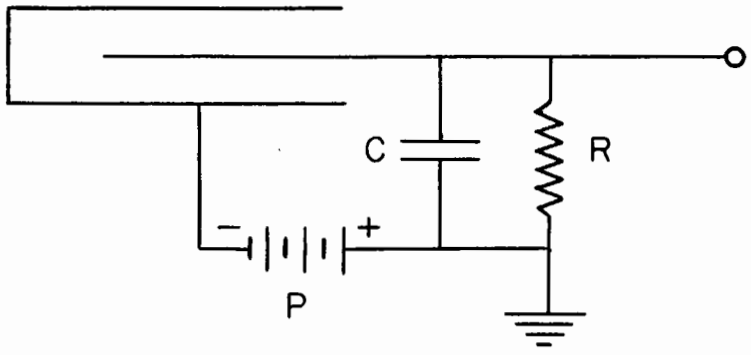

(b)

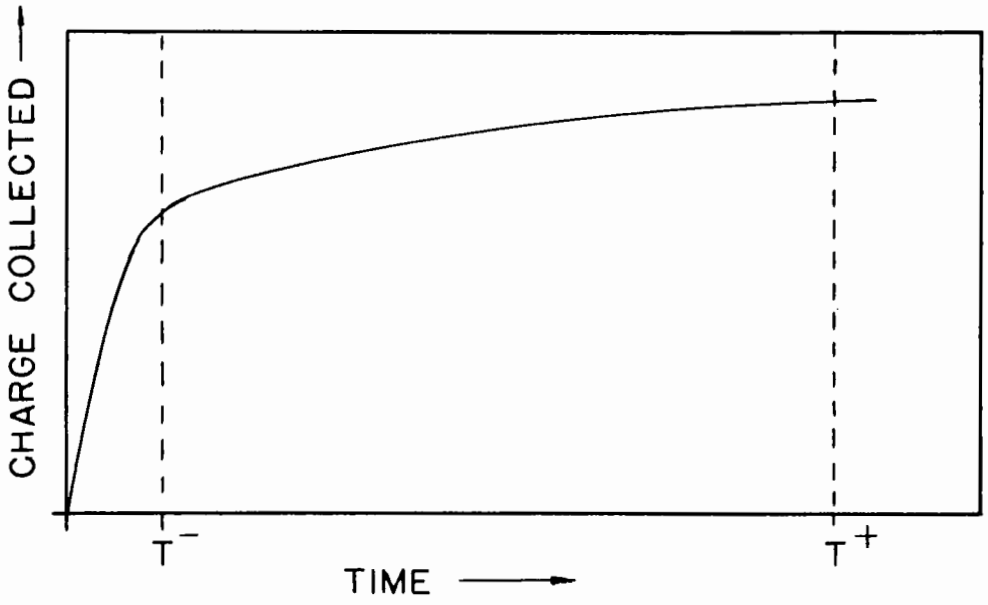

(c)

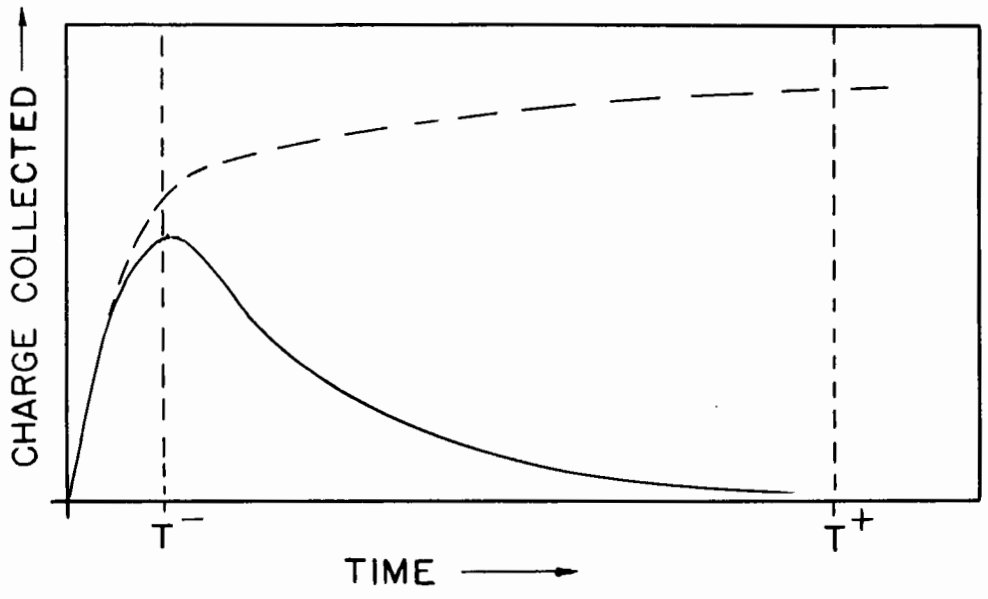

slower rise up to time T^+ due to that of the positive ions. Hence such a system will integrate the ion current due to collection of the ions from successive ionizing events, and chambers of this design (ionization-current chambers) are used in the type of measurement outlined in part (a) above.

If however, the time constant of the resistor-capacitor circuit is reduced so that

$$T^- < RC < T^+$$

(by reduction of the resistance of R for example) then the rate of leakage of the charge from R will compete with its rate of arrival, and accumulation of charge on R will only take place for rapid rates of collection of charge at the electrodes. The variation during one ionizing event will therefore be as shown in Figure 3 (c) with the charge accumulating during the electron collection and leaking away approximately exponentially thereafter. The chamber is then said to behave as an ionization-pulse chamber, and since T^- can be made very small (owing to the high mobility of electrons) such chambers will respond to ionizing events very closely spaced in time.

Proportional Counters

We have already described how, at higher chamber potentials, the electrons moving under the influence of the external field acquire sufficient energy between collisions with gas molecules to cause ionization and produce secondary electrons. These electrons are in turn accelerated, cause ionization and so on, so that an electron-cascade towards the anode is obtained.

This process, called electron multiplication, takes place primarily in a narrow region within a few millimeters of the anode. The electron-bombardment of gas molecules causes excitation in addition to ionization, and the photons emitted in the de-excitation process may lead to photo-electron production in cathode surfaces or in molecules of constituents of the gas-mixture with a sufficiently low ionization potential.

Thus a possibility exists of a cyclic process occurring in the chamber, such as

1. An initial electron produced in the chamber
2. Initiates electron cascade
3. Cascade leads to excitation of gas molecules
4. Gas molecules de-excite by photon emission
5. Photons travel to cathode and produce photo-electrons
6. Photo-electrons initiate new cascades.

The character of the discharge is differentiated according to whether this cyclic process contributes significantly or not. We may obtain a measure of the significance of the contribution by means of a parameter γ, which is the probability that each electron produced by the cascade at stage 2. will produce at least <u>one</u> photo-electron at stage 6.

Then if the initial electron at stage 1. produces n electrons in the cascade of stage 2., the n secondaries will produce $n\gamma$ photo-electrons which produce $n^2\gamma$ electrons by multiplication, and so on. Hence the total number of electrons formed in all the cascades from one initial ionization electron (the so called Multiplication Factor)

$$M = \frac{n}{1 - n\gamma} \qquad \ldots\ldots(17)$$

If $\gamma \ll 1$, (the photon process is unimportant), then the chamber is said to operate as a proportional counter. M is approximately constant, at a value of n, and the amplitude of the output pulse (proportional to the quantity of charge collected at the anode) is proportional to the amount of ionization produced in the original ionizing event, which is a function of incident particle energy.

Rose and Korff (116) have given an expression for M

$$M = \exp\left[k \cdot \sqrt{\frac{V_o ap}{\log_e(b/a)}}\left(\sqrt{\frac{V_o}{V_t}} - 1\right)\right] \qquad .....(18)$$

where k is a constant characteristic of the gas, p is gas pressure, b and a are the radius of cathode and anode surfaces respectively, V_o is the applied polarization potential and V_t is a threshold potential given by

$$V_t = aE_c \log_e \frac{b}{a} \qquad .....(19)$$

where E_c is the critical potential field strength at which multiplication commences. Experimental data are found to agree with equation 18, and counters with values of M as high as 10^4 have been described (65) which have been used for measurements of low energy radiation.

It is evident that the phenomenon of gas-multiplication, presenting an electron pulse of very much greater amplitude to the collection system than in the case of an ionization chamber, allows individual ionizing events to be registered with an external amplification system of very much lower gain than would otherwise be required. However the value of M observed is not an invariant quantity, but will exhibit statistical fluctuations from event to event, in much

the same way as the original ionization process.

The variance of M was examined theoretically by Snyder (136) and Frisch (51) who found that

$$V_M = M \qquad .....(20)$$

Thus the total variance V of the output pulse amplitude of a counter expressed as an equivalent variance of the original ionization J_o will be

$$V = FJ_o + J_o \qquad .....(21)$$

The observations of Hanna et al. (65) at 250 ev, 2.8 keV and 17.4 keV indicated that a value of

$$V = J_o \qquad .....(22)$$

describes the experimental results more exactly. Since F (see equation 11) is not expected to be very small, the variance of the gas multiplication must be less than given by equation 20, confirming the observations of Curran et al. (37).

Among the advantages which may be cited for the proportional counter, compared with the until recently more widely used G-M counter, the stability of the system (provided good amplifying equipment is employed) and especially the short resolving time are most important. The latter may be as small as 5 microseconds or less (if an amplifier of short resolving-time is used) provided a counter gas with low electron-attachment tendency is used. Suitable gases are the rare gases, nitrogen, hydrogen, methane and higher hydrocarbons, carbon dioxide, boron trifluoride and others, used either singly or better in combination.

A further advantage arises from the common operation of proportional counters at atmospheric pressure, which facilitates the filling of the chamber after insertion of an internal source, compared with a

G-M counter which commonly requires an operating pressure of about 10 cm. Hg., unless very high applied potentials are used.

Geiger-Müller Counters

If the polarization potential is raised further, above that range of values at which the chamber is acting as a proportional counter, the value of γ is no longer negligible for those ionizing events producing the greatest amounts of ionization, and the chamber is said to be operating in the region of limited proportionality since pulse size is no longer proportional to original ionization at high energies (see below). At higher potentials still, $m\gamma = 1$ (see equation 17) for all ionizing events, and the counter operates as a Geiger-Müller counter.

Under these conditions, photons are produced in every electron cascade, and produce photo-electrons, which initiate further cascades. Thus a series of cascades will occur in the chamber, each cascade leaving a number of positive ions in the vicinity of the anode, and the process continues until the effect of the positive ion sheath in depressing the effective potential field near the anode becomes large enough to terminate the discharge.

The output pulses are thus observed to be of approximately constant amplitude for all ionizing events, since one electron produced in the chamber by an ionizing event is sufficient to discharge the counter. This leads to important advantages for the G-M counter, namely high sensitivity, and a large output pulse which needs the minimum of amplification with simple ancillary equipment before being supplied to a recording system.

However the positive ion sheath at the anode, left behind by the multiple cascade process described above, moves out to the cathode in a few hundred microseconds, and its interaction with the cathode surface gives rise to further secondary electron production, which in turn leads to further electron cascades. Thus unless measures are taken to ensure the contrary, once triggered, the counter will enter into a series of discharges spaced at intervals of somewhat less than a millisecond.

This process may be prevented, or quenched, in several ways. Thus internal quenching may be effected by addition of a proportion of a suitable poly-atomic gas to the counter filling. Thus ethyl alcohol is frequently added in proportions of about 10 percent to argon, the usual filling for G-M tubes. Then the positive argon ions moving to the cathode interact with neutral alcohol molecules to form argon atoms and alcohol ions, the cross-section for this so called "charge exchange" process being large due to the relative magnitudes of the ionization-potentials of argon and ethyl-alcohol (15.7 and 11.5 V resp.). The alcohol ions, arriving at the cathode "predissociate" rather than form secondary electrons, so no sequence of discharges is observed.

Alternatively the discharge may be quenched externally, for instance by causing the first pulse from an ionizing event to trigger an electronic circuit which then lowers the polarization-potential of the counter sufficiently to cause it to cease operation in the G-M region, for a time-interval longer than the time required for the migration to the cathode of the positive ion sheath.

With either mechanism the resolution time of the counter is much longer than that of a proportional counter, and usually lies in the range from 200 to 600 microseconds. This is an important disadvantage compared with proportional counter operation. Other disadvantages which may be cited are a limited life, due for instance to consumption of quenching agent, and the tendency for counter characteristics to change as the end of the life is approached.

With either mode of counter operation it is necessary to allow for the failure of the counter, at higher counting rates, to respond to ionizing events which occur in the time interval when the chamber is recovering from a discharge. When the dead-time is fixed at a definite value, as in the method of external quenching described above, formulae quoted in the literature (146) may be employed. eg.

$$n = n_o e^{-n_o t} \qquad \text{.....(23)}$$

and

$$n_o = \frac{n}{1 - nt} \qquad \text{.....(24)}$$

where n_o and n are the mean rates of occurrence of events, and of recording events respectively, and t is the dead-time. However when no fixed dead time is applied to the system, it is best calibrated empirically.

We may now proceed to discuss the methods of absolute disintegration-rate measurement which have employed particle counters. These generally use proportional counters and Geiger-Müller counters interchangeably, and differ mainly in their method of defining that proportion of the radiation emitted by the source which is observed by the detector.

(i) Coincidence-Counting Method

The use of an electrical coincidence arrangement for the detection of the simultaneous emission from a source of two particles was first reported by von Baeyer (4) in 1935, and was discussed in detail by Dunworth (38) and Wiedenbeck and Chu (144, 145). The application of coincidence measurements to absolute disintegration-rate determination has been described by Putman (113) and Seliger and Schwebel (130).

The principle of this method may be outlined as follows. Consider a source of β and γ radiation placed between two counters, one a β-counter of geometrical efficiency e_β, the other a γ-counter of efficiency e_γ. Then the counting-rate of the β-counter is given by

$$R_\beta = N_o e_\beta \qquad .....(25)$$

and that of the γ-counter by

$$R_\gamma = N_o e_\gamma \qquad .....(26)$$

where N_o is the source disintegration-rate. Also the β-γ coincidence-rate between the β- and γ-counters, that is the rate at which particles emitted simultaneously by the source are registered one by each of the counters, is given by

$$R_{\beta-\gamma} = N_o e_\beta e_\gamma \qquad .....(27)$$

Hence from equations 25 to 27

$$\frac{R_\beta R_\gamma}{R_{\beta-\gamma}} = \frac{N_o^2 e_\beta e_\gamma}{N_o e_\beta e_\gamma} = N_o \qquad .....(28)$$

In this derivation it has been assumed that

(i) the source is of uniform activity over its whole area

(ii) the β-counter is of uniform efficiency to radiation from all

parts of the source

(iii) the γ-counter is also of uniform efficiency.

Putman has shown (113) that equation (28) can be applied directly if any two of (i), (ii) and (iii) are valid. Thus, provided the source is uniformly distributed, and is thin enough for γ self-absorption to be negligible (not a very difficult circumstance to arrange) then self-absorption of β-radiation, which is at the moment the main source of error in 4π β-counting, does not exert a disturbing influence. Similarly equation (28) is valid despite the continuous energy distribution of β-radiation, and the variation of e_β with energy, since in its derivation e_β could equally well be replaced by $\overline{e_\beta}$, a mean efficiency over the energy spectrum. Likewise cases where β-emission is followed by the emission of more than one photon, or by alternative modes of photon emission, are also covered, if the appropriate mean efficiency $\overline{e_\gamma}$ is used.

Nuclides which constitute cases where direct application of equation (28) is not possible are the following.

(i) Nuclides which exhibit a branched β-decay scheme. Consider β particles belonging to two different energy spectra, counted with efficiences $e_\beta(1)$ and $e_\beta(2)$, of branching ratios A and (1-A), the mean γ-counting efficiencies for the photons following each beta transition being $e_\gamma(1)$ and $e_\gamma(2)$. Then the separate rates analogous to equations (25), (26) and (27) are

$$R_\beta = N_o \left[Ae_\beta(1) + (1-A)e_\beta(2) \right] \qquad .....(29)$$

$$R_\gamma = N_o \left[Ae_\gamma(1) + (1-A)e_\gamma(2) \right] \qquad .....(30)$$

$$R_{\beta-\gamma} = N_o \left[Ae_\beta(1)e_\gamma(1) + (1-A)e_\beta(2)e_\gamma(2) \right] \qquad .....(31)$$

$$\frac{R_\beta R_\gamma}{R_{\beta-\gamma}} = N_o \left[1 + \frac{A(1-A)(e_\beta(1)-e_\beta(2))(e_\gamma(1)-e_\gamma(2))}{Ae_\beta(1)e_\gamma(1) + (1-A)e_\beta(2)e_\gamma(2)} \right] \quad .....(32)$$

Hence the simple quotient no longer gives the disintegration-rate N_o, unless $e_\beta(1) = e_\beta(2)$ or $e_\gamma(1) = e_\gamma(2)$. The latter condition is in general not fulfilled, but in the case of a Geiger counter, the efficiency towards all energies of β-radiation can be made unity if window and air-absorption can be evaluated and corrected for (see below) and the source mounted so that self absorption and scattering effects are negligible (see below). However now the method has lost its unique character and is little better in accuracy than the "defined solid angle methods" discussed below.

(ii) Nuclides in which internal conversion is important, particularly those emitting low-energy photons. The effect of internal conversion has been examined by Wiedenbeck and Chu (145), and may be outlined as follows. In the case of the simple β-γ transition considered in the derivation of equation (28), let the conversion coefficient of the γ-radiation be α. Then if e_β is the efficiency of the β-counter for β-radiation and e_c for conversion electrons, then analogous relationships to equations (25), (26), and (27) are

$$R_\beta = N_o(e_\beta + \frac{\alpha e_c}{1+\alpha} - \frac{\alpha e_\beta e_c}{1+\alpha}) \quad .....(33)$$

$$R_\gamma = N_o e_\gamma(\frac{1}{1+\alpha}) \quad .....(34)$$

$$R_{\beta-\gamma} = N_o e_\beta e_\gamma(\frac{1}{1+\alpha}) \quad .....(35)$$

$$\frac{R_\beta R_\gamma}{R_{\beta-\gamma}} = N_o\left[1 + \frac{\alpha e_c}{1+\alpha} \cdot \frac{1-e_\beta}{e_\beta}\right] \quad .....(36)$$

Thus if e_c is not negligible, a knowledge of the conversion coefficient α to an accuracy at least equal to that required for the value of N_o is

required for the determination in this case.

Further sources of error to which the method is susceptible are the following.

(i) Sensitivity of the β-counter to γ-radiation and vice-versa. This may be measured and corrections applied by means of measurements with suitable absorbers between source and counter (113), or if scintillation counters are used for both β- and γ-counting (130) by pulse height analysis.

(ii) Dead time losses in the separate counters, which may be considerable, since quite intense sources need to be used if coincidence counting-rates are to be measured to good statistical precision.

(iii) Natural background effects. The correction for this error is somewhat more complex than in a simple counter system, since in the usual coincidence-counting arrangement with the β- and γ-counters vertically above one another, that component of the background due to cosmic radiation will have a fair probability of triggering both counters coincidently.

(iv) Random coincidences. If t_β and t_γ are the separate resolution times of the β- and γ-channels, then a contribution to the coincidence rate

$$R = R_\beta R_\gamma (t_\beta + t_\gamma) \qquad \ldots\ldots(37)$$

will be observed due to the failure of the coincidence apparatus to resolve unrelated events occurring within a time interval less than $t_\beta + t_\gamma$.

Thus one may summarize: the coincidence method is easily and with good accuracy applicable only to nuclides which decay by a single

β^--transition to an excited state of the product nucleus of very short half-life (ie. emitting prompt γ-radiation). The nuclides satisfying this criterion form a very small proportion of those it is of interest to observe (33). However, for those nuclides to which it may be applied, it is said to offer an accuracy of better than $\pm$ 0.5 percent (130). This surpasses the results of any other method (including the results hitherto obtained with 4π β-counting).

The remaining methods relying on particle-counting can be classified according to the solid angle subtended at the source by the sensitive volume of the counter, ie. either as low geometry counting (where the angle is $<< 2\pi$ steradians) or as high geometry counting (where the angle is 4π steradians).

(ii) Low Geometry Counting

The low geometry counting method represents the application of the conventional end-window Geiger-Müller counting system to absolute-disintegration rate determination. The G-M counter has the considerable advantage of registering essentially all particles that penetrate to the sensitive volume of the counter. However its application to the problem at hand necessitates a careful evaluation of the many sources of error to which the system is liable - disturbing influences which modify the spatial distribution of radiation from the source, or absorb this radiation before it triggers the counter.

Zumwalt (153) has given an expression relating the counting rate of an end-window counter, R, to the disintegration rate of the source, N_o.

$$R = N_o G f_w f_A f_B f_H f_S \qquad .....(38)$$

where G is the solid angle subtended by the counter at the source divided by 4π steradians ("geometrical efficiency"), and the f's are factors relating to

W - absorption of radiation in the counter window and air between the source and counter

A - the scattering of particles into the counter, that would otherwise not enter it, by air around the system

B - backscattering of radiation from the source mount

H - the scattering effects due to the counter support and housing

S - the absorption and scattering of radiation within the material of the source itself.

A number of workers (1, 25, 108, 113, 148, 153) have studied the phenomena enumerated, and have obtained the value of the various correction factors as a function of source, mount or absorber thickness etc.

(1) The "geometrical efficiency" has been determined by calibration of the system (with all the f-values known) with standard sources. These were either calibrated by another β-counting method such as coincidence counting (1, 153) or prepared from the RaD-E-F equilibrium mixture (25, 108), standardized by knowledge of the weight of uranium parent from which it was separated, or by α-counting of the RaF (Po^{210}) constituent.

However the quantity G was found not to be constant for emitters of radiation of different energy. This was taken to be due to a change in the dimensions of the "sensitive volume" of the counter, and attempts to correct for this error led to a modification of the apparatus which has been called the "defined solid angle" technique (113). The solid

angle within which radiation must be emitted to reach the counter was defined by a circular opening in a mask between the counter and source (1, 113). Changes in sensitive-volume with particle energy were then without effect, since only the central part of the chamber was used, and the factor G could now be computed from the dimensions of the system.

(2) The correction for absorption in the counter window was generally obtained by plotting an absorption curve from readings of counting-rates with increasing thicknesses of aluminum in front of the window, and extrapolating past the zero thickness point a distance equal to the window thickness (1, 25, 108, 153). However a possible error could arise from this procedure, since it would not detect and correct for a soft component of the radiation completely absorbed in the counter-window. For this reason the use of a windowless counter (113) would be preferable.

(3) The effects of air between the source and counter were studied, either by placing a series of layers of a plastic material, with a value of mean atomic number close to that of air, between source and counter (153), or replacing the air with other gases or a vacuum (1).

(4) The effect of housing scattering of radiation has been studied by devising a system in which most of the heavy material surrounding the system was replaced by air (148). Lining the conventional lead housing with low-$\overline{Z}$ material was also found to reduce the correction necessary.

(5) The backscattering effects and self-absorption and scattering effects were studied by measuring recorded counting-rates and angular

distributions of radiation as a function of source and mount thickness. The results of these investigations are discussed in detail in sections D and E of this thesis.

In addition to the above, corrections needed to be made for counter background, and dead-time losses (see earlier) and for the effects of γ-radiation if present. It is clear that in view of the multitude of corrections that had to be applied, no great accuracy was to be expected from this kind of method. In fact the best results obtained were accurate to little better than ± 5 percent.

2π Counters

A counter sensitive to radiation emitted into a solid angle of 2π-steradians, ie. into a complete hemisphere, would possess several advantages despite the difficulties associated with the necessary internal mounting of sources. Thus Zumwalt's factor G (see earlier) is fixed at a known value, while f_W f_A and f_H become unity.

However 2π counters have been little used in absolute counting, since their development was immediately followed by that of 4π-counters, which possess all the advantages of 2π counters and many advantages in addition.

Counting with a Geometry of 4π-steradians

A counting geometry of 4π-steradians, ie. a system in which all particles emitted by a source are counted, may be obtained in three ways - with a counter filled with a gas-mixture containing a gaseous source material, with the radioactive material dispersed in the phosphor of a scintillation-counter, or with a solid source placed between two counters, each with a geometry of 2π steradians.

(iii) Gas Counting

The theoretical advantages of using a gaseous source as part of the filling of, for example, a Geiger counter are quite important. In such a system most of the sources of error of other counting arrangements disappear since β-particles initiate electron cascades immediately after emission, and before the intervention of scattering or absorption effects. The benefit accruing from the complete absence of self-absorption effects is of most potential importance in radio-biological tracer applications, using C^{14} and S^{35}. Sources for assay resulting from these studies contain a very low energy β-emitter, usually in material of very low specific activity.

In 1946 Henriques et al. (71, 73, 74) described a system in which suitable compounds of C^{14}, S^{35} and H^3 were used as filling for an ionization chamber attached to a Lauritsen electroscope. This was successfully employed for assay of the nuclides mentioned, although not in an absolute sense.

The first success in the use of CO_2 as a filling of a G-M counter was reported in 1947 (101). CO_2 did not exhibit suitable characteristics when pure, but did so after addition of small quantities of CS_2. This gas mixture was later used in absolute counting of C^{14} (66, 67, 94). (However there are reports that this gas mixture is not 100 percent efficient) The addition of small quantities of $C^{14}O_2$ to the usual argon-alcohol filling for G-M counters (41) has also been employed.

The sources of error, to which absolute counting measurements in these systems are subject, are threefold.

(1) Adsorption of radioactive materials on the counter walls resulting in cross-contamination from one determination to the next. This can be made negligible by suitable pretreatment of wall-materials (41).

(2) End effects. The measurement of the activity of the volume of gas defined by the geometrical dimensions of the cylindrical counter cathode may be in error in two ways. Firstly there will be a contribution to the measured activity from material outside the specified volume but from which radiation will penetrate into the counter proper and register. Secondly, and more important, the counter field strength towards the ends of the tube will tend to be lower than in the centre, and low counting-rate in these parts will be observed. Corrections for end effects can be made experimentally by use of two or more counting tubes of different lengths, but with similar diameters and end-geometries (and presumably end effects). Then (41) if R and r are the observed counting rates per unit volume for counters of length L and l, and if p is the counting-rate per unit volume with a counting efficiency of 100 percent, then

$$p(L-l) = RL - rl \qquad \ldots\ldots(39)$$

from which the true counting rate for a counter of a given volume may be calculated.

(3) Wall effects. It is expected that disintegrations from a thin layer of gas adjacent to the cathode surface resulting in a β-particle emitted in the direction of the cathode, which is absorbed before triggering the counter, will not be registered. This effect, although reduced by backscattering effects, may not be negligible. Experiments

using similar gas fillings in tubes of different diameters, etc., indicated that the effect was less than ~ 2 percent (67).

Thus the gas counting method might be expected to be of considerable use for the assay of materials emitting soft radiation, and of low specific activity. However it will not often be possible to find a suitable gaseous compound of the element studied, which moreover must not exert a deleterious influence when introduced into a counting-tube, and gas-counting has not frequently appeared in the literature on absolute-counting of recent years.

(iv) Scintillation Counting

Scintillation-counter systems, in which a source to phosphor geometry of 4π steradians were obtained, have been used for specialized applications. Thallium activated potassium iodide phosphors containing natural K^{40} activity (50) and thallium activated rubidium iodide phosphors containing Rb^{87} (92) have been used in half-life studies, while studies of nuclear decay mechanisms have been made with C^{11} in anthracene (131) and Tl^{204} in thallium activated sodium iodide (98).

Other methods of introducing source material into the phosphor system have been used. Thin evaporated sources of Hg^{203} have been sandwiched between two NaI(Tl) crystals (7), while the immersion of a source carried on a thin foil into a liquid phosphor (18) was also successful. Attempts to disperse radioactive materials in a liquid phosphor system are generally unsuccessful, owing to the depressing effect exerted by foreign material on the scintillation efficiency, although a recent report (87) suggests that incorporation of C^{14} compounds in a liquid phosphor has been successful.

This method is clearly useful for certain specific applications, where dispersion of the source throughout the phosphor can successfully be achieved. However systems in which a source on a suitable mount is sandwiched between two crystals, or any such arrangement, will possess many of the inherent errors of 4π gas-ion counting without that method's flexibility and applicability to routine usage.

The method of absolute disintegration-rate determination by particle counting remaining to be described is that examined in this thesis, namely 4π-counting. This term, although strictly embracing methods (iii) and (iv) above, is customarily reserved for specific application to a counter system, with a source to detector geometry of 4π-steradians, composed of a solid source between two proportional or G-M counters, each with a geometry of 2π steradians.

We consider this system in detail below.

3) 4π-COUNTING

(a) History

This method owes its origin to Simpson (133) who in 1944 described a system in which the source was disposed in a re-entrant cavity in a G-M counter, the radiation entering the counter volume through thin foil windows. The source-to-counter geometry thus approached 4π-steradians.

The first counter in which this geometry was accurately obtained was due to L. Meyer-Schützmeister and was described in 1948 by Haxel and Houtermans (69). Since that time a variety of designs of 4π-counter have been described (14, 20, 28, 29, 30, 31, 68, 69, 76, 95, 100, 117, 124, 128, 133, 135, 140, 141, 142). These have been designed to operate as proportional and as G-M counters, and the chambers have been

of cylindrical and spherical form.

All, however, have had several essential features in common. The chamber is divided symmetrically into two halves, each of which is a self-contained counter unit. The two halves are electrostatically screened from one another by a plate or sheet of conducting material. The source is mounted at the centre of the plate, the central portion of which, at least in the vicinity of the source, is thin in order to reduce absorption of the radiations emitted. Thus the radiation enters one half counter directly without any intervening material, and the other half-counter via a thin layer of source-mounting material.

Of those systems which can be devised with a 4π-steradian geometry, that just described is the most convenient for routine usage. Nearly all radioactive materials can be converted to a form suitable for mounting on a thin backing, and provided a backing material of adequate strength can be found in the required thickness, little chance of counter-contamination and cross-contamination from sample to sample exists, particularly since source mounting systems are devised so as to be expendable.

(b) Advantages of a 4π-counting Geometry

A counter with a geometry of 4π steradians will clearly be more sensitive and be able to measure to good statistical accurcay much smaller samples than a low geometry counter. However the increased sensitivity is among the least important of the advantages of this system.

It has been appreciated for many years that a counter sensitive to radiation emitted over an angle of 4π steradians will have peculiar

advantages resulting from the fact that all particles emitted from a source are counted, and hence that any event subsequent to charged particle emission which occurs within the resolution time of the instrument will not be registered separately. This fact has two very desirable consequences.

(i) The interpretation of counting data is independent of a knowledge of the relevant decay scheme in the majority of cases. That is provided the primary events of the nuclear transition studied include charge particle emission with a total probability of unity, one count will be registered per disintegration - the observed counting-rate (corrected for background and resolution losses) is identically equal to the disintegration rate. This remains undisturbed by the emission of secondary particles, nuclear gamma radiation, or annihilation radiation, when these occur within the counter resolution time, as is usually the case.

This state of affairs is in sharp contradistinction to all counting-methods without a 4π-steradian geometry. The difference is particularly important in the case of nuclides decaying by positron emission - the 4π-counter being probably the only satisfactory means of accurately assaying these materials. The trouble with other counting methods arises from the fact that (in addition to nuclear gamma radiation from the source) annihilation radiation (photons of 0.511 Mev) is emitted when the positron annihilates with a negative electron at the end of its path. Thus the photons may originate at a considerable distance from the source proper, and will be counted with a geometry much different from that for the positron itself. In the 4π-counter

however all the positrons register, and the counter discharges due to any annihilation-radiation are in coincidence with the corresponding positron-induced discharges, and thus not differentiated from them.

Cases of nuclear transitions, for the assay of which some data from the decay scheme are required, include those when particle emission occurs with a probability of less than unity (which includes orbital electron capture) and transitions leading to a metastable excited state of the product nucleus. In such cases, the accuracy of the disintegration-rate determination will clearly depend on the accuracy of the nuclear data employed, (as is true for the other counting systems discussed) in addition to that of the 4π-counting system itself.

(ii) Scattering of radiation either by source material, source mount, gas or counter walls is without effect on the observed counting-rate. Any discharges (subsequent to that corresponding to the primary event) caused by repeated scattering of one particle will occur within the counter resolution time. The same is true of secondary radiation production due to interaction of primary particles with the gas, wall or other material within the counter.

Hence in Zumwalt's relationship (equation 38), for a 4π-counting system the following is true:

$$G \longrightarrow \text{unity}$$

$$f_A \equiv \text{unity}$$

$$f_B \equiv \text{unity}$$

$$f_H \equiv \text{unity}$$

and most of the large corrections of uncertain accuracy required in

low-geometry systems are eliminated. The only sources of error still to be corrected for in the calculation of disintegration rates from 4π-counter data are due to

(i) Failure of the counter to respond once to every ionizing particle arising from a nuclear disintegration which reaches the counter gas.

(ii) Absorption of radiation by the mount on which the source is deposited.

(iii) Absorption of radiation by the source-material itself (self-absorption).

(iv) Statistical fluctuations in the disintegration rate of the source and in the background counting-rate of the counter.

Errors from term (iv) can be reduced to within any desired limits by extension of the number of events observed (provided the combination of source intensity and half-life is such as to allow this), and the error in any given case can be evaluated in accordance with the laws of statistics.

Thus since nuclear disintegrations are randomly distributed in time, the distribution of the number of events observed in a given time about the mean number (n) occurring in the same interval will be a Poisson distribution. Hence the variance V_n of n

$$V_n = n \qquad \text{.....(40)}$$

or the standard deviation σ_n of n is

$$\sigma_n = \sqrt{V_n} = \sqrt{n} \qquad \text{.....(41)}$$

Errors from (i) to (iii) should on the other hand be amenable to reduction by evolution of suitable techniques. However this has not up to the present time been possible apparently, since the results of intercomparison of standards (130) by 4π β-counting show a scatter of several percent, in contrast to good agreement with β-γ coincidence counting results. Nevertheless the 4π-counting method has no inherent inaccuracies of this magnitude, and in this thesis we shall examine the items listed above, in sections B, C and D respectively, with a view to the reduction of the error from these causes. In section E, we shall discuss certain more theoretical topics on which certain of the experimental work may be made to give information.

B. COUNTER RESPONSE PROBABILITY

1) INTRODUCTION

For the purposes of the present discussion it is convenient to define a quantity, which we shall call the response probability of a counter. This is the probability that a discharge triggering the recorder be produced when a charged particle or photon originating from a nuclear disintegration in the source reaches the counter gas. (We will deliberately avoid employing the term "efficiency" since this has been used in different contexts by different authors, sometimes being used in the sense of the above definition, but more often including the counter geometry ratio and effects due to scattering, absorption and so on.).

Thus the object of this section of the thesis may be restated in terms of the above definition: we shall investigate the errors arising in disintegration-rate determinations by 4π-counting owing to a departure of the counter-response probability towards the particular form of radiation studied from a value of unity. The response probability towards charged particles for instance will under suitable conditions be close to unity, whereas to photons it will be very much less than unity. However provided the counter has nearly unit response probability towards at least one of the products of disintegration, then as outlined earlier the response probability of the counter to the nuclear transition as a whole will be of a similar magnitude.

We shall effect the investigation by examining the variation of the response probability towards particular forms of radiation with changes in the conditions under which the counter is operated. There

are several variables to be considered. Some can be adjusted to ensure that no deleterious effect on the response probability arises from those sources. Others however cannot be completely controlled in this fashion. In these cases we must determine the conditions under which a minimum disturbance is observed, and determine the value of the response probability under these conditions, so that the disintegration-rate value obtained may be corrected.

The conditions under which the counter response probability may differ from unity are the following: it may be <u>less</u> than unity if

(a) the gas multiplication and electron collection efficiency of the chamber is less than a minimum value,

(b) the "effective" geometry of the chamber is less than 4π steradians,

(c) at higher counting rates the probability becomes appreciable that particles from successive disintegrations be emitted within a time interval of one another less than the resolution-time of the counter. "Resolution-losses" will then occur.

It may be <u>more</u> than unity, ie. more than one count be registered per disintegration, if

(d) at higher polarization potentials, the character of the discharge phenomena alters, approaching that of a G-M counter. Under these conditions, $n\gamma$ approaches unity (see Section A) and photons arising from excited gas molecules in the neighbourhood of the electron cascade produce photo-electrons at the cathode surfaces.

At the same time a second process also becomes important, namely bombardment of the cathode by positive ions, which also leads to the production of delayed electron cascades, leading to multiple pulsing as described earlier.

(e) the counter gas contains more than a limiting concentration of electronegative impurities. Then electron attachment (see Section A) may lead to delayed electron collection, and hence multiple pulsing.

(a) Gas Multiplication and Electron-collection Efficiency

In order that the passage of an ionizing entity through the chamber shall register a count, the ionization produced, after gas multiplication, collection at the counter anodes, and external amplification, must produce a pulse at the output of the amplifier system larger than the discriminator bias potential applied to the signal. Whether this condition is satisfied depends on the relative magnitudes of the multiplication factor, amplifier gain, capacitance of the chamber anode system and amplifier input, and of the bias potential. These quantities may all be measured, but, aside from the discriminator bias, which cannot be reduced below a minimum value, the only one normally varied in the system is the gas-multiplication factor. As outlined in section A, this is a function of polarization potential and must be adjusted, by increasing the polarization potential, until the situation described above is obtained. However, the polarization potential cannot be raised indefinitely, since above a limiting value the secondary processes described under (d) above set in. Thus it is important to determine whether the gas multiplication can be raised sufficiently to bring the response probability of the chamber close to a value of unity for the radiation producing the least amount of ionization in the chamber. (This is clearly particularly important when beta-radiation is to be examined, since the energy spectrum

includes a proportion of particles with very low energies, a proportion which increases with decreasing spectrum end-point energy.)

(i) Determination of polarization conditions for optimum gas multiplication and electron collection.

One may adopt two lines of investigation. First the change in counting rate as the gas-multiplication is varied within the range available may be observed. Secondly the various quantites described above may be measured, the gas multiplication as a function of polarization potential, and the total response probability of the counter under given conditions for the softest beta-radiation liable to be examined may be calculated. Both these methods have been used in the present investigation.

In addition to being a function of the polarization potential, the gas multiplication and electron collection efficiency are also dependent on several other variables.

(ii) Source position.

The polarization field strength is a function of position inside the chamber, and therefore the electron collection efficiency will be a function of source position both within the normal source-mount plane, and for movements at right angles to this plane. However since the chamber is usually operated at a potential that ensures a collection and gas multiplication factor more than adequate for registering particles from disintegrations in material situated at the centre of the chamber, it is probable that they are also adequate for positions some distance removed from the centre of the chamber. Hence it is expected that a region of constant response probability

would exist, and that the operation of the counter will be insensitive to small source movements within this region.

(iii) Conductivity of source mount.

Since the efficiency of electron-collection and gas multiplication are rapidly varying functions of polarization field strength, it is important to ensure that this field strength is reasonably constant and at an optimum value in the vicinity of the source. This is especially important for the measurement of soft β-emitters of which the radiation will have a short range in the counter gas, and hence produce most of its ionization in the immediate source vicinity. The design of counting-chamber we have used (see later) ensures this provided the source mount is conducting to the cathode surface. A mount made of a poor conductor will disturb the field strength in such a manner that a position of low field strength occurs at the source position, between the anodes, and poor collection and multiplication results.

Seliger and Cavallo (128) claimed that the loss in efficiency due to the use of a non-conducting film mounted over an aperture in an aluminum diaphragm was negligible provided the aperture diameter was limited to minimise the field disturbance. However, in a later paper (95) they agreed with most observers that, for reliable results, the film had to be rendered conducting. This is satisfactorily accomplished by gold-coating the film by distillation in vacuo. A rapid routine method for estimating the thickness of the gold-layer will be described in section C (below). It is of considerable importance to reduce the superficial density of the source mount used as

far as possible in order to reduce absorption of radiation (see section C). It is thus essential to know the minimum superficial density of gold required for satisfactory counter operation, since it is fruitless to reduce the film superficial density much below this figure. Little quantitative information is available on this point, or on whether one or both sides of the film need be coated. Hawkings (68) has used 25 $\mu g./cm^2$ of gold on both sides of a 50 $\mu g./cm^2$ formvar film with success.

(iv) The electron collection and multiplication process will clearly be affected to some extent if the counter gas contains a significant proportion of electron-accepting impurities since electron attachment leads to slow moving negative ions in place of highly mobile electrons. It is therefore of importance to determine the limiting concentration which can be tolerated without the counter operation being affected.

(b) Counter "Geometry"

The response probability will be reduced from a value of unity if conditions are such that a proportion of the emitted radiation is absorbed (other than by source material, or the mounting film) before it can produce in the gas-space the necessary minimum number of ions required to trigger the recorder. It must therefore be verified that with the aperture sizes used by us, this effect is not serious.

(c) Resolution Losses

Operation of the chamber as a proportional counter serves to increase the value of the response probability at high counting rates, by effectively reducing the resolution time of the apparatus, compared with that obtained with the counter operated as a Geiger-Müller counter

(see section A). The use of the 4π-counter over a wide range of counting rates nevertheless demands that the resolution loss be accurately known as a function of counting rate. Due to the variety of processes which may cause resolution losses in the proportional counter and associated electronic equipment this function is best obtained empirically. The availability of thin films, described in the next section, has made possible a very precise determination of the coincidence loss function by a modification of the conventional multiple source technique.

2) COUNTING APPARATUS

The counting apparatus used for the work to be described is shown in the photographs in Figure 4, both in general appearance and in more detailed views of the counting chamber itself. The apparatus as shown has the necessary duplication of H.T. and amplifier units for the coincidence studies described in section E of this thesis, but is normally connected to a single amplifying system with the anodes in parallel, for the remainder of the experimental work to be described and for routine counting work.

The counting chamber is essentially of the design described by Hawkings et al. (68) and is illustrated diagrammatically in Figure 5. It consists basically of two hemispherical brass cathodes of 7 cms. diameter and two ring shaped anodes of 0.001 inch diameter tungsten wire. Insulation of the anodes and anode leads from the cathodes is effected by large teflon insulators, and the source mount consists of a plastic film of superficial density 5-10 $\mu g./cm^2$, rendered

Figure 4

The 4π-counting Apparatus

(a) General view, showing lead castle and preamplifiers at the left, main rack and methane cylinder to right. Units in rack are, from bottom upwards: flow-meters and automatic timer, scaler and recorder (AEP 908), Nichols High Voltage supply (AEP 1007B), Power supply for preamplifiers, and a second High Voltage supply for coincidence experiments.

(b) View of open castle, flow-meters and automatic clock. Chamber in closed operating condition.

(a)

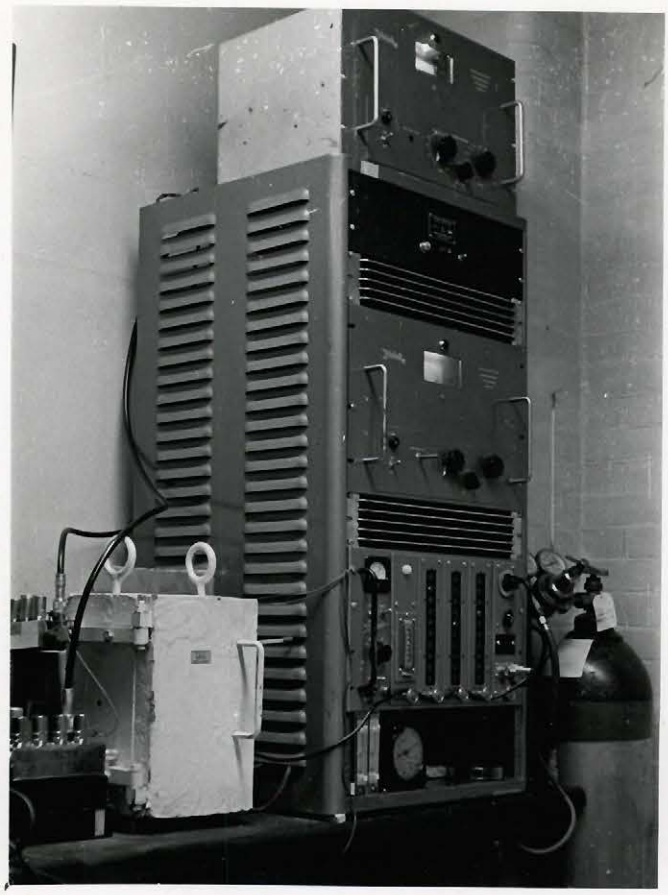

(b)

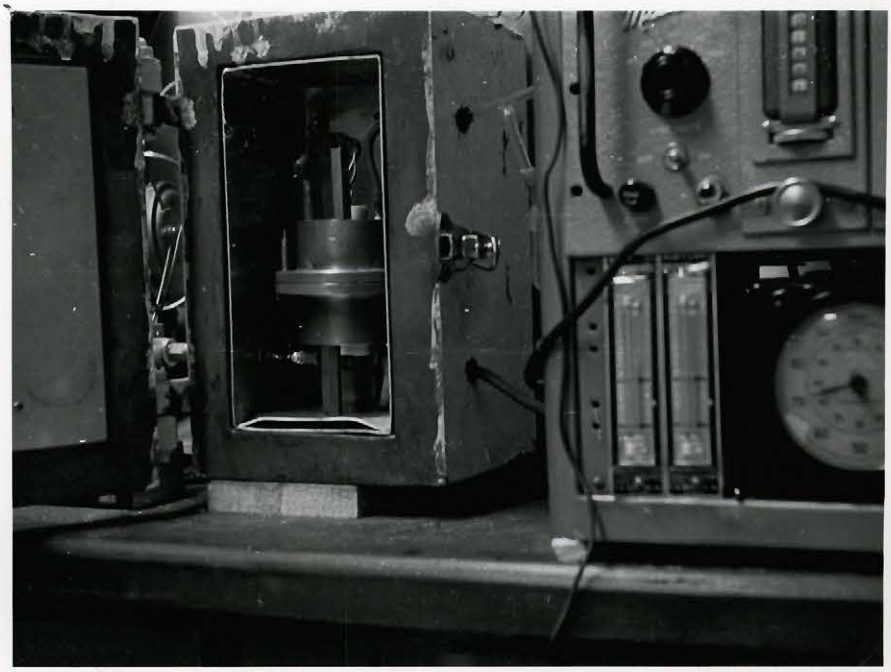

Figure 4

The 4π-counting Apparatus

(c) Detailed view of interior of castle, showing arrangement of anode leads, and chamber open for insertion of sample. Anode leads connect to single preamplifier lead (top left) for normal operation, each half-counter separately to two preamplifiers for coincidence experiments. Second amplifier lead is seen at bottom left.

(d) Chamber disassembled, showing diaphragm with 0.5 cm. diameter aperture at left.

(c)

(d)

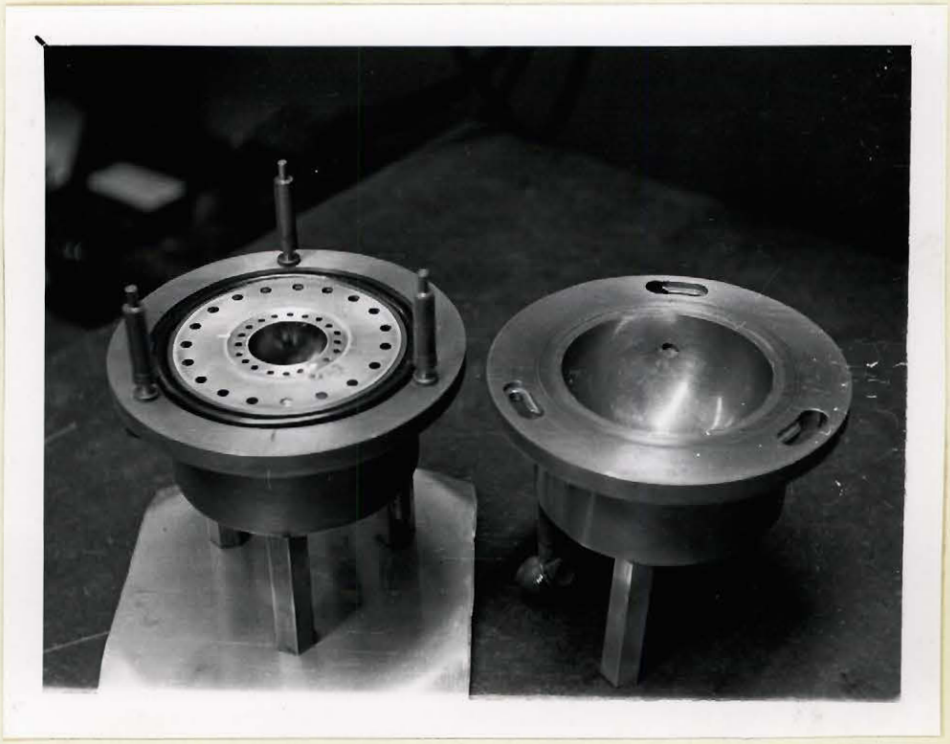

Figure 5

4π-counting Chamber (diagrammatic)

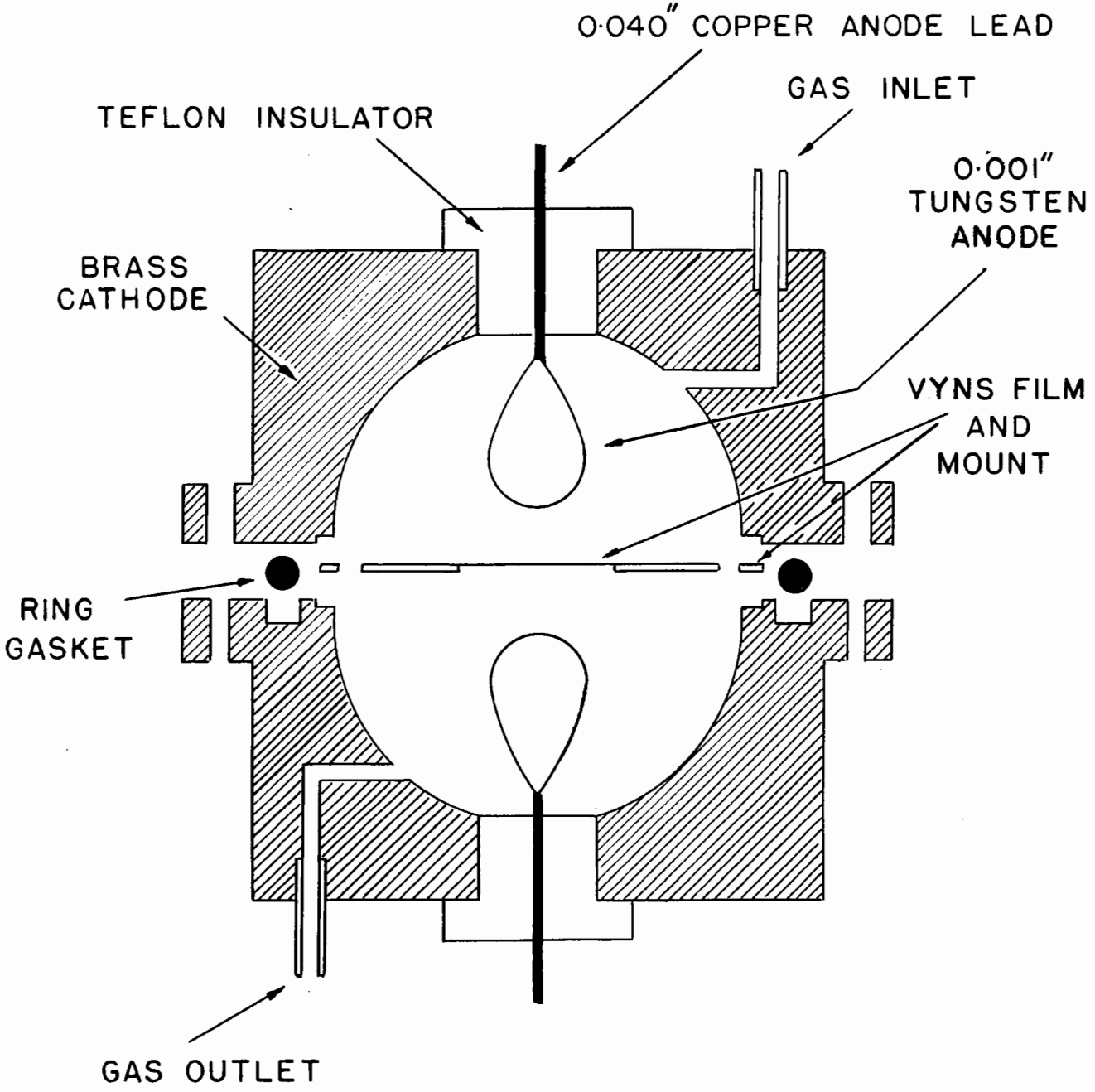
0·040" COPPER ANODE LEAD
GAS INLET
TEFLON INSULATOR
0·001" TUNGSTEN ANODE
BRASS CATHODE
VYNS FILM AND MOUNT
RING GASKET
GAS OUTLET

conducting by a 2 $\mu g./cm^2$ layer of gold applied by distillation in vacuo to one side of the film. The film is mounted over an aperture in an aluminum plate 1 mm. thick. The aperture diameter is usually 2.5 cms. and occasionally 5.0 cm.

The chamber is used in conjunction with a Nicholls high voltage supply (AEP 1007B). The anodes of the chamber are connected in parallel to an Atomic Instrument pre-amplifier (205-B) which has been modified to obtain a low "noise" level. The output from this is fed into an Atomic Energy of Canada Ltd. amplifer (AEP 1448) and thence after discrimination into a Marconi scaling unit of 1000 (AEP 908). The overall gain of the amplifying system is 30,000 and a bias voltage up to 50 volts can be applied by the discriminator to the output signal.

The counter chamber is operated in the proportional region, the counting gas used being C.P. methane at atmospheric pressure dried by passage over silica gel. After insertion of a sample the counter is flushed for about two minutes at a rapid flow rate and the rate then moderated to a standard rate of 0.5 ml. methane per second (see figure 19 b). Gas flow rates are measured by means of a simple flow-meter system.

The excellence of the high voltage characteristics obtained with this system (shown below), particularly in respect to the length and very small slope of the 'plateau', is largely attributable to the high quality of the amplifying equipment used, especially the AEP 1448 main amplifier. This unit, of which the circuit diagram is shown in Appendix A, has been specially designed, so that a high degree of 'saturation' may occur (ie. the input pulse amplitude may exceed the

maximum the equipment can handle to a very great extent) without production of multiple or spurious pulses following the primary pulse, due to "ringing" effects becoming apparent. These so-called non-overloading characteristics are illustrated in Figure 6. This shows a series of pulse forms as observed at the output of the amplifying system with a cathode-ray oscilloscope as the input pulse amplitude from the counting chamber was increased by increasing the polarization potential. The absence of secondary pulsing under conditions of primary pulse saturation is clearly seen.

3) EXPERIMENTAL TECHNIQUES, RESULTS AND DISCUSSION

The sources of radiation used in the work to be described in this and the next section were all of so high a specific activity that essentially "weightless" deposits were obtained. No modification of radiation energy or spatial distribution by self scattering or absorption processes in the source material was therefore to be anticipated. Samples approximating "point-sources" were prepared by evaporation of a suitably sized aliquot of stock solution on the mounting film by means of infra-red radiation. One exception to this procedure was the case of $Tc^{99}m$. This nuclide was co-separated with rhenium in the normal fission product procedure (59) by distillation of Tc_2O_7 from concentrated H_2SO_4 followed by $Fe(OH)_3$ scavenging operations. Thence to the final stage when the Re - Tc mixture was precipitated as the sulphide. The sulphide was slurried with water and a portion evaporated on the film.

The half-life, mode of decay, radiation characteristics and source of supply of the nuclides used are shown in Table I.

Figure 6

Output Waveform of AEP 1448 Amplifier Unit

Pulse observed with a C.R.O. at output of amplifier for increasing polarization potential on chamber. Using a Ni^{63} source (β^--emitter).

(a) Polarization potential 2.0 kv

(b) Polarization potential 2.2 kv

(c) Polarization potential 2.6 kv

(d) Pulse at output of discriminator circuit.

All with C.R.O. self-synchronized, time base 3 μ.sec/cm., vertical sensitivity 1 volt/cm.

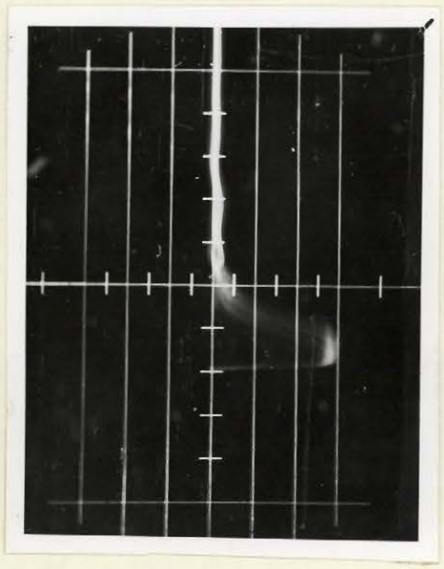

(b)

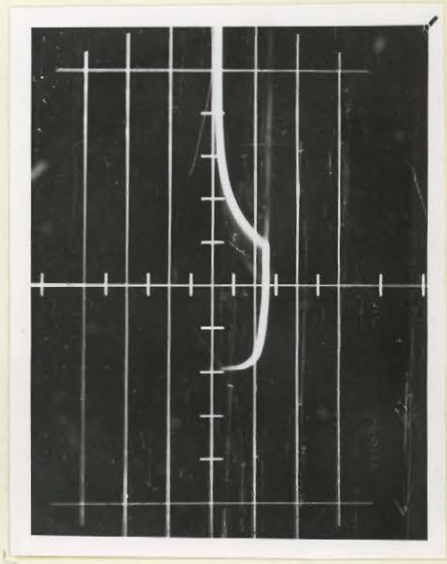

(d)

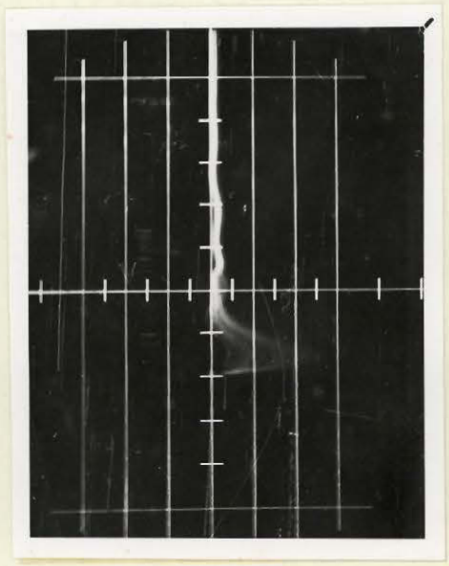

(a)

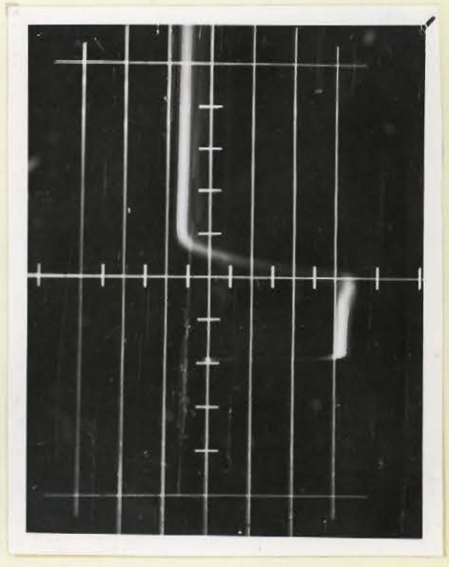

(c)

TABLE I

Characteristics and Source of Supply of Radioactive Nuclides

Nuclide	Half-life	Mode of decay	Maximum Energy of Particle Mev	Source of Supply
Ni^{63}	80 y	β^-, no γ	0.067	A.E.C.L.
S^{35}	87 d	β^-, no γ	0.167	A.E.C.L.
Ca^{45}	152 d	β^-, no γ	0.254	A.E.C.L.
Tl^{204}	4.0 y	β^-, no γ	0.765	A.E.C.L.
Bi^{210}	5.0 d	β^-, no γ	1.17	Separated from RaD-E-F from A.E.C.L.
P^{32}	14.4 d	β^-, no γ	1.70	A.E.C.L.
La^{140}	40.3 h	β^-, γ	2.26	Separated from fission products of uranium irradiated in BEPO, A.E.R.E., Harwell, England
Po^{210}	138 d	α, γ	5.30 (mono-energetic)	Separated from RaD-E-F from A.E.C.L.
Na^{22}	2.6 y	β^+, γ	1.8	A.E.C.L.
Co^{60}	5.3 y	β^-, γ	0.319	A.E.C.L.
Tc^{99m}	6.0 h	IT, γ	0.142 (mono-energetic)	Separated from fission products of uranium irradiated in BEPO, Harwell.

(a) Gas Multiplication

(i) High Voltage Characteristics of the Counter

High voltage characteristic curves were obtained in the usual way for a series of sources of β^- radiation of increasing maximum energy at a constant discriminator bias level. The nuclides employed, with the exception of La^{140} all emit β^- particles without accompanying γ radiation. Their nuclear properties are described in the top half of Table I. Figure 7 thus indicates the response of the counter to β^- radiation. Standard deviations on the quantities measured lie within the areas of the points as plotted (as for all succeeding figures in this thesis unless otherwise indicated).

The data shown in Figure 7 indicate that the chamber used in this work is certainly suitable for measurements of β^- emitters with maximum energies down to 0.067 Mev. The plateaus obtained in no case show any perceptible slope. The maximum figure which can be calculated on a basis of the statistics of the measurements concerned is less than 0.1 percent per 100 volts. There is, therefore, little ambiguity as to the correct counting rate figure to be used as a basis for calculating the disintegration rate, and little doubt of the fact that substantially all of the particles in the spectrum are being registered. At polarization potentials of about 100 volts in excess of the threshold value, the response probability certainly approximates very closely to unity. However, obviously, any polarization potential on the plateau may equally well be used if this is desirable.

The displacement of the curves to higher potential values observed with increasing particle energy is due to the reduced amount

Figure 7

High Voltage Characteristics of the Counter for β^-

Radiation of Increasing Maximum Energy

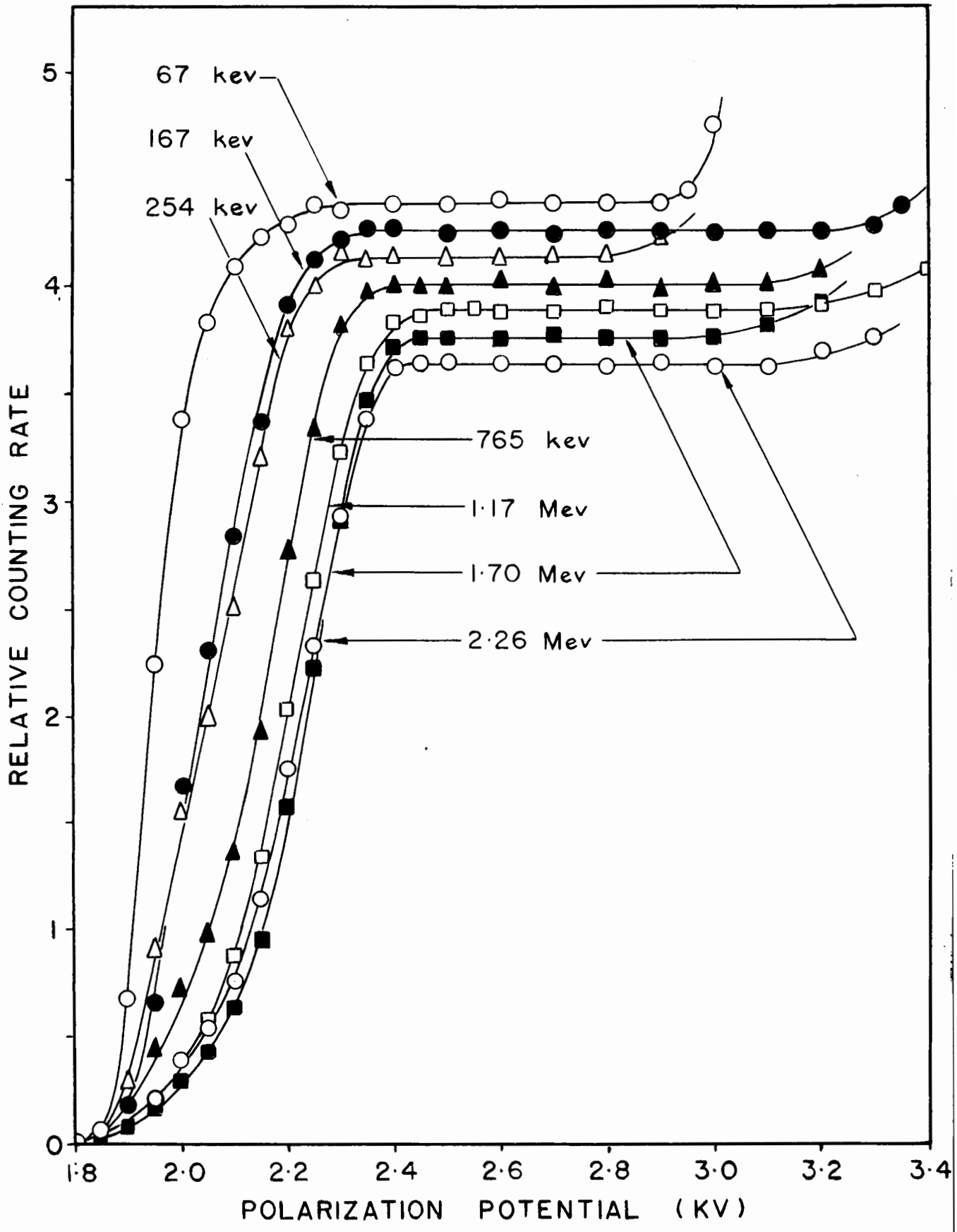
67 kev
167 kev
254 kev
765 kev
1·17 Mev
1·70 Mev
2·26 Mev
RELATIVE COUNTING RATE
0
1
2
3
4
5
1·8
2·0
2·2
2·4
2·6
2·8
3·0
3·2
3·4
POLARIZATION POTENTIAL (KV)

of ionization produced in the region of maximum polarization field strength by the more energetic radiation. (The variation of ionization with particle energy was discussed in section A.) The effect is less marked at the higher end of the energy scale since there is very little variation of specific ionization with energy in this region.

The length of the plateaus observed with β^- emitters is never less than 400 volts and may be as much as twice this. The polarization potential at which multiple pulsing sets in, causing an increasing counting rate, is dependent on many factors such as condition of source and temperature of the chamber, and varied somewhat from source to source.

Figure 8 (a) shows a series of characteristics obtained using Ni^{63} (maximum energy 0.067 Mev) taken at increasing discriminator bias values. Figure 9 shows a similar series using La^{140} (maximum energy 2.26 Mev). Plateaus taken at increasing bias values are displaced to higher polarization potential values since increased gas multiplication is necessary to produce pulses larger than the increased bias levels, but the curves are otherwise exactly superposable.

Figure 8 (b) shows a discriminator bias characteristic for Ni^{63} at a polarization potential of 2.6 kv, which is typical of those obtained with this equipment. It demonstrates the usual absence of low amplitude spurious pulses, and shows a constant counting rate up to a bias of at least 30 v, in accordance with the observations of the previous paragraph.

Figure 10 shows characteristics obtained with nuclides decaying by the emission of alpha particles, positrons, negative electrons accompanied by gamma radiation and by isomeric transition. These data

Figure 8 (a)

High Voltage Characteristics for Ni^{63} β^- Radiation

as a Function of Applied Discriminator Bias

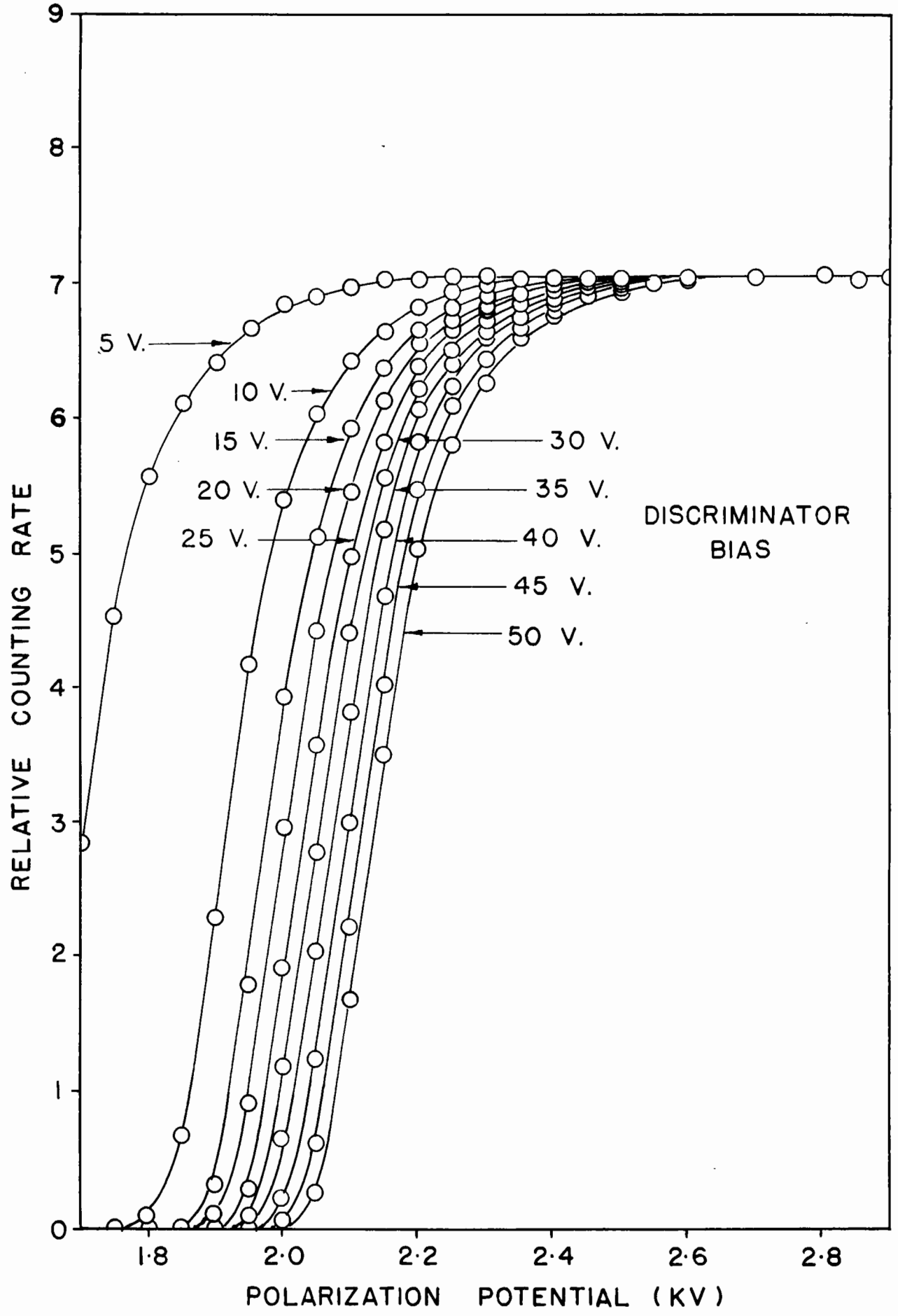
RELATIVE COUNTING RATE
POLARIZATION POTENTIAL (KV)
DISCRIMINATOR BIAS
5 V.
10 V.
15 V.
20 V.
25 V.
30 V.
35 V.
40 V.
45 V.
50 V.
0
1
2
3
4
5
6
7
8
9
1·8
2·0
2·2
2·4
2·6
2·8

Figure 8 (b)

Discriminator Bias Characteristics for Ni^{63}

β^- Radiation at a Polarization Potential of 2.6 kv.

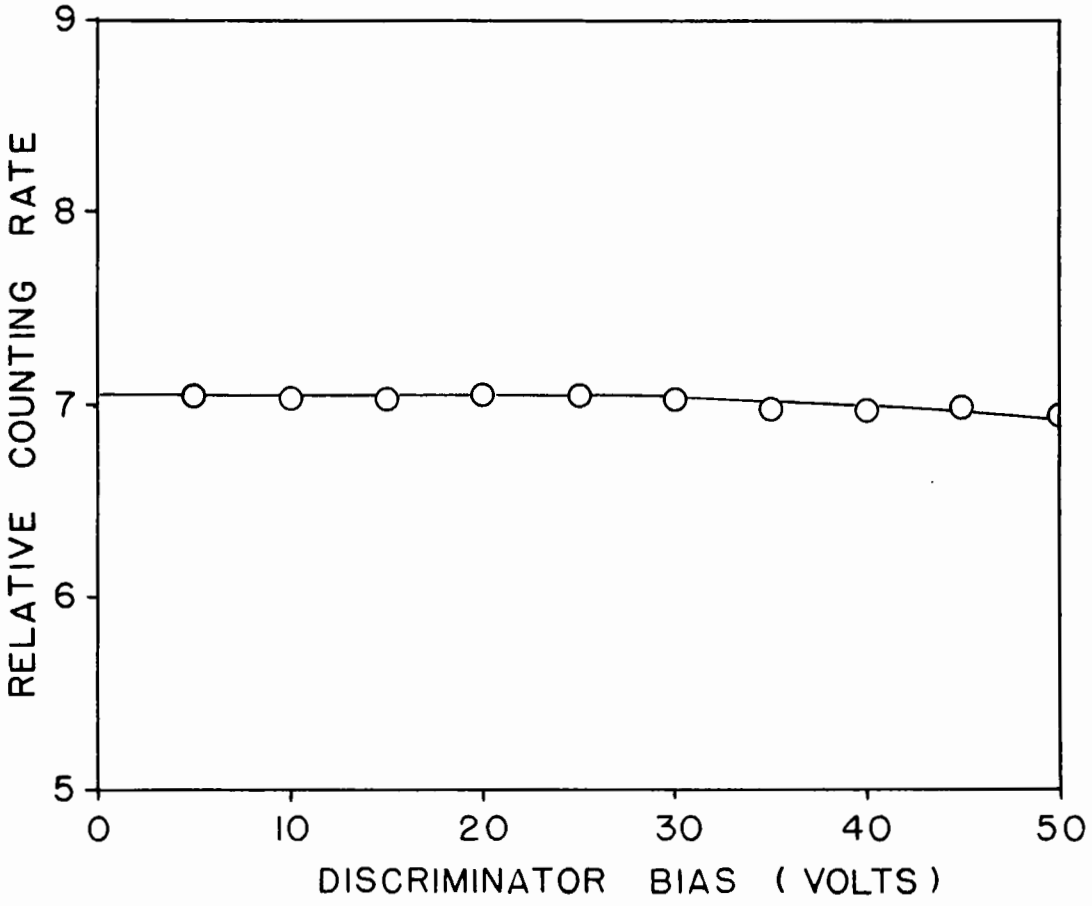
9
8
7
6
5
RELATIVE COUNTING RATE
0
10
20
30
40
50
DISCRIMINATOR BIAS (VOLTS)

Figure 9

High Voltage Characteristics for La^{140} β-radiation

as a Function of Applied Discriminator Bias

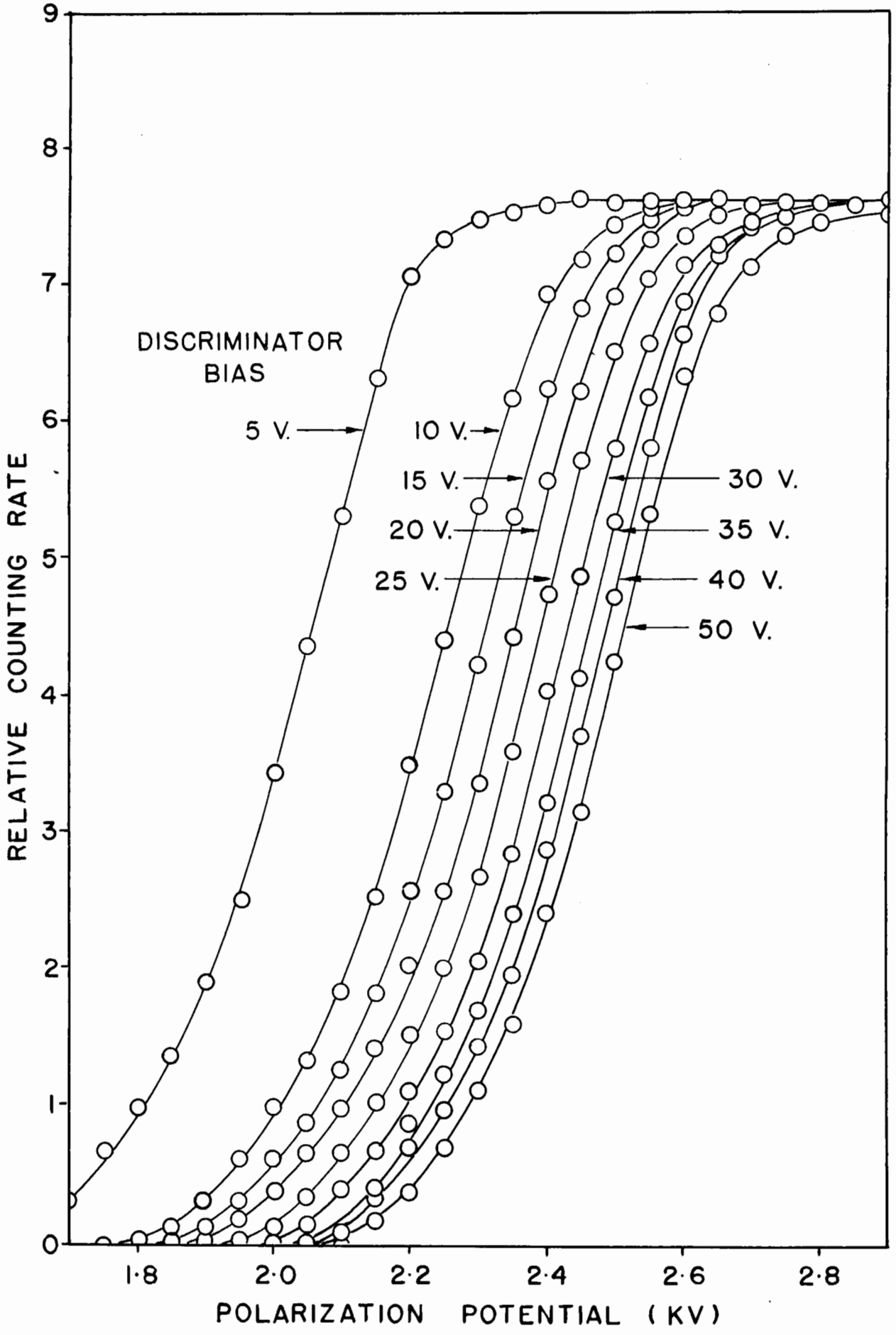
DISCRIMINATOR
BIAS
5 V.
10 V.
15 V.
20 V.
25 V.
30 V.
35 V.
40 V.
50 V.
RELATIVE COUNTING RATE
0
1
2
3
4
5
6
7
8
9
1·8
2·0
2·2
2·4
2·6
2·8
POLARIZATION POTENTIAL (KV)

Figure 10

High Voltage Characteristics for Various Forms of Radiation

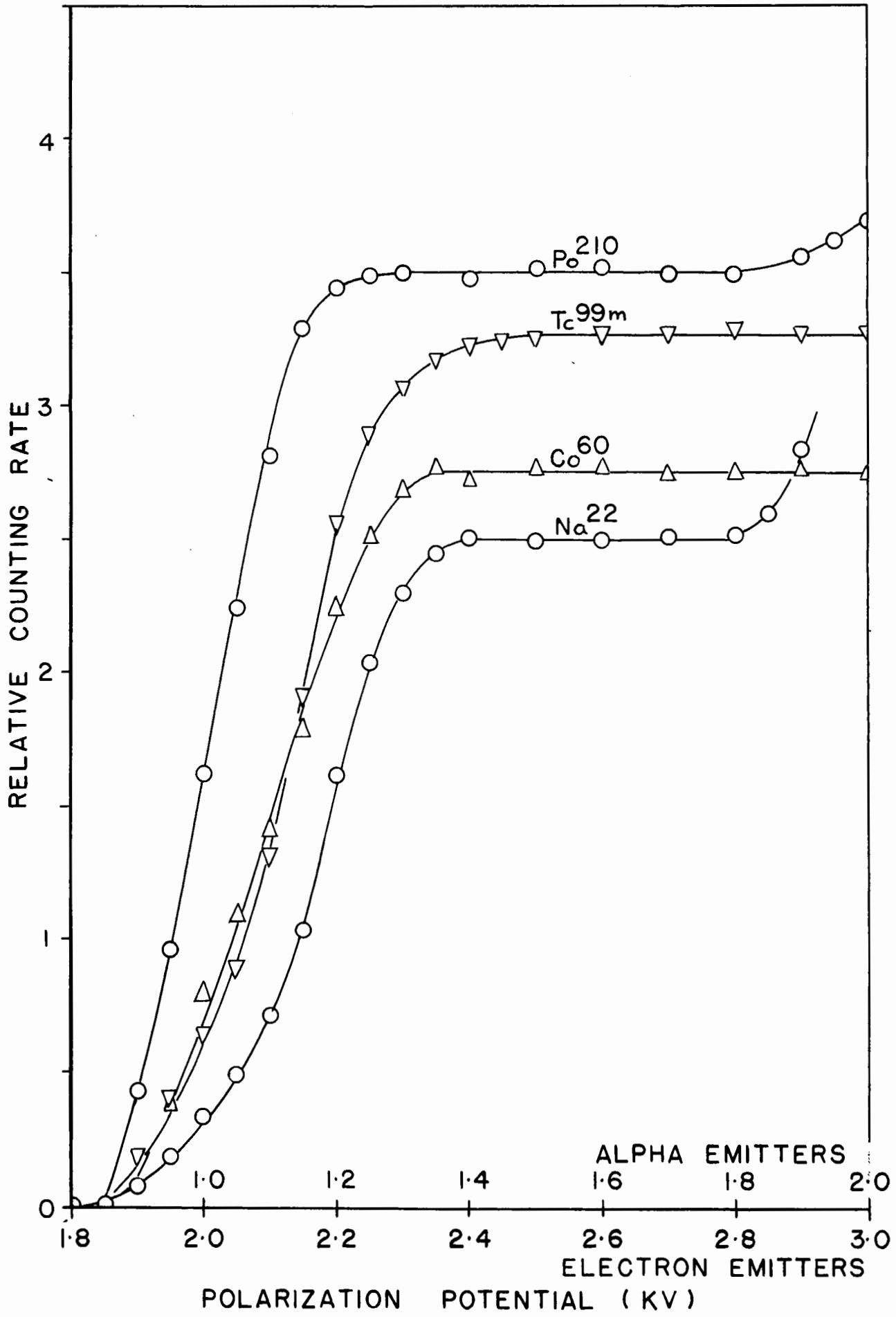
RELATIVE COUNTING RATE
0
1
2
3
4
Po 210
Tc 99m
Co 60
Na 22
ALPHA EMITTERS
1·0
1·2
1·4
1·6
1·8
2·0
1·8
2·0
2·2
2·4
2·6
2·8
3·0
ELECTRON EMITTERS
POLARIZATION POTENTIAL (KV)

indicate that the present chamber makes a satisfactory counter for many forms of radiation. Absolute measurements with α, β^+ and β^- emitting nuclides with or without accompanying γ radiation are clearly straightforward. With nuclides decaying by means of isomeric transition the same is true if the pertinent nuclear data are available.

Figure 11 shows the variation of the characteristic with increasing disintegration rate. A series of P^{32} sources of known strength was prepared on 5-10 $\mu g./cm^2$ films. The disintegration rates (about 500 dis/sec) were below the region where resolution losses were significant. A series of secondary sources was then prepared from these, by lamination, the total disintegration rate being calculated by summing those of the component sources. (It will be shown in the next section that the absorption of radiation from P^{32} even with 10 or more of these component films can be neglected.) The results of measurements of the laminated sources at two values of discriminator bias are shown. The calculated disintegration rate for each source used is shown for comparison purposes.

These results show clearly that satisfactory characteristics are retained at least up to a counting rate of 3×10^3 counts per second. The irregular shape of the curves above this figure, presumably due to a variable resolution loss, show that it is meaningless to quote a resolution loss for a counting system unless this is given for definite polarization conditions.

The observed variation of resolution loss with polarization potential may be due to a variety of reasons. For example, since the

Figure 11

High Voltage Characteristics as a Function of

Disintegration-Rate

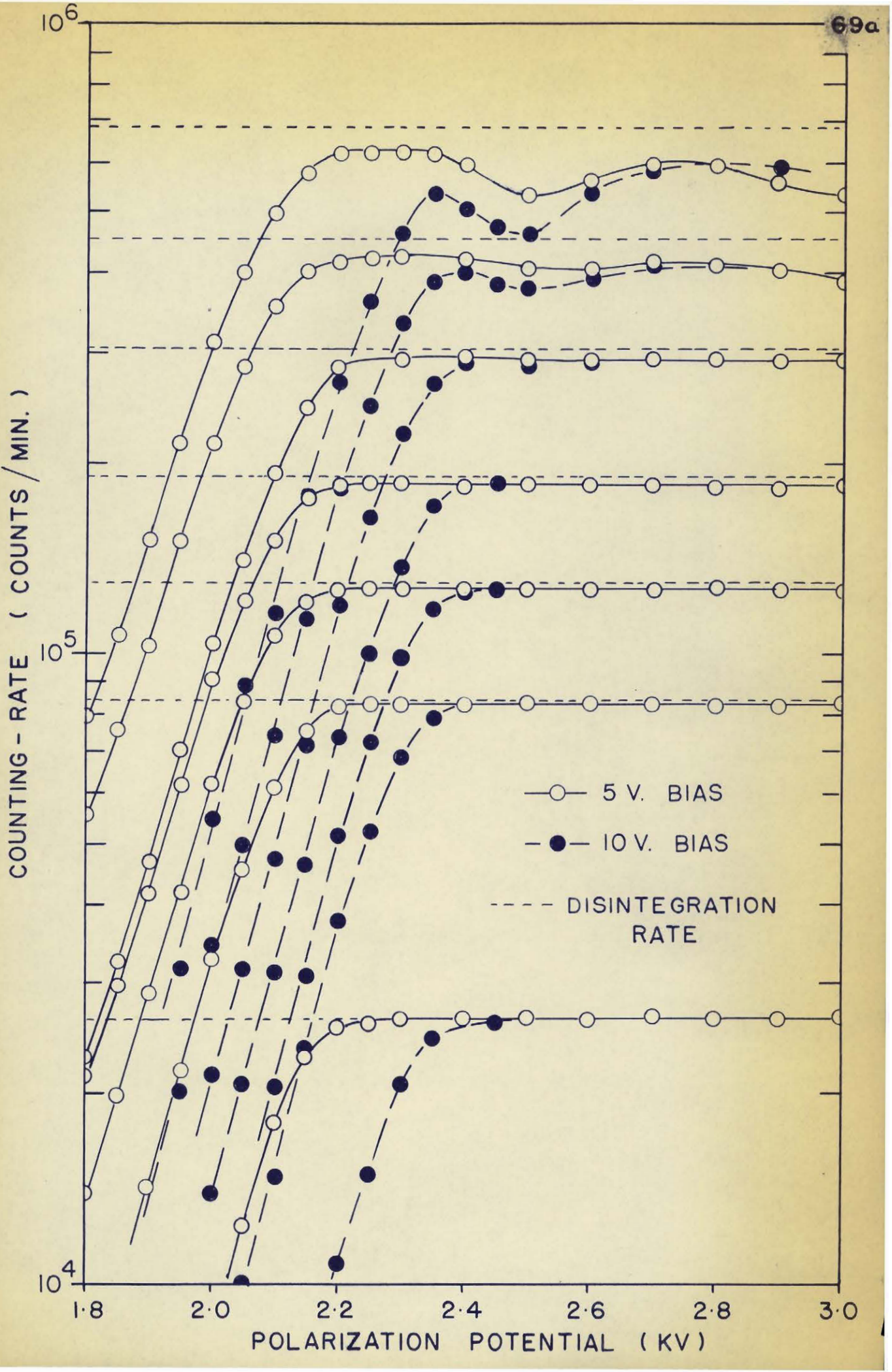
10^6
10^5
10^4
COUNTING - RATE (COUNTS / MIN.)
5 V. BIAS
10 V. BIAS
DISINTEGRATION RATE
1·8
2·0
2·2
2·4
2·6
2·8
3·0
POLARIZATION POTENTIAL (KV)

discharge mechanism results in a local and partial reduction of the polarization field, the counter may enter ito successive discharge processes with the effective counter field at different stages of recovery. Thus the second discharge of a pair occurring within a short time interval may result in a smaller pulse amplitude due to reduced gas multiplication, and hence a pulse which does not register. The reduction of pulse height will however be compensated by an increase in polarization potential. Likewise, the resolution of the electronic equipment for closely spaced pulses of one size corresponding to one polarization potential will be expected to differ from that for another pulse size and potential. This too would be expected to contribute to the observed effect, and resolution losses in the electronic equipment may well be more important than those in the chamber itself.

The Response Probability of the Counter to Very Low Energy Particles

From Figure 7 it is seen that over a wide range of potentials an essentially constant counting rate with Ni^{63} and S^{35} was observed, suggesting that a unit response probability had been obtained. However it was felt desirable to check this.

The ionization produced by very energetic particles is more than adequate to ensure a response probability of unity under normal operating conditions. With low energy particles this is however not so, and a small fraction of any spectrum of β-radiation, ie. that fraction with a very low energy, will not count with unit probability. This fraction increases as the maximum energy of the spectrum decreases. Therefore in order to calculate the response probability to the radiation

of a β-emitter as a whole, it is necessary to allow for this low-energy effect by computing the expected response probability as a function of energy, and integrating the result using the known β-energy distribution.

We have calculated the response probabilities of the counter towards the entire spectrum of the β-radiation of Ni^{63} and S^{35} since these were the softest β-radiations studied. The calculations are conveniently made in three stages. First, the minimum total charge pulse arriving at the counter anode system which will trigger the recording mechanism was calculated from the measured electronic parameters.

	Amplifier Gain	3×10^4	(measured with a calibrated pulse generator and oscilloscope)
	Minimum Bias Level	3 volts	(ie. a pulse greater than this will trigger the scaler circuit)
Hence	Minimum Input	0.1 mv	(calculated from above)
	Capacitance of chamber anode system and amplifier input	25 $\mu\mu f$	(measured by resonance bridge method)

Therefore, the 0.1 mv input signal corresponds to a charge arriving at the anode of 2.5×10^{-15} coulombs or 1.6×10^4 electronic charges, ie. this quanity of charge is the minimum which will trigger the recorder.

The mean gas multiplication was determined in the following way. Using the α particles from Po^{210} the maximum pulse height obtained at the chamber anode system was measured with a cathode ray oscilloscope, care being taken that pulses were not large enough to produce amplifier saturation or distortion of the proportional counter action. The observed pulse amplitude was independent of polarization potential between 250 and 500 volts. Here the chamber is acting as a saturated ion-chamber

and the gas multiplication is unity. Readings, taken at increasing potentials, were normalized to this value. When the danger of saturation or distortion became apparent a Ni^{63} source was substituted for the Po^{210}. A large range existed where both could be used so that no errors were introduced by the substitution.

The results are shown in Figure 12. At 2.6 kv the mean gas multiplication (M) has a value of 2.6×10^3 and at 2.9 kv, of 1.6×10^4. Therefore at these polarization potentials the counter will respond to a mean of 6 and 1 ion pairs respectively.

In Figure 12, we have resolved the experimental curve into two parts (dotted lines) one corresponding to a constant amplitude at the value of unity for the "saturation ion-chamber" region, and another, seen to be approximately exponential, corresponding to the increasing multiplication value. The exponential character of the latter is in accordance to the predictions of Rose and Korff (116) discussed in section A.

Secondly, the probability that a given particle energy will produce a certain minimum number of ion pairs should be calculable if the appropriate data were available. Curran et al. (36) note that the mean energy (W) necessary to produce 1 ion pair increases with particle energy at low energies, but give no quantitative data. They also note that W for both argon and nitrogen (both non-electron acceptors like methane) is substantially independent of energy down to 500 ev. This confirms theoretical predictions made by Fano (43). As a first approximation (adequate for present purposes) one can assume that the value due to Schmeider (127) of $W \sim 30$ ev applies in the region of interest.

Figure 12

Gas Multiplication Function of the Counter

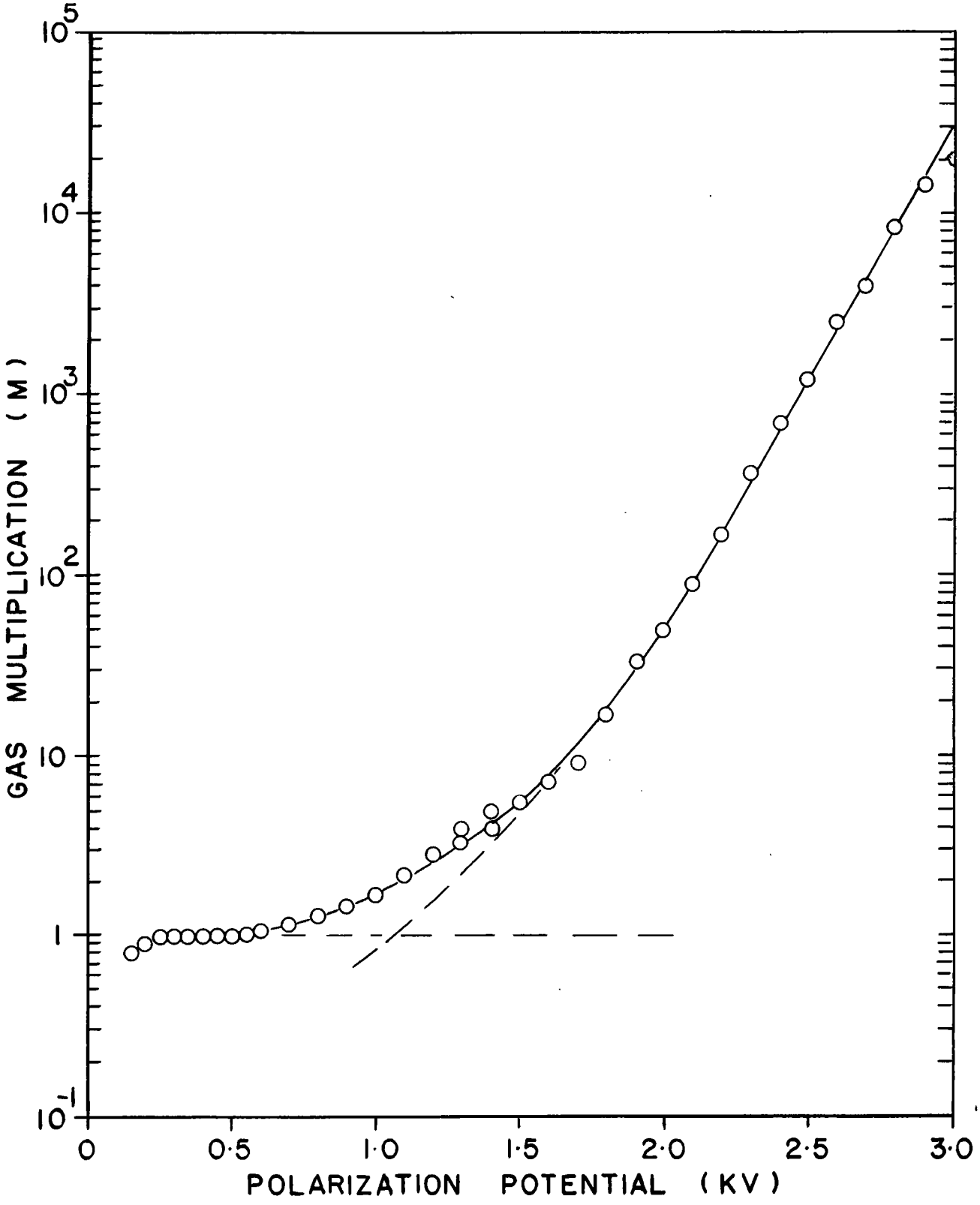
GAS MULTIPLICATION (M)
10^5
10^4
10^3
10^2
10
1
10^{-1}
0
0·5
1·0
1·5
2·0
2·5
3·0
POLARIZATION POTENTIAL (KV)

Both the ionization process and gas multiplication are subject to statistical variation, and it was shown in section A that the total effect observed as a variance on the output pulse amplitude was equivalent to a variance of the original ionization processes corresponding to a Poisson distribution of numbers of ions, about the mean number, n, given by

$$n = \frac{E}{W} \qquad \text{.....see equation 8}$$

On this basis then one may calculate the probability that at least J ion pairs be produced as a function of particle energy. The probability that x ion-pairs be produced under conditions giving a mean value of n is given by

$$p(x) = e^{-n} \cdot \frac{n^x}{x!} \qquad \text{.....(42)}$$

Then the probability of producing 1 or more ion pairs is

$$P_1 = 1 - p(o) = 1 - e^{-n} \qquad \text{.....(43)}$$

and the probability of producing J or more ion pairs is

$$P_J = 1 - \sum_{x=o}^{J-1} p(x) \qquad \text{.....(44)}$$

$$= 1 - e^{-n} \sum_{x=o}^{J-1} \frac{n^x}{x!}$$

$$= 1 - e^{-n} \left(1 + \frac{n}{1!} + \frac{n^2}{2!} + \ldots + \frac{n^{J-1}}{(J-1)!}\right) \qquad \text{.....(45)}$$

The functions corresponding to equation 45 are shown in Figure 13. Since a minimum of one ion pair will trigger the counter at a polarization potential of 2.9 kv, the curve for J = 1 represents the counter response probability function under this condition. Similarly, the curve for J = 6 gives the response probability at 2.6 kv. Clearly, at low E values these calculations are in error, but certainly show

Figure 13

Counter Response Probability as a Function of Electron Energy When it is Responding to a Minimum Ionization of 1 and 6 Ion Pairs

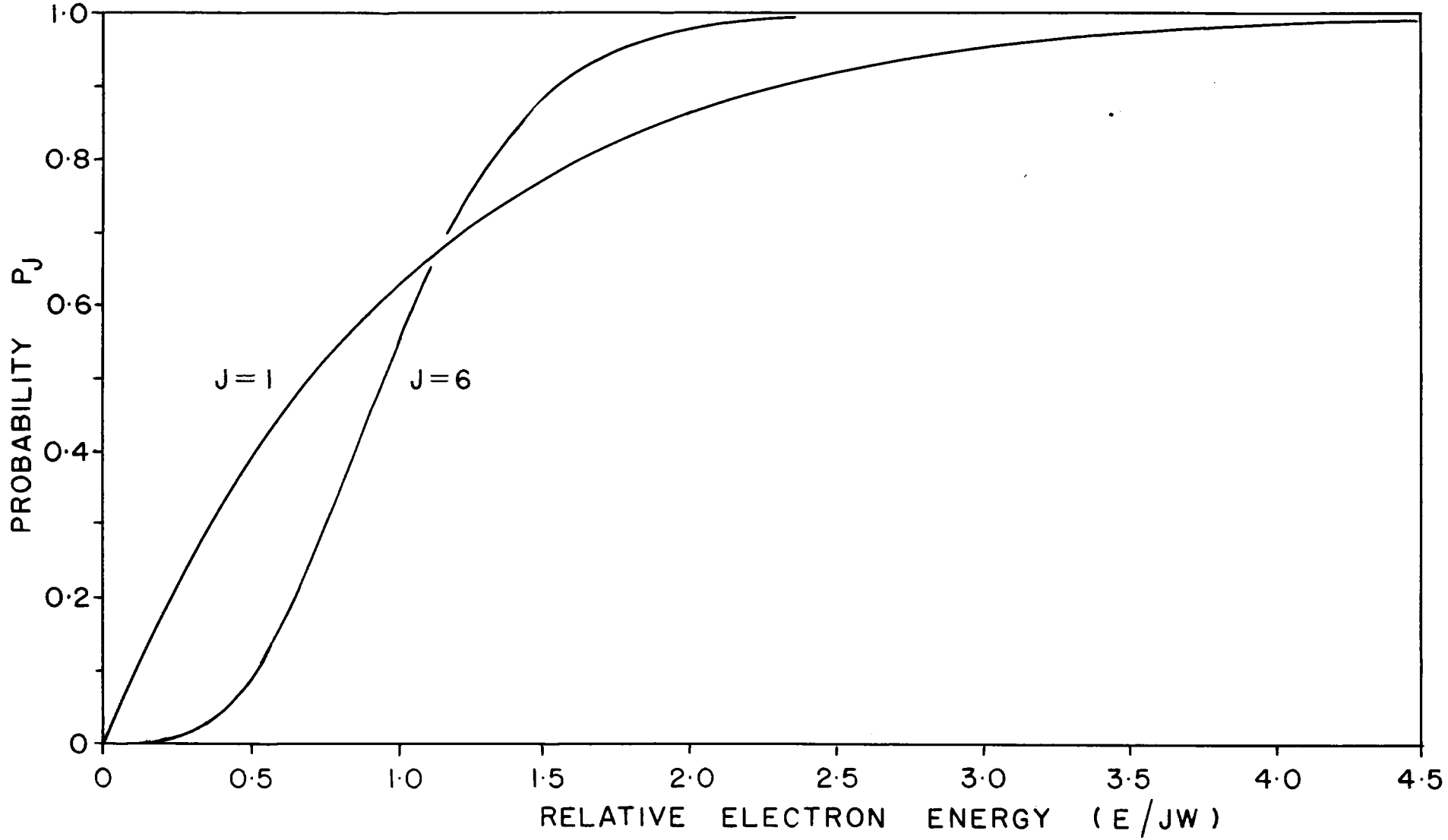
1·0
0·8
0·6
0·4
0·2
0
PROBABILITY P_J
J = 1
J = 6
0
0·5
1·0
1·5
2·0
2·5
3·0
3·5
4·0
4·5
RELATIVE ELECTRON ENERGY (E/JW)

at worst an order of magnitude for P at these energies.

Thirdly, from the probability curves of Figure 13 it is now possible to obtain a total response probability for a radiation of any known energy distribution. We have calculated the values for Ni^{63} and S^{35} at applied potentials of 2.6 and 2.9 kv. The relevant probability function has been integrated using the energy spectra for these two nuclides shown in Figures 59 and 60, which were calculated by the methods outlined in section E, from the data of Kobayashi et al. (82) for Ni^{63} and Langer et al. (90) for S^{35}.

(The data for Ni^{63} was presented (82) as a Kurie plot, assuming the transition to be first forbidden $-\Delta J = 2$, yes - and we have adopted the same assumption to obtain the original momentum data and thus the β-energy spectrum. The S^{35} spectrum corresponds to an allowed transition.)

The results of these calculations are shown in Table II.

TABLE II

Counter Response Probability

Nuclide	Polarization Potential (kv)	Mean Number of Ion Pairs Detected	Probability
Ni^{63}	2.6	6	0.9953
Ni^{63}	2.9	1	0.9992
S^{35}	2.6	6	0.9998
S^{35}	2.9	1	0.9999

Due to the low energy of the emitted radiation, Ni^{63} and S^{35} are the two nuclides of those we have studied which are most likely to have a low response probability. The response probability in the two cases is seen to be very close to unity. This conclusion is also, of course, corroborated by the observations recorded in Figure 7. The counting rates obtained with all energies remained essentially unchanged even when for example in the case of S^{35}, the applied potential was increased from 2.4 to 3.2 kv, corresponding to a change in the gas multiplication by a factor of about 160.

(ii) Response Probability as a Function of Source Position

We have examined the variation of response probability of the counter for sources of radiation as a function of their location in the source mount plane in a manner essentially similar to that employed by Hawkings et al. (68) for P^{32}, using β^--emitters of varying energy from 0.067 Mev to 2.26 Mev at various polarization potentials and bias voltages.

The source was mounted on a small area of 5-10 $\mu g./cm^2$ film supported over an aperture of 5 mm. diameter in a slide of aluminum foil. The slide was arranged to move between two parallel wires so that the source could be adjusted to any position along a diameter of the source mounting diaphragm. This movement, combined with the rotation of the diaphragm allowed the source to be brought to any point within the plane of the source mount. The whole was screened electrostatically from the electrode system by being sandwiched between two gold-coated 10 $\mu g./cm^2$ films. Attenuation of the β-radiation by absorption in the small layer of gas trapped between the films could be neglected for

purposes of this experiment. The counting rate was observed with the source in 90 different positions, each at two values of polarization potential and two discriminator bias settings. Typical contours of equal response probability are shown in Figures 14 and 15.

The contours are essentially similar to those obtained by Hawkings et al. (66) for P^{32}. The area over which the response probability is unity for a particular applied voltage and bias level can be seen to be smaller for Ni^{63} than for La^{140}, because of the reduced range of the weaker radiation in the counter gas. The curves show an expansion of the contours with increasing polarization and decreasing bias voltage, corresponding to the expected variation of response probability under these conditions.

From these data it is clear that a source diameter of up to at least 1 cm. can be tolerated by the counter for all particle energies studied without a significant drop in response probability.

It will be seen from Figure 5 that the counting chamber is constructed in such a manner that both hemispheres are recessed to accommodate an aluminum source-mount diaphragm. This allowed us to investigate the variation of response probability when a source of S^{35} was moved 1 mm. from the medial position towards each anode. (The source-mounting film is customarily affixed to one side of the aluminum diaphragm, and the source material deposited on the side of the film away from the diaphragm.) The results as shown in Table III, show that a displacement of at least 1 mm. in either direction (the maximum allowed by the counter design) may occur without adversely affecting the counting rate.

Figure 14

Contours of Equal Response Probability for Ni^{63} β-radiation

(a) at 2.6 kv, 5 v discriminator bias

(b) at 2.6 kv, 30 v discriminator bias

(c) at 3.0 kv, 30 v discriminator bias

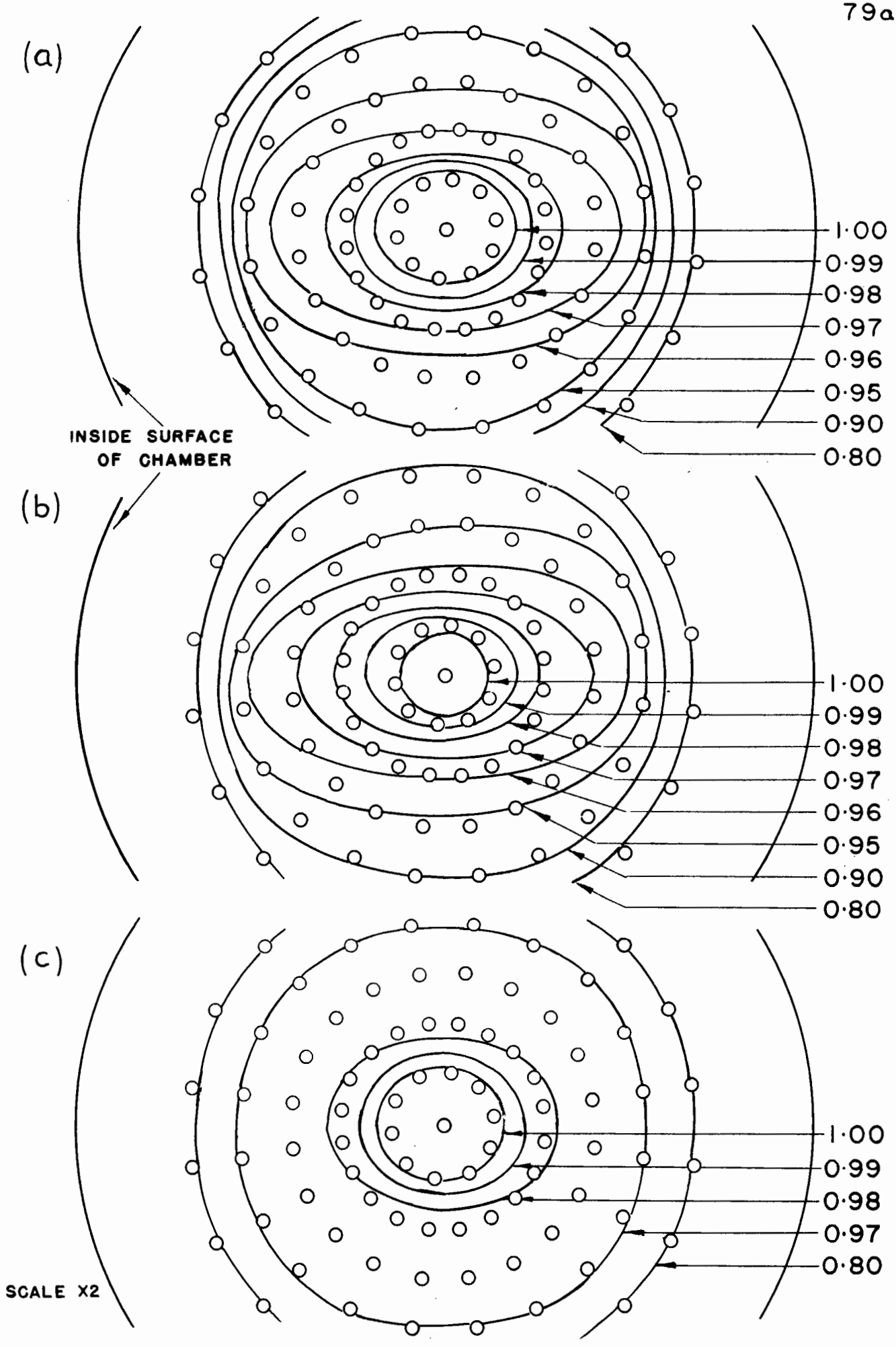
(a)
INSIDE SURFACE
OF CHAMBER
1·00
0·99
0·98
0·97
0·96
0·95
0·90
0·80
(b)
1·00
0·99
0·98
0·97
0·96
0·95
0·90
0·80
(c)
1·00
0·99
0·98
0·97
0·80
SCALE X2

Figure 15

Contours of Equal Response Probability for La^{140} β-radiation

(a) at 2.6 kv, 5 v discriminator bias

(b) at 2.6 kv, 30 v discriminator bias

(c) at 3.0 kv, 30 v discriminator bias

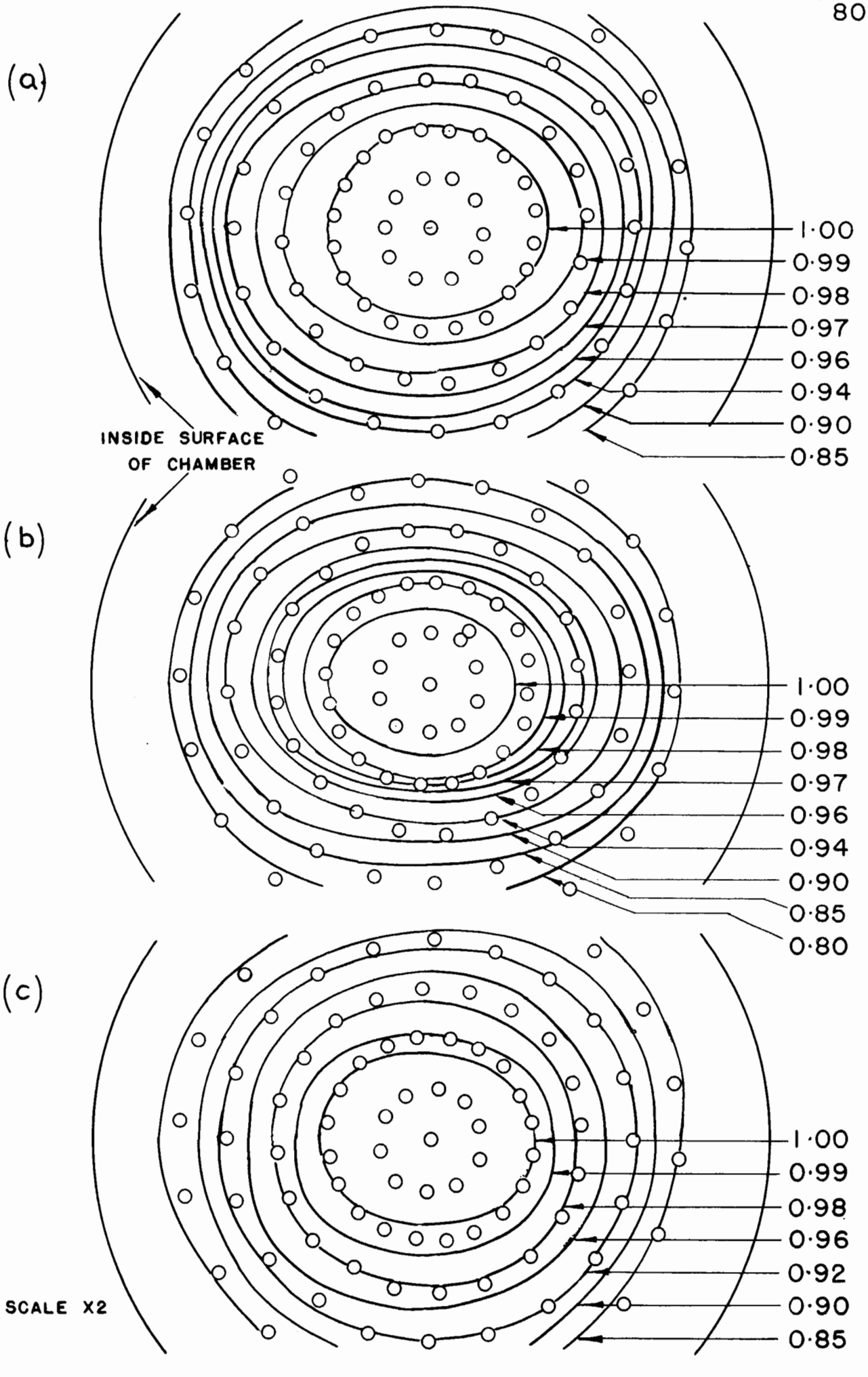
(a)
1·00
0·99
0·98
0·97
0·96
0·94
0·90
0·85
INSIDE SURFACE
OF CHAMBER
(b)
1·00
0·99
0·98
0·97
0·96
0·94
0·90
0·85
0·80
(c)
1·00
0·99
0·98
0·96
0·92
0·90
0·85
SCALE X2

TABLE III

Effect on Response Probability of Vertical Source Displacement

Position	Observed Counting Rate (counts/min.)
Source central facing upwards	39,070 ± 140
Source displaced 1 mm. towards top anode facing upwards	39,170 ± 140
Source central facing downwards	39,240 ± 140
Source displaced 1 mm. towards bottom anode, facing downwards	39,280 ± 140

(iii) Effect of Variation of Gold Thickness of Source Mount Films

The effect on counter response probability of variation of gold thickness on films has been investigated in two sets of experiments, one each for Ni^{63} and P^{32} radiation. Sets of VYNS films (all of 5-10 $\mu g./cm^2$ superficial density and mounted over diaphragm apertures of 5 cms. diameter) were coated on one side with a range of gold thicknesses. The superficial density of gold applied was measured spectrophotometrically as described in section C. For each film, a source was applied centrally to the side of the film on which the gold had been deposited. The high voltage characteristic at a constant discriminator bias setting obtained with this arrangement was recorded. A diaphragm with aperture diameter of 2.5 cms. was then placed over the first, forming effectively a system in which a film with the same gold superficial density was mounted over a smaller aperture. The characteristic curve was again determined. The film, on the original diaphragm, was then removed from the counter and 10 $\mu g./cm^2$ gold dis-

tilled on to it. In one-half of the experiments the gold was applied to the side of the film carrying the source and in the other half to the reverse side. The voltage characteristic was again determined. Finally, a further 10 $\mu g./cm^2$ of gold was applied, this time to the opposite side to the above (both sides now had at least 10 $\mu g./cm^2$ of gold) and a fourth characteristic was measured.

The results of the effect of gold thickness are as follows:

1. In all cases the last two characteristics were identical. Identical voltage characteristics were obtained regardless whether the gold was on the source side, reverse side or both sides. Representative characteristic curves are shown in Figure 16.

2. The appearance of the characteristics obtained with increasing thickness of gold is shown in Figure 17 for Ni^{63} and Figure 18 for P^{32}. In order to render the data comparable, the counting rates are expressed as a fraction of that found for the source after application of 10 $\mu g./cm^2$ of gold to the source mount. The figures plotted apply to a diaphragm aperture of 5 cms. The smaller aperture of 2.5 cms. had the effect of displacing the characteristic for a given gold thickness to a higher polarization potential. However, the gold thickness at which normal characteristics occurred (> 2 $\mu g./cm^2$) was the same for both aperture sizes.

(iv) Effect of Purity of Counting Gas

The effect of using a counter gas of inferior quality is shown in Figure 19 (a). This shows a series of characteristics using Ni^{63} as the radioactive source and Technical Grade methane as the counting gas. The mass spectrometric analysis of a sample of C.P. methane,

Figure 16

High Voltage Characteristics as a Function of the Side of Source Mount to which Gold is Applied

(a) 5 μg./cm^2 of gold on source side - Ni^{63}

(b) 5 μg./cm^2 of gold on reverse side - Ni^{63}

(c) 5 μg./cm^2 of gold on source side - P^{32}

(d) 5 μg./cm^2 of gold on reverse side - P^{32}

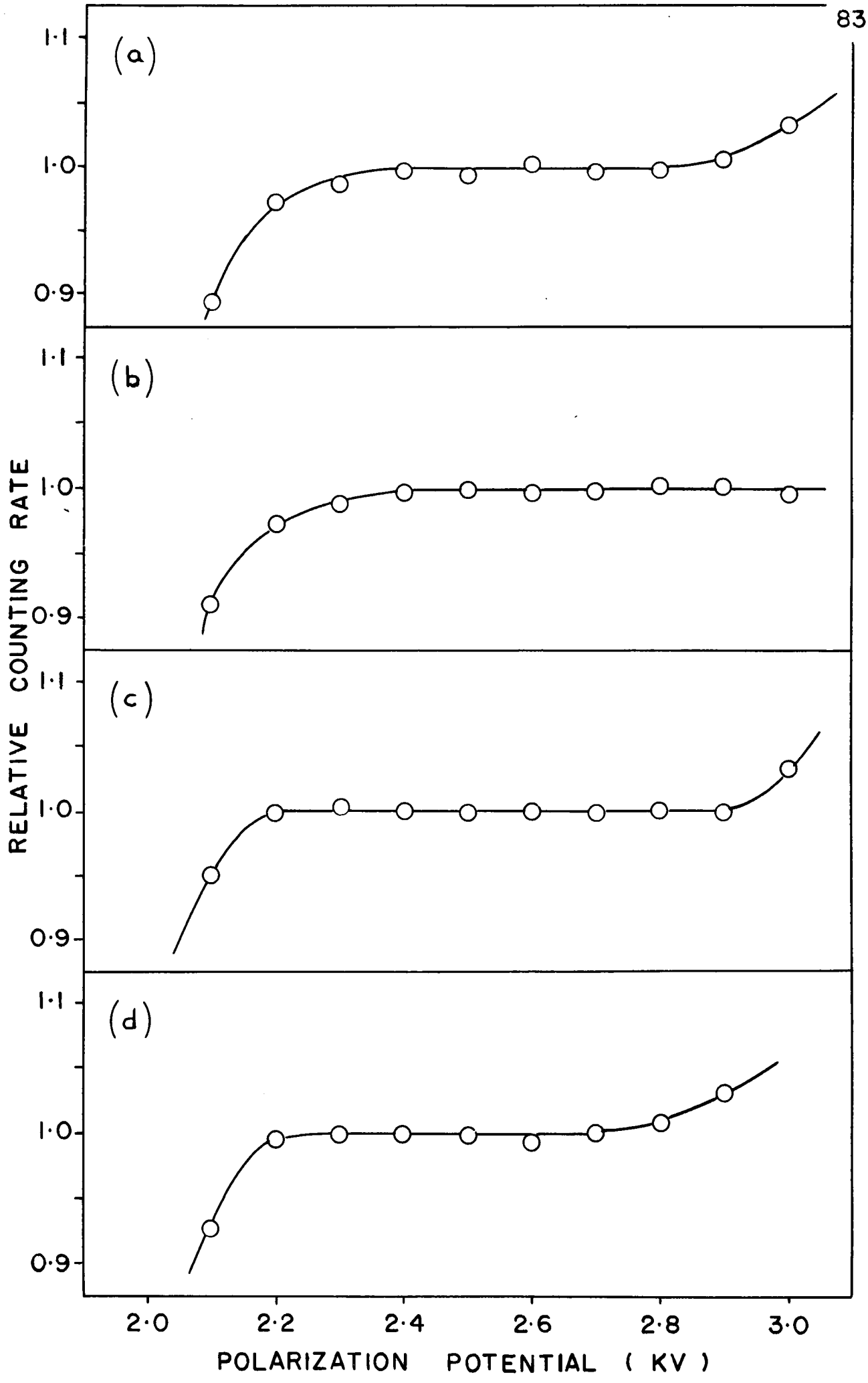
(a)
(b)
(c)
(d)
1·1
1·0
0·9
RELATIVE COUNTING RATE
2·0
2·2
2·4
2·6
2·8
3·0
POLARIZATION POTENTIAL (KV)

Figure 17

High Voltage Characteristics for Ni^{63} as a Function of Gold Thickness on Source Mount

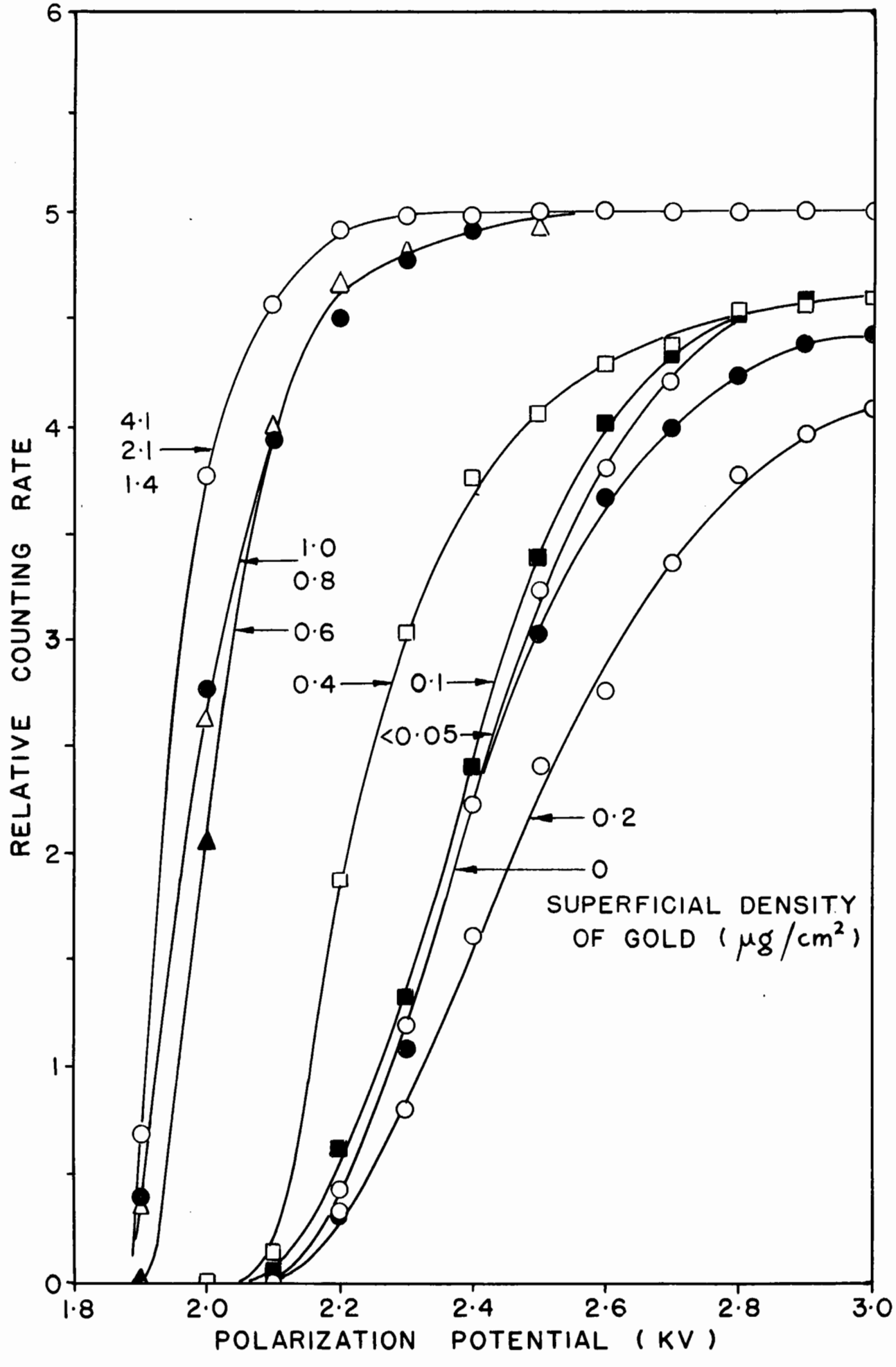
RELATIVE COUNTING RATE
POLARIZATION POTENTIAL (KV)
SUPERFICIAL DENSITY OF GOLD (μg/cm²)
4·1
2·1
1·4
1·0
0·8
0·6
0·4
0·1
<0·05
0·2
0
0
1
2
3
4
5
6
1·8
2·0
2·2
2·4
2·6
2·8
3·0

Figure 18

High Voltage Characteristics for P^{32} as a Function of Gold Thickness on Source Mount

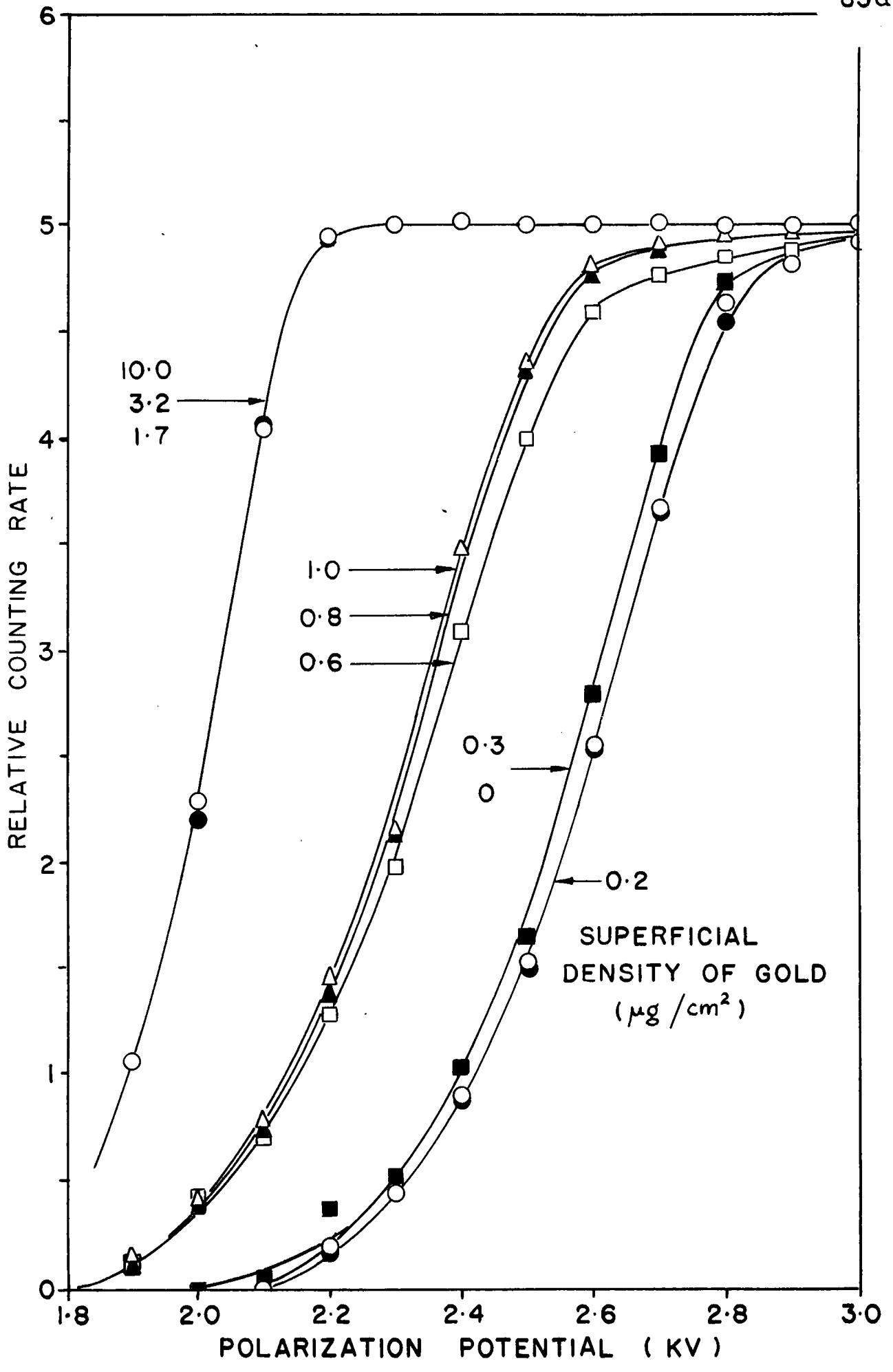
RELATIVE COUNTING RATE
POLARIZATION POTENTIAL (KV)
SUPERFICIAL DENSITY OF GOLD (μg /cm²)
10·0
3·2
1·7
1·0
0·8
0·6
0·3
0
0·2
0
1
2
3
4
5
6
1·8
2·0
2·2
2·4
2·6
2·8
3·0

Figure 19 (a)

High Voltage Characteristics Obtained with Impure Methane for Ni^{63} β-radiation

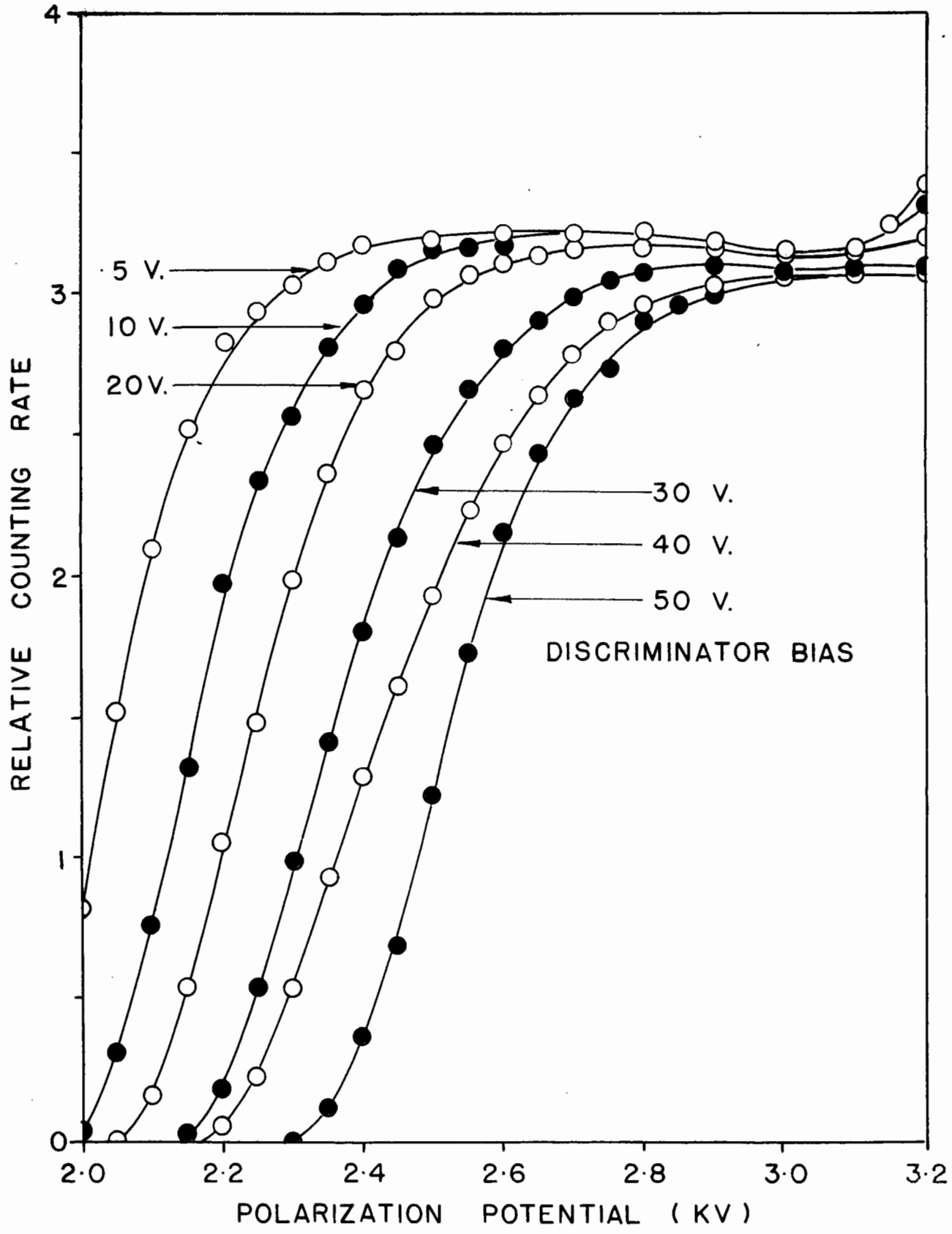
4
3
2
1
0
RELATIVE COUNTING RATE
5 V.
10 V.
20V.
30 V.
40 V.
50 V.
DISCRIMINATOR BIAS
2·0
2·2
2·4
2·6
2·8
3·0
3·2
POLARIZATION POTENTIAL (KV)

giving normal performance, is shown in Table IV. We do not give an analysis for Technical Grade methane as this varies from one cylinder to another. (The variation is so great that occasionally a cylinder of Technical Grade methane has been found to give satisfactory results.)

TABLE IV

Mass-Spectrometric Anaylis of C.P. Methane *

Constituent	Concentration (percent by weight)
H_2	0.1
C_2H_4	0.01
C_2H_6	0.59
N_2	0.5
O_2	0.01
CO_2	0.15
C_3, C_4	0.01
CH_4	Remainder

Experiments performed with synthetically prepared gas mixtures showed that the counter was relatively insensitive to the presence of higher saturated and unsaturated hydrocarbons in the gas mixtures. The presence of small quantities of air or oxygen however, is injurious, possibly due to the electron affinity of the latter.

---

* The author is indebted to Professor H. I. Schiff of this department for this analysis.

This latter effect is also demonstrated in the "flushing-curves" of Figure 19 (b). These show the increase of counting-rate with time (measured from the time of insertion of the source, RaD-E-F, and closing of the chamber) for a series of counting gas flow-rates. The counting-rates do not reach a constant value, indicative of normal operation, until essentially all the air has been flushed out of the chamber. We have used these curves to determine the period of time which must be allowed for complete counter flushing, before measurements can be made.

(b) "Counter Geometry"

Experimental techniques for determining the effect of a reduction of diaphragm aperture diameter on the counter characteristics are described in section (iii) of (a).

Characteristics for Ni^{63} and P^{32} are shown in Figure 20 for both large and small diaphragm apertures. The gold thicknesses used in this experiment were greater than the limit at which regular behavior commenced.

Several workers (68, 95, 100) have discussed the effect of using a relatively thick metal diaphragm in order to support the source-mounting film or foil. Calculations have been made of the fraction of particles emitted which will be "lost" due to collision with the diaphragm aperture walls. Experiments have also been performed at a single value of the polarization potential to determine the effect of reduction of aperture size.

Figure 20 shows clearly that no decrease in counter response occurs when the diaphragm aperture diameter is decreased from 5.0 to

Figure 19 (b)

Effect of Incomplete Counter Flushing.

Counting-rate as a Function of Time for a Series of Counting Gas Flow-rates, with a RaD-E-F source.

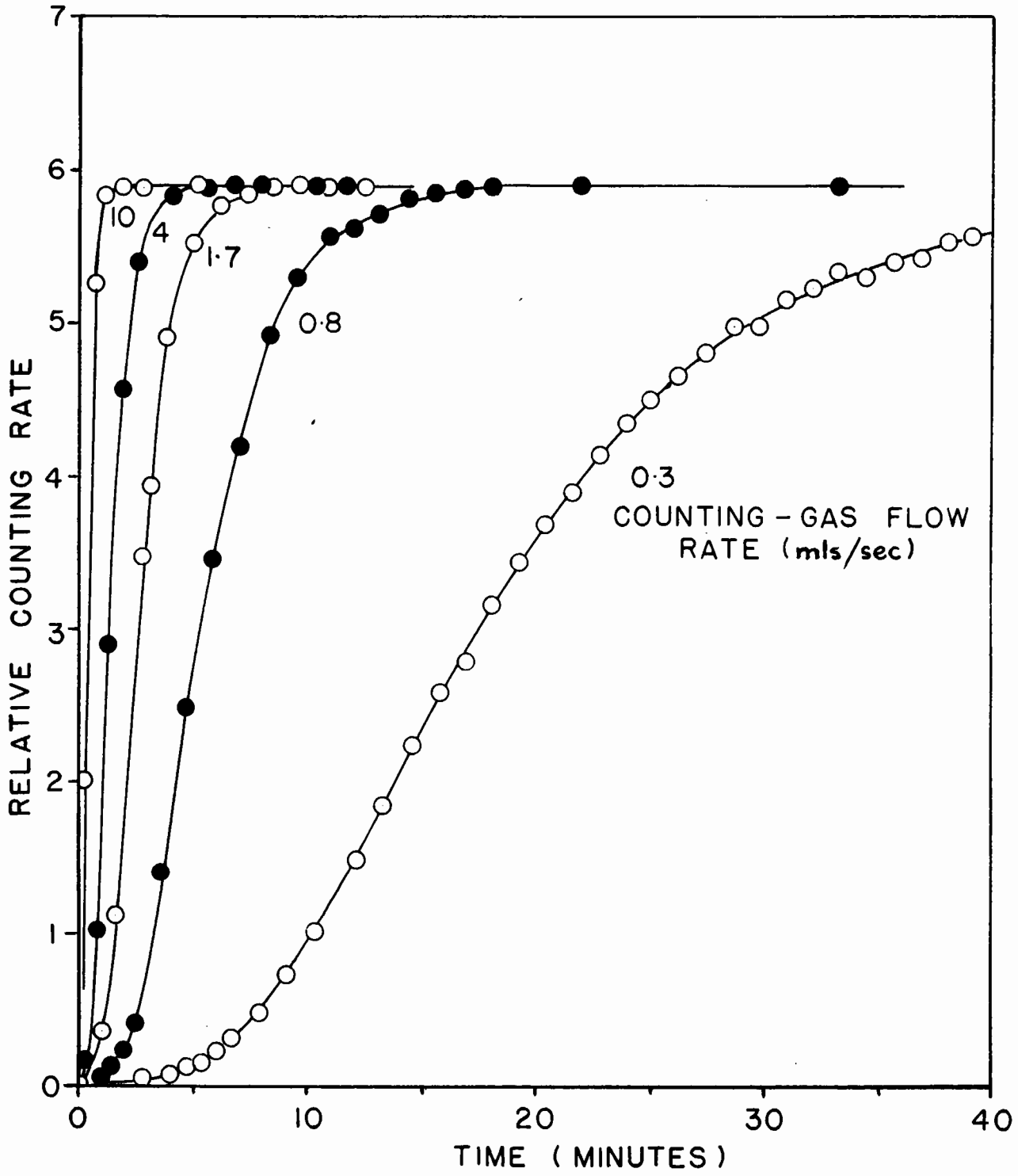
RELATIVE COUNTING RATE
TIME (MINUTES)
10
4
1·7
0·8
0·3
COUNTING - GAS FLOW RATE (mls/sec)
0
1
2
3
4
5
6
7
0
10
20
30
40

Figure 20

High Voltage Characteristics Obtained with Varying Size of Diaphragm Aperture

(a) 2.5 cm. diameter Ni^{63}

(b) 5.0 cm. diameter Ni^{63}

(c) 2.5 cm. diameter P^{32}

(d) 5.0 cm. diameter P^{32}

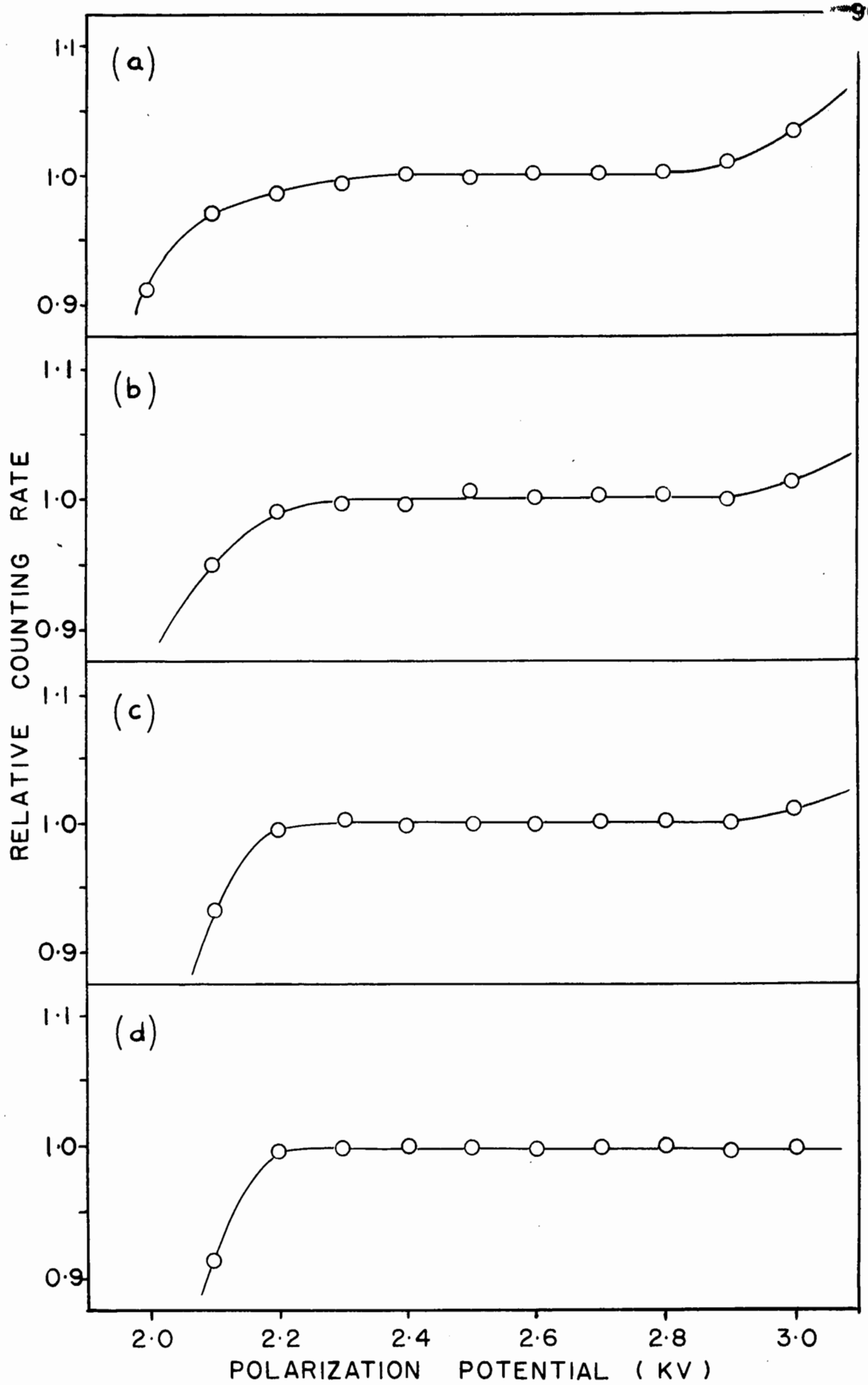
(a)
(b)
(c)
(d)
1·1
1·0
0·9
RELATIVE COUNTING RATE
2·0
2·2
2·4
2·6
2·8
3·0
POLARIZATION POTENTIAL (KV)

2.5 cms. Provided that a particle produces the necessary minimum number of ions before being absorbed in the aperture wall, it will be registered. As the polarization potential is increased, the probability of this minimum number being produced approaches unity. Thus, the effect of a reduced aperture size is to displace the polarization characteristic to higher polarization potentials and does not reduce the effective counter geometry from 4π steradians.

(c) Response Probability at Higher Counting Rates

The resolution loss function of the present counting system has been determined using the method previously described to examine the effect of disintegration rate on the characteristic curve of the counter. A series of 12 sources of P^{32} with disintegration rates ranging between 3×10^2 and 10^4 dis./sec. was prepared and the counting rates of the single and laminated sources obtained. The results, expressed as "resolution loss" as a function of the observed counting rate, are shown in Figure 21 plotted with logarithmic coordinates. Some points for the curve were also obtained by studying the departure from exponential decay of a source of Na^{24}.

The results obtained in Figure 21 clearly illustrate the loss in counting rate of this counter assembly with increasing disintegration rate. The presentation of the data on a "log-log" plot results in a curve which is linear and thus facilitates extrapolation to lower counting rates. This correction curve can be used with confidence for our arrangement up to an apparent counting rate of 2×10^5 counts/min. As can be seen from Figure 11, up to that point the correction is essentially

Figure 21

Resolution Loss Function of the Counter at 2.6 kv

High Voltage and 15 volts Discriminator Bias

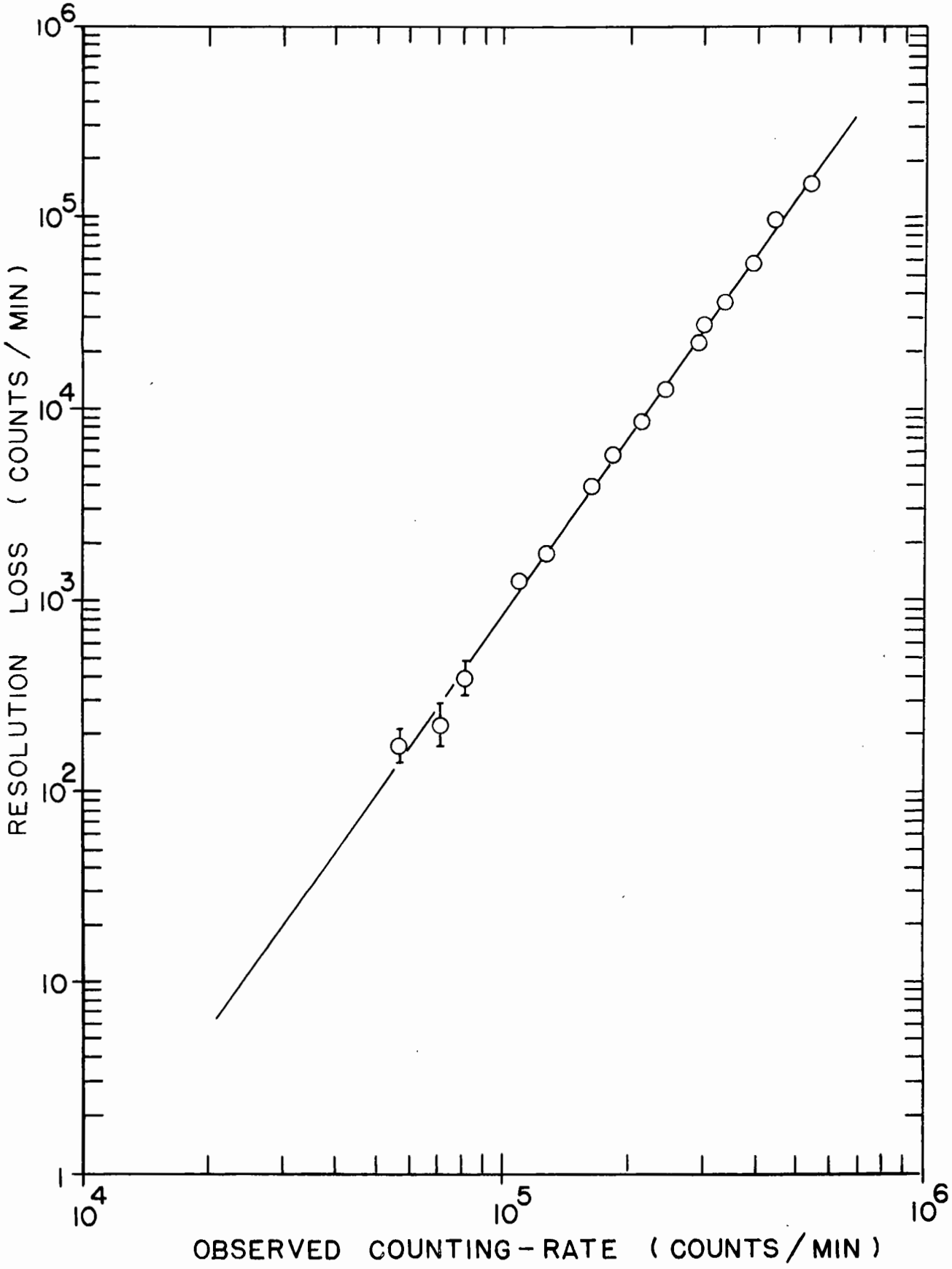
RESOLUTION LOSS (COUNTS / MIN)
10^6
10^5
10^4
10^3
10^2
10
1
10^4
10^5
10^6
OBSERVED COUNTING-RATE (COUNTS / MIN)

independent of polarization potential and discriminator bias. It should be noted that the slope of the curve in Figure 21 corresponds very nearly to a cubic relationship between counting rate and resolution loss. This is quite at variance with the standard dead time correction formulae discussed in section A, (equations 23 and 24), which were derived assuming a constant "dead-time" and suggests that the resolution losses in the electronic circuitry may well be playing a more important part in our case than is assumed in the simple G-M counter system.

4) CONCLUSIONS

On the basis of the experimental work discussed in this section, it is concluded that the error in disintegration-rate determination due to the departure of the response probability of a 4π-counter from a value of unity may be reduced to less than 0.1 percent. For our apparatus, the conditions under which this is realized are the following:

Source mounting film of 5-10 $\mu g./cm^2$ of VYNS resin mounted over a diaphragm aperture of 2.5 or 5.0 cms. diameter and coated with at least 2 $\mu g./cm^2$ of gold.

Counting gas C.P. methane.

Polarization potential 2.6 kv

Discriminator bias 15 volts.

The absence of perceptible slope on the plateaus of the high voltage characteristics of the chamber when functioning correctly allows a considerable latitude in the conditions under which the system may be satisfactorily operated. It further allows a rapid verification

that the system is so operating. If an increase of 200 volts in the polarization potential or 10 volts decrease in the discriminator bias causes no change in counting rate observed, then a response probability close to a value of unity is indicated.

C. THE FABRICATION AND CALIBRATION OF VERY THIN FILMS: ABSORPTION OF RADIATION BY THE SOURCE-MOUNT

1) INTRODUCTION

The second source of error in disintegration rate determination by 4π-counting to be considered is due to absorption of radiation, which would otherwise trigger the lower half-counter, in the foil or film used to support the source. We shall show that this error can be reduced to a figure of the same order of magnitude as the error considered in section B, both being substantially less for a given radiation energy than the error at present arising from self-absorption effects, considered in section C.

In this section we shall consider this source-mount absorption effect purely as it affects the correction of observed counting measurements in the calculation of disintegration-rates. Later in section E, we shall analyse the data in more detail, and relate the magnitude of the observed effects to the combined influence of the several absorption and scattering processes.

In the present investigation, we shall again adopt a two-fold approach. Firstly, we attempt to reduce the magnitude of the error arising from source-mount absorption as far as is practical by the use of films of very low superficial density, made from synthetic resin of low average atomic number. However a limit is set to the extent to which the thickness of these films can be reduced by the requirement of adequate mechanical film strength for the intended purpose. Secondly, therefore, it is necessary to develop a method of determining the extent

of absorption of radiation in the film which still occurs, to the accuracy required. We shall discuss these topics separately.

2) THE FABRICATION AND THICKNESS CALIBRATION OF VERY THIN FILMS

(a) Introduction

There exists a pressing need for very thin films of low $\overline{Z}$ material, strong enough to act as source-mounts, not only in 4π-counting but also in beta-spectrometry and allied fields. The techniques to be described have been successful in the fabrication of films of material of $\overline{Z} = 5.1$, of good chemical and mechanical stability, of superficial densities down to below 1 $\mu g./cm^2$ (thickness < 7 $m\mu$) and of area up to 100 cm^2.

Materials used for the production of source-mounts for the purposes of 4π-counting or beta-spectrometry must satisfy a number of criteria. They must be of:

(a) minimal superficial density and low average atomic number, in order to reduce absorption and scattering of radiation:

(b) adequate mechanical strength to withstand shocks received during normal, careful handling and the pipetting out of radioactive solutions:

(c) adequate chemical resistance to reagents present during the rapid evaporation of these solutions, eg. under infrared irradiation:

(d) adequate thermal resistance to withstand infrared irradiation during this evaporation procedure and during metallizing procedures if these are required (see later).

The use of a number of materials has been reported in the literature. Aluminum foil has been used (28, 29, 30, 31, 140, 142)

in superficial densities as low as 260 $\mu g./cm^2$ (135). Such foils will however be very weak mechanically, and in addition aluminum does not exhibit very good chemical resistance to acids or alkalies. Certain synthetic resins have been found to lend themselves to the fabrication of thin films suitable for source mounts and have been used extensively with conventional low-geometry counters and in beta-spectrometry where back-scattering effects were to be minimized (33, 108). Formvar (33, 54, 148),a polyvinylformal, has excellent mechanical properties, being strong and resistant to abrasion (52, 125, 126). A method (8) to produce films of less than 10 $\mu g./cm^2$ superficial density by means of very specialized handling techniques has recently been described. Unfortunately Formvar is readily attacked by acids, concentrated alkalies, and organic solvents. It has however found application in laminates with films of polystyrene or Zapon (52, 68, 95) which possess better chemical properties, but are alone too fragile.

Cellulose nitrate (5, 76, 100) and acetate (135) are probably the most successful of the materials used up to this time. They are resistant to hydrochloric acid in all concentrations, oxidizing acids in concentrations up to 12 N, and dilute alkalies. They are attacked however by concentrated alkalies, and other substances, eg. an aqueous slurry of a metallic sulphide. Films of these materials with a superficial density of as low as 3 $\mu g./cm^2$ have been reported. However these are of small area, and it is found that films of less than 40 $\mu g./cm^2$ do not make satisfactory mounts owing to increasing fragility which impedes their manufacture, handling, and use during pipetting operations.

When it is desired to work with source-mounting films of

5-10 $\mu g./cm^2$, therefore, it is clear that a material with much better characteristics is required. We propose the use of VYNS resin* (a polyvinylchloride-acetate copolymer). Films of this material can be made with superficial densities below 1 $\mu g./cm^2$. These show remarkable tensile strength, and excellent chemical resistance to acids and alkalies in all concentrations and to most organic solvents. The only common chemicals found to attack the films are ketonic compounds and esters which act as solvents for the resin. These properties, together with resistance to all but the severest of shocks, make VYNS resin an ideal material for source mounts.

(b) Procedures

(i) Film Production

VYNS resin as supplied by the manufacturers is a finely ground white powder. The most convenient solvent is found to be cyclohexanone, one volume of resin requiring about two volumes of solvent for complete dissolution. First addition of solvent to the resin produces a gel, which dissolves in further solvent only slowly in the course of several days. The process can however be accelerated somewhat by maintaining the mixture at 50-60°C for several hours. The saturated solution thus obtained forms a convenient stock solution. This is diluted with further cyclohexanone before use to give a one-third saturated solution.

---

* This material is a product of the Bakelite Co. N.Y., available in Canada through Canadian Resins and Chemicals Ltd., Montreal. The author is indebted to Mr. I. Maclaine of Dominion Oilcloth and Linoleum Ltd. for introduction to this material, and to Mr. F. M. King of Canadian Resins and Chemicals Ltd. for a supply of the resin for experimental purposes.

VYNS in cyclohexanone does not spread satisfactorily on a water surface, and dilution with a second solvent produces on evaporation very weak and uneven films. The conventional techniques for film formation are therefore not applicable, and a new method has had to be developed. This is found to produce films whose constancy of thickness is better than previously obtainable, and possesses the additional merit of improving the tensile strength of the thinner films, possibly by orientation of polymer molecules.

The procedure used is as follows. A trough or sink is filled with water at room temperature and a floating wooden barrier placed in contact with one end. One to two milliliters of resin solution are pipetted between the barrier and the trough, so as to wet both the side of the trough and the barrier; the latter is released and the resin solution allowed to expand into a band about 2-3 cm. wide, the outer edge (nearest the barrier) of which immediately begins to solidify. The barrier is lifted from the water, lowered lightly on to the solidified film, and then moved away along the water surface at a speed of about 30-40 cm. per second. During this process a film of resin is observed to feed out of the solution band, and continues to do so covering the water surface, until either the barrier reaches the far end of the trough, or the band of solution is exhausted. The thickness of film produced is governed by the speed at which the barrier is pulled out, the thinnest films being obtained with the highest speeds. The evenness of the film in one direction is conditioned by the evenness of the original pipetting operation, and in the other by the constancy of barrier velocity. Success in operation of this procedure is largely

a matter of manual dexterity, which can easily be obtained.

The film produced is quite dry and may be lifted from the water surface for use immediately. The lifting may be accomplished by the use of wire frames (coated with VYNS to give better film adhesion) which allow larger areas of film to be obtained, eg. up to 40 cm. x 20 cm. of 10-20 $\mu g./cm^2$ film. The film may then be transferred to other supports which have previously been wetted with water. Alternatively, the supports, in our apparatus aluminum annuli of area 40 cm^2, may be used to pick up the film directly, 30 or 40 rings being covered in one operation. In either case the support or frame is lowered to contact the upper surface of the film, the latter torn away at the edges, and the film lifted with a rolling motion, one edge separating first. This procedure often gives a film completely free of water droplets. Any that may be left can be cautiously pulled to the edge of the film with a wisp of absorbent material. An alternative procedure, useful for the thinnest films, is to sink the film and support carefully and to bring them out through the water surface at right angles, reducing the effect of surface tension forces. Marks remaining after evaporation of water droplets left by this procedure may be avoided by dipping the film on edge below the surface of some distilled water. VYNS is hydrophobic, and films produced by this method, once any adhering water is removed, are quite dry and ready for use. No appreciable change in weight is observed over long periods of time, either with plain films or after metallizing (see later).

This simple technique as described is suitable for the production of uniform films of up to 20 $\mu g./cm^2$ superficial density.

Films of greater thicknesses are conveniently produced by lamination, two films placed in contact adhering readily; laminates of greater than 100 $\mu g./cm^2$ and quite even in thickness have been made in this way. Alternatively, one can use a mechanical means of ensuring constant barrier speed to produce the thicker films. The manual method does not operate too satisfactorily in this region.

It is standard procedure in this laboratory to store films on edge. This arrangement renders the stock of films less liable to damage by vibration, and further allows a large number of films to be stored in a small space.

Electron micrographs[*] of a plain VYNS film at a magnification of 10^4 reveal no evidence of structure in the film. (see Figure 22 (a).) However if the film is shadowed with gold applied by distillation (see later) at an angle of 20° to the surface, a series of surface ridges becomes visible (Figure 22 (b)), presumably running in the direction in which the film was pulled out.

(ii) Measurement of Film Superficial Density

Optical Reflection Method

As is well known, thin films are often observed to be brilliantly colored by reflected light, owing to the occurrence of interference and

---

[*] The author is indebted to Dr. A. W. Tickner of the Applied Chemistry Group, National Research Council, Ottawa, Ont. for the opportunity of using this group's electron-microscope facilities, both for these pictures, and those that follow.

Figure 22

Electron Micrographs (x 10^4)

(a) Plain VYNS film, 10 $\mu g/cm^2$, without shadowing

(b) VYNS film, 10 $\mu g/cm^2$, shadowed with Gold

(a)

(b)

reinforcement between the light reflected from the top and bottom surfaces of the film. The conditions for reinforcement and destructive interference for light of wave length λ are given by:

$$\text{reinforcement:} \quad (n + \tfrac{1}{2})\lambda = 2\mu d \cos \theta \qquad .....(46)$$

$$\text{destruction:} \quad n\lambda = 2\mu d \cos \theta \qquad .....(47)$$

where μ is the film refractive index (for VYNS = 1.5), d is the film thickness, θ is the angle of reflection, and n is an integer. The wave lengths for which interference is expected for various VYNS film thicknesses with normally incident light, together with the color actually observed, are listed in Table V. The effects observed below 10 $\mu g./cm^2$ are due to a falling off in reflectivity of the film.

TABLE V

Superficial density of film ($\mu g./cm^2$)	Film Thickness ($m\mu$)	Wave length for reinforcement calculated ($m\mu$)	Wave length for destructive interference calculated ($m\mu$)	Color Observed
1	7	(14)	(21)	Dark gray
5	36	(72)	(108)	Light gray
10	70	(140)	(210)	White
20	140	280	420	Light yellow
25	180	360	540	Yellow-brown
30	210	420	630	Purple) First
35	250	500	750	Blue) order
40	290	580	870	Yellow) spectrum
45	320	640	960	Red) (n = 1)
50 and above	360 and above	-	-	Second order and above (n ≥ 2). Colors of diminishing intensity

We have used these color differences, as observed visually, for the rough sorting of films of differing thicknesses, and especially for the selection of areas of film of the desired thickness and evenness for lifting from the water surface. It is clear that this could be made into a precision method, if desired, by use of a spectrophotometer with a reflection attachment.

Gravimetric Method

A five decimal place analytical balance is capable of measuring the superficial density of 40 cm^2 (for our apparatus) of 5 $\mu g./cm^2$ film with an accuracy of 5 percent. This gives a very useful, absolute means of superficial density standardization. We have used films specially selected for their uniformity and calibrated gravimetrically to standardize other methods of determination. As a routine method, however, weighing has certain disadvantages:

(i) Measurements to the required accuracy are very tedious and time-consuming.

(ii) The superficial density measured is an average for the whole film, not for the region of interest (the centre). This method is not therefore applicable to films with peripheral irregularities which are nevertheless quite suitable for source mounts.

(iii) Finally the mounting of a film on a weighed support is not easily accomplished without a concomitant change in support weight, and measurements are subject to random errors far in excess of those imposed by the sensitivity limit of the balance used.

Beta Radiation Absorption Method

Figure 23 shows as a function of their superficial density the transmission of VYNS films for the beta radiation of Ni^{63} (which has a maximum energy of 67 Kev). Providing the radiation measurements can be made to the necessary precision, the method is limited by the accuracy of the superficial density values of the films used for calibration. We estimate that measurements can be made to 2 $\mu g./cm^2$ in the range 0-30 $\mu g./cm^2$, and with a somewhat larger error at greater thicknesses. The actual form of the curves obtained depends a great deal on the radiation scattering and other characteristics of the apparatus used, but the details of procedure as used by us are as follows.

A Ni^{63} source of about 2×10^3 dis./sec. is deposited in a depression at the centre of an aluminum plate, and the whole is covered with a VYNS film of about 50 $\mu g./cm^2$ to give a completely planar surface. This is then mounted in a conventional hemispherical 2π-proportional counter, and the counting rate measured to the required accuracy. Curves of transmission versus superficial density are then obtained, using specially selected gravimetrically calibrated films which are placed in contact with the plate. Advantages of the method include insensitivity to peripheral film irregularities - the superficial density measured is that observed by a source centrally located on the film used for a source mount - and a rapidity of operation much greater than for the gravimetric method. Disadvantages include the tendency for films of less than 10 $\mu g./cm^2$ to adhere to the plate and subsequently to rupture (which can to some extent be ameliorated by a light dusting

Figure 23

Transmission of VYNS film to Ni^{63} Beta Radiation

(a) Film superficial density range 0-30 $\mu g./cm^2$

(b) Film superficial density range 0-600 $\mu g./cm^2$

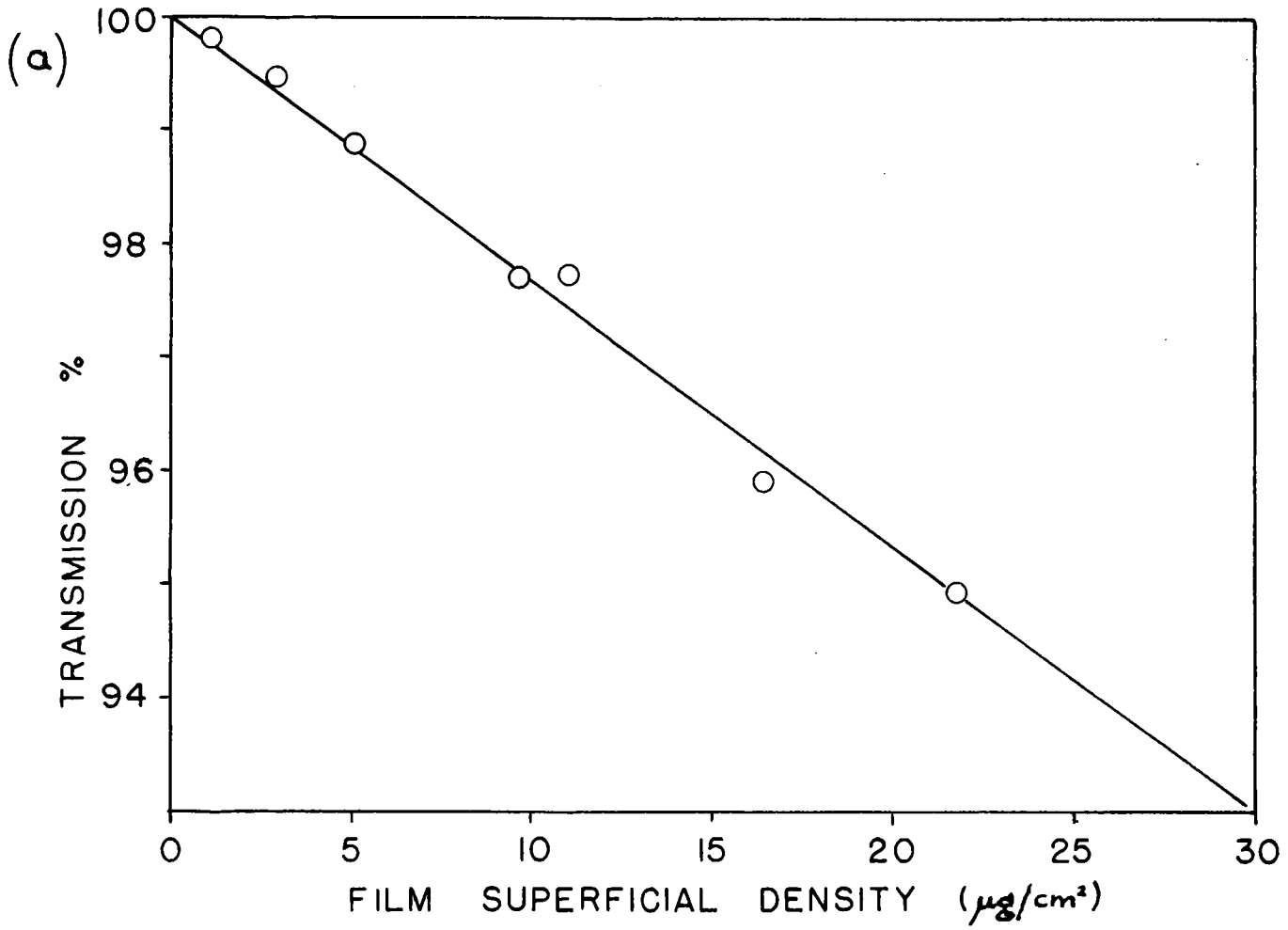
(a)
100
98
96
94
TRANSMISSION %
0
5
10
15
20
25
30
FILM SUPERFICIAL DENSITY (μg/cm²)

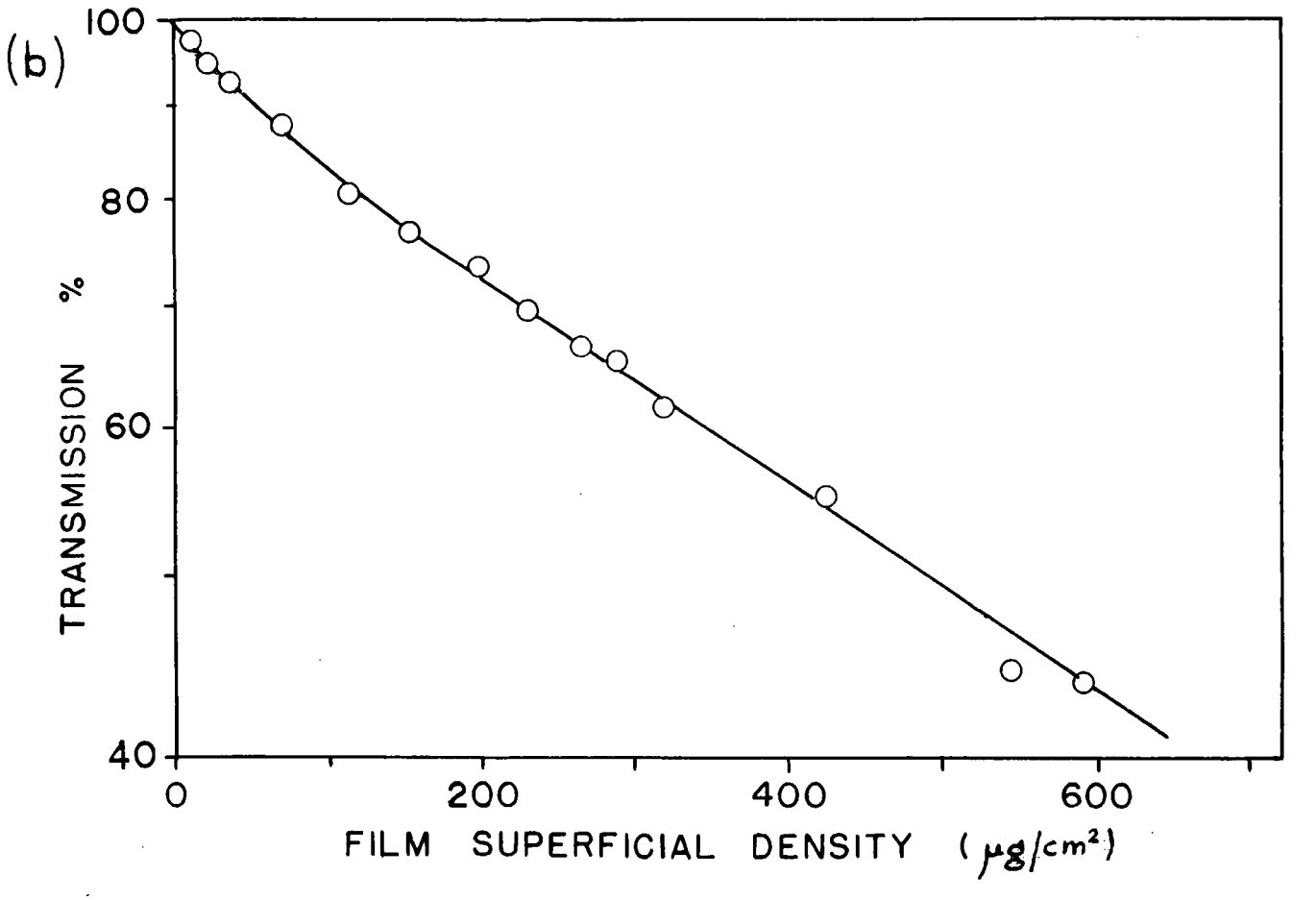
(b)
100
80
60
40
TRANSMISSION %
0
200
400
600
FILM SUPERFICIAL DENSITY (μg/cm²)

of talc away from the central part of the film), the need for ensuring close contact between the film and plate (since a layer of methane counting-gas entrapped between them can cause considerable error in the apparent film thickness), and the need for electronic counting apparatus, etc.

Optical Absorption Method*

This method is now in routine use in this laboratory, and proves quite satisfactory for the measurement of superficial densities in the range 0-30 $\mu g./cm^2$. We employ a Beckman Model DU Spectrophotometer, which is first balanced against air, and then used to measure the optical transmission at a wave length of 360, 600 or 1300 $m\mu$ according to the thickness range and accuracy required.

These wavelengths were chosen as a result of determination of the optical absorption spectra of a series of films of increasing thickness. These spectra are shown in Figure 24. The curves obtained exhibit periodic oscillations of transmission with increasing wavelength, the number of oscillations observed in a given wavelength interval increasing with increasing film thickness. This effect is presumably due to an interference phenomenon.

The curves of transmission versus superficial density at the three chosen wavelengths, calibrated with selected weighed films, are

---

* The author wishes to thank Mr. W. L. Elsdon of Dr. C. A. Winkler's laboratory for valuable discussions on the spectrophotometric measurement of thin films.

Figure 24

Optical Transmission Spectrum of VYNS film, at

Increasing Superficial Density

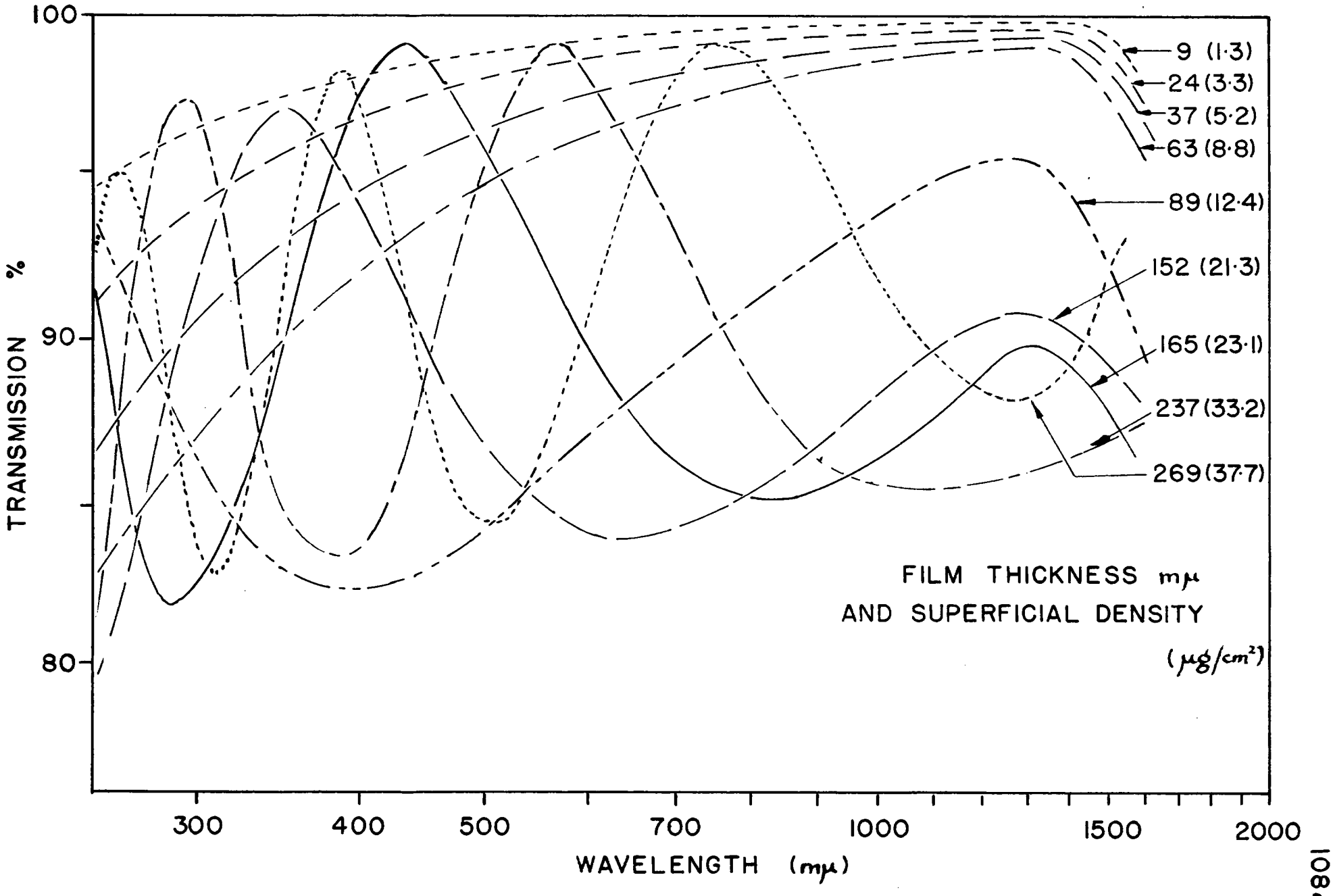
100
90
80
TRANSMISSION %
9 (1·3)
24 (3·3)
37 (5·2)
63 (8·8)
89 (12·4)
152 (21·3)
165 (23·1)
237 (33·2)
269 (37·7)
FILM THICKNESS mμ
AND SUPERFICIAL DENSITY
(μg/cm²)
300
400
500
700
1000
1500
2000
WAVELENGTH (mμ)

1084

shown in Figure 25.

The potential precision of the method is about 0.05 $\mu g./cm^2$, but calibration difficulties impose at the moment a limit of $\pm$ 0.5 $\mu g./cm^2$, which is nevertheless adequate for the present purposes. The method is found to be very rapid and facile in operation, and is applicable to the thinnest films since they need not be placed in contact with anything. It also measures the thickness of the centre of the film, and is useful in measuring small irregularities of superficial density in this area.

(iii) Gold Coating

The plastic film used for mounting a source within a 4π-counting chamber (or for beta-spectrometry) must be conducting in order that the counter shall function correctly. (see Section A) Films may be rendered conducting by a suitable coating, either of Aqua-dag (88, 108) or of metal applied by sputtering or distillation in vacuo. The use of aluminum (135), copper (76, 100), silver (3), and gold (20, 68) has been reported. We find gold coating of one side of the film by distillation from a tungsten ribbon filament at about 1200°C. and under < 1 μ Hg to be satisfactory.

Low distillation rates of gold give approximately isotropic distribution of metal, and several films may be coated simultaneously if arranged spherically around the filament.

The progress of distillation may be followed by observing the color of the film by reflected light from the reverse face to that being coated. With an initially uncolored film of 5-10 $\mu g./cm^2$ for example, a faint purple coloration is first noticed at a superficial

Figure 25

Optical Transmission of VYNS Film as a Function of Superficial Density

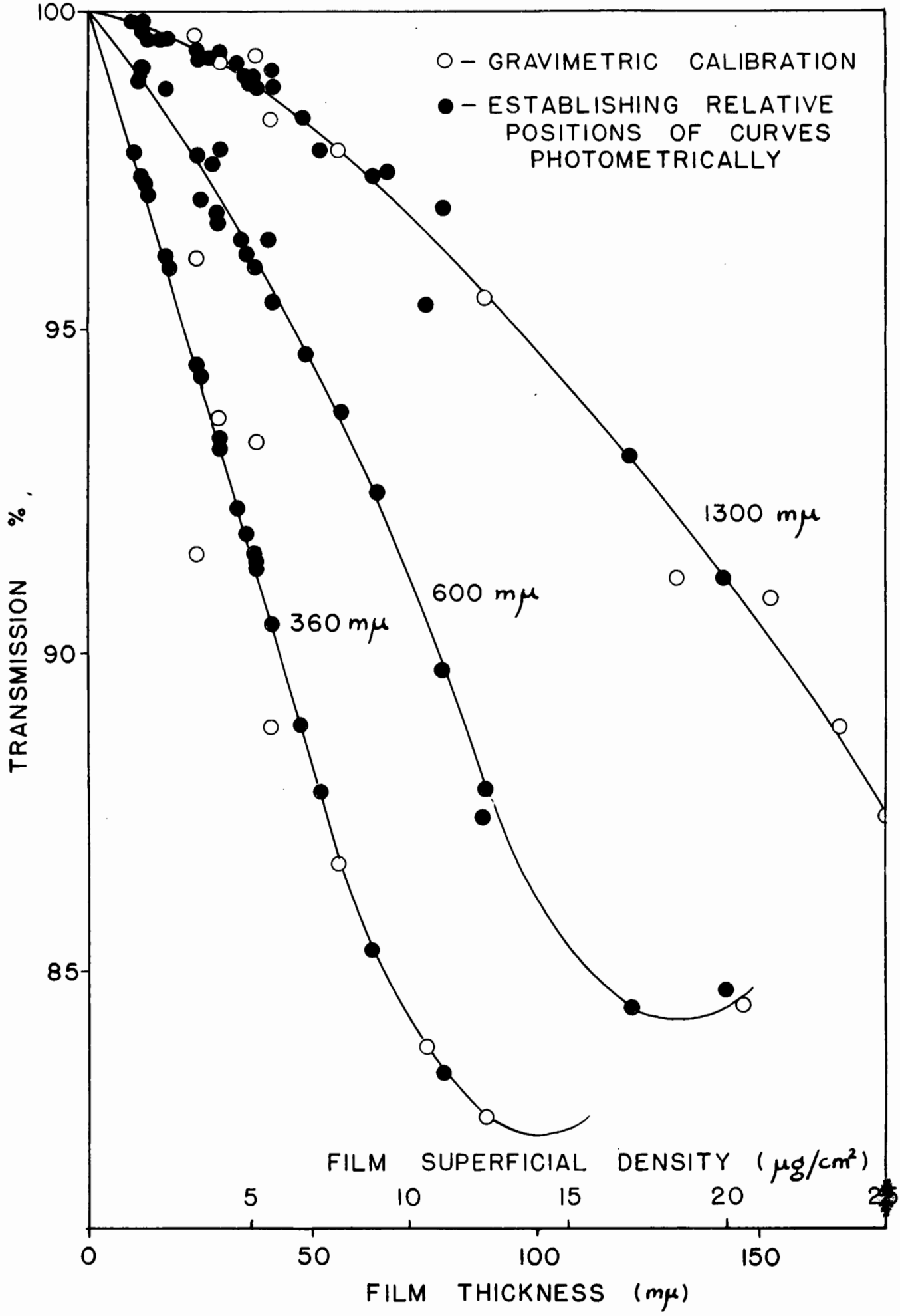
100
95
90
85
TRANSMISSION %
○ – GRAVIMETRIC CALIBRATION
● – ESTABLISHING RELATIVE POSITIONS OF CURVES PHOTOMETRICALLY
1300 mμ
600 mμ
360 mμ
FILM SUPERFICIAL DENSITY (μg/cm²)
5
10
15
20
0
50
100
150
FILM THICKNESS (mμ)

density of 0.4 $\mu g./cm^2$ gold, and this progressively deepens in shade until at 5 $\mu g./cm^2$ a rich red-purple coloration is obtained. By transmitted light gold layers appear as increasing intensity of blue, due to absorption or reflection of light at about 600 mμ. Absorption spectra of a series of gold films on VYNS (duly corrected for the VYNS absorption) are shown in Figure 26. The absorption at 600 mμ. has been made the basis of a satisfactory precision method of measuring the thickness of a gold layer applied. The Beckman Spectrophotometer is again used, balanced against air, and the transmission at 600 mμ of a series of films of known gold superficial density is measured, the film being arranged so that the light beam is incident on it from the uncoated side. A satisfactory method of preparing the calibration films is to employ increasing distillation times from a filament of constant distillation rate, which is known from gravimetric measurements. The optical transmission of the film plus gold as measured is the product of the transmission of the film, and that of the gold. The former may be read from the 600 mμ curve in Figure 25, and the curve of the gold transmission thus calculated versus gold superficial density is given in Figure 27. Spectrophotometer readings can be taken with an accuracy which gives a precision for the method of 0.05 $\mu g./cm^2$ of gold, and in this case the calibration is probably of comparable accuracy.

We have examined the structure of the gold film also, by electron-microscopy. Figure 28 shows a micrograph of a layer of 5 $\mu g./cm^2$ superficial density with a magnification of 3×10^4; the crystal size of the gold deposit appears to be in the neighbourhood of 60 mμ diameter.

Figure 26

Optical Transmission Spectrum of Gold at

Increasing Superficial Density

(These data were obtained in collaboration with Mr. W. L. Elsdon of Dr. Winkler's laboratory.)

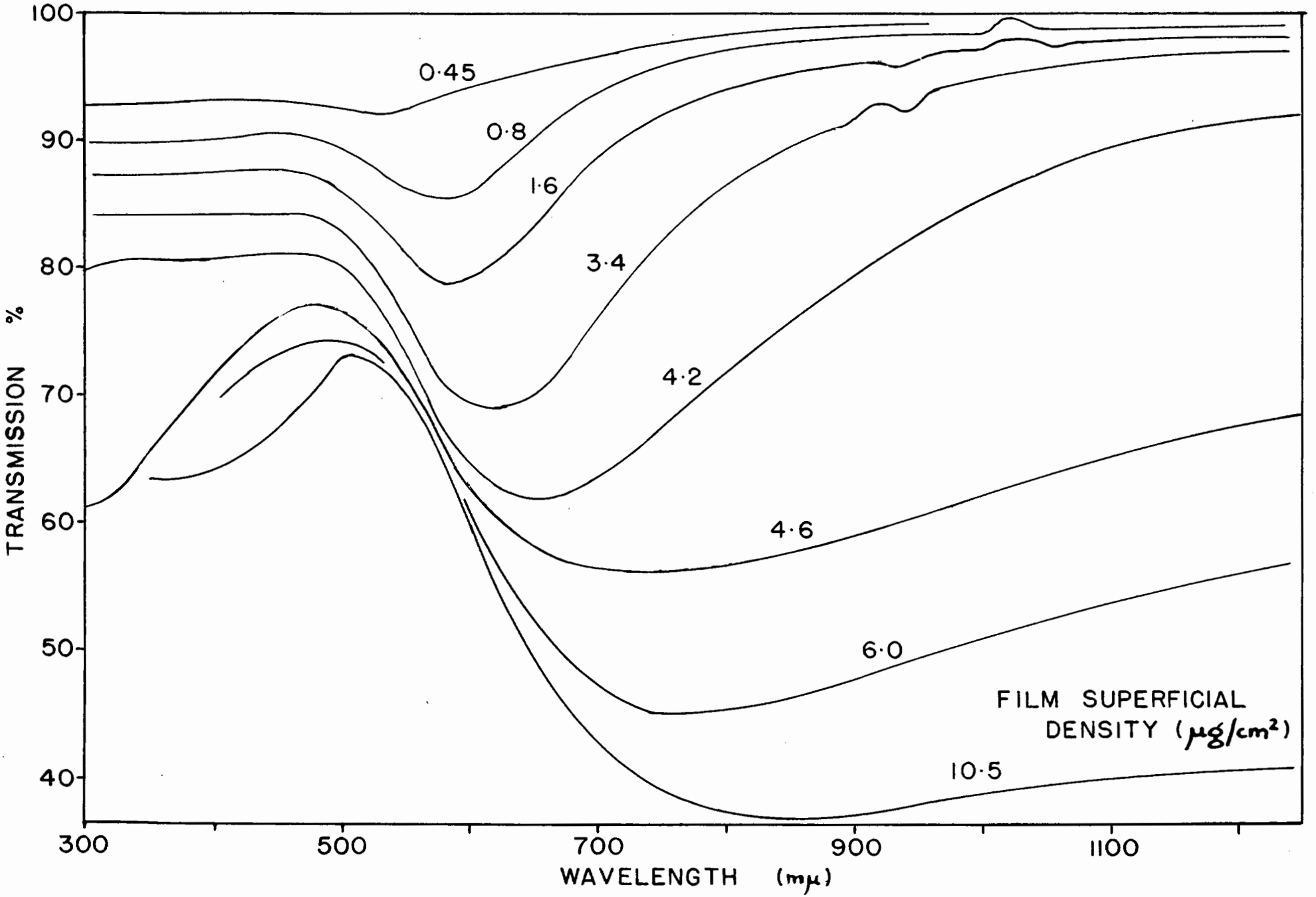
100
90
80
70
60
50
40
TRANSMISSION %
0·45
0·8
1·6
3·4
4·2
4·6
6·0
10·5
FILM SUPERFICIAL DENSITY (μg/cm²)
300
500
700
900
1100
WAVELENGTH (mμ)

Figure 27

Optical Transmission of Gold on VYNS film at 600 mμ Wavelength,

as a Function of Superficial Density

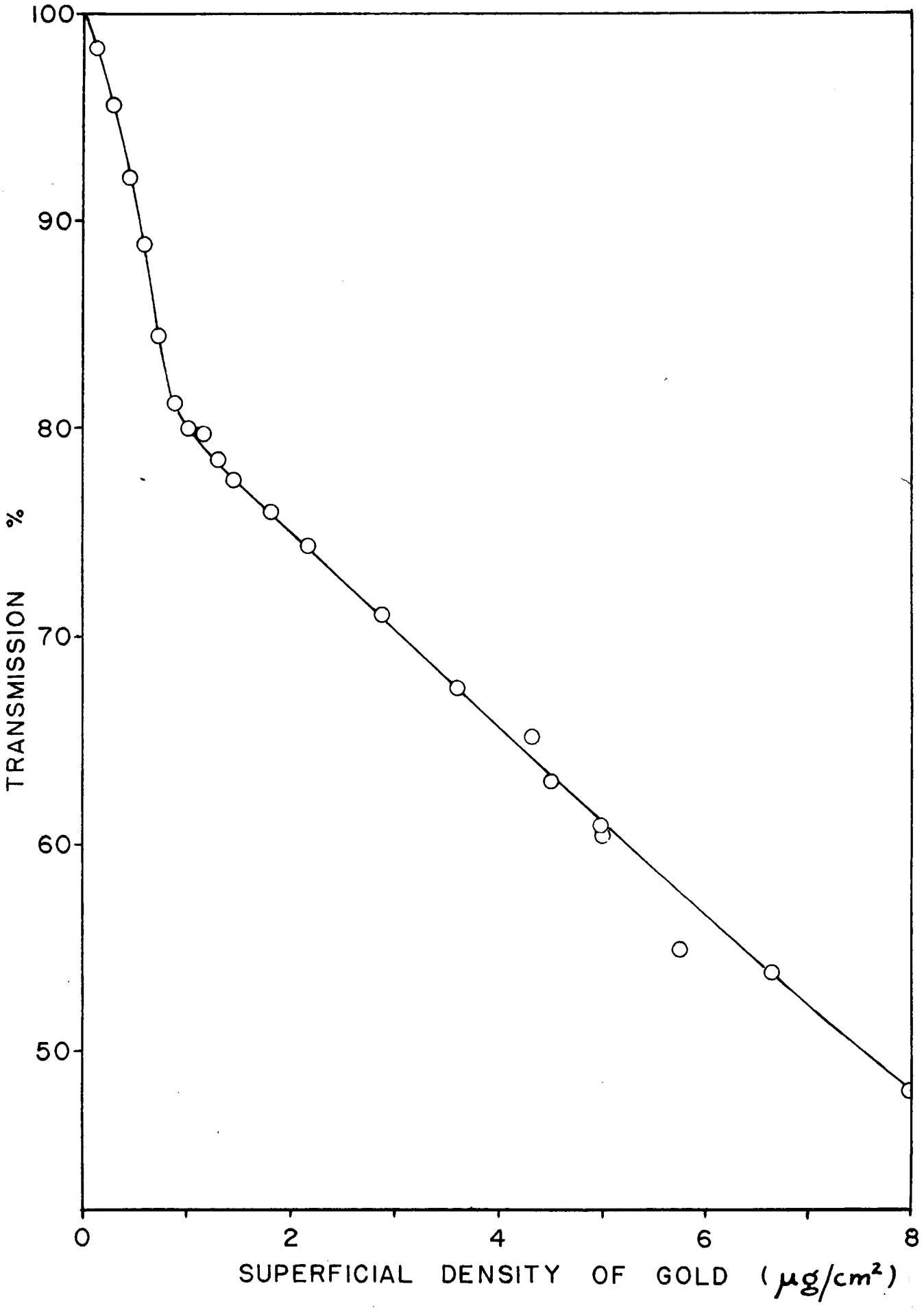
100
90
80
70
60
50
TRANSMISSION %
0
2
4
6
8
SUPERFICIAL DENSITY OF GOLD (μg/cm²)

Figure 28

Electromicrograph (3×10^4) of 10 $\mu g./cm^2$ of Gold on VYNS Film

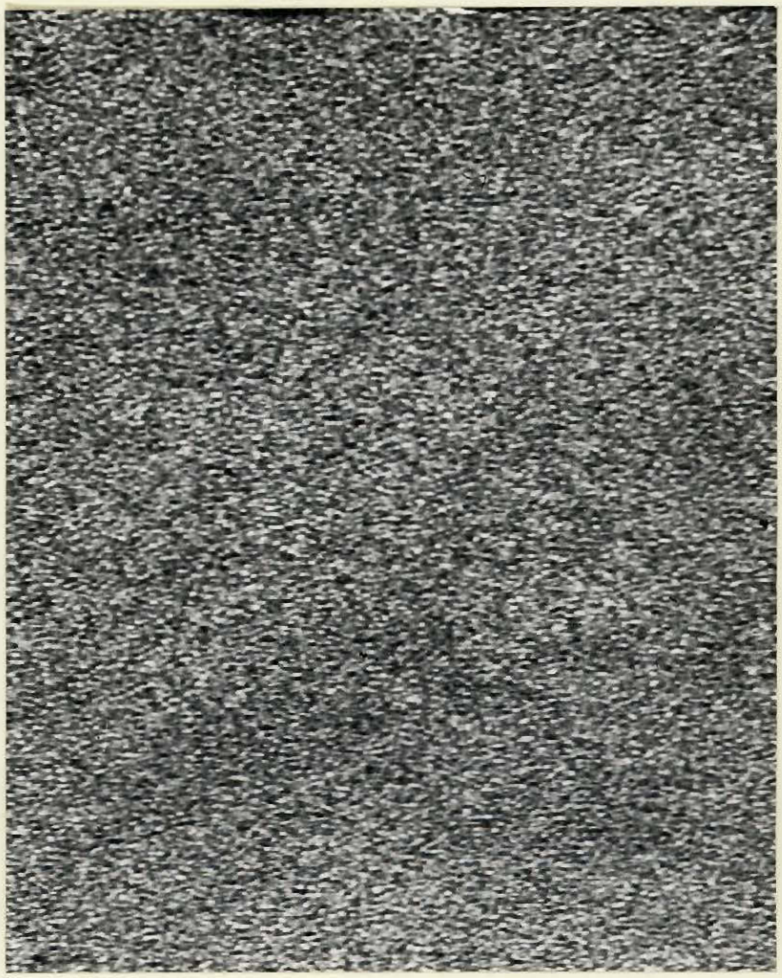

Several interesting features are apparent in the results of the spectral studies and in the electron micrograph of the gold deposits, which may be related to changes in structure at definite deposit thicknesses. For instance, there is a marked change of slope in the transmission curve of Figure 27 at about 1.0 $\mu g./cm^2$. This does not appear to be associated with a change of the spectral form shown in Figure 26, although such a change does occur between 4.2 and 4.6 $\mu g./cm^2$ superficial density, a transmission peak at about 500 $m\mu$ replacing an absorption peak at about 600 to 700 $m\mu$. We have already noted in section B, that a marked change in conductivity of the gold film occurs between 1 and 2 $\mu g./cm^2$, the high-voltage characteristic of the 4π-counter assuming a form corresponding to "regular" behavior when the source mounting film has 2 $\mu g./cm^2$ of gold coating.

It is possible that these changes in behavior are associated with the completion of structural units as progressively larger quantities of gold are distilled on to a film.

Thus assuming an effective radius for the gold atom of 1.4 Å, a single layer of atoms arranged as close packed spheres is calculated to contain 1.3×10^{15} atoms per cm^2, which corresponds to

$$\frac{1.3 \times 10^{15} \times 200}{6 \times 10^{23}} = 5 \times 10^{-5} \text{ g/cm}^2$$

or 0.5 $\mu g./cm^2$. Therefore, bearing in mind that the density of the metal in a film of this thickness may differ from that in the bulk metal, we may tentatively correlate the break in the absorption curve of Figure 27 at 1.0 $\mu g./cm^2$ and the increase in film conductivity observed

in section B between 1 and 2 $\mu g./cm^2$ with the "completion" of an atomic layer.

In Figure 28, it is seen that at 5 $\mu g./cm^2$ superficial density the deposit is composed of crystals of dimension of the order of 60 $m\mu$. If one calculates the number of spherical particles of radius 30 $m\mu$, arranged as a single layer of close-packed spheres, accommodated on the surface, one arrives at a figure of about

$$2 \times 10^{10} \text{ per } cm^2$$

which assuming a density for gold of about 20 is equivalent to a superficial density of

$$2 \times 10^{10} \times 2.5 \times 10^{-15}$$

$$= 5 \times 10^{-5} \text{ g/cm}^2 = 5 \ \mu g./cm^2$$

Thus the change of spectral form between 4.2 and 4.6 $\mu g./cm^2$ superficial density, may then be due to a completion of a single layer of these crystals, although one must again bear in mind the approximation involved.

It is hoped to perform at a later date further experimental work on the conductivity of these gold films, in an attempt to secure more data on this question of structure.

3) CORRECTION FOR SOURCE-MOUNT ABSORPTION

(a) Introduction

The availability of VYNS films of a superficial density of 5-10 $\mu g./cm^2$ for use as source-mounts in 4π-counting allows source-mount radiation absorption to be neglected in disintegration-rate determinations of moderate precision for α-radiation or β-radiation of moderate or high energy. For work of the greatest precision, however,

and particularly that with the weaker β-emitters, the absorption loss must be accurately evaluated and a correction made. The use of very thin films is nevertheless still of considerable advantage, since the magnitude of the correction is reduced, and the final disintegration-rate value less sensitive to errors in the correction.

Three methods of determining the absorption correction have been described in the literature: the so-called "sandwich" procedure, calculation from 2π and 4π counting-rates, and the use of absorption curves.

(i) The "sandwich" procedure has been described by Hawkings et al. (68). The counting rate given by a source mounted on a known thickness of mounting film is determined, and then a second determination made with an identical film superimposed over the first so as to sandwich the source. The observed reduction of counting-rate was applied as a correction to the single film value to arrive at the source disintegration-rate, and the validity of this procedure was taken to be apparent "from a consideration of the contribution to the counting rate from each hemisphere". However Smith (135) found that applying the sandwich procedure to similar sources of, for instance, S^{35} using sets of films of differing superficial density lead to results for the disintegration rate differing by as much as 7 percent. The results should of course be independent of the thickness of films used.

(ii) Seliger and co-workers (95, 128) have attempted to develop mathematical relationships which would allow calculation of the source disintegration-rate from measured 2π and 4π-, single and sandwiched film counting rates. The resulting formulae as quoted in the second

and more rigorous of the two papers (95) were:

(a) $$\frac{N_a - N_b}{N_T - N_b} = 2\beta_f + t \sim t \qquad .....(48)$$

where N_a and N_b are the counting rates observed in the top and bottom half-counters respectively, N_T is the counting rate observed from both halves combined, β_f is the fractional backscattering factor and t the fractional absorption factor for the film used as source mount.

(b) $$\frac{N_T - N_S}{2N_T - N_S} = \frac{t}{2} \qquad .....(49)$$

where N_S is the total counting-rate observed with the source sandwiched between two similar films. The value of t obtained from these equations was then to be substituted into

$$N_o = \frac{N_T}{1 - t/2} \qquad .....(50)$$

to obtain N_o, the disintegration rate.

As is common with calculations of this sort (eg. 135) the combination of a continuous distribution of beta energies with energy-dependent scattering and absorption coefficients and a complex geometrical arrangement make the problem analytically very difficult without the adoption of several simplifications. For example: Among those employed by Seliger et al. were the supposition that the absorption and scattering characteristics of β-radiation were unaffected by the scattering process (eg. degradation of the energy spectrum was neglected) and, in several places in the derivation, the assumption that β_f and t were small compared to unity.

The latter may be true in the region of beta-energies and film thicknesses where the absorption correction is in any case insignificant, but with lower beta-energies where an accurate correction is required, both coefficients are by no means negligible, and vary rapidly with changing beta energy. In particular, the backscattering effect observed in a 4π geometry is found to be considerably larger than in conventional counter systems. The 4π-counter will respond to particles having undergone scattering at low angles to the source mount, and low angle scattering is evidently important even with thin films of low average atomic number. Using a 4π-counter, Meyer-Schützmeister and Vincent (100) have reported an 8 percent backscattering for S^{35} β-particles from 30-40 $\mu g./cm^2$ cellulose films, Houtermans et al. (76) report similar results for P^{32}, and Borkowski (20) found 5 percent backscattering of Na^{24} β-radiation from 50 $\mu g./cm^2$ of Formvar.

Thus the overall 2 percent accuracy claimed by Mann and Seliger (95) for their absorption correction is probably optimistic when one is using β-emitters of low energy (eg. Ni^{63}, C^{14}, S^{35} etc.).

(iii) The "absorption curve method" used to correct the results obtained from end-window counters for the absorption of radiation, suggests itself as a corrective technique applicable to this case also. A procedure of this sort was used by the workers at Göttingen (76, 100). They made a series of counting-rate measurements with a source mounted on a film, and with increasing thicknesses of aluminum foil placed over the source, and used the curves obtained to correct the original counting rate. However, such a procedure would appear to be open to the same objections as the ordinary sandwich procedure.

Studying the variation of counting-rate as a function of the actual mount thickness was first employed by Smith (135). He commenced with a source mounted on aluminum of 260 $\mu g./cm^2$ and took measurements of the counting rates obtained with the source backed by increasing thicknesses of this material. The curve obtained on plotting the results was observed to be approximately linear, and Smith assumed that the value obtained by extrapolating back to zero mount-thickness represented the source disintegration-rate. However, this value was found to be low compared with the counting-rate observed with a similar source mounted on 30 $\mu g./cm^2$ of cellulose acetate, by 3 percent in the case of S^{35}, and 1.5 percent in the case of Co^{60}. The discrepancy probably arose from a change of slope in the absorption curve below 260 $\mu g./cm^2$ superficial density, such as was observed by Suzor and Charpak in another connection (141). Provided sufficiently thin films and a suitable technique were used, this type of procedure would be expected to produce the most accurate means of correcting for mount-absorption, the results being independent of any assumptions regarding counter mechanisms and so on. The anomalous backscattering effects observed by Yaffe and Justus (148) and Glendenin and co-workers (57) would not be expected to cause any disturbing effects.

(b) Experimental Procedure and Results

For the following experiments, we have used the chamber and ancillary equipment described in the previous section operating under the conditions found to give unit response probability. We have performed two sets of experiments:

(i) Single Film Source Mount Characteristics

A series of counting rate measurements was taken for each nuclide of the series of seven β-emitters of increasing end-point energy, and four emitters of differing forms of radiation, whose nuclear characteristics were described earlier (section B). For each of a series of increasing source-mount superficial densities, we have measured the total counter counting rate (N_T) with the anodes connected in parallel to the amplifying system. The source mounts used were of gold-coated VYNS film mounted on a 1 mm. aluminum diaphragm of aperture 2.5 cms. in diameter. The thinnest films employed were of 5 to 10 $\mu g./cm^2$ superficial density, and increasing thickness was obtained

(a) up to about 70 $\mu g./cm^2$ by allowing a series of films of known superficial density to adhere to the back of the initial mount.

(b) above 70 $\mu g./cm^2$ by temporarily placing in contact with the back surface of the mount, in position in the chamber, each of a series of standardized films of increasing superficial density.

The results of these experiments are shown plotted in Figures 29 and 30. Data as shown are for "weightless" sources. Experiments with Ni^{63} have shown that identical results are obtained even for source thicknesses where self-absorption of the order of 80-90 percent occurs.

(ii) Sandwich Characteristics

A second series of measurements was taken using the series of seven β-emitters described above as shown in Figure 29. In this case sources of each nuclide were prepared on a series of films of increasing superficial density and the following quantities measured: the total counting-rate with the anodes in parallel with a single mount (N_T), and

Figure 29

Source Mount Absorption Curves for β-radiation of

Increasing End-point Energy

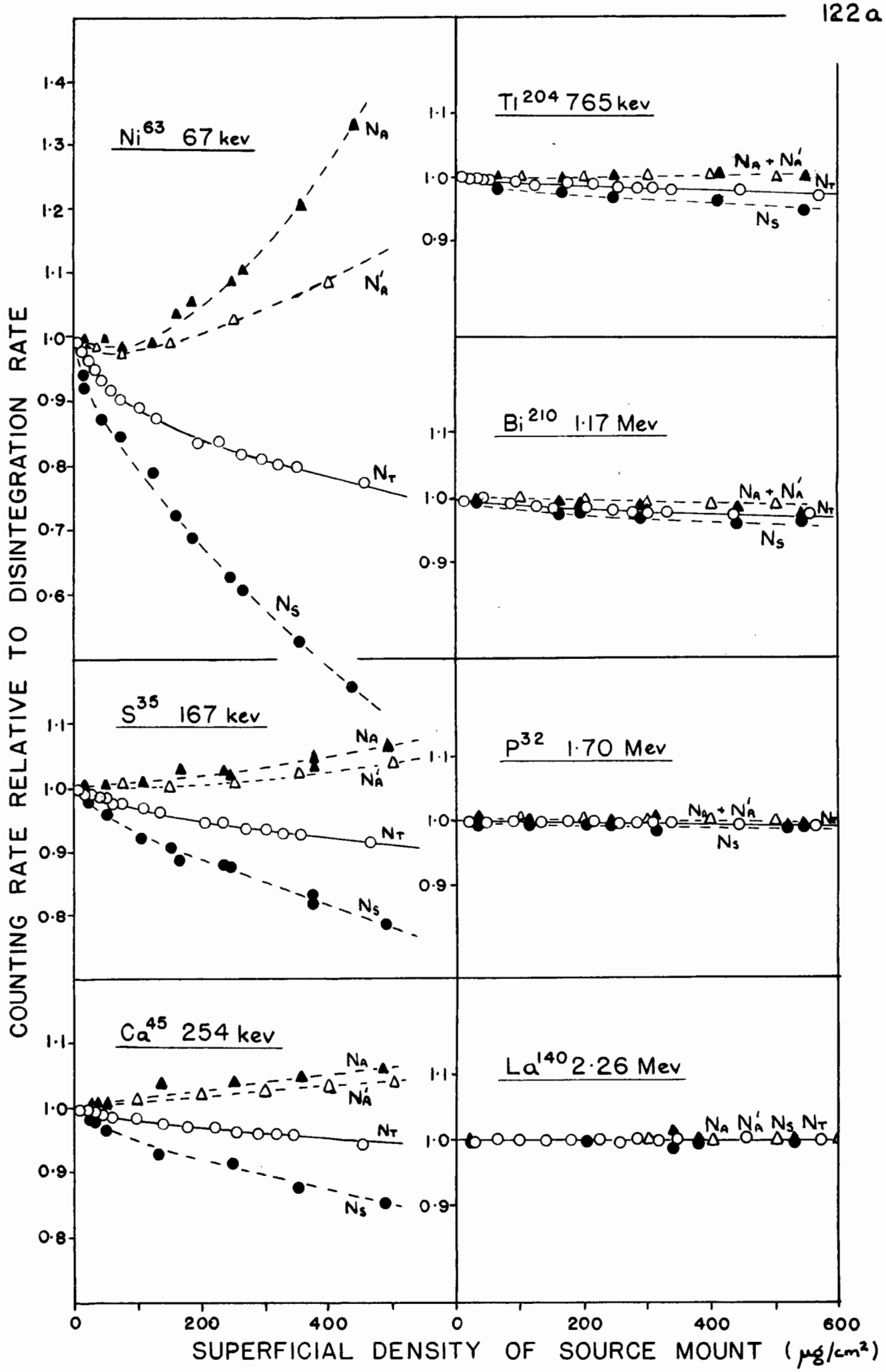
Ni 63 67 kev
Tl 204 765 kev
Bi 210 1·17 Mev
S 35 167 kev
P 32 1·70 Mev
Ca 45 254 kev
La 140 2·26 Mev
N_A
N'_A
N_T
N_S
N_A + N'_A
COUNTING RATE RELATIVE TO DISINTEGRATION RATE
SUPERFICIAL DENSITY OF SOURCE MOUNT (μg/cm²)

Figure 30

Source Mount Absorption Curves for Various Forms of Radiation

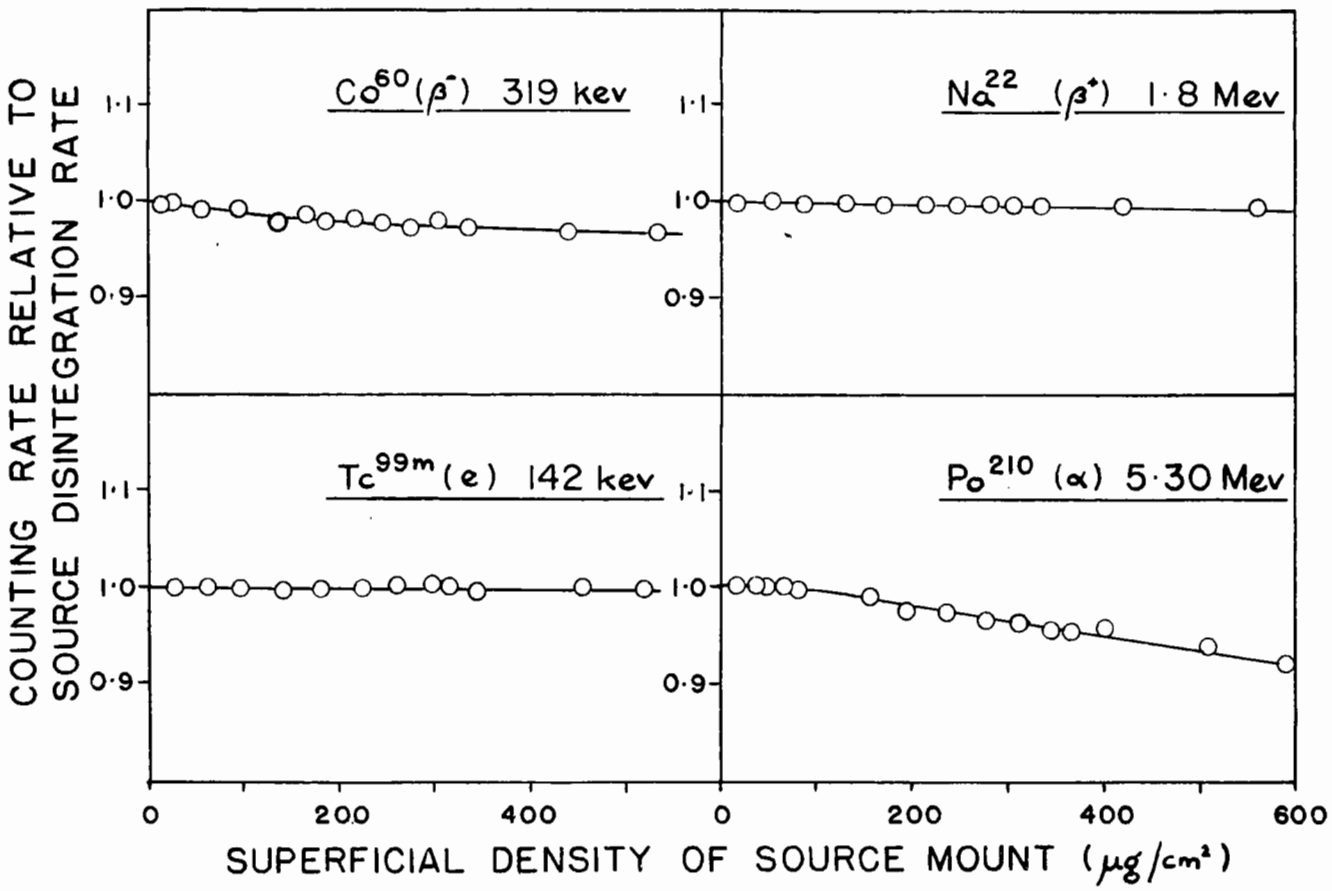
COUNTING RATE RELATIVE TO SOURCE DISINTEGRATION RATE
Co60 (β⁻) 319 kev
Na22 (β⁺) 1·8 Mev
Tc99m (e) 142 kev
Po210 (α) 5·30 Mev
1·1
1·0
0·9
0
200
400
600
SUPERFICIAL DENSITY OF SOURCE MOUNT (μg/cm²)

the total counting-rate with a second identical sandwiching film added (N_S). From these values the expected disintegration rate of the sources used has been calculated by the procedure of Hawkings et al. (N_A) and by the more rigorous of the procedures of Seliger and co-workers (N_A'). The results are shown as a function of source mount superficial density in Figure 29, with the true source disintegration rates normalized to a common value for each nuclide using the curves for N_T obtained in the first series of experiments.

(c) Discussion

(i) The Sandwich Procedure

The results shown in Figure 29 give a fairly complete picture of the accuracy of the sandwich procedure as a function of mount thickness and β end-point energy, whether applied by the method of Hawkings et al. (68) or by the N.B.S. method (95, 128, 130), and are in accord with those found by Smith (135). Though the procedure may be said to work fairly well at higher particle energies, where the mount absorption loss is small in any case, at lower energies, where accurate information is desirable, it becomes progressively less and less useful. The fact that the calculation of the disintegration rate leads to results that vary considerably (for example in the case of Ni^{63}) with source mount thickness would indicate that the mathematical treatment was oversimplified.

(ii) The Absorption Curve Procedure

The anomalous results obtained by this method by Smith (135) using mounts with a superficial density in excess of 260 $\mu g./cm^2$ are readily understood on a basis of the curves for N_T shown in Figure 29. Extrapolation of the approximately linear portion of the curves obtained

at higher mount thicknesses would take no account of the initial fall in counting rate observed at very low mount thicknesses. This fall in counting rate, particularly pronounced at low β end-point energies, is due to progressive absorption by the source mount of the softest radiation in the beta energy spectrum.

For work of moderate precision the data in Figure 29 may be used directly to correct observed single-film results for source-mount absorption. In order to allow interpolation to intermediate β-energies, the data are replotted in Figure 31 with the absorption parameter (N_T/N_o) as a function of beta end-point energy for a series of film thicknesses. Clearly several approximations are introduced by use of the data in this way, including a neglect of variation in the form of the β-energy spectrum with nature of the beta-transition (degree of forbiddenness etc.) and of the additional complication of nuclear gamma emission when this is present. Also, obviously the transition must be recognized as a beta-transition and the end-point energy known.

For work of maximum precision the procedure adopted to obtain our experimental results is recommended. In this case, the source material is mounted on the thinnest film available, and the counting rate N_T measured as a function of increasing mount thickness as outlined above. The disintegration rate is obtained by extrapolating to zero mount thickness.

The accuracy of the disintegration rate value, arrived at in this way, can also be judged from Figure 29. It is limited by the statistical deviation of the counting rates measured, and by the accuracy with which the superficial density values are known (see above). No

Figure 31

Source Mount Absorption as a Function of β End-point Energy, for Films of Increasing Superficial Density

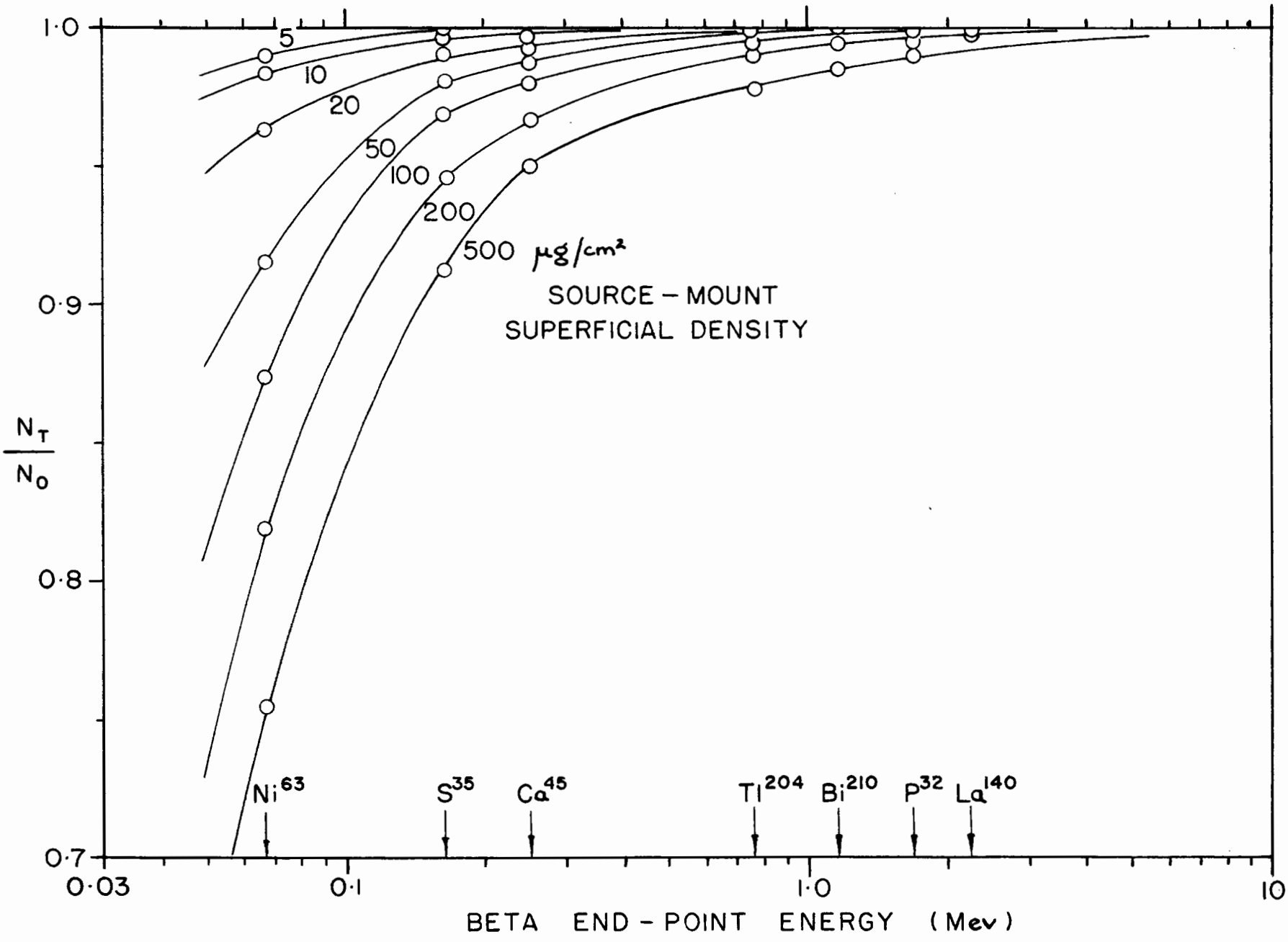
1·0
0·9
0·8
0·7
$\frac{N_T}{N_0}$
5
10
20
50
100
200
500 μg/cm²
SOURCE – MOUNT
SUPERFICIAL DENSITY
Ni⁶³
S³⁵
Ca⁴⁵
Tl²⁰⁴
Bi²¹⁰
P³²
La¹⁴⁰
0·03
0·1
1·0
10
BETA END – POINT ENERGY (Mev)

126a

error of significance should be introduced by the technique of allowing additional films to adhere to the original mount, and we estimate that the error in the final disintegration rate value can be reduced to about ± 0.2 percent in the case of the weakest beta-radiation studied, and probably to less than this at higher particle energies. We find this method satisfactory in routine use, the necessary measurements and manipulations taking very little more time than those required for the conventional sandwich procedure.

In the case of a β-emitter of unknown energy, once the disintegration rate is known from the absorption curve procedure, Figure 31 may be used to derive from the observed value of N_T/N_o a crude but nevertheless useful estimate of the end-point energy of the spectrum. This technique replaces those commonly used with end-window counters, which are inapplicable in a 4π steradian geometry.

The reasons why the value of source disintegration-rate predicted by the sandwich procedure should vary with increasing source mount thickness, and in general differ (widely at low β-energies) from the figure unequivocally indicated by the absorption curve method, and the reasons for variations in the separate counting-rates of the hemispheres above and below the source mount, and in the rate of coincidences between the two half-counters, will be discussed in section E.

One should, however, consider here the data for N_T for Po^{210} shown in Figure 30. Po^{210} is an α-emitter of 5.30 Mev energy, which has a range of $\sim$ 5.1 mg/cm^2 in air, and therefore (using known atomic stopping powers (13)) a range of 4.9 mg/cm^2 in film material. Hence,

with film superficial densities of up to 600 $\mu g./cm^2$ with a collimated beam of radiation or a low counting geometry, no fall of N_T with increasing film thickness would be expected. The variation observed in a 4π geometry is definitely due to absorption of α-radiation in the film however, since as seen in Figure 50 (section E) in this case one observes that the rate of coincidences between the two half-counters is very small (< 1 percent of N_o) in contrast with the situation with β-emitters (see section E), and that N_T is substantially the sum of the counting rates of the upper hemisphere (n_a constant with increasing film thickness) and lower hemisphere (n_b decreasing almost linearly with increasing film thickness).

The observed effect may be shown to be due to the absorption of those α-particles emitted at a small angle to the film surface and which follow an oblique path in the film material. We may calculate the fraction of the total isotropically emitted α-radiation which may be expected to be absorbed at any film thickness. If, as in Figure 32, the film thickness is d, and the range of the radiation (emitted from the source S) in film material is R, then of those α-particles emitted in the 2π-steradian angle towards the film, only those inside the cone of half-angle θ will emerge into the gas volume and register. The proportion of the total radiation emitted outside this cone and totally absorbed in the film can be shown to be approximately

$$\frac{2\pi r.d}{4\pi R^2} \quad \text{for large } \theta \qquad \ldots\ldots(51)$$

$$= \frac{rd}{2R^2} \sim \frac{d}{2R} \qquad \ldots\ldots(52)$$

in agreement with observed linearity with d.

Figure 32

Absorption of Monoenergetic Radiation in Source-Mount
(diagrammatic)

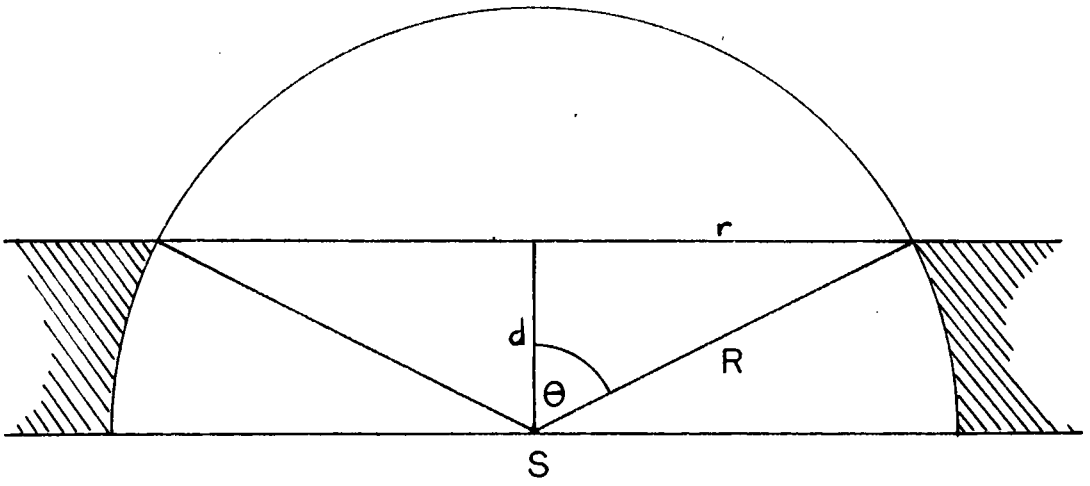
r
d
θ
R
S

In a film thickness d corresponding to 600 $\mu g./cm^2$, the loss by absorption is found to be 6.5 percent compared to an observed value of 7.5 percent. The agreement is fair, considering the assumptions made regarding the range of Po^{210} α-particles in film material. Also with very oblique paths, a finite probability exists that an α-particle will scatter out of the film into the gas-space and register before being absorbed, resulting in decreased absorption. This effect also may be responsible for the constancy of N_T at low film thicknesses.

The absence of apparent decrease of N_T with d in the case of the (monoenergetic) conversion electrons of Tc^{99m} (Figure 30) is presumably due to their longer range (26 mg/cm^2) and the influence of backscattering.

D. SELF-ABSORPTION

1) INTRODUCTION

In this section we shall discuss the third source of error, to which 4π-counting is subject, namely absorption of radiation in the material of the source itself - most commonly called self-absorption. This process is at present, and will most likely remain for some time, the limiting factor in disintegration-rate determinations with the 4π-counter, or with any other method (except coincidence counting) which employs the sample mounted in solid form.

The degree to which self-absorption effects will affect the precision ultimately attainable with 4π-counting techniques depends on the energy and type of radiation to be measured. With fairly high specific activity sources of electronic radiation of moderate or high energy, self-absorption effects are small, and should be measurable to sufficient precision to prevent any great error being introduced into the final disintegration-rate value. For electronic radiation of lower energy, and for α-radiation however, self-absorption effects are much more significant. It is probable that by means of techniques, such as those we shall describe below, the self-absorption error in materials of high specific activity can eventually be estimated to the same degree of precision as the errors described in sections B and C, and allowance made for it. (Such will be the case in the standardization of isotopes, eg. for therapeutic purposes.) For material of low specific activity however, such as commonly arises in the use of S^{35} or C^{14} in biological work, this is less likely, and 4π-counting of solid samples is ultimately liable to be less successful than counting methods using source material

in the gaseous phase, although up to now no great success has been achieved in this direction.

The application of 4π-counting methods to routine radiochemical work, in which in this laboratory we are particularly interested, will therefore demand the reduction of the quantities of inactive isotopic carrier used in radiochemical separations particularly for emitters of lower energy radiation.

Self-absorption is a source of error common both to 4π-counting and to conventional absolute counting-methods, such as that involving a calibrated end-window Geiger-Müller counter. It is instructive then to review previous work on self-absorption, performed in the main on such a system where the angle over which the radiation from the source is observed is very much less than 2π steradians.

Much of the work up to the last few years has been concerned with C^{14} and S^{35}, β^--emitters with end-point energies of 155 and 167 kev respectively. The reason for this was that, until recently, the error due to self-absorption with emitters of more energetic radiation was considerably less than those due to the other scattering and absorption processes important in the end-window system (see section A). With C^{14} and S^{35} however, particularly in low specific-activity sources, self-absorption is very important, and the magnitude of the effect was estimated by measuring the specific activity of suitably mounted sources as a function of their superficial density (2, 70, 71, 93, 115, 137, 149, 150) usually in the range 0-30 mg/cm^2.

Attempts to treat the phenomenon theoretically were faced with the problem, common to all processes involving beta-radiation, of the

complexity produced by the continuous distribution of particle energies, and lack of all but empirical data of the absorption and multiple scattering processes. The earliest self-absorption relationships proposed (71, 93) were based on the assumption that the absorption of beta-radiation resulted in an exponential decrease of radiation-intensity with increasing sample thickness. Thus the observed activity, da, due to a layer of thickness, dx, a distance x below the surface of a source of specific activity, a_o, was taken to be

$$da = a_o e^{-\mu x} dx \qquad .....(53)$$

where μ is the external absorption coefficient for the β-radiation studied in the source material used. This expression integrated over a total source thickness (or surface density) d gives a total <u>observed</u> activity

$$A = \frac{a_o}{\mu} (1 - e^{-\mu d}) \qquad .....(54)$$

$$\text{or} \quad a = \frac{a_o}{\mu d} (1 - e^{-\mu d}) \qquad .....(55)$$

where a is the <u>observed specific</u> activity.

The process of absorption of β-radiation by external absorbers may or may not be observed to be exponential under given conditions (eg. 32, 107, 137, 153). The exact form of absorption curves observed depends on the relative contributions of absorption and scattering effects obtained in a given counting geometry, and maxima in the curves may be observed (32, 107, 153) for instance if more radiation is scattered into the counting chamber by the thinnest absorbing layers than is lost by absorption.

The conditions under which exponential absorption may be expected have been discussed by Feather (47), and approximately exponential effects are sufficiently common for values of μ to be quoted by experimenters. In any case the expression above derived from this assumption was found to describe the self-absorption process fairly well over the range of sample superficial density commonly used (2, 22, 71, 72, 137).

Further verification of the original calculations was obtained by Broda et al. (22). They considered the ratio of the "external absorption half-thickness" $\epsilon_{\frac{1}{2}}$ to the source superficial density at which the observed specific activity was reduced to one half the true value, $\eta_{\frac{1}{2}}$. From the expression

$$\frac{a}{a_o} = \frac{1 - e^{-\mu d}}{\mu d}$$ See equation (55)

setting $a/a_o = \frac{1}{2}$ for a value of $d = \eta_{\frac{1}{2}}$ they obtained

$$\frac{1}{2} = \frac{1 - e^{-\mu \eta_{\frac{1}{2}}}}{\mu \eta_{\frac{1}{2}}}$$

$$\text{ie. } e^{-\mu \eta_{\frac{1}{2}}} = 1 - \frac{\mu \eta_{\frac{1}{2}}}{2} \qquad \text{.....(56)}$$

The solution for this equation is

$$\mu \eta_{\frac{1}{2}} = 1.53$$

and since $\epsilon_{\frac{1}{2}} = 0.693/\mu$

$$\text{then} \quad \frac{\eta_{\frac{1}{2}}}{\epsilon_{\frac{1}{2}}} = 2.21 \qquad \text{.....(57)}$$

Experimental values of this ratio for a number of beta-emitters with a range of beta-energies were, with a few exceptions, in agreement with the theoretical figure.

On the basis of this simple theory then, three main methods of correcting for self-absorption effects were available.

i) For material of high specific activity, a plot of observed specific activity against source superficial density could be extrapolated to zero superficial density to obtain the corrected value, or once a system was calibrated, the self-absorption correction for a source of given mass could be read directly from the calibration plot.

ii) For material of low specific activity, measurements could be made at "infinite source thickness", ie. under such conditions that the radiation from the lowest layers of the source were entirely absorbed in the source material. Under these conditions the expression for observed total activity

$$A = \frac{a_o}{\mu}(1 - e^{-\mu d}) \qquad \text{.....} \quad \text{Equation (54)}$$

becomes

$$\lim_{d \to \infty} A = \frac{a_o}{\mu} \qquad \text{.....(58)}$$

and A is therefore a direct measure of specific activity and is independent of d.

iii) For strictly relative measurements of two or more sources, if these were made of identical mass, identically mounted, then no self-absorption correction was necessary.

As more precise data were accumulated, however, it was found that the picture was not quite as simple as had been suggested. The first intimation of this was the appearance of maxima in curves of specific activity versus source superficial density at low superficial density values. As early as 1943, Hendricks et al. (70) had presented

data giving evidence of this effect, but had not commented on it. Solomon et al. (137) in 1947 published a curve showing a clearly defined maximum in the observed specific activity of $BaC^{14}O_3$ at about 1 mg/cm^2 source superficial density. This was at first assumed due to the incomplete recovery of radiocarbon from solution during the $BaC^{14}O_3$ precipitation, but it was pointed out to the authors by L. E. Glendenin that the effect was in fact due to self-scattering, an effect analogous to the external scattering effects which had been observed as early as 1910 (86) in external absorption curves. Many subsequent publications on self-absorption have also shown curves with maxima (5, 32, 106).

The effects of external scattering and self-scattering had been investigated and treated mathematically by Elliott and co-workers in 1943 and 1944, but the results were not published until 1951 (39, 40, 42, 107). They first (39) showed that from very thin layers of source material, radiation was approximately isotropic, while from thicker layers the intensity observed at an angle θ to the normal approached a value $\propto$ cosine θ. This again could be explained on the basis of an assumption of exponential absorption. Thus the simple self-absorption expression

$$a = \frac{a_o}{\mu d}(1 - e^{-\mu d}) \qquad \text{....Equation (55)}$$

applies for a direction of observation of the radiation normal to the source surface. If the observation is made at an angle θ to the normal, the effective source thickness becomes $\frac{d}{\cos \theta}$ and

$$a_\theta = \frac{a_o \cos \theta}{\mu d}\left(1 - e^{-\frac{\mu d}{\cos \theta}}\right) \qquad \text{.....(59)}$$

which reduces to the experimental cosine θ distribution at large d. In later papers (40, 107) they showed that experimental results were consistent with scattered radiation also having a cosine distribution, and the isotropic and cosine θ radiation distributions for thin and thick sources have since been confirmed by Collie et al. (32).

The significance of the existence of the self-scattering effects were twofold.

(i) The anisotropy of radiation from sources of finite thickness had the effect of concentrating radiation more and more in the direction of the normal to the source plane with increasing source thickness. This meant that the extent of self-absorption effects observed was a function of the angle over which the radiation intensity was measured (ie. of counter-geometry). It would be at a minimum for a counting system of small geometry, observing radiation in a direction normal to the source surface, as constituted by the conventional end-window system.

(ii) Unless care was exercised in obtaining accurate observations of radiation intensity at low source thicknesses, the customary procedure of extrapolation of the observed specific activity versus thickness curve to zero thickness would lead to erroneous (high) values for the true specific activity. So too would calculations using the simple formula, and a value of the self-absorption coefficient $\mu_{S.A.}$ obtained from the region of source superficial densities say between 2 and 30 mg/cm^2.

Further since scattering was now recognized as making a significant contribution to the effects observed, the question of the influence of the effective atomic number of the source material became

important. So long as the process was considered to be purely one of absorption, self-absorption effects of similar magnitude were to be expected in different materials. This was by analogy with external absorption phenomena where a change in Z did not produce a very marked change in observed absorption effects (93) due probably to a fortuitous cancellation of increased fore scattering against increased loss by absorption. Thus some of the earlier publications on self-absorption (93, 115) report little Z-dependence of the effect.

Later workers however noted evidence for a marked dependence of self-absorption effects on effective atomic number, in accordance with the expected state of affairs if scattering effects were important. Yankwich and Weigl (151) noted a ratio of 1.27 between the magnitude of self-absorption for C^{14} in barium carbonate and ceresin wax at moderate source thicknesses. This they successfully correlated to the observed backscattering from the two materials, and Glendenin and Solomon (58) likewise noted a displacement of self-absorption curves for S^{35} in $CaSO_4$, $BaSO_4$, $PbSO_4$.

The work of Collie et al. (32) gave further evidence both on Z-dependence, and on the contribution of back-scattering and side-scattering within the source material to the total self-absorption observed. They found it possible to obtain semi-quantitative agreement with experiment by constructing a self-absorption curve from empirical external absorption curves (with maxima) and empirical back-scattering curves obtained for the source material in separate experiments.

Finally the dependence of source material atomic number was again demonstrated in the work of Nervik and Stephenson (106) which

also showed very effectively that self-scattering effects could dominate over absorption effects, and produce observed specific activities 30 percent higher than the true value with high-energy β-emitters and high Z source materials. They published curves of self-absorption-scattering effects for a range of β-emitters with end-point energies from 0.167 Mev to 2 Mev, each mounted in NaCl and in $Pb(NO_3)_2$. All the curves gave evidence of a rise to "saturation scattering" in the first 5 mg/cm^2 of source superficial density (cf back-scattering 153) and it was not until higher superficial density values that absorption became more or less important according to beta-energy. The scattering effects in $Pb(NO_3)_2$ were about 1.5 times larger than in NaCl as expected.

The dependence of the self-absorption factor observed on the counting geometry of the counter system (described above) has been discussed theoretically by Reid et al. (114, 115). The expression for the activity observed at an angle θ to the normal has already been given (equation (59)). If one integrates over the cone of half angle ⊕ representing the solid angle over which radiation from a point source is detected (ie. representing the effective counting geometry) the specific activity observed under these conditions with a source thickness, d, is given by

$$a_{\oplus,d} = 2\pi \int_0^{\oplus} a_{\theta,d} \sin\theta \, d\theta \qquad \ldots\ldots(60)$$

where $2\pi \sin\theta \, d\theta$ is the solid angle element of integration. Substituting for $a_{\theta,d}$ and replacing a_o by a'_o the "specific activity per unit solid angle"

$$a_{\Theta,d} = \frac{1}{2}\int_0^{\Theta} \frac{a'_o \cos\theta}{\mu d}\left(1 - e^{-\mu d/\cos\theta}\right) \sin\theta \, d\theta \qquad .....(61)$$

which Reid et al. (115) expand to give

$$\frac{a_{\Theta,d}}{a'_o} = \frac{1}{2}\left[e^{-\mu d} - \mu^2 d^2 + \frac{\mu^3 t^3}{2.2!} - \frac{\mu^4 t^4}{3.3!} + \ldots\right]$$

$$- \frac{1}{2}\left[\cos\Theta \, e^{-\mu d/\cos\Theta} - \mu d \ln\cos\Theta - \frac{\mu^2 d^2}{\cos\Theta} + \ldots\right]$$

$$.....(62)$$

The expected variation of self-absorption with geometry predicted by equation 62 was checked against experiment by Yankwich et al. (150). They obtained data for C^{14} and S^{35} in geometrics ranging from 7.6 to 20.5 percent of 2π steradians. The results however failed to show the predicted 20 percent difference in self-absorption over this range, and indeed showed no effect greater than the scatter due to mounting and counting errors. This may possibly have been due to the experimental conditions not corresponding to those assumed in the calculations, ie. a point source of thickness such that the cosine θ radiation distribution is established.

A more rigorous check on the affect of geometry was made by Baker and Katz (5). They first obtained self-absorption curves in a geometry approaching 4π steradians obtained by an array of G.M. tubes arranged round the sample. The curves were found to be well described by the simple self-absorption formula (equation (55)), over the source thickness range 0-500 mg/cm^2 with beta energies in the range 1 to 3 Mev, and not an expression of the form of equations (60) and (61) nor the result (equation (62)) obtained by Reid et al. The values of $\mu_{S.A.}$ obtained from these curves were found, along with those of Broda et al.

(22) whose counting geometry had approached 2π steradians (using a cylindrical G-M tube) to satisfy the relation

$$\mu = 0.0155\ E_m^{-1.41} \qquad .....(63)$$

where E_m, the madimum energy of the beta spectrum, is in Mev, and μ in cm^2/mg.

Baker and Katz then investigated self-absorption phenomena observed in a system of very small geometry G. The angular distribution of radiation was first examined as a function of source thickness and was found to be isotropic at low source thicknesses and a cosine distribution at higher thicknesses as described earlier (39). They then obtained from these curves a plot of the ratio $\frac{a_{0,d}}{\bar{a}_d}$ against d, where $a_{0,d}$ is the limit for small θ of $a_{\theta,d}$ the counting rate in small geometry at an angle θ to the normal and source thickness d, and $\bar{a}_d$ is the counting rate at this geometry averaged over all angles

$$\bar{a}_d = \frac{1}{2\pi} \int_0^{\frac{\pi}{2}} a_{\theta,d}\ 2\pi \sin\theta\ d\theta \qquad .....(64)$$

cf. (60)

$\bar{a}_d$ being related to the total number of beta particles leaving the source surface

$$Ad = \bar{a}_d\ (4\pi/G) \qquad .....(65)$$

G, the solid angle, being in radians. If d the source thickness were expressed in terms of R the maximum range of the beta particles in the source materials, curves of $a_{0,d}/\bar{a}_d$ were found to be superposable for different beta energies, and the ratio was observed to reach a value of 2 at values of $d > 0.2$ R, corresponding to an adoption of cosine θ radiation-distribution at or above this d-value.

A comparison of self absorption curves for 4π steradian and very small counting geometry normal to the source then showed that the former was represented by

$$f_{4\pi} = \frac{1 - e^{-\mu d}}{\mu d} \qquad .....(66)$$

and the latter by

$$f_o = \frac{a_{0,d}}{\bar{a}_d} \cdot \frac{(1 - e^{-\mu d})}{\mu d} \qquad .....(67)$$

ie. the product of the 4π-steradian function, and the anisotropy function plotted earlier. More generally for any counter geometry G_Θ given by

$$G_\Theta = 2\pi(1 - \cos \Theta) \qquad .....(68)$$

one has $$f_\Theta = \frac{1}{(1 - \cos \Theta)} \frac{1 - e^{-\mu d}}{\mu d} \int_o^\Theta \frac{a_{\theta,d}}{\bar{a}_d} \sin \theta \, d\theta \qquad .....(69)$$

For $\theta \dashrightarrow o$ this reduces to equation (67).

It is seen that, since the factor $a_{\theta,d} / \bar{a}_d$ has a value of 2 for d values in excess of 0.2 R, extrapolating the curve of equation (66) to zero d from counting values obtained at d values greater than this will lead to a corrected apparent disintegration-rate value twice the true value. This may be seen by factoring out of equation (69) the θ-dependent part and substituting for $a_{\theta,d}$

$$a_{\theta,d} = a_{0,d} \cdot \cos \theta \qquad .....(70)$$

from the cosine distribution at $d > 0.2$ R to give

$$S = \frac{1}{1 - \cos \theta} \int_o^\theta \cos \theta \sin \theta \, d\theta$$

$$= \frac{\sin^2 \theta}{1 - \cos \theta} \qquad .....(71)$$

The value of S varies from unity at $\theta = \frac{\pi}{2}$ (2π steradian geometry) to 2 at small angles (geometry approaching zero) and will have intermediate values in between.

The failure of Baker and Katz to obtain better agreement between their data and the result of the integration of equation (61) may have been due to the poor approximation of their geometry to 4π steradians or to an incorrect or approximate integration procedure (they do not quote their final expression). A rigorous integration procedure is given by Gora and Hickey (60) and they report agreement between the result and data obtained by them and by Yankwich et al. (150, 151). Their starting integral

$$a_{\Theta,d} = \frac{1}{\Omega_\Theta}\int_0^\Theta \frac{a_o \cos\theta}{\mu d}\left(1 - e^{-\mu d/\cos\theta}\right) d\Omega \qquad .....(72)$$

is analagous to equation (61) except that the volume element is written as $d\Omega = 2\pi \sin\theta \, d\theta$

and the expression is divided through by

$$\Omega_\Theta = 2\pi(1 - \cos\Theta)$$

so that $a_{\Theta,d}$ becomes a_o, the observed counting rate in a cone of half angle Θ when $d = 0$, ie. for an "infinitely thin" source with zero self-absorption. If λ is written for μd and $y = \frac{\lambda}{\cos\theta}$ equation (72) becomes

$$a_{\Theta,\lambda} = \frac{a_o\lambda}{1 - \cos\Theta}\int_\lambda^{\frac{\lambda}{\cos\Theta}} \frac{(1 - e^{-y})}{y^3}\, dy \qquad .....(73)$$

$$= a_o f(\Theta,\lambda) \qquad .....(74)$$

where $$f(\Theta,\lambda) = F(\lambda) - \cos\Theta \, F\left(\frac{\lambda}{\cos\Theta}\right) \qquad .....(75)$$

and $$F(\lambda) = \frac{1}{2}\left[\frac{1 - e^{-\lambda}}{\lambda} + e^{-\lambda} + \lambda\, Ei(-\lambda)\right] \qquad .....(76)$$

The exponential integral function

$$Ei(-\lambda) = -\int_{\lambda}^{\infty} \frac{e^{-t}}{t}\, dt$$

has been tabulated (78).

The limiting cases of this result are as follows.

$\lambda \dashrightarrow 0$, ie. small μ or d

$$F(\lambda) \sim 1 \qquad f(\theta,\lambda) \sim 1 \qquad a_{\theta,\lambda} = a_o$$

ie. no absorption effects

$\lambda \gg 1$, ie. d large

$$F(\lambda) \sim \frac{1}{2\lambda}$$

$$f(\theta,\lambda) = \frac{\frac{1}{2\lambda} - \frac{(\cos^2\theta)}{2\lambda}}{1 - \cos\theta}$$

$$= \frac{1 + \cos\theta}{2\lambda}$$

ie. $f(0,\lambda) = 1/\lambda$ and $f(\frac{\pi}{2},\lambda) = \frac{1}{2\lambda}$

Thus from equation (74) it is seen that the observed specific activity $a_{\theta,\lambda}$ should decrease about twice as quickly with increasing d in a 2π steradian geometry as in a narrow angle geometry, a result similar to that observed experimentally by Baker and Katz. Gora and Hickey point out that this result means that a value quoted for $\mu_{S.A.}$ for a particular nuclide is not meaningful unless the geometry for which it is measured is stipulated. These authors provide data obtained with a 2π steradian and narrow angle geometry, and these are observed to agree well with the

self-absorption curves for the geometries quoted. This is despite the fact that (a) the computations were based on the usual assumption of exponential absorption and (b) they took no account of self-scattering processes, unless the cosine θ radiation distribution corollary of the exponential absorption rule can be considered to do so.

The 4π-counter

In the field of 4π-counting, very little attention has been paid to self-absorption losses. This again may have been due to the fact that until recently, these losses were considered less serious than other errors to which the method has been subject.

Meyer-Schützmeister and Vincent (100) were aware of the extent of self-absorption in S^{35} sources however. Their method of source mounting (vacuum-drying of solutions) produced crystals of 2-3 μ in diameter. If the material was deposited so as to be concentrated into one crystal of 20 μ diameter the observed activity was observed to be lower by 30 percent. In order to allow for self-absorption, the authors assumed the crystals to be spherical in shape and computed radiation absorption using a value of μ from external absorption measurements, assuming absorption to be exponential. Corrections were usually of the order of 4 percent.

Hawkings et al. (68) proposed a better method of correcting for, or rather ensuring the absence of, significant absorption effects. Their procedure was the progressive dilution of the stock solution from which sources were prepared, until a constant specific activity (after correction for the dilution) was observed. Alternatively an

extrapolation of a plot of the logarithm of the counting-rate against the aliquot used could be extrapolated to infinite dilution. This method applicable in general to high specific activity materials only, is however not infallible. Material from dilute solution will, unless elaborate precautions are taken, in general crystallize into local aggregates and even with precautions, crystal size cannot be reduced indefinitely. Thus self-absorption may still be significant, and further dilution will not necessarily produce an improvement in the situation.

A recent paper by Seliger and Schwebel (130) emphasizes the importance of the method of source preparation. Different methods of mounting Sr^{90} were found to give sources differing in counting-rate by 5 percent, and similar but larger effects were found for Co^{60}, mounted by evaporation of a solution with and without prior precipitation by ammonia. Micrographic examination of even the best residues showed clumping of source material. No systematic attempt was made to determine and correct for absorption losses, such corrections as were made being mostly quite arbitrary.

Thus the subject of the determination and correction for self-absorption in the 4π-counter is virtually untouched.

The calculations of Gora and Hickey may be carried over into a counting geometry of 4π steradians. The absence of consideration of scattering effects is less serious here since, as was pointed out in section A, any modification of radiation distribution due to scattering processes is without effect on the measured disintegration-rate (all emerging particles being counted). Only those particles which are

absorbed before being counted, either in the source material or source mount, will not be registered. The assumption of exponential absorption however is liable to be more important, since the results of section C clearly indicate that absorption of beta-radiation of a range of energies is not exponential over the first 300 $\mu g./cm^2$ of absorber, the region in which we shall be interested.

Equation (72) and its solution apply directly to the 4π steradian geometry since $a_{\frac{\pi}{2},d}$ bears the same relation to a_o (the rate of emission of particles into the cone of half angle $\frac{\pi}{2}$ radians, ie. a hemisphere, in the absence of absorption effects) as does $a_{\pi,d}$ to N_o, the total disintegration rate. Thus the values of $f(\frac{\pi}{2},\lambda)$ and of $F(\lambda)$ computed by Gora and Hickey may be used directly.

The problem of correcting for self-absorption in a precise way divides itself into two parts.

(a) The preparation of samples of radioactive material in a uniform and reproducible form.

(b) The determination of the extent of absorption in the sample so produced as a function of its measured superficial density, and consequent correction of the observed disintegration-rate.

We shall discuss each in turn.

2) EXPERIMENTAL TECHNIQUES AND RESULTS

(a) Source Preparation

The methods of sample mounting used in conventional counter systems, mostly involving manipulations of material in the solid state, are inapplicable to the case of a 4π-counter. This follows from the use of very thin and comparatively fragile plastic films for the source

mount, replacing the filter paper or metal tray ordinarily used. Handling of solids in the form of slurries is likewise unsatisfactory, since these tend to form large aggregates, or tear the film on drying.

The usual method of mounting 4π-counter sources then is by evaporation of a suitable aliquot of a stock solution (68, 100, 113). However as mentioned above, such an evaporation procedure will usually lead to local agglomerates of crystals (most often at the periphery of the original drop) rather than an even layer of material. This is especially the case when the source-mounting film is particularly hydrophobic like VYNS, and under these conditions self-absorption effects will be neither minimal nor reproducible.

A more evenly spread deposit is obtained (88) if the surface of the film is rendered hydrophilic ie. by treatment with a solution of a protein such as albumin or insulin (90, 91, 126). Under these conditions the deposit is distributed over a wider area, and is more uniform in a macro sense. However the actual crystal sizes obtained are still quite large and very variable.

The vacuum evaporation of solutions, as used by Meyer-Schützmeister and Vincent (100), certainly produces smaller crystal sizes. However when used with the 5-10 $\mu g./cm^2$ VYNS films in our apparatus (described earlier), this method is found to produce numerous tears in the film under the source, due probably to the expansion of the droplet on freezing under the conditions of rapid evaporation.

An improved method of source preparation is therefore required and a suitable technique appears to be the use of vacuum distillation of source material directly on to the film, starting with solid material.

As a method of producing thin even layers of metals and salts, this is of course both of long-standing and widespread employment (75). Its use in this laboratory to coat VYNS source-mounting films with gold has already been described. Further it has already been used to mount radioactive materials both for beta-spectrometry (90, 112) and in 4π-counters (69, 124). However a more systematic application of the method seemed desirable.

The apparatus used by us is shown diagrammatically in Figure 33 and in photographs in Figure 34. The furnace section consists of a vacuum jacket of pyrex glass containing a platinum crucible A. This contains a charge C of radioactive material to be distilled, and is heated by means of a radio-frequency induction coil B. This coil consisted of 12 turns of number 20 gauge copper wire, coated with poly-tetrafluorethylene (teflon), in order that the insulation between turns should be unaffected by heating (by radiation from the interior of the furnace) to 200 to 300°C. *

The temperature of the crucible is measured by means of a Chomel-Alumel thermocouple D and millivoltmeter. About 1 cm. from the mouth of the crucible is positioned an aluminum mask E with a central circular aperture of 1 cm^2 area. Immediately behind this is placed the source mounting film F.

The lower end of the furnace is connected, via two liquid-nitrogen cooled traps in series to remove any activities carried in the

---

* The author is indebted to Mr. S. Fromson of Canadian Vickers Ltd. who prepared the wire from which the induction coil was made.

Figure 33

Radio-frequency Induction Vacuum-Furnace (diagrammatic)

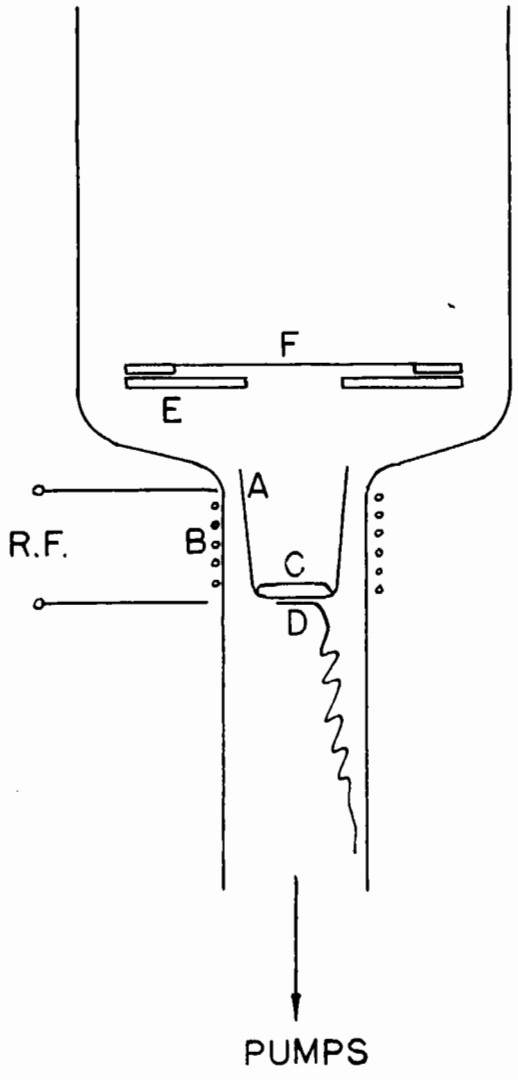
F
E
A
R.F.
B
C
D
PUMPS

Figure 34

Vacuum Distillation Apparatus

(a) General view, with radio-frequency generator to the right, and millivoltmeter indicating furnace temperature at centre. Vacuum system is to the left.

(b) Detailed view of vacuum system. Furnace chamber is to the left, double liquid air traps central, and the McLeod gauge to the right.

(a)

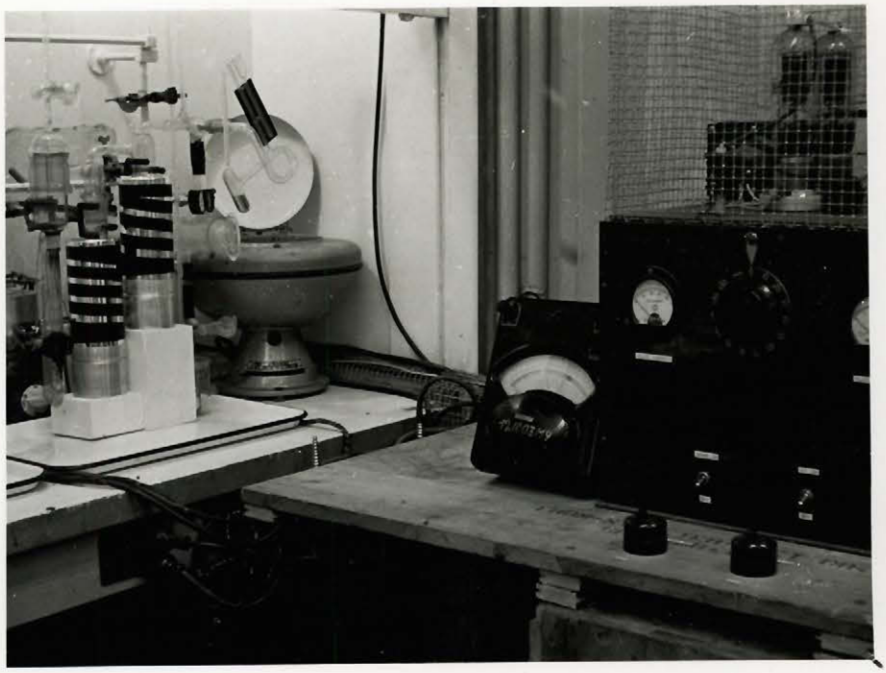

(b)

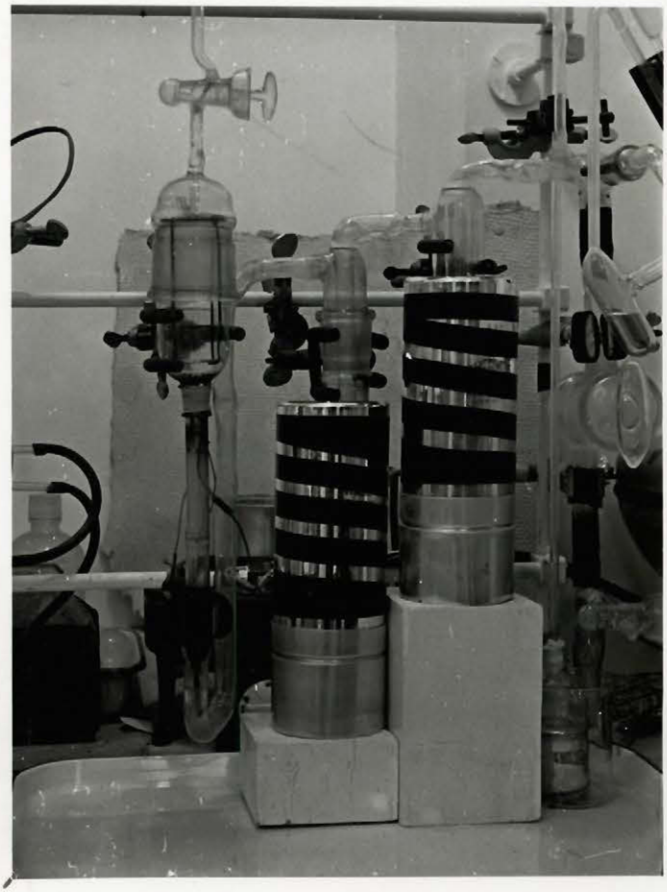

gas phase, to a rotary pump capable of maintaining a pressure in the system of 0.1 μ Hg. The exhaust from the pumping system was finally vented into the fume hood as a further precaution. Controlled crucible temperatures up to 900°C are at present attainable, and a mounting film shows no sign of deterioration in proximity to the hot crucible under vacuum after 10 minutes. The crucible is cooled nearly to room temperature before the system is opened by venting a small air leak above the furnace, and allowing air to be pumped past the heated surfaces.

The deposits produced in the arrangement at present in use are found to be precisely defined in area, and very uniform. The latter condition is demonstrated by a single interference colour (viewed by reflection) being seen across the diameter of the deposit (cf. section C of this thesis) and a uniformity of better than $\pm$ 1 percent is indicated by spectrophotometric measurements (see later).

The appearance of changing interference colours in light reflected from the reverse face of the film as the deposit increases in thickness is a very sensitive index of the state of progress of the distillation. Colourless materials or layers of coloured materials so thin as to be invisible by transmitted light can clearly be seen and controlled in this way.

Of the materials that can be successfully distilled with the temperature range and pressure at present available to us, compounds containing large organic groupings have been found to be the most suitable. Such compounds can be readily prepared for a number of radioactive species, and these are found to be readily volatile (under the pressure quoted) at moderate crucible temperatures, and produce a

deposit of which the weight and composition do not alter appreciably on prolonged exposure in moist air.

Providing reasonably close ($\pm$ 10°C) temperature control during the distillation is maintained, charring is not a problem. These compounds are generally of low $\overline{Z}$, and also frequently show optical absorption bands in the visible or near-visible region which are useful in estimating the (usual) absence of, or extent of, decomposition (should this inadvertently occur) during distillation, and more especially in measurement of deposit thickness by optical means. This can be used as a quantitative transference or aliquoting method.

In this section we shall be concerned with measurements on Ni^{63}, S^{35}, and Co^{60}. For preparing sources of these materials we have employed nickel dimethylglyoxime, benzidene sulphate, and cobalt α-nitroso-β-naphthol respectively (the $\overline{Z}$ values in these cases being 4.19, 4.91 and 4.48 respectively). These compounds were prepared from solutions of the appropriate nuclide, to which isotopic carrier had been added where necessary, by the standard methods of gravimetric analysis modified where necessary. The actual procedures used were as follows:

(i) Nickel Dimethylglyoxime

To the slightly acid Ni^{63} solution was added a two-fold excess of 1 percent alcholic dimethylglyoxime, followed by a slight excess of ammonia. The precipitate was centrifuged, and washed three times with water. It was finally slurried with water and transferred to the platinum crucible, being subsequently dried by infra-red irradiation. Distillation was found to proceed satisfactorily at a crucible tempera-

ture of 250°C under a pressure of less than 1 μ Hg.

(ii) Benzidene Sulphate

To the neutral or slightly acid S^{35} solution, containing the sulphur activity as sulphate, was added a slight excess of 1 percent aqueous benzidene hydrochloride. The precipitate was allowed to age for 15 minutes, after which it was centrifuged and washed three times with water. Slurrying, transfer to the crucible and drying were then effected as before. Distillation was found to proceed satisfactorily at 360°C under 1 μ Hg. pressure.

(iii) Cobalt α-Nitroso-β-naphthol

To a weakly acid solution of Co^{60} were added 10 drops of 30 percent hydrogen peroxide, followed by 2 M sodium hydroxide to slight excess. The cobaltic hydroxide precipitate was redissolved with heating in glacial acetic acid, and the solution diluted 10-fold with boiling water. Excess of a solution of α-nitroso-β-naphthol in 50 percent acetic acid was then added and the precipitate centrifuged and washed three times with boiling water. Slurrying, transfer to the crucible, and drying were effected as before, and distillation proceeded satisfactorily at 200°C under 1 μ Hg. pressure.

Figure 35 (a), (b) and (c) shows absorption spectra obtained from these deposits using a Beckman D.U. spectrophotometer balanced against a film identical with that used as a mount. In Figure 35 (a), two spectra of nickel dimethylglyoxime are presented, one for the solid deposit, the other for the starting material in a colloidal solution protected with gelatin. These are seen to be identical apart from the absence, in the case of the solid deposit, of the background of scattered

Figure 35 (a)

Absorption Spectra Obtained From Vacuum Distilled Material

Nickel Dimethylglyoxime

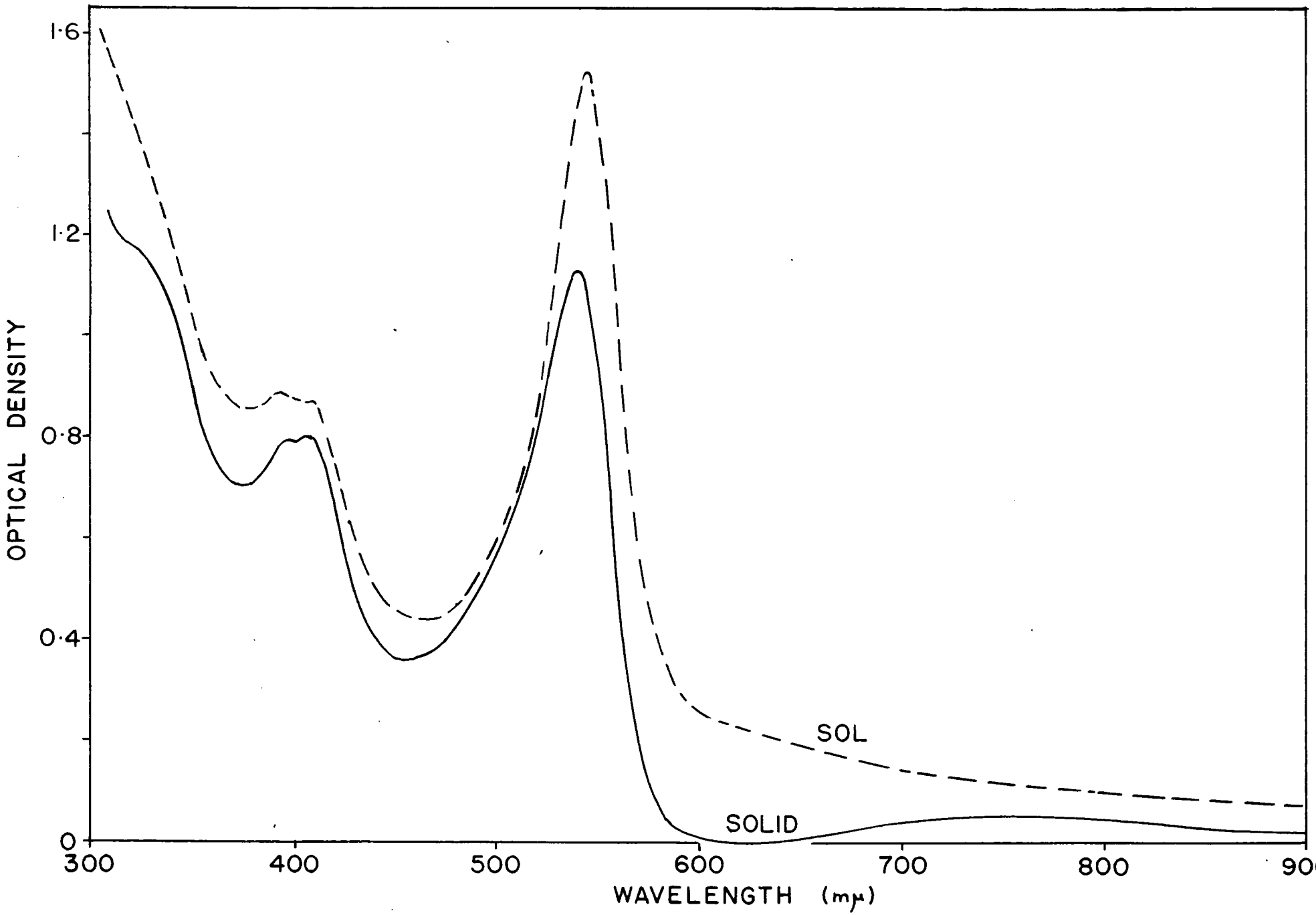
1·6
1·2
0·8
0·4
0
OPTICAL DENSITY
300
400
500
600
700
800
900
WAVELENGTH (mμ)
SOL
SOLID

155a

Figure 35 (b)

Absorption Spectra Obtained From Vacuum Distilled Material

Benzidene Sulphate

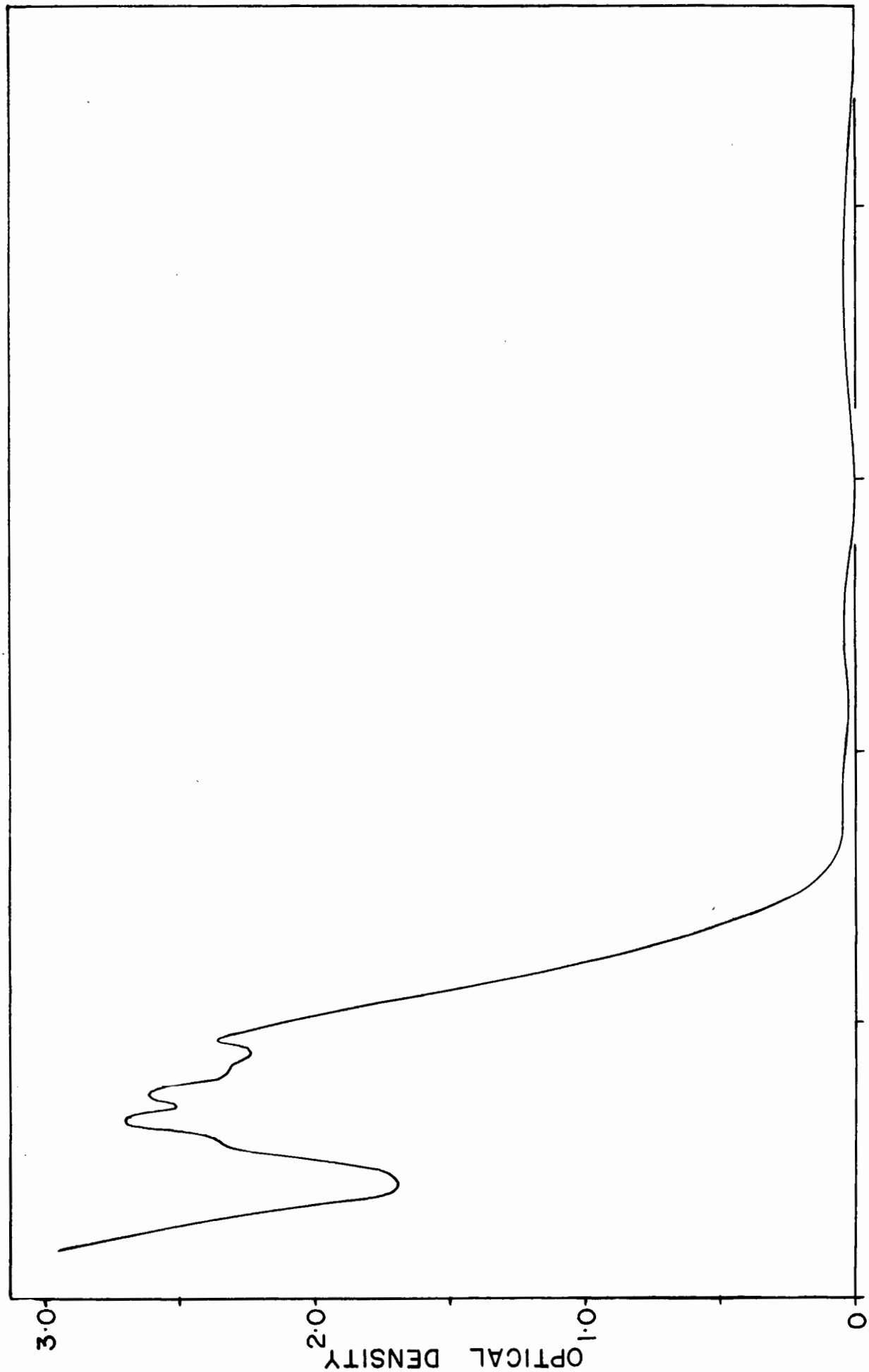
OPTICAL DENSITY
3.0
2.0
1.0
0
200
300
400
500
600
WAVELENGTH (mμ)

Figure 35 (c)

Absorption Spectra Obtained From Vacuum Distilled Material

Cobalt α-nitroso-β-naphthol

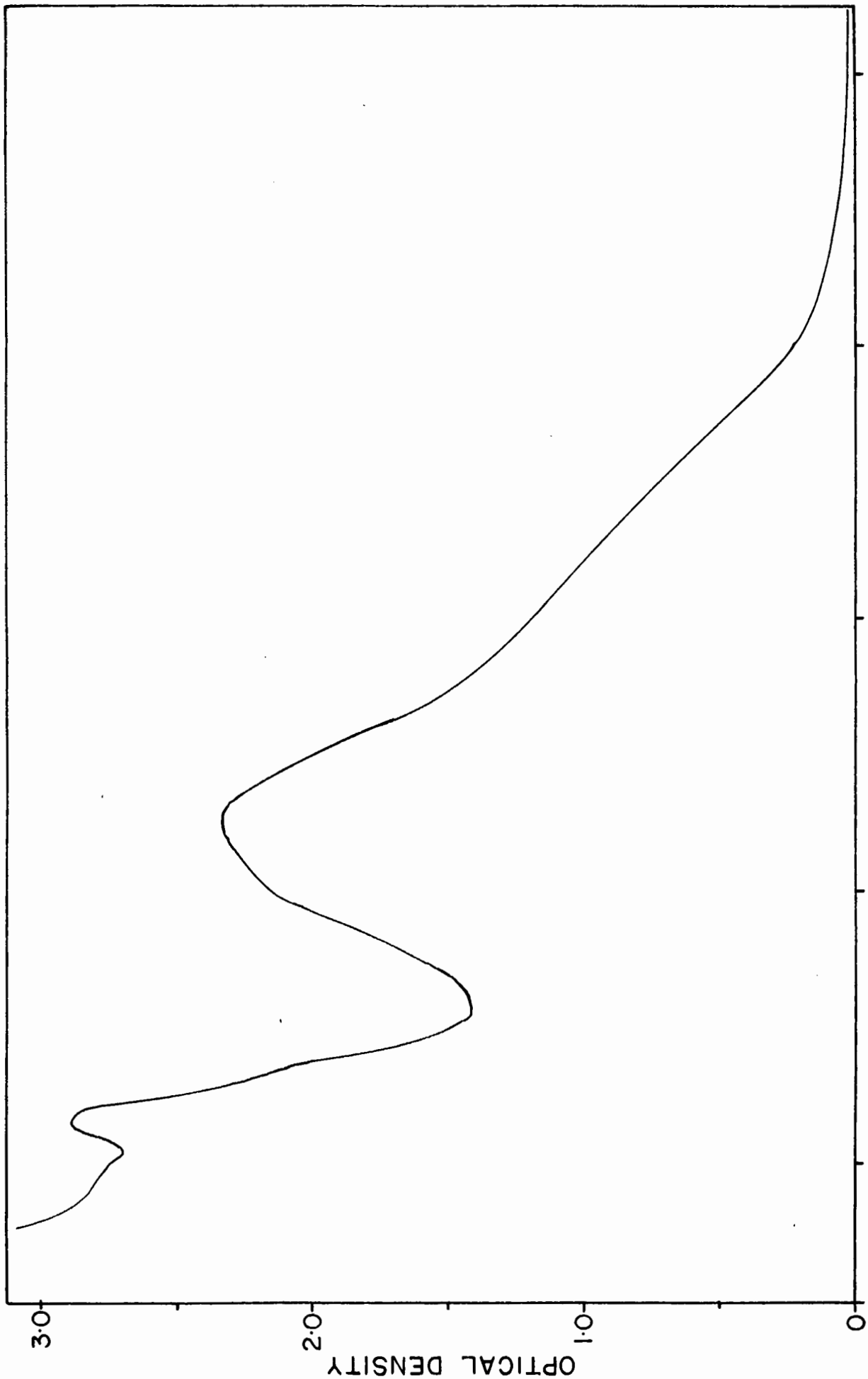
OPTICAL DENSITY
3·0
2·0
1·0
0
300
400
500
600
700
WAVELENGTH (mμ)

light observed with the colloidal solution. This indicates that the nickel dimethylglyoxime at least distils without significant decomposition.

Clearly, aside from its application to the present problem, the mounting of material on thin films by this method will have applications in absorption spectrophotometry generally. It was seen in Figure 25 that the spectrum for 5-10 $\mu g./cm^2$ VYNS film exhibits no absorption peaks in the wavelength region studied and will not interfere with spectrophotometric measurements in this wavelength range. (In parts (a), (b) and (c) of Figure 35, compensation was made for the film spectrum) Thicker films however will not be so convenient as interference effects become important.

We have used photospectrometric measurements for a rapid and accurate means of thickness calibration of the deposits obtained by distillation. The wavelengths of light used were selected with regard to the position of peaks observed in Figure 35, the sensitivity required, and the limits of accuracy imposed by the means of gravimetric calibration presently available to us.

Figure 36 shows curves of optical transmission of the deposits of the three materials studied (corrected for film transmission) against deposit superficial density. Over their initial portions, the curves are seen to be approximately exponential in accordance with Lambert's law.

In Figure 37 we compare the deposits obtained by the three mounting methods investigated. Figure 37 (a) shows a photo-micrograph of the result of evaporating under infra-red irradiation a solution of

Figure 36 (a)

Optical Transmission of Vacuum Distilled Material, as a Function of Deposit Superficial Density

Nickel Dimethylglyoxime

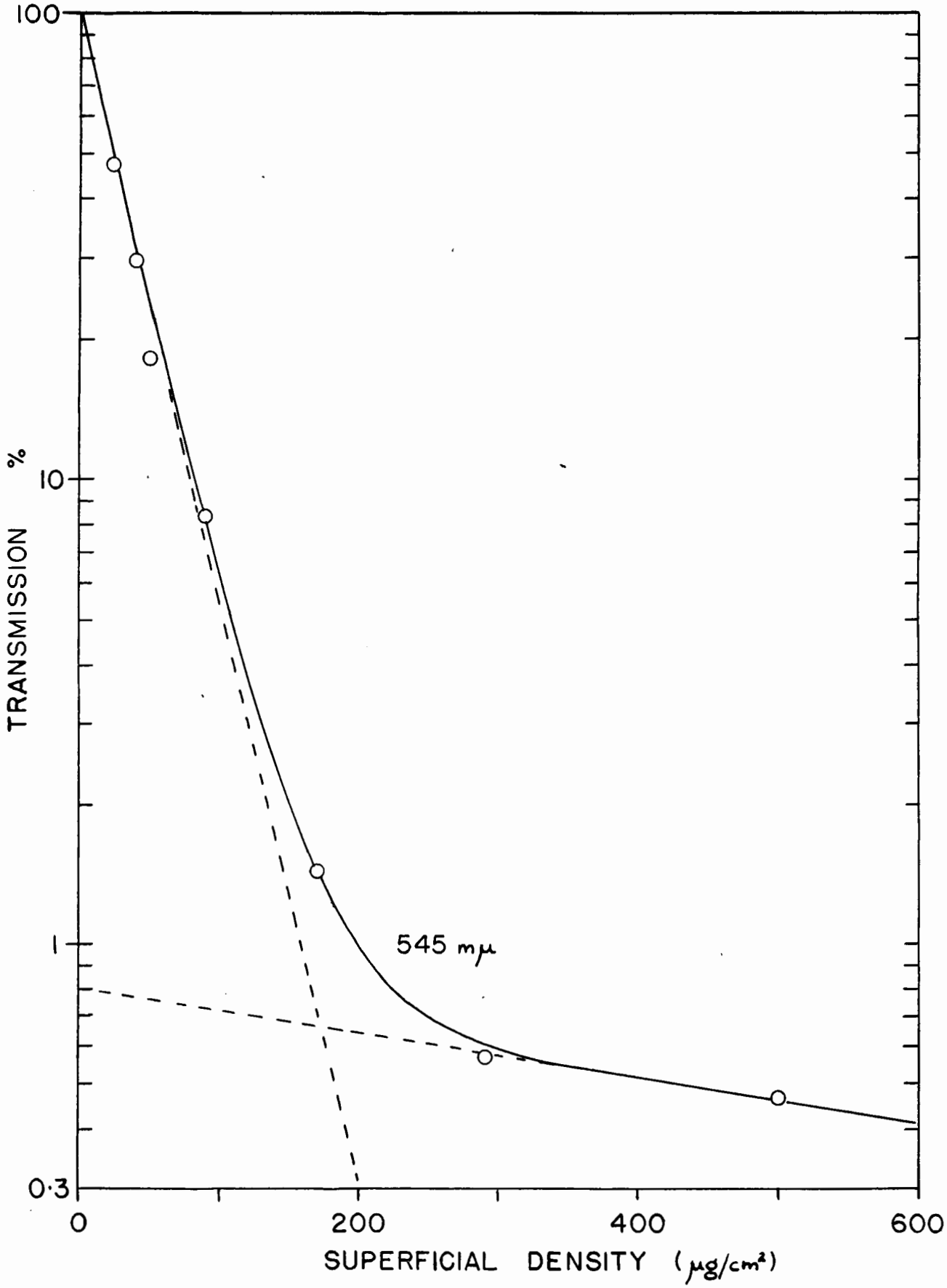
100
10
1
0·3
TRANSMISSION %
545 mμ
0
200
400
600
SUPERFICIAL DENSITY (μg/cm²)

Figure 36 (b)

Optical Transmission of Vacuum Distilled Material, as a Function of Deposit Superficial Density

Benzidene Sulphate

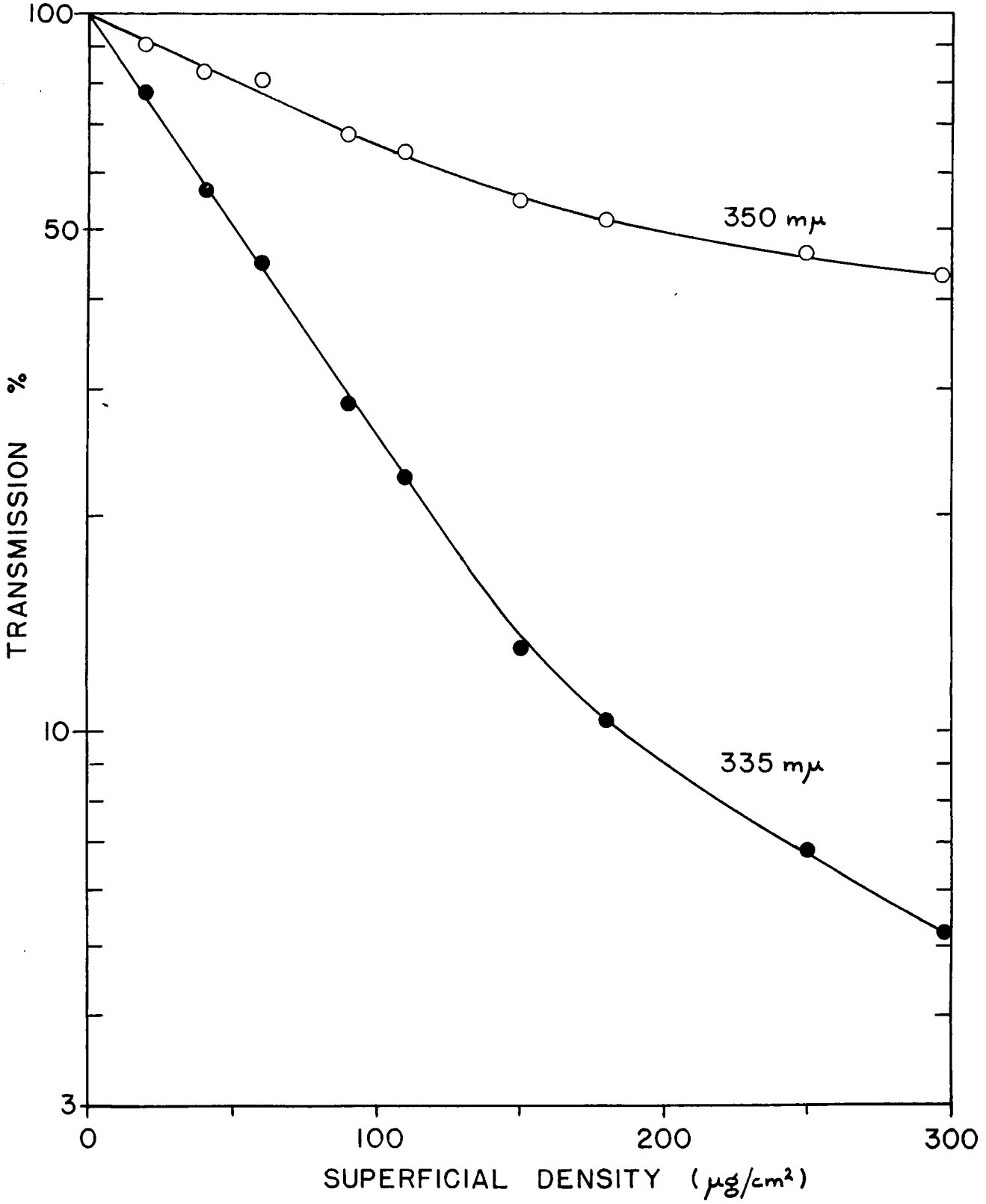
100
50
10
3
TRANSMISSION %
350 mμ
335 mμ
0
100
200
300
SUPERFICIAL DENSITY (μg/cm²)

Figure 36 (c)

Optical Transmission of Vacuum Distilled Material, as a Function of Deposit Superficial Density

Cobalt α-nitroso-β-naphthol

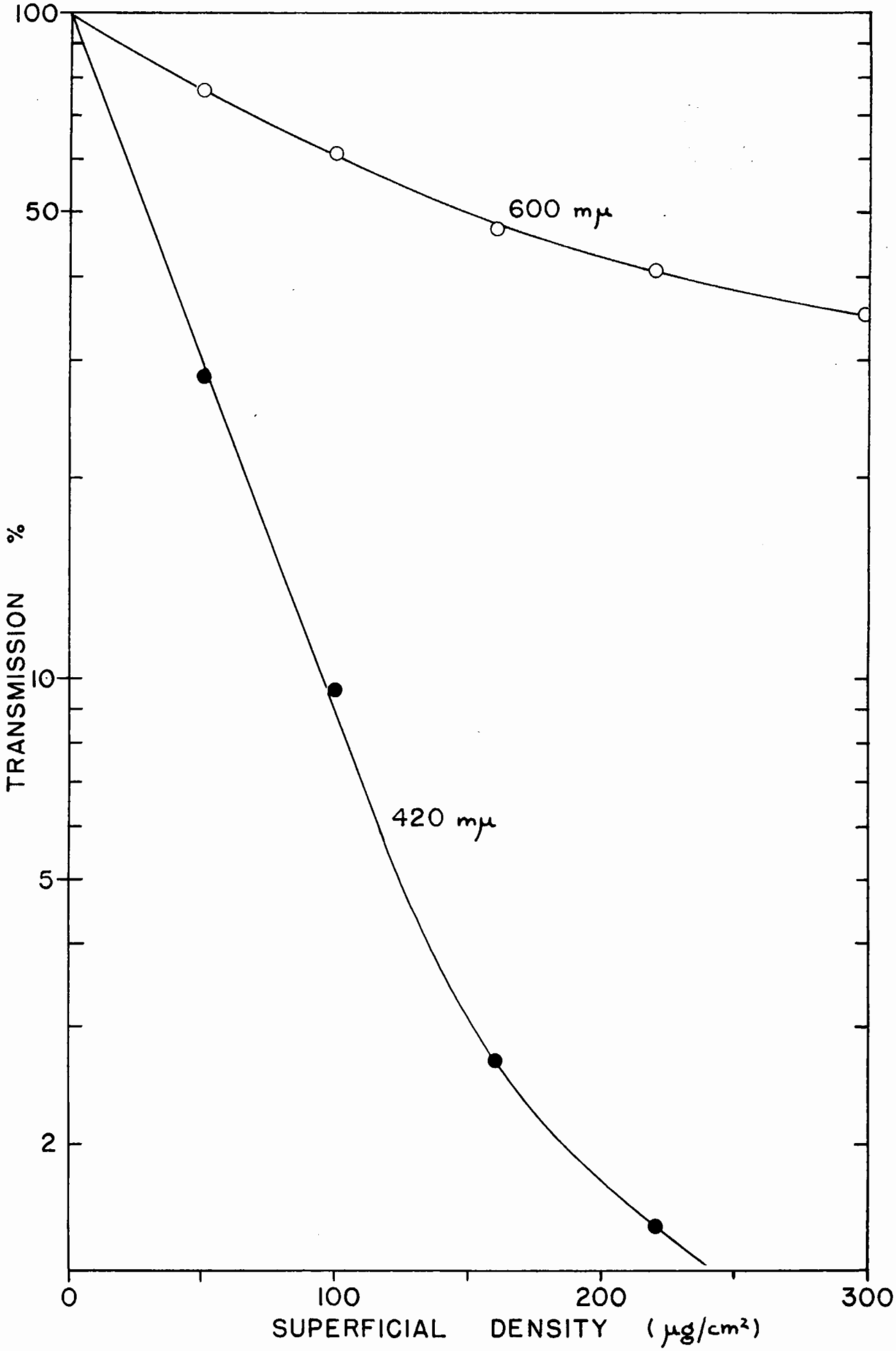
100
50
10
5
2
TRANSMISSION %
600 mμ
420 mμ
0
100
200
300
SUPERFICIAL DENSITY (μg/cm²)

Figure 37

Microstructure of the Results of Various Source-mounting Techniques

(a) Photomicrograph (x 20) of deposit from evaporation of Na_2SO_4 solution on 5 $\mu g./cm^2$ VYNS film without insulin. Original periphery of drop is seen as thin line of deposit near top of picture.

(b) Photomicrograph (x 20) of deposit from evaporation of Na_2SO_4 solution on 5 $\mu g./cm^2$ VYNS film after wetting film with 5 percent insulin solution.

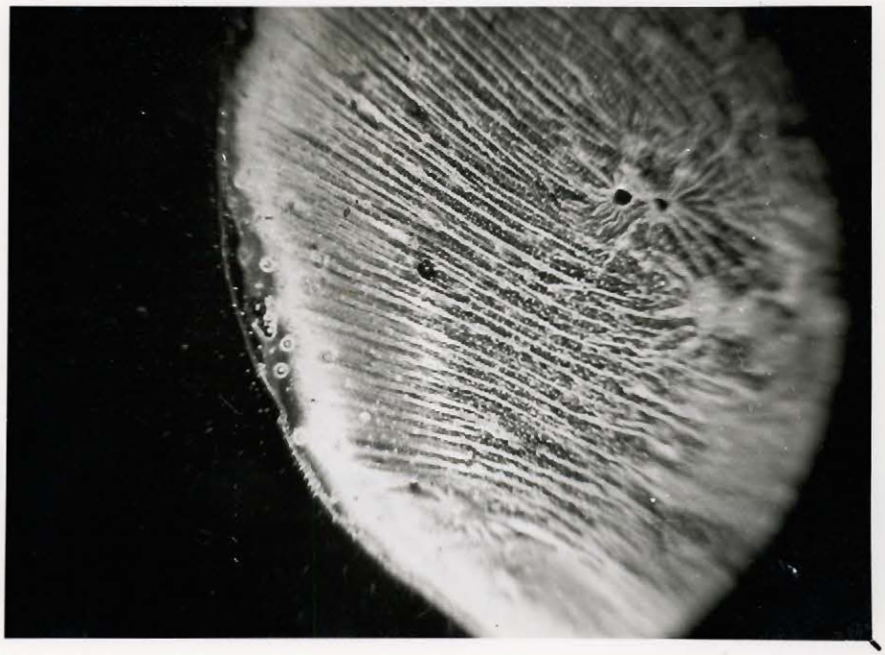

(b)

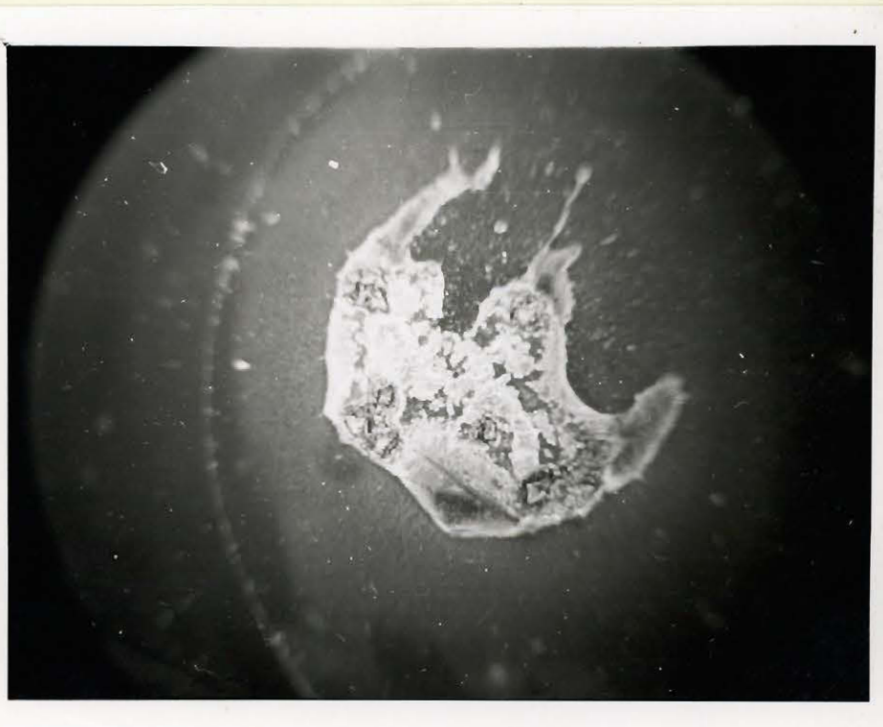

(a)

Figure 37

Microstructure of the Results of Various Source-mounting Techniques

(c) Electron micrograph (x 10^4) of deposit of cobalt α-nitroso-β-naphthol on VYNS film produced by vacuum distillation. Deposit superficial density 1.2 $\mu g./cm^2$.

(d) Electron micrograph (x 10^4) of deposit of nickel dimethylglyoxime on VYNS film produced by vacuum distillation. Deposit superficial density 5 $\mu g./cm^2$.

(d)

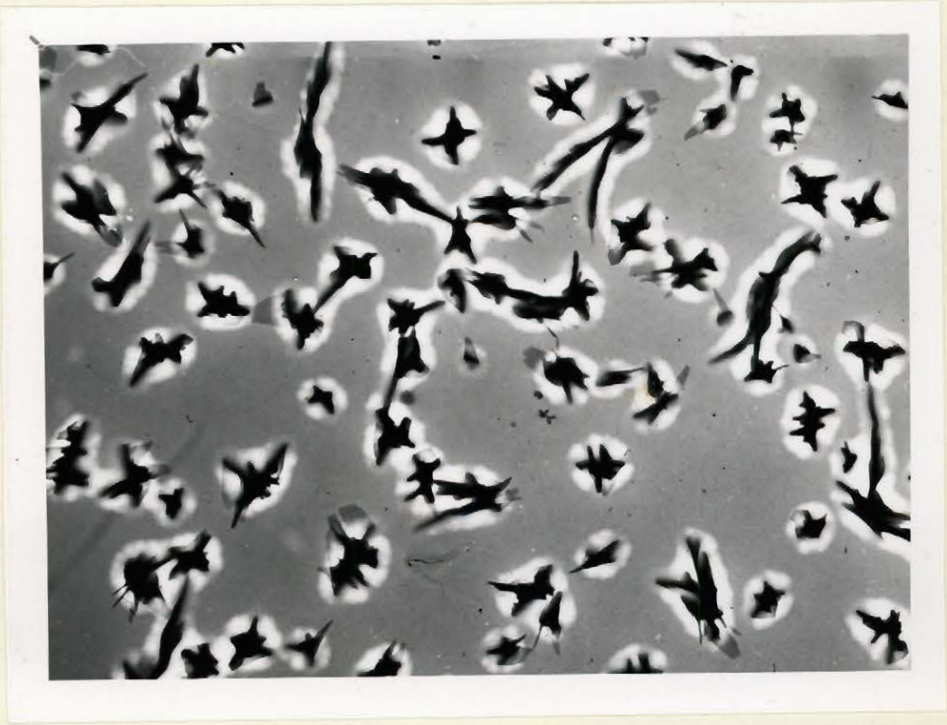

(c)

sodium sulphate without insulin on a film of 5 $\mu g./cm^2$ VYNS. Figure 37 (b) shows a photo-micrograph of the result of similar evaporation with prior treatment of the film with 5 percent insulin solution. The solid material is seen to be more evenly spread than in (a), but considerable irregularity still remains. Much of the solid material is concentrated into local aggregates but single crystals where they exist are needle-shaped of 30 to 100 μ in diameter. Figures 37 (c) and 37 (d) show electron micrographs of cobalt α-nitroso-β-naphthol at 1.2 $\mu g./cm^2$ superficial density and nickel dimethylglyoxime at 5 $\mu g./cm^2$ superficial density respectively. These pictures are representative of several taken over different areas of deposit all showing a uniform distribution of crystals of about 1 μ in diameter. It appears that this crystal size is maintained throughout the process of completion of successive crystal layers.

(b) Estimation of Self-Absorption

We shall in this section present preliminary data obtained for the self-absorption of Ni^{63}, S^{35} and Co^{60} in the compounds listed above. The results were obtained by a method analagous to that used by experimenters working with end-window counter systems. The counting-rate obtained with sources prepared by successive depositions from the same charge of radioactive material was measured as a function of deposit thickness, determined between 0 and 200 $\mu g./cm^2$ spectrophotometrically as described above and thence gravimetrically. From these data was computed the observed specific activity after each deposition, and this was plotted against source superficial density.

Figures 38 and 39 show the results so obtained. Figure 38 (a)

Figure 38

Self-absorption of Ni^{63}, in a 4π-geometry

(a) Source superficial density range 0-80 $\mu g./cm^2$

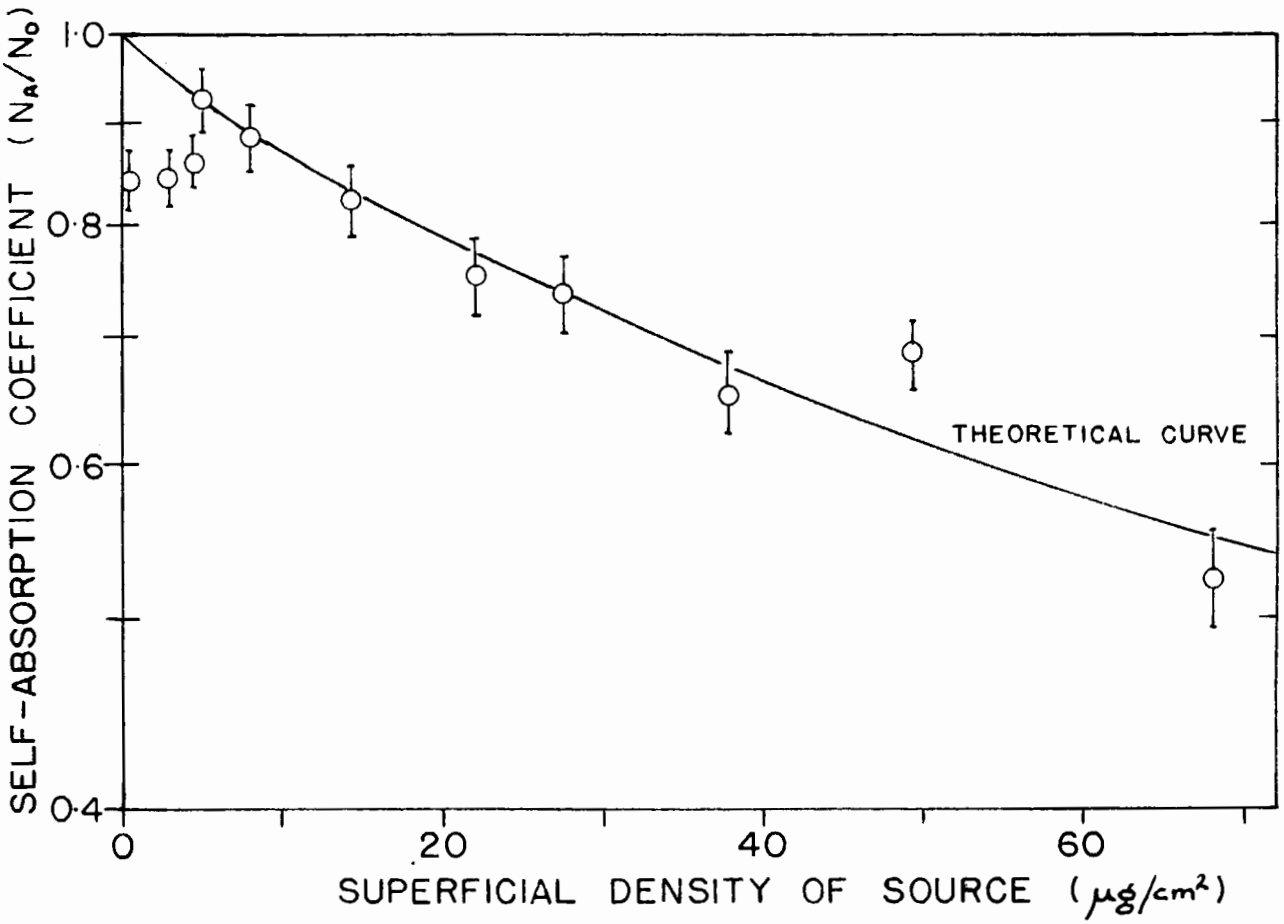
SELF-ABSORPTION COEFFICIENT (N_A/N_0)
1·0
0·8
0·6
0·4
0
20
40
60
SUPERFICIAL DENSITY OF SOURCE ($\mu g/cm^2$)
THEORETICAL CURVE

Figure 38

Self-absorption of Ni^{63}, in a 4π-geometry

(b) Source superficial density range 0-3 mg/cm^2

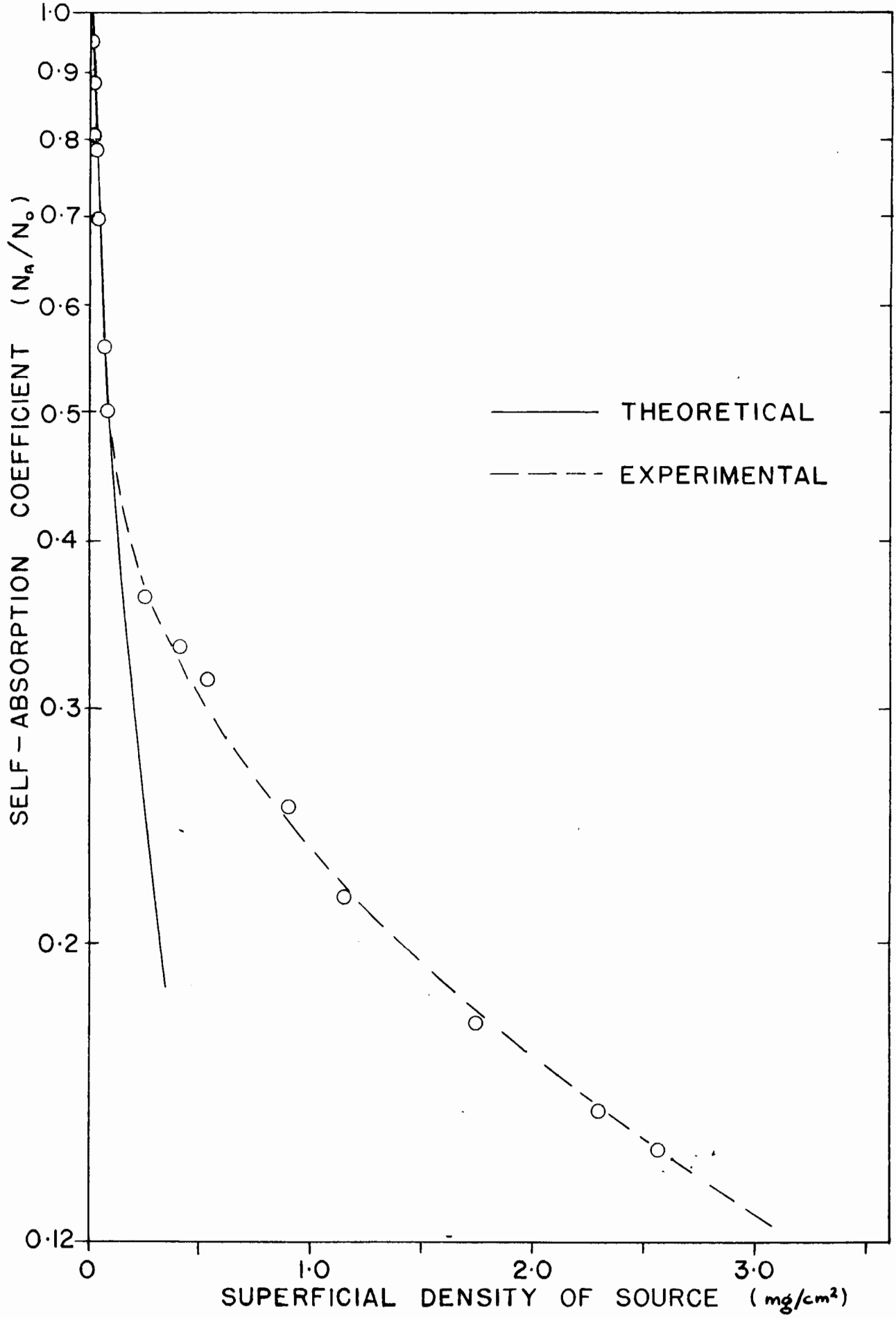
1·0
0·9
0·8
0·7
0·6
0·5
0·4
0·3
0·2
0·12
SELF-ABSORPTION COEFFICIENT (N_a/N_o)
THEORETICAL
EXPERIMENTAL
0
1·0
2·0
3·0
SUPERFICIAL DENSITY OF SOURCE (mg/cm²)

Figure 39

Self-absorption in a 4π-geometry of Ni^{63}, S^{35} and Co^{60};

Source Superficial Density Range 0-400 $\mu g./cm^2$

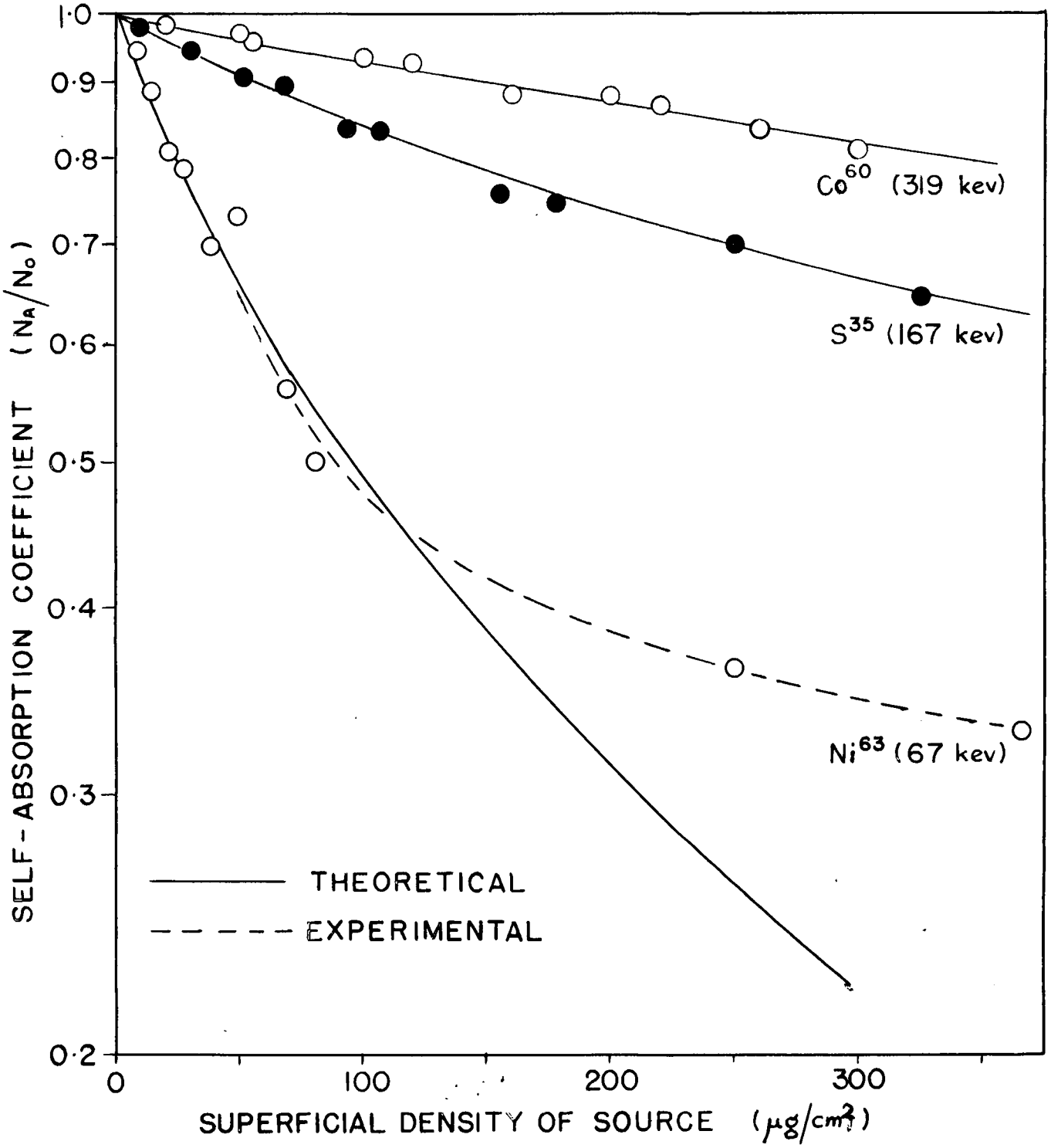
1·0
0·9
0·8
0·7
0·6
0·5
0·4
0·3
0·2
SELF-ABSORPTION COEFFICIENT (NA/No)
Co60 (319 kev)
S35 (167 kev)
Ni63 (67 kev)
THEORETICAL
EXPERIMENTAL
0
100
200
300
SUPERFICIAL DENSITY OF SOURCE (μg/cm2)

shows the data for Ni^{63} for a range of source superficial densities of 0-80 $\mu g./cm^2$. Figure 38 (b) shows the extension of the data to the range 0-3 mg/cm^2. Figure 39 compares the self-absorption of Ni^{63}, S^{35} and Co^{60} in the range of superficial densities between 0 and 300 $\mu g./cm^2$.

3) DISCUSSION

A relationship of the form obtained by Gora and Hickey (60) from the integration of equation (72), that is of the forms of equations (73) to (76), may be compared with the experimental results obtained by us in a 4π-geometry, if relationship (75) is evaluated for $\Phi = \frac{\pi}{2}$. Such equations have been fitted to the experimental data in Figures 38 and 39, the values of μ selected to give the best agreement being indicated in column 2 of table VI.

Agreement is seen to be satisfactory over the initial part of the curve where $\mu d < 0.6$. However, if one examines the results for Ni^{63} it is seen that at higher source thicknesses the self-absorption curve changes slope, in the sense that the data are now best fitted by a smaller μ-value. This effect is similar to that observed in the case of external absorption in a 4π-geometry with very thin absorbers, discussed in section E. There it will be seen that the external absorption data can be fitted to the sum of two curves derived from two different μ-values, and it is probable that a similar two component curve could be used in the case of Ni^{63} self-absorption. It is also likely that if the observations on the self-absorption of S^{35}, Co^{60} and emitters of more energetic radiation were continued to higher source-thicknesses

a similar state of affairs would be found to exist in these cases also. At the moment however we will restrict our attention to the values of μ found to agree with the self-absorption data over the range of source superficial densities examined in Figure 39.

The values of $\mu_{S.A.}$ predicted by the relationship (equation (63)) given by Baker and Katz (5), which are generally of the same order as those previously reported, are compared with our values in table VI, and are seen to be very much the smaller. This is as would be expected since their relationship applied to μ-values obtained with source-thicknesses much greater than the range we have studied, and their thicknesses were probably greater than the value at which the change to a curve of smaller slope (referred to above) occurred for the nuclides studied.

TABLE VI

Nuclide	μ Observed cm^2/mg	μ Predicted by Baker and Katz cm^2/mg	External Absorption μ_0 cm^2/mg	μ_{300} cm^2/mg
Ni^{63}	7.8	0.35	9	3.2
S^{35}	1.0	0.21	3.3	0.88
Co^{60}	0.38	0.09	-	-

In section E of this thesis we shall analyse half counter and coincidence rates so as to obtain curves of pure scattering and absorption probabilities of β-particles as observed in a 4π steradian geometry.

In Table VI we anticipate the results quoted there by listing values of μ_0 and μ_{300} for Ni^{63} and S^{35} (columns 4 and 5). These are the external absorption coefficients corresponding to an exponential absorption curve tangential to the observed absorption relationship at d = 0 and d = 300 $\mu g./cm^2$ respectively. The value of μ observed for the self-absorption curve lies between the two.

This is as expected since the electrons emitted from a source of superficial density, say 300 $\mu g./cm^2$, will have been subjected to absorption through thicknesses of material ranging from 0 to 300 $\mu g./cm^2$. Thus the mean absorption may be expected to be equivalent to that due to a superficial density value in between.

(It is meaningful to compare the absorption of β-radiation in the source materials used and in the VYNS mounting film in this way, since the latter has an arithmetic mean Z value of about 5.1, closely similar to the values given earlier for the source materials. We neglect to first order approximation the absorption and scattering effects (129) of the 2 $\mu g./cm^2$ of gold required to render the source mounting films conducting.)

Hence from our results, substantiated by agreement in order of magnitude with the results of "external" absorption measurements, it is clear that self-absorption effects in a 4π-geometry for very low source superficial densities are of much greater magnitude than was expected from previous work.

One may perhaps comment on the low values of specific activity observed in the case of Ni^{63} for superficial density values below 5 $\mu g./cm^2$. This effect bears a superficial resemblance to the maximum

observed in self-absorption curves obtained with << 2π steradian geometries. It is however a quite different effect. It will be observed from Figure 37 (c) that in layers of source material of less than about 5 $\mu g./cm^2$ superficial density, the source area is not completely covered, but rather consists of uniformly distributed 1 μ diameter crystals with spaces between. Thus the effective superficial density of the source material is much greater than the value obtained by weighing the deposit spread over a known area, or probably by the optical method. The observed specific activities will therefore not lie on the curve obtained from higher superficial density values until one or more complete crystal layers are built up, which appears from Figure 37 (d) to occur at $d > 5$ $\mu g./cm^2$. There is however in this case no error involved in extrapolating the curve from higher thicknesses to zero thickness, since the value of specific activity obtained is that required - ie. for a source of evenly spread material of zero superficial density.

Thus for materials of fairly high specific activity (ie. high enough to give an accurately measurable counting rate from sources of the thicknesses used) there are two available methods of correcting for self-absorption.

(i) The platinum crucible may be charged with a suitable compound of the nuclide being studied, and the observed specific activity determined as a function of source thickness (accurately measured) after successive distillations. Extrapolation of a suitable plot then produces the required specific activity with zero self-absorption. In the case of materials of specific activity, so high that the quantities of

precipitates etc. handled are impracticably small, it may be necessary to add additional measured quantities of isotopic carrier, to render the method accurately quantitative. For materials of the highest specific activity, of course, self-absorption effects are liable to be so small that direct solution evaporation produces "weightless" sources giving true specific activity measurements, provided the solution contains very little dissolved solid inactive material.

(ii) If self-absorption curves for the nuclide in the compound used are available, then a single measurement from a source of known superficial density will allow the true specific activity to be computed.

Eventually it is hoped to produce a complete series of such curves for all β-energies. However at the moment, the method is limited in two ways.

(i) The design of furnace is such that a collection efficiency of a few percent only is possible. This will doubtless be improved by a redesigned system.

(ii) The calibration of the optical method for superficial density determination is limited, together with the direct gravimetric estimation, by the weighing facilities at present available. The result is a scatter in the experimental values, seen clearly in Figure 38 (a), since both ordinate and abscissa are affected. Hence an extrapolation of the Ni^{63} curve produces a specific activity value accurate only to ± 3-4 percent.

For S^{35} and Co^{60} however it is seen that a value accurate to

about ± 1 percent can be obtained, and the accuracy obtainable will increase with increasing end-point energy. Further work on the experimental techniques involved in this method of correction for self-absorption should make possible a precision of better than ± 0.5 percent for all the beta-energy range studied, since the method is certainly of sufficient sensitivity. This will reduce self-absorption errors to an order of magnitude similar to that of the errors described in sections B and C.

E. ABSORPTION AND SCATTERING OF BETA-RADIATION IN A COUNTER GEOMETRY OF 4π STERADIANS

1) INTRODUCTION

In the three previous sections, we have discussed the three sources of error to which disintegration-rate determinationsby 4π-counting are subject, and proposed suitable methods for the reduction of the magnitude of error in such determinations.

In addition to the experimental work performed in evolving these methods, other experiments were performed which allow an analysis of the various electronic scattering and absorption processes which occur inside the 4π-counting chamber. Such an analysis is of interest as a means of explaining the results of source-mounting film absorption measurements, reported in section C, which were found to be at variance with previous theoretical predictions. It is also of interest since a comparison becomes possible between the absorption and backscattering of beta-radiation taking place in a 4π-counting chamber, and equivalent processes which have been observed by experimenters working with a source-to-counter geometry of much less than 2π steradians.

Before describing this additional experimental work, however, we shall discuss the nature of the absorption and backscattering processes, as observed in a conventional counter geometry, and also describe previous work on phenomena which give coincidences between the two halves of the 4π-counter, the examination of which is the first step in the analytical process.

(a) Absorption of Beta-Radiation

The penetration of electronic radiation through matter is a very complex phenomenon owing to the number of processes by which interaction may occur.(13). With an initially well-collimated beam of monoenergetic electrons, interaction with a layer of material of superficial density up to a few hundred $\mu g./cm^2$ occurs by means of a few scattering events per electron resulting in a spreading of the beam without too great a loss of energy, or intensity. With thicker layers more scattering events per electron occur, and a transition to "multiple scattering" occurs. With layers of absorber thicker than a certain limit, the electrons no longer have a preferred direction of motion, and a situation best described in terms of a diffusion process results (12). In these circumstances the number of electrons observed to emerge from the foil decreases with increasing thickness of foil, a process described as absorption of the radiation.

Single scattering events involving electrons of a given energy can be successfully treated theoretically (9, 104), while with multiple scattering and diffusion processes only an approximate treatment has been possible (12). In systems with the further complication of the continuous energy distribution of beta-radiation added, any rigorous theoretical treatment has up to now proved impossible, and the data available is handled only in a semi-empirical way.

The absorption of beta radiation is of interest to workers on absolute β-counting for two reasons:

(i) Absorption of radiation in for instance the window of an end-window counter and in the air between source and counter produces an

error in disintegration-rate measurements (see earlier) for which correction must be made by the methods already outlined.

(ii) The absorption process makes possible a simple method of determination of beta-energies.

Beta-energy determination, or more especially determination of the end-point energy of the energy spectrum, characteristic of a given beta-emitter, is most accurately effected by means of electron spectrometry. If a less precise value, say ± 5 percent, is acceptable, eg. for identification purposes and if the decay scheme is simple, the determination of the maximum range of the beta-radiation through a suitable absorber material, usually aluminum, using a simple end-window counting system, will suffice. A plot of transmission versus absorber thickness, termed an absorption curve, is prepared and the beta-radiation range obtained from this conveniently by the method of Feather (46). Empirical relationships between energy and range observed have been given both for monoenergetic electrons and for beta-spectra of differing end-point energies (46, 49, 55, 93, 97, 122). These may be used to compute the maximum energy in the case studied, or alternatively the empirical curve due to Glendenin (56) which also embodies the data of Glendenin and Coryell (55), Marshall and Ward (97) and earlier workers quoted by Rutherford, Chadwick and Ellis (121) may be used. Alternatively the method of Bleuler and Zünti (16) may be applied directly to the absorption curve.

As was discussed in the previous section, the earliest workers on the absorption of beta-radiation found that the transmission of an absorber to beta-radiation decreased approximately exponentially with

increasing absorber superficial density, due to a fortuitous combination of the effects due to the form of the low energy end of the beta-energy spectrum and those due to scattering of electrons in the absorber. The closeness of approximation to an exponential relationship observed will depend (47) among other things on the relative positions of the source counter and absorber. There have been several publications (eg. 32, 107, 137) in which external absorption curves showing maxima appear. These were obtained in arrangements in which the scattering of electrons into the counter was more important at low absorber thicknesses than the loss of electrons by absorption, ie. with the absorber nearer to the source than the counter, and using an absorber material of high atomic number.

In a system where a source-to-counter geometry of 2π or 4π steradians exists, however, the anisotropy of radiation distribution from the source before or after penetration of an absorber will be without effect on intensity measurements as was outlined in section A. In the case of a 4π-counter for instance all particles emerging into the gas space, ie. all those emerging from source or absorber, are registered, and any diminution of intensity with increasing absorber thickness must be due to absorption effects alone.

However the effects observed will be expected to differ from those observed in a narrow angle geometry in other ways. The counter subtending 2π steradians at the source will register particles emerging at small angles to and hence incident at small angles to the absorber surface. Hence the path length of the majority of these particles in the absorber material will exceed the absorber thickness d, and greater

absorption effects than those corresponding to a path length d will be expected.

It may be possible to compute the expected absorption effect as a function of d, in a fashion analagous to that outlined in section D. However the situation is complicated by the fact that particles will in general emerge at an angle dissimilar to that at which they were incident upon the absorber surface. Thus particles entering the absorber at small angles to the surface will in general have a greater probability of being scattered into the gas space, after a path length less than that computed from the angle of incidence.

In films of thicknesses towards the lower end of the range studied (< 100 $\mu g./cm^2$), the electron diffusion process is not expected to have been set up. The path-length traversed in aluminum before the diffusion process becomes important was computed as a function of electron energy by Zumwalt (153) from the theoretical expression of Bethe et al. (12). It was found to be 100 $\mu g./cm^2$ for 10 kev electrons and increased with increasing energy. Electrons with energies up to 10 kev form a small fraction of the beta-energy spectrum from those nuclides studied, with the possible exception of Ni^{63}.

Prior to the present investigation no measurement of absorption effects in a 4π-counter have been reported. Measurements of the variation of the total-counter, half-counter and coincidence-counting rates with source-mount thickness have previously been reported (76, 135, 141, 142). None of these alone, however, corresponds to the absorption of the original beta-radiation. Analysis of the data, when attempted, was effected at constant source-mount thickness only, and a

true "absorption curve" did not result.

Absorption measurements in the absorber thickness range up to a few hundred $\mu g./cm^2$ have not hitherto been reported. Such measurements are liable to be of considerable interest, particularly when conducted with weightless sources where self-absorption effects are virtually absent, since it is the electrons of lowest energy in the beta-spectrum (i.e. those electrons about which least is known) that are absorbed. The results of section C, and of Suzor and Charpak (141, 142) indicate that unexpected changes of observed counting-rate take place in this absorber thickness region.

(b) Backscattering of Beta-Radiation

The importance of the backscattering of electrons in absolute counting systems using low-geometry counters has been briefly discussed in section A. Indeed most of our knowledge of the phenomenon derives from experimental work performed in this connection (25, 33, 148, 153), since, as in the case of beta-radiation absorption, the phenomena involved are too complex to lend themselves to theoretical evaluation at this time. In the thicknesses of backscattering material employed in the experimental work referred to, the electron diffusion process would again be expected to be important, but thus far the theory of Bethe et al. (12) has proved of only limited usefulness (153).

The broad features of the backscattering phenomena observed in a counter-geometry of much less than 2π steradians are as follows:

(i) The extent of backscattering increases with thickness of backing up to a fixed value and then remains constant. The fixed value characterizes a condition called "saturation backscattering".

(ii) The saturation backscattering value increases with increasing atomic number of the backing material, being about 12 percent for aluminum and > 50 percent for lead.

(iii) The mass of backing required for saturation backscattering is roughly independent of its atomic number, but is an increasing function of the end-point energy of the beta-spectrum (ie. about 30 mg/cm^2 for a 170 kev beta-particle, 110 mg/cm^2 for a 1 Mev particle) and is very roughly equal to one fifth the range of the beta-radiation studied.

(iv) The value of saturation backscattering at a constant Z of backing material is independent of end-point energy of the beta-spectrum. Earliest results showed a decrease of saturation backscattering with decreasing end-point energy, but Glendenin and Solomon (58) showed that this was probably due to the preferential absorption of backscattered radiation in the counter window.

(v) The backscattered radiation is degraded in energy. Absorption curves (86, 148, 153) show forms generally similar to the incident beta radiation but with the half-thickness or range reduced to between 0.4 and 0.8 that of the beta-radiation. The energy spectrum of the radiation produced by the backscattering of monoenergetic electrons has been given by Balfour (6). The results are in accordance with those obtained with β-radiation.

(vi) The backscattered radiation is anisotropic in distribution being primarily concentrated in a direction normal to the surface of the backscatterer for materials of large Z (148). Hence when the beta-radiation from a weightless source (isotropic) and the backscattered radiation are compared, effects of different magnitude will be observed

for different counter geometries. Zumwalt (153) compared his results for a narrow angle geometry with those of Borkowski for a 2π geometry, observing that backscattering was larger in a 2π geometry for materials of low Z and smaller for materials of high Z.

The latter result was confirmed by Conway and Rasmussen (34) using a high Z backing in a 2π counter. Several instances of unexpectedly large differences in counting-rate between the halves of a 4π-counter, using low Z backing have also been observed. Thus 8 percent backscatter of S^{35} from 30-40 $\mu g./cm^2$ of cellulose film was reported by Meyer-Schützmeister and Vincent (100), and a 5 percent difference in counting rate between the halves of a 4π-counter using Na^{24} mounted on 50 $\mu g./cm^2$ of Formvar was attributed by Borkowski (20) to scattering, since significant absorption of the 1.4 Mev β-radiation in the film was unlikely. A similar effect was reported by Houtermans et al. (76) with P^{32} on 25 $\mu g./cm^2$ of cellulose.

The magnitude of scattering effects observed from such thin films in a 2π or 4π geometry is at variance with the use of these films as mounts in the work with small geometry-counters, since backscattering was considered under these conditions to be negligible. However as pointed out by Mann and Seliger (95), the phenomenon giving rise to increased scattering in a 2π geometry is probably small-angle single scattering. This is likely to be important for film thicknesses much below those at which the electron diffusion process, responsible for conventional backscattering, occurs. The scattered electrons emerging at small angles from the film surface will be registered by a 2π-counter, but not with a counter of smaller geometry. Seliger (129) has shown that

the single scattering process thus observed will be relatively independent of scatterer atomic number, and hence will be little disturbed by the gold-coating on films used as source mounts in a 4π-counter.

(c) Coincidences in a 4π-counter

We shall define a coincidence in a 4π-counter as being an event in which a discharge occurs in both halves of the counter within the resolution time of the recording apparatus, used to observe the system. This phenomenon must clearly be differentiated from the resolution loss phenomenon described in sections A and B which leads to an erroneous measure of the disintegration rate at high counting-rates, owing to the discharges due to successive disintegrations occurring within the counter resolution time of one another. The coincidence processes we shall discuss in this section occur in discharge phenomena resulting from up to 20 percent of disintegrations, but do not result in any error in the disintegration-rate determination since they occur within the resolving time of the equipment.

Previous workers with 4π-counters have been aware that coincident discharges occurred in a chamber of this sort. Haxel and Houtermans (69) observed the phenomenon during a disintegration-rate determination of Rb^{87}, and ascribed it to conversion electrons emitted simultaneously with the β-radiation. A fairly comprehensive study of the variation with mount thickness of the half-counter and coincidence rates in a G-M 4π-counter was made by Suzor and Charpak (28, 29, 140, 141, 142) although in a higher superficial density range than we have employed. They concluded (141) that there were three possible causes for coincidences.

(i) Secondary electronic radiation resulting from interaction of the primary beta-radiation with the source-mount, one each of the beta-particle and secondary electron triggering each half counter. They considered that electromagnetic radiation such as X-radiation or bremsstrahlung would be incapable of causing an effect of the magnitude observed.

(ii) Electronic radiation from the source, in addition to the beta-particle. Haxel and Houterman's conversion electrons come into this category, although coincidences were noted in as great an extent with beta-emitters where nuclear gamma radiation was known to be absent. Another possibility was the inner bremsstrahlung electrons described by Bruner (24) although the energy spectrum he quoted did not account very satisfactorily for the observed absorption effects.

(iii) Very soft gamma radiation from the source, eg. a 10 kev gamma photon emitted in 10-20 percent of disintegrations.

The results of the analysis of half-counter and coincidence rates by Smith (135) were interpreted by him on the basis of processes (i) and (ii). With S^{35} mounted on 260 $\mu g./cm^2$ aluminum he found a 7 percent probability for the production of secondary electrons by interaction of the beta-radiation with the mount, and 3 percent probability for the emission of an inner-bremsstrahlung electron per disintegration.

Meyer-Schützmeister and Vincent (100) did not however agree with these results. By studying the variation of coincidence-rate with varying diameter of the aperture in the metal plate dividing the chamber over which the film was mounted, and with counter-gas pressure, they came to the conclusion that the prime cause of the effect, in the case

of S^{35} at least, was backscattering of radiation by the counter-gas from one half-counter to the other. There was a smaller contribution from scattering at the counter-walls at larger aperture diameters. They also concluded that of the coincidence rate (in general of the order of 5 percent of the disintegration-rate), less than a few tenths of a percent was attributable to inner-bremsstrahlung electrons in the cases of S^{35} and P^{32}.

This latter observation is in accordance with more recent experimental work on the effect (118) in which I B electron emission was found to occur very much less frequently than was reported by Bruner.

Thus the first problem in this section is the positive identification of the phenomena leading to coincident discharges. Then follows an analysis of the data from half-counter and coincidence rates observed as a function of source-mount thickness to obtain absorption and backscattering curves as observed in a 4π-steradian counter geometry. These may then be correlated with the energy distribution in the appropriate parts of the beta-energy spectrum, and with theories of scattering and absorption.

2) EXPERIMENTAL TECHNIQUES AND RESULTS

There are two possible ways of measuring the rate at which coincident discharges occur in the 4π-counter. It will be shown later that the total counting-rate (ie. that observed with the counter anodes connected in parallel) N_T is related to the counting rates above (n_a) and below (n_b) the source mount, and to the coincidence rate (n_c), by the relationship:

$$N_T = n_a + n_b - n_c \qquad \ldots\ldots(77)$$

Therefore one may either measure N_T, n_a and n_b separately, by disconnecting one anode and then the other for example, and from this information compute n_c, or one may measure n_c directly by electronic means, and compute N_T from measured values of n_a and n_b. The first method has the disadvantage that the value for n_c is obtained only as the small difference between large quantities on which there are statistical deviations, and hence is subject to a disproportionate error. We have therefore adopted the second procedure.

In the apparatus for the experimental work to be described in this section, the chamber and interior arrangements were as before. However the two anodes were no longer connected, separate H.T. supplies, (205-B) preamplifiers, AEP 1448 amplifiers, and AEP 908 scalers being connected to each. The output signals of the two amplifiers, taken after discrimination from the output of the multivibrator stage, were fed into a coincidence unit (of which a circuit diagram appears in the appendix), the output of this being fed into a third AEP 908 scaler. The arrangement of the anode leads and preamplifiers can be seen in Figure 4 in section B, and a block diagram of the equipment appears in Figure 40.

It was considered important that the High Voltage supplies and amplifier-systems used in conjunction with the separate half-counters should be matched, so that each system would give a similar performance. This was checked by comparing high-voltage characteristics for Ni^{63} for each separate half-counter. The potentials at which counting commenced, and at which the plateau commenced, were found to agree well enough for the purposes of this experiment.

Figure 40

Block Diagram of Apparatus Used for Coincidence Experiments

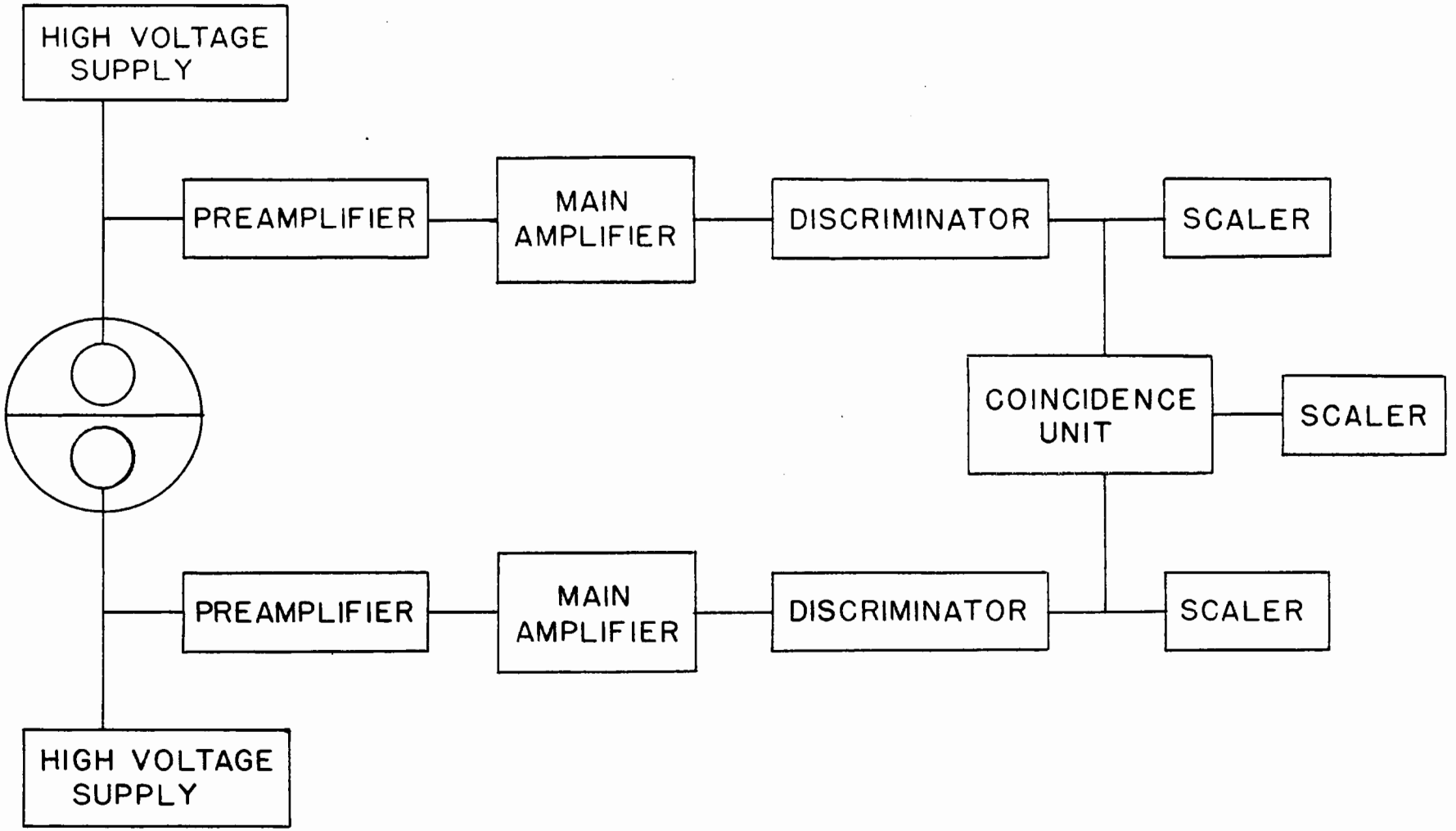
HIGH VOLTAGE SUPPLY
PREAMPLIFIER
MAIN AMPLIFIER
DISCRIMINATOR
SCALER
COINCIDENCE UNIT
SCALER
PREAMPLIFIER
MAIN AMPLIFIER
DISCRIMINATOR
SCALER
HIGH VOLTAGE SUPPLY

The resolution time of the coincidence circuitry was determined by feeding in the output signals of two amplifiers when connected to separate proportional counters which act as sources of pulses randomly distributed in time. The resolution time t is given to good approximation by

$$N = n_1 \cdot n_2 \cdot t \qquad \ldots.(78)$$

where N is the coincidence rate observed with separate pulse rates of n_1 and n_2 applied to the coincidence circuit input. For a range of values of n_1 and n_2, t was found to be 10.3 μ.sec. This figure was subsequently used to correct all observed coincidence-rates for random coincidences, due to unrelated events occurring within the circuit resolution time of each other, and all values of n_c reported are so corrected unless otherwise stated.

The pulses fed into the coincidence unit were the square pulses of > 10 volts amplitude produced by the multivibrator stage of the discriminator circuit. These would be expected to trigger the coincidence circuit satisfactorily, and result in the observed output pulse-rate of the circuit corresponding accurately to the coincidence rate in the system examined.

To check this, periodic comparisons were made of the value of N_T obtained via equation (77) from the half-counter and coincidence-rates, observed with the coincidence circuit, and the value of N_T obtained directly by observations with the anodes connected in parallel. In all cases the discrepancy was well within the expected statistical deviations on the quantities involved, indicating satisfactory operation of the coincidence circuitry.

The electronic method of measuring coincidence-rates in a 4π-counter is not however free from disadvantages. The worst of these is the appearance of positive pulses at the amplifier output in addition to the negative pulses associated with the electron cascade.

In Figure 41 are shown photographs of oscilloscope traces, with the instrument connected to the amplifier output. Figures 41 (a), (b) and (c) show the positive pulse wave-forms obtained at the output of the amplifier connected to one half-counter (A say) with the time-base triggered by the pulses (negative) from the other (say half-counter B). Half-counter A is unpolarized, while polarization potentials of 2.2, 2.4 and 2.6 kv are applied to B. The positive pulses in A are seen to be in coincidence with negative pulses in B, and to increase in magnitude with increasing polarization of B.

In Figures 41 (d), (e), (f) and (g) is seen the effect on positive pulses in A when the polarization in B is held constant at 2.6 kv and that in A increased from 1.8 to 2.4 kv. The positive pulses in A remain of constant amplitude, and negative pulses due to electron cascades in A appear and increase in magnitude, as in Figure 6 of section B.

The positive pulses in themselves are not disturbing, since, although amplified as positive pulses by the amplifying system, they fail to trigger the multivibrator circuit of the discriminator, and hence fail to register. However when the polarization potential of the other hemisphere exceeds 2.6 kv, the negative overswing following the positive pulse becomes large enough to trigger the recorder, and hence is registered as an additional count. This effect is demonstrated in Figures 42 and 43, where high-voltage characteristics (with both N_T

Figure 41

Positive Pulses Observed with Coincidence Apparatus

Observed with a C.R.O. at output of amplifier A (C.R.O. synchronized with negative pulses from amplifier B). Time base 3 μ.sec/cm. Vertical sensitivity 1 volt/cm.

Hemisphere A unpolarized

Hemisphere B: a) 2.2 kv b) 2.4 kv c) 2.6 kv

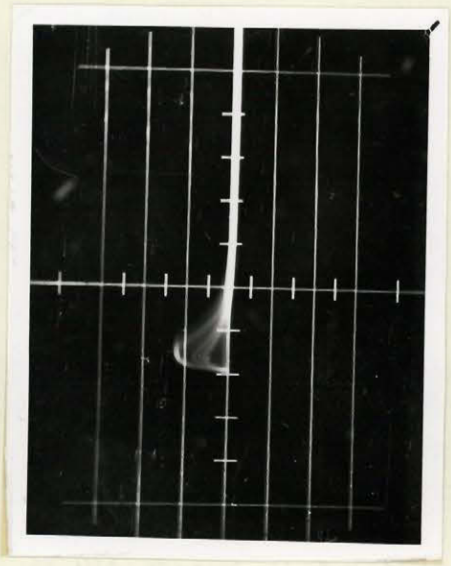

(b)

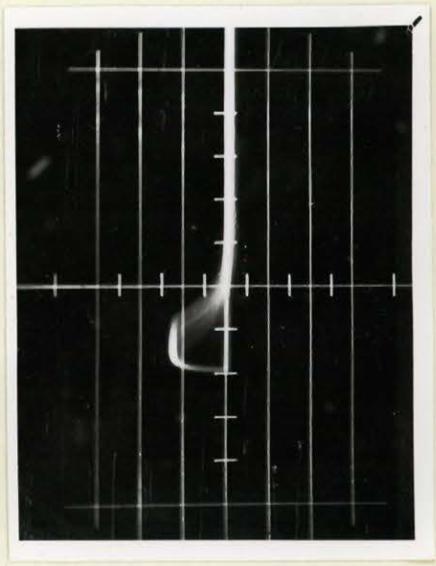

(c)

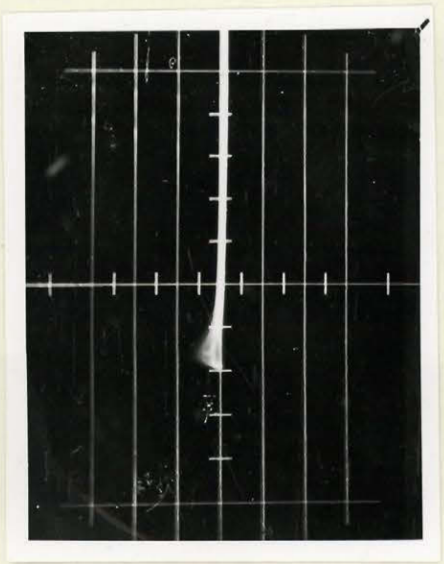

(a)

Figure 41

Positive Pulses Observed with Coincidence Apparatus

Observed with a C.R.O. at output of amplifier A (C.R.O. synchronized with negative pulses from amplifier B).
Time base 3 μ.sec/cm. Vertical sensitivity 1 volt/cm.

Hemisphere B at 2.6 kv.

Hemisphere A: d) 1.8 kv e) 2.0 kv f) 2.2 kv g) 2.4 kv

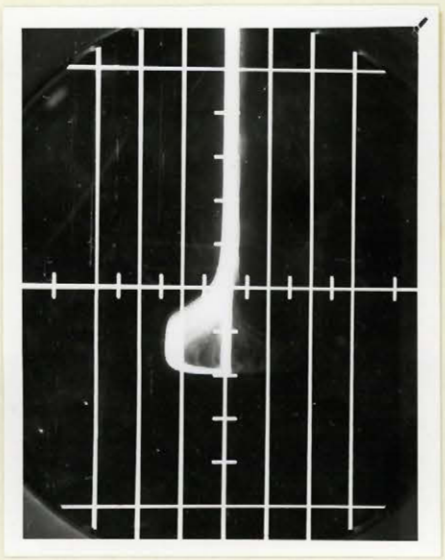

(e)

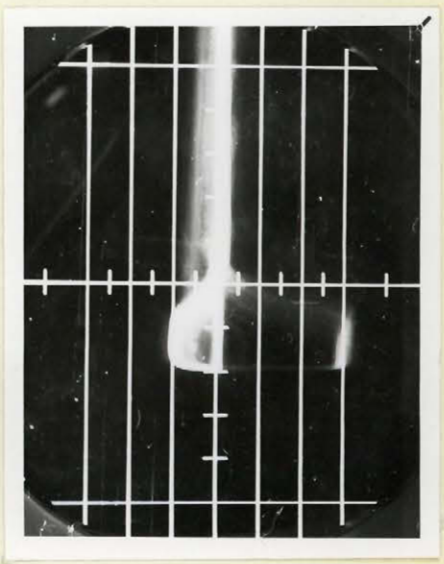

(g)

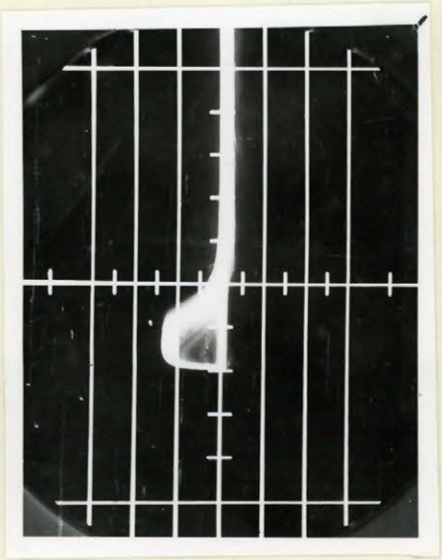

(d)

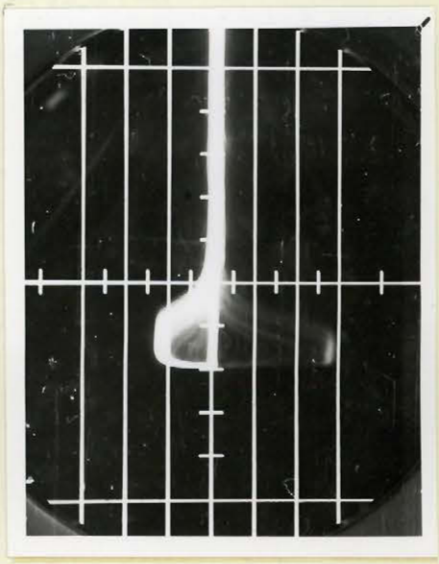

(f)

Figure 42

High-Voltage Characteristic for Ni^{63} Obtained with

Coincidence Apparatus, as a Function of Diaphragm Aperture Diameter

(Counting Gas C.P. CH_4)

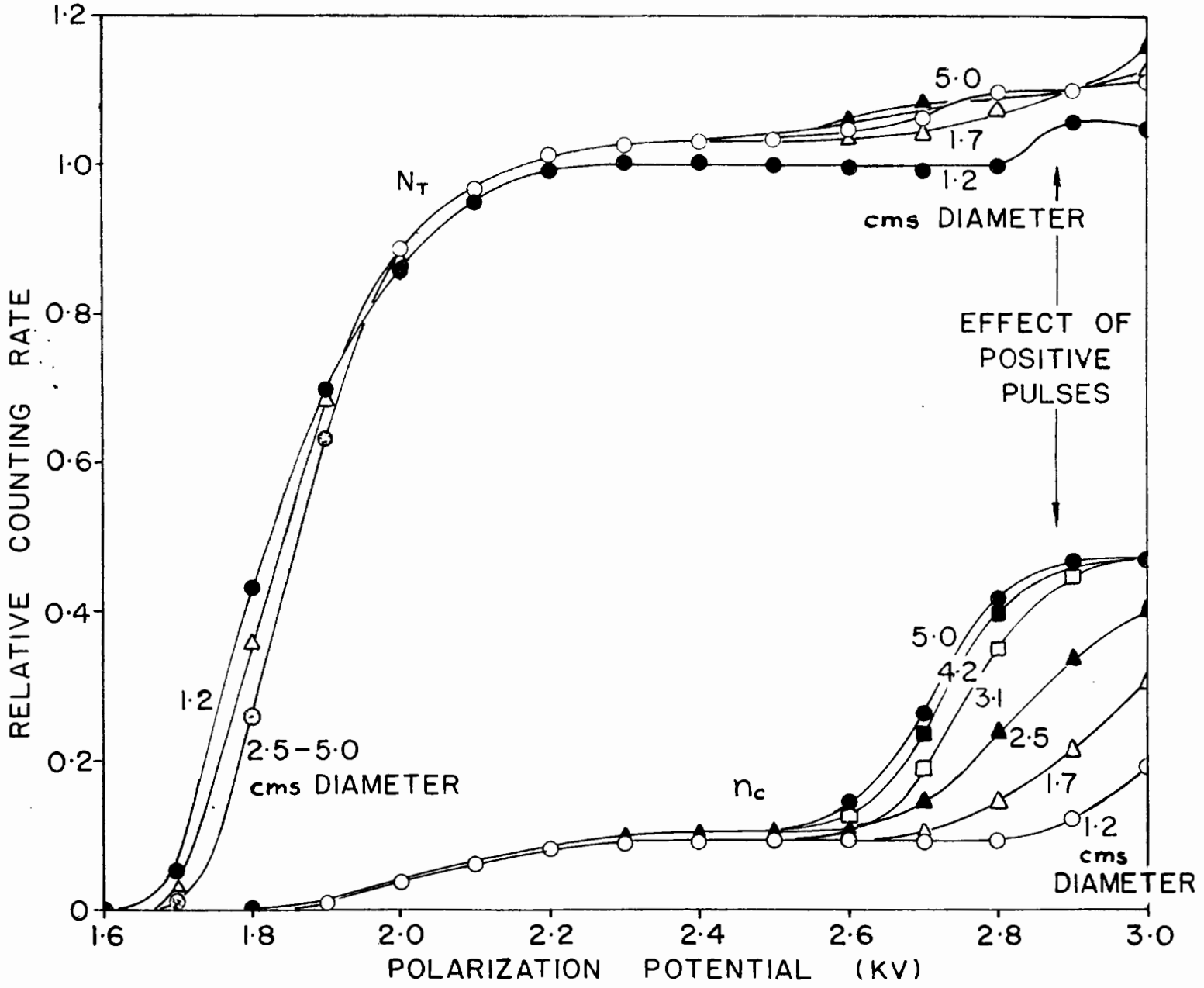
1·2
1·0
0·8
0·6
0·4
0·2
0
RELATIVE COUNTING RATE
5·0
1·7
1·2
N_T
cms DIAMETER
EFFECT OF POSITIVE PULSES
1·2
2·5–5·0
cms DIAMETER
n_c
5·0
4·2
3·1
2·5
1·7
1·2
cms DIAMETER
1·6
1·8
2·0
2·2
2·4
2·6
2·8
3·0
POLARIZATION POTENTIAL (KV)

1914

Figure 43

High-Voltage Characteristics for P^{32} Obtained with

Coincidence Apparatus as a Function of Diaphragm Aperture Diameter

(Counting Gas C.P. CH_4)

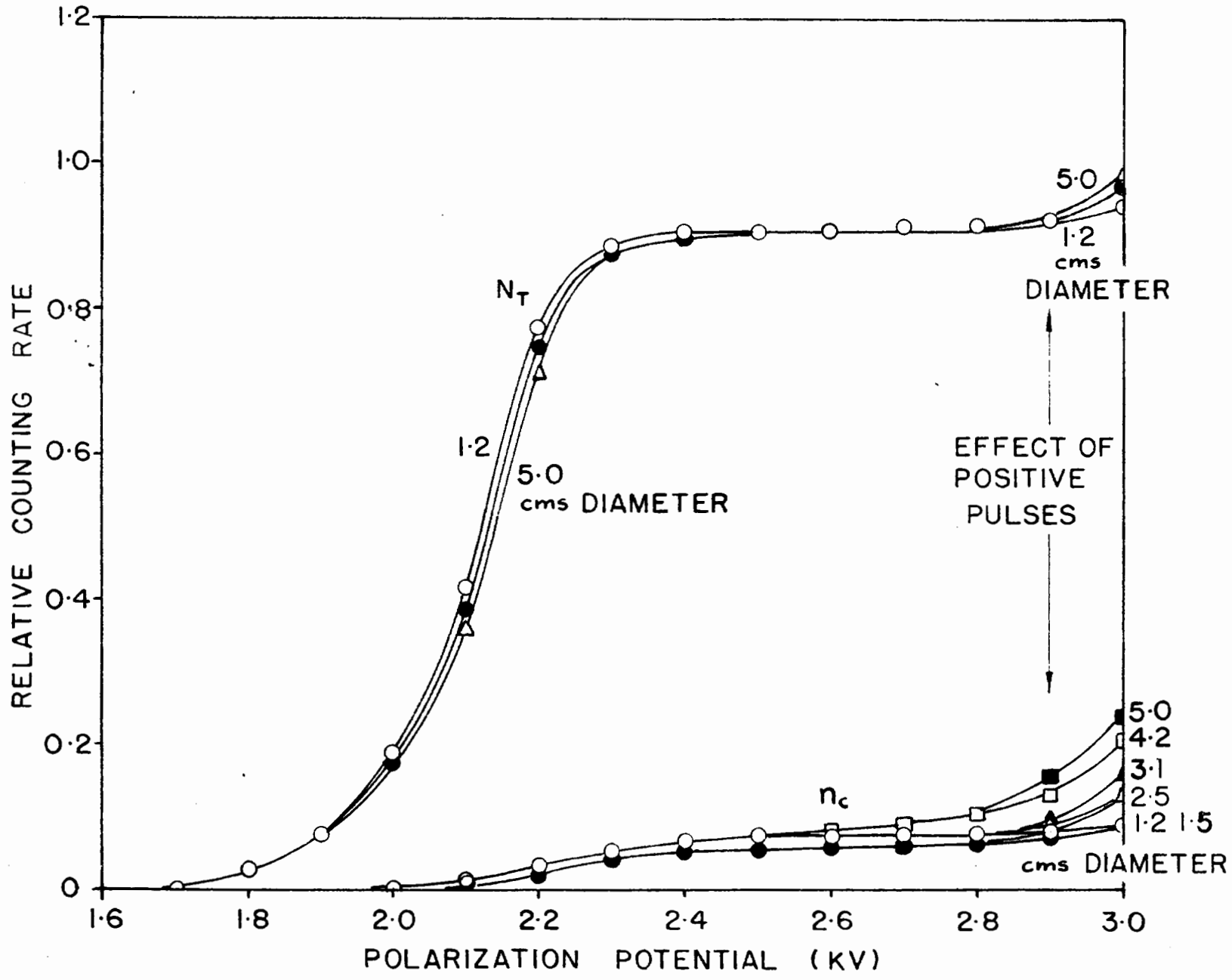
1·2
1·0
0·8
0·6
0·4
0·2
0
RELATIVE COUNTING RATE
1·6
1·8
2·0
2·2
2·4
2·6
2·8
3·0
POLARIZATION POTENTIAL (KV)
N_T
1·2
5·0
cms DIAMETER
5·0
1·2
cms
DIAMETER
EFFECT OF
POSITIVE
PULSES
n_c
5·0
4·2
3·1
2·5
1·2 1·5
cms DIAMETER

and n_c plotted) for Ni^{63} and P^{32} are shown as a function of diaphragm aperture diameter. The number of events due to positive pulses, which show up in both the N_T and n_c curves, is seen to increase with increasing aperture diameter, and similar results to those seen in these figures are also obtained with intermediate β-energies.

All the foregoing phenomena are consistent with the positive pulses being due to an induction effect. The electron cascade moving towards the anode in one hemisphere represents the movement of the same amount of charge away from the anode in the other, and hence would be expected to produce a pulse in the second of opposite sign to that in the first. Certainly the electrons in the cascade are much nearer to the first anode than the second, but it will be recalled from Figure 5 of section B that the anodes are only of the order of 5-6 mm. apart over the source.

The effects observed with varying aperture size can be attributed to changing electrostatic screening between the hemispheres. Thus although screening due to the diaphragm plus the gold-coated plastic film is very incomplete, it improves with decreasing aperture diameter. Expressed differently, more of the induction current (negative) reaching the first anode is supplied from ground via the aluminum diaphragm (rather than from the other anode) with small aperture diameters than at large ones.

With the anodes connected in parallel, of course, as is the case in normal counter operation, the positive pulses, being in coincidence with the larger negative pulses at the other anode, do not appear. They result merely in a small reduction of the amplitude of the output

negative pulse. Thus they are not a feature of normal counter operation, and appear only because of the separation of the anode systems for the purposes of this experimental work. They are then to be regarded merely as a nuisance, having the effect of somewhat reducing the available plateau length, and to some extent spoiling the excellent high-voltage characteristics displayed in section B.

However sufficient high-voltage plateau was found to exist in all cases examined, below the polarization potential at which the positive pulse effect becomes disturbing, for the counter to be operated under conditions at which unit response probability could be assumed. We shall therefore not discuss this effect further.

The experimental work to be presented here falls into two categories.

(a) The coincidence rate n_c was measured (in terms of the disintegration rate N_o) for five of the range of beta-emitting nuclides described in section B (covering an end-point energy range from 67 kev to 1.7 Mev) over a range of diaphragm aperture sizes and with two different counter gases. In all cases, except that of Ni^{63} (in which a 12 $\mu g./cm^2$ source of nickel dimethylglyoxime prepared as described in section D was employed), the sources used were point sources produced by evaporation of a suitable aliquot of carrier-free stock solution as before.

The experimental technique was as follows. The source was first prepared on a 5-10 $\mu g./cm^2$ gold-coated film mounted on a 5 cm. diameter aperture, and the appropriate measurements of n_c, n_a and n_b made and N_T computed. A diaphragm with a smaller aperture was then

placed over the film, forming effectively a system in which the film was mounted over the smaller aperture. These measurements were repeated for a series of aperture sizes.

Each measurement was duplicated, using first C.P. methane, and then argon + 10 percent methane as counting gas. The polarization potential was of course suitably adjusted in the second case since suitable operating conditions were found to lie at a potential about 1.0 kv less than with methane.

The results of this series of measurements are plotted in Figure 44. The solid curves on this figure are the theoretical parabolas (see later) fitted to the data.

(b) The coincidence and half-counter counting rates were measured for the same series of nuclides and with Po^{210} as a function of source-mounting film thickness, with each of the counting-gases mentioned. The aperture diameter was maintained constant at a value of 2.5 cms. The results are shown in Figures 45 to 50.

In all cases except that of Ni^{63}, the sources were "weightless" point sources prepared by evaporation of a suitable aliquot of a carrier free stock solution. For Ni^{63}, 1 cm^2 area sources of nickel dimethylglyoxime were again used, both of 12 $\mu g./cm^2$ and 2.6 mg/cm^2 superficial density. The corresponding curves are plotted separately in Figure 45. The curves for the 2.6 mg/cm^2 Ni source show no features differing from those for the 12 $\mu g./cm^2$ source other than those expected from the absorption of radiation in a 1 cm^2 area of 2.6 mg/cm^2 thickness in the source mount.

The experimental technique used was as follows. The original

Figure 44

Coincidence Rate as a Function of Diaphragm Aperture Radius, for a Series of β-emitters of Increasing End-point Energy

(a) with C.P. CH_4 counting gas.

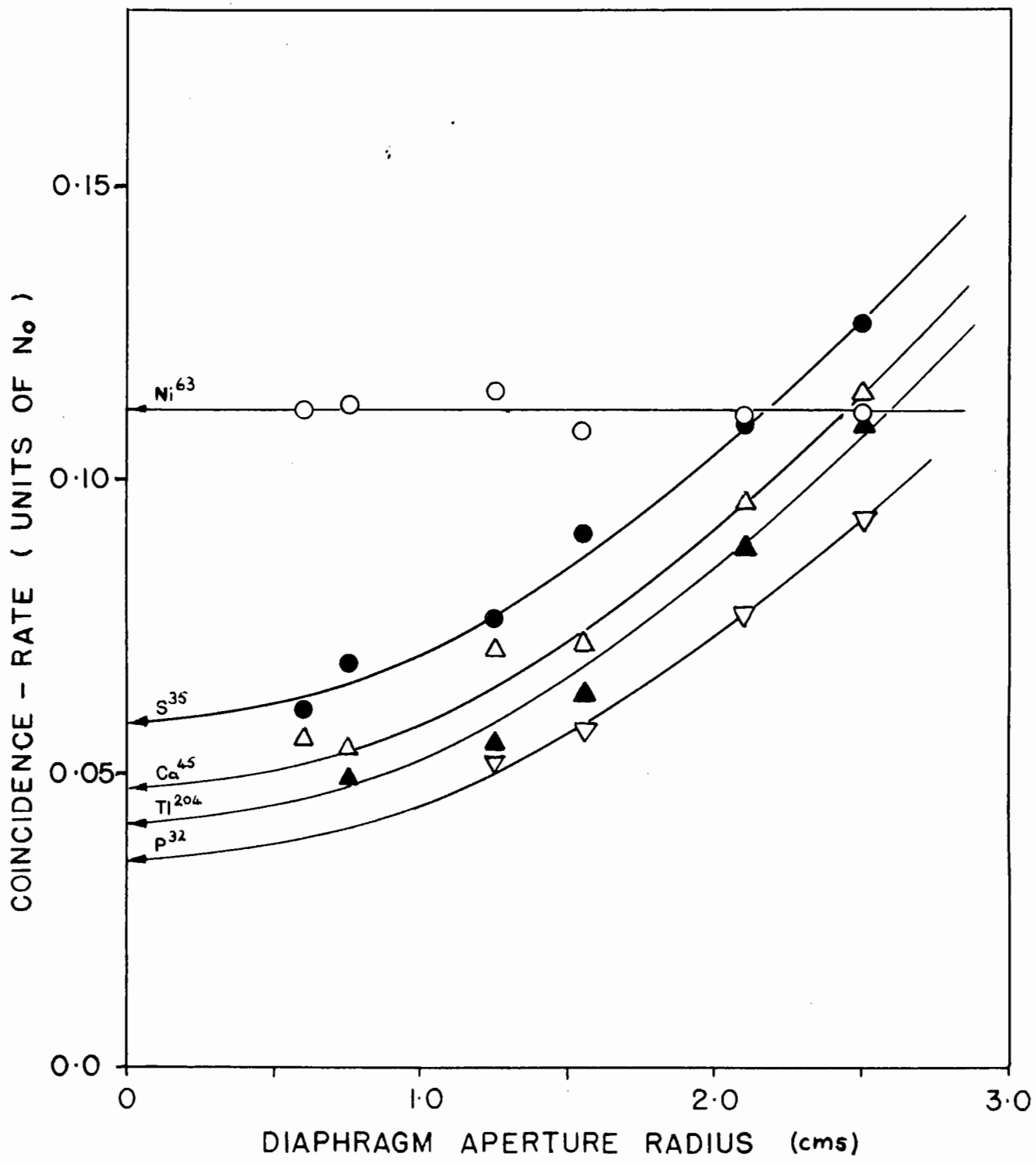
0·15
0·10
0·05
0·0
COINCIDENCE – RATE (UNITS OF No)
Ni63
S35
Ca45
Tl204
P32
0
1·0
2·0
3·0
DIAPHRAGM APERTURE RADIUS (cms)

Figure 44

Coincidence Rate as a Function of Diaphragm Aperture Radius,

for a Series of β-emitters of Increasing End-point Energy

(b) with A + 10 percent CH_4 counting gas

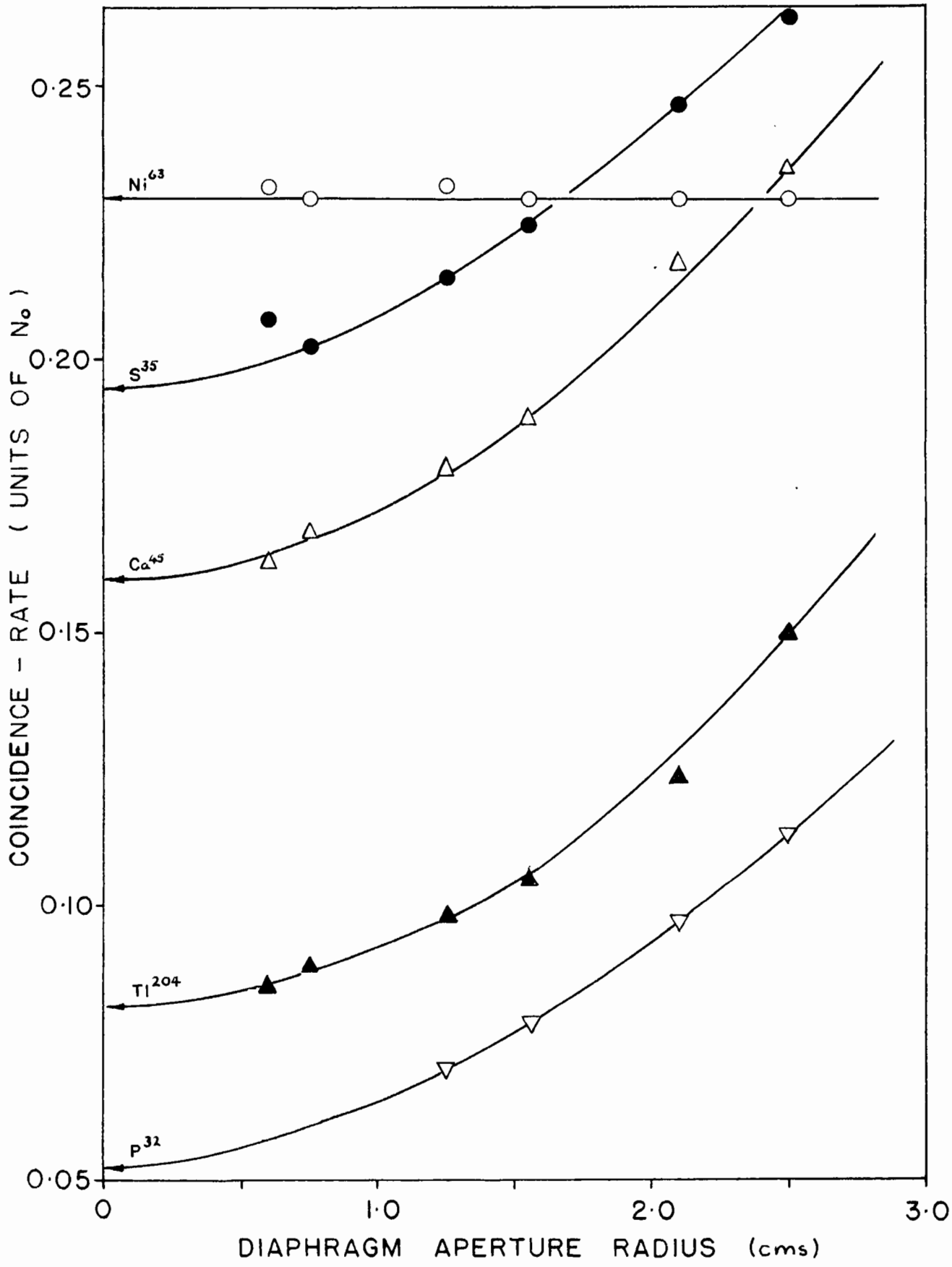
0·25
0·20
0·15
0·10
0·05
COINCIDENCE - RATE (UNITS OF N_0)
Ni^{63}
S^{35}
Ca^{45}
Tl^{204}
P^{32}
0
1·0
2·0
3·0
DIAPHRAGM APERTURE RADIUS (cms)

Figure 45

Source Mount Absorption Characteristics for Ni^{63}

(Beta end-point energy 67 kev)

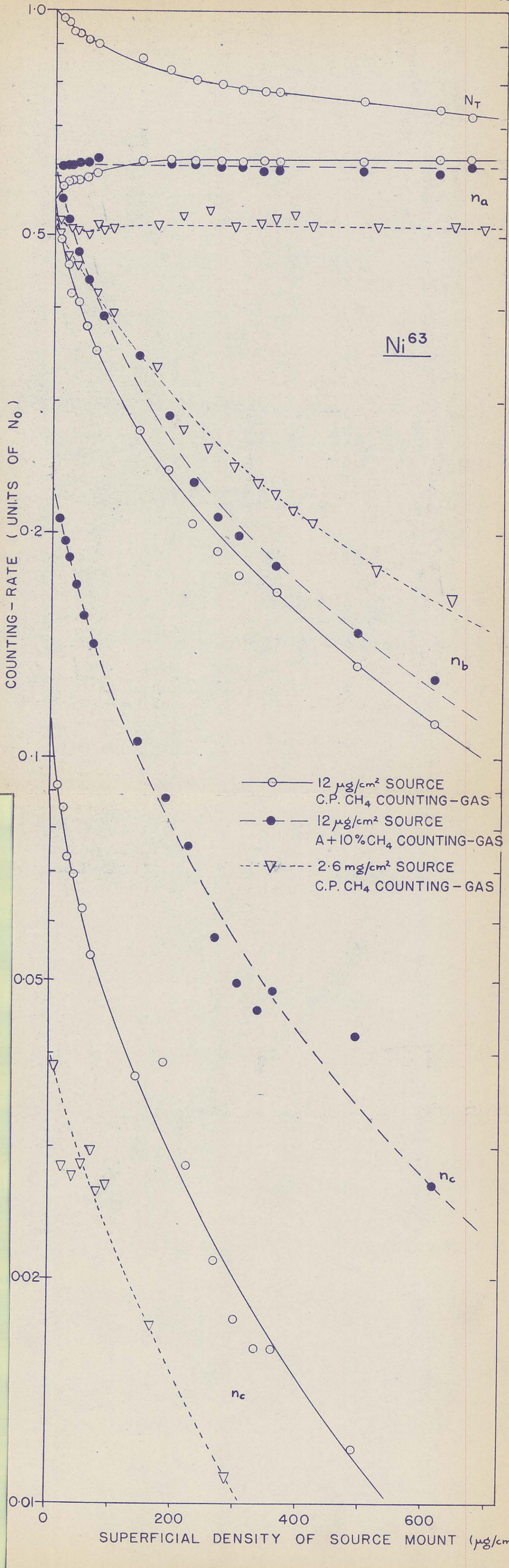
1·0
0·5
0·2
0·1
0·05
0·02
0·01
COUNTING-RATE (UNITS OF N_0)
N_T
n_a
n_b
n_c
n_c
Ni^{63}
12 μg/cm² SOURCE
C.P. CH_4 COUNTING-GAS
12 μg/cm² SOURCE
A+10%CH_4 COUNTING-GAS
2·6 mg/cm² SOURCE
C.P. CH_4 COUNTING-GAS
0
200
400
600
SUPERFICIAL DENSITY OF SOURCE MOUNT (μg/cm²)

Figure 46

Source Mount Absorption Characteristics for S^{35}

(Beta end-point energy 167 kev)

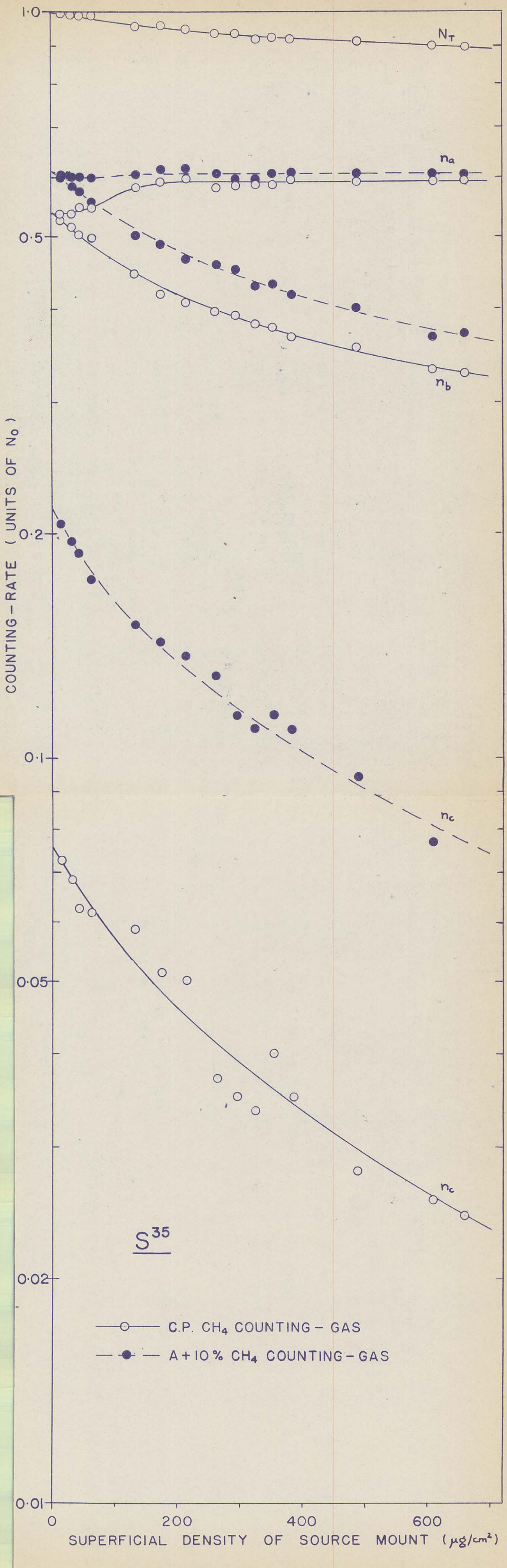
1·0
0·5
0·2
0·1
0·05
0·02
0·01
COUNTING-RATE (UNITS OF N₀)
N_T
n_a
n_b
n_c
n_c
S 35
C.P. CH₄ COUNTING-GAS
A+10% CH₄ COUNTING-GAS
0
200
400
600
SUPERFICIAL DENSITY OF SOURCE MOUNT (μg/cm²)

Figure 47

Source Mount Absorption Characteristics for Ca^{45}

(Beta end-point energy 254 kev)

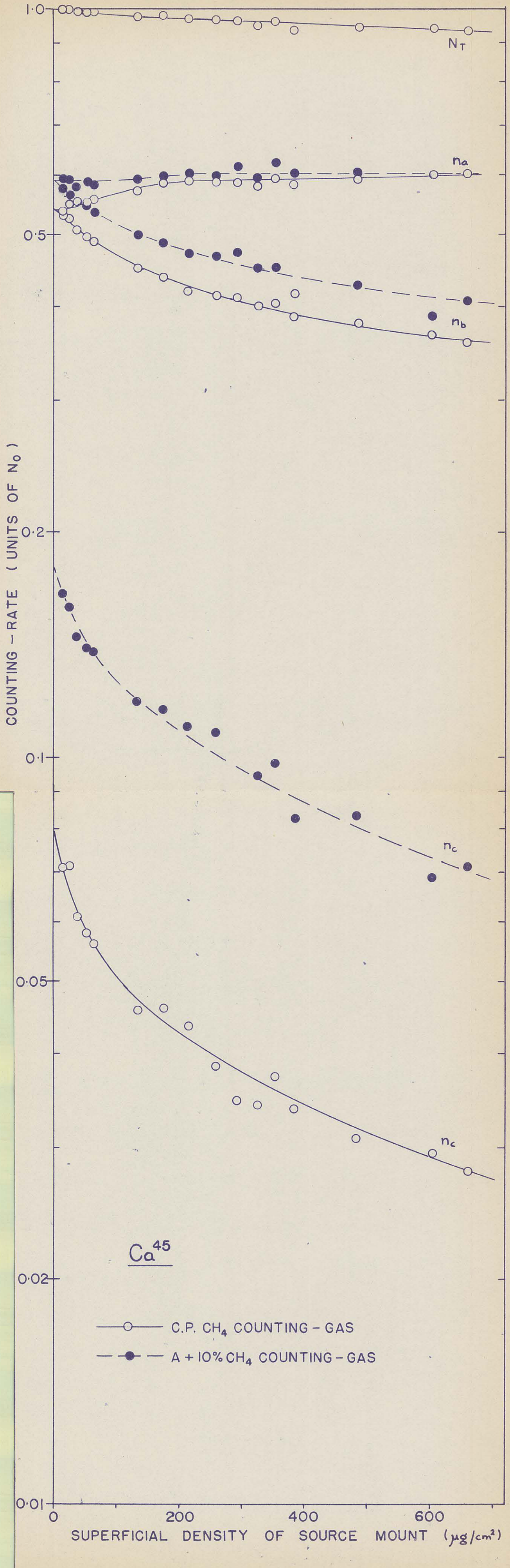
1·0
0·5
0·2
0·1
0·05
0·02
0·01
COUNTING – RATE (UNITS OF N_0)
N_T
n_a
n_b
n_c
n_c
Ca^{45}
C.P. CH_4 COUNTING – GAS
A + 10% CH_4 COUNTING – GAS
0
200
400
600
SUPERFICIAL DENSITY OF SOURCE MOUNT (μg/cm²)

Figure 48

Source Mount Absorption Characteristics for Tl^{204}

(Beta end-point energy 765 kev)

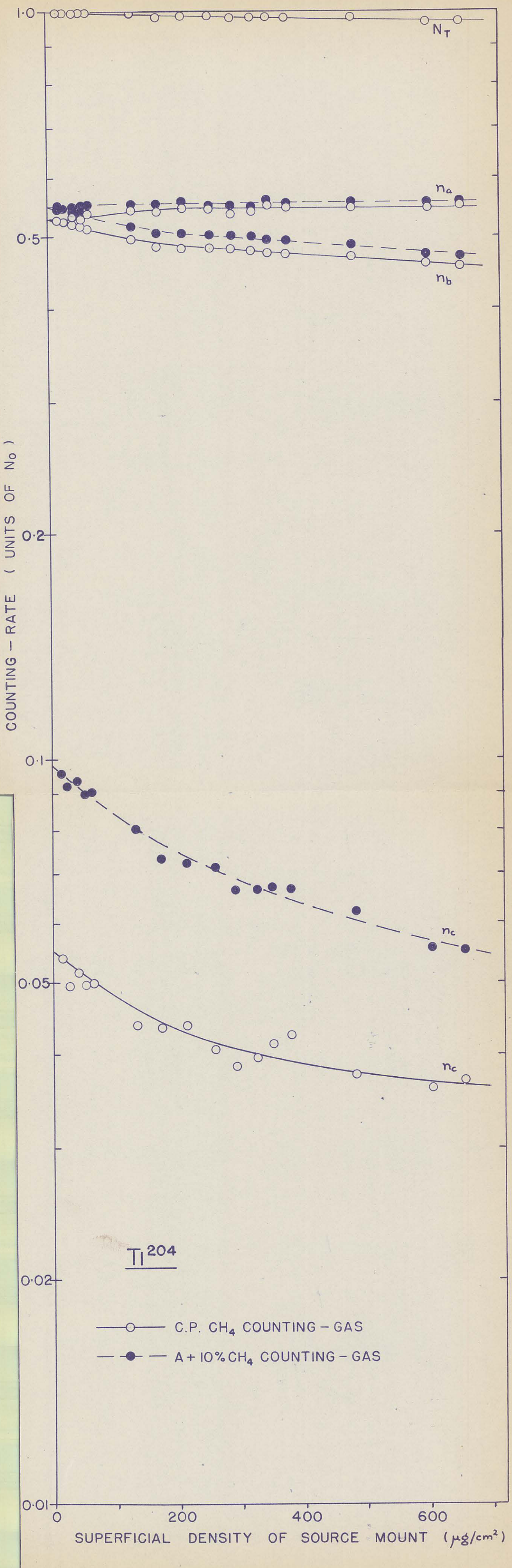
1·0
0·5
0·2
0·1
0·05
0·02
0·01
COUNTING – RATE (UNITS OF N_0)
N_T
n_a
n_b
n_c
n_c
Tl^{204}
C.P. CH_4 COUNTING – GAS
A + 10% CH_4 COUNTING – GAS
0
200
400
600
SUPERFICIAL DENSITY OF SOURCE MOUNT ($\mu g/cm^2$)

Figure 49

Source Mount Absorption Characteristics for P^{32}

(Beta end-point energy 1.70 Mev)

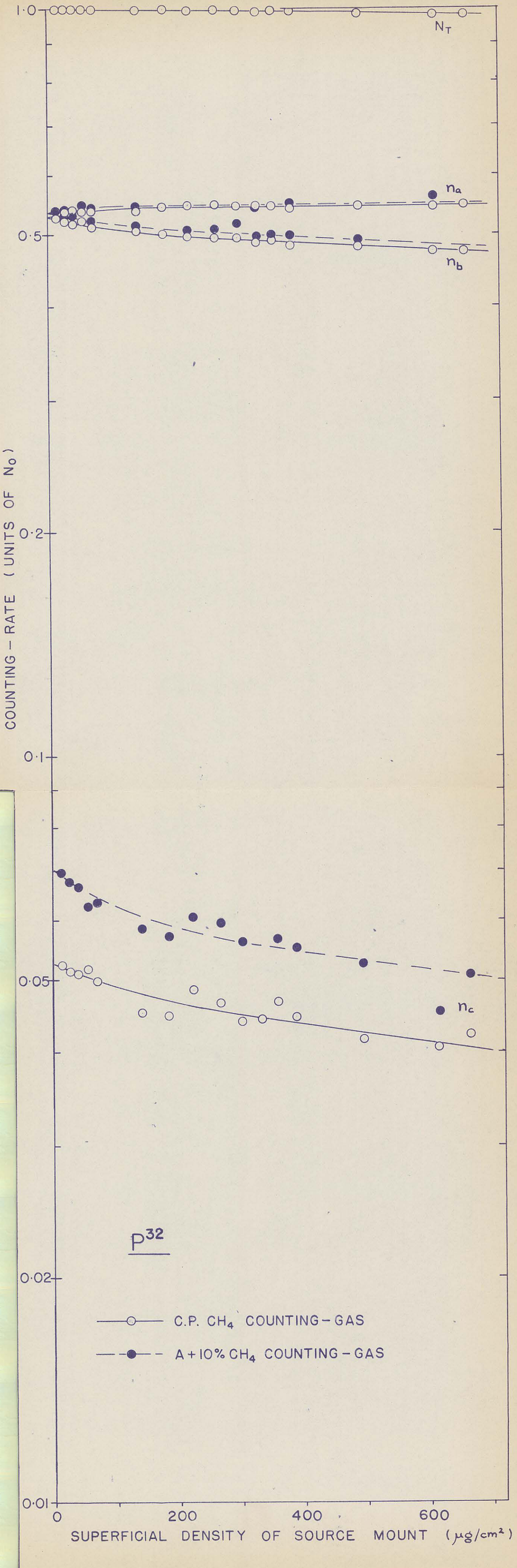
1·0
0·5
0·2
0·1
0·05
0·02
0·01
COUNTING – RATE (UNITS OF N_0)
N_T
n_a
n_b
n_c
P32
C.P. CH_4 COUNTING – GAS
A + 10% CH_4 COUNTING – GAS
0
200
400
600
SUPERFICIAL DENSITY OF SOURCE MOUNT ($\mu g/cm^2$)

Figure 50

Source Mount Absorption Characteristics for Po^{210}

(Alpha-energy 5.30 Mev)

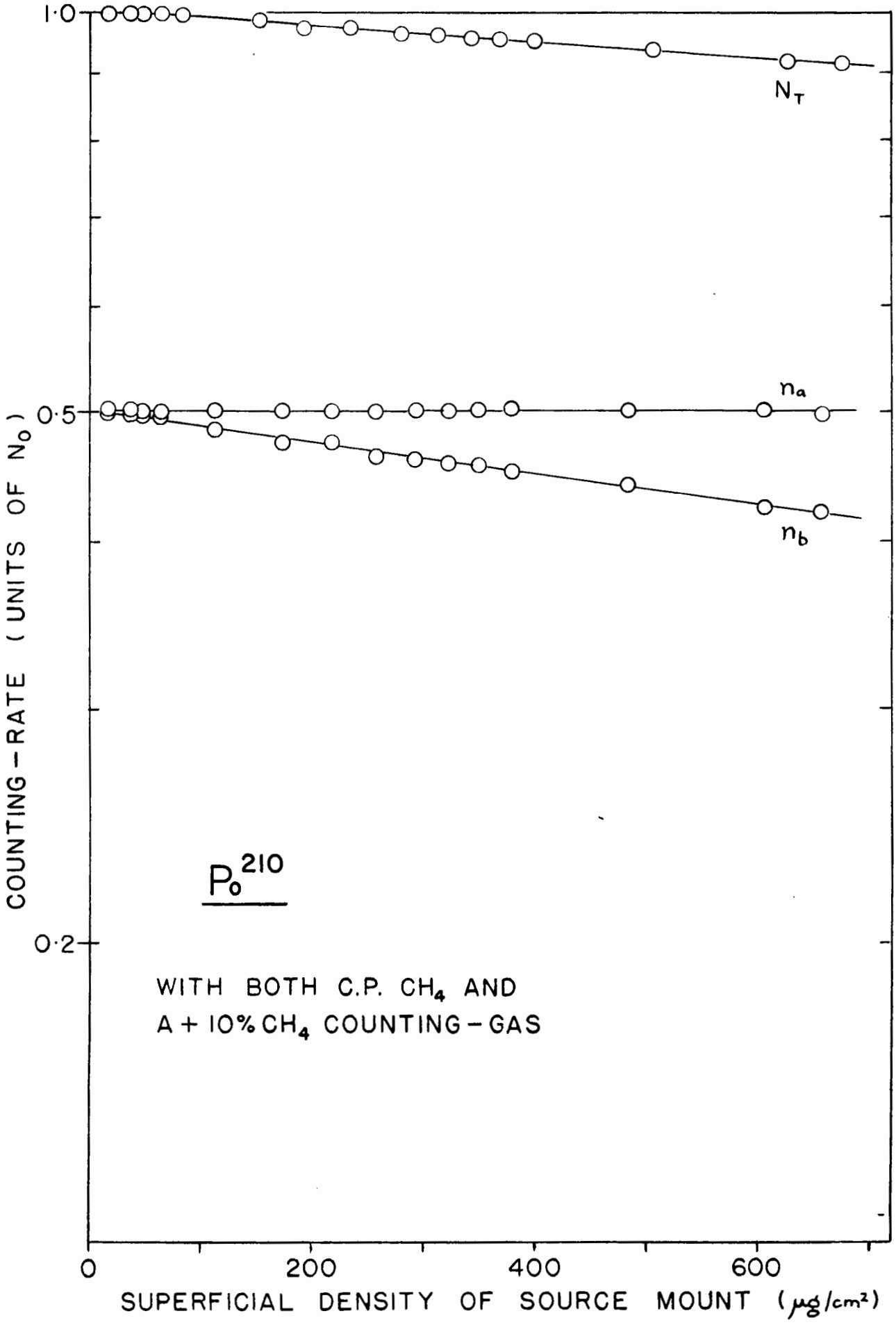
1·0
0·5
0·2
COUNTING-RATE (UNITS OF N_0)
N_T
n_a
n_b
P_o^{210}
WITH BOTH C.P. CH_4 AND
A + 10% CH_4 COUNTING-GAS
0
200
400
600
SUPERFICIAL DENSITY OF SOURCE MOUNT (μg/cm²)

source was prepared on a 5-10 $\mu g./cm^2$ gold-coated film, the total superficial density of which had been calibrated as described in section C, and the counting rates n_a, n_b and n_c measured. A second calibrated film was then caused to adhere to the back of the first (ie. on the side opposite to the source), the measurements repeated, and so on until a film thickness of about 70 $\mu g./cm^2$ had been built up. From then on each of a series of calibrated films of up to 600 $\mu g./cm^2$ superficial density was temporarily placed in contact with the back of the source-mounting film to produce source-mounts of greater thicknesses, the measurements being repeated at each thickness. For each set of measurements, the value of N_T was computed, and the curves of N_T against film superficial density obtained agreed well with those obtained directly as described in section C.

Each measurement was made twice, once each with C.P. methane and argon + 10 percent methane as counting-gas, with appropriate adjustments of polarization potential as described earlier. The period over which the counting-rate on each channel was measured was extended to ensure adequate statistical accuracy. Generally more than 1000 coincidence events were recorded at each measurement giving a standard deviation of about $\pm$ 3 percent. This was considered adequate for the purposes of the present experiment.

In order to check on the operation of the counter with greater mount thicknesses determination of the high voltage characteristic was repeated in the case of Ni^{63} at intervals during the above experiment. The results, shown in Figure 51, give characteristics at film superficial densities up to 490 $\mu g./cm^2$. These show no shift in location of the plateau, nor any other unexpected features.

Figure 51

High Voltage Characteristics as a Function of Source Mount Thickness with Ni^{63}. Counting Gas C.P. CH_4

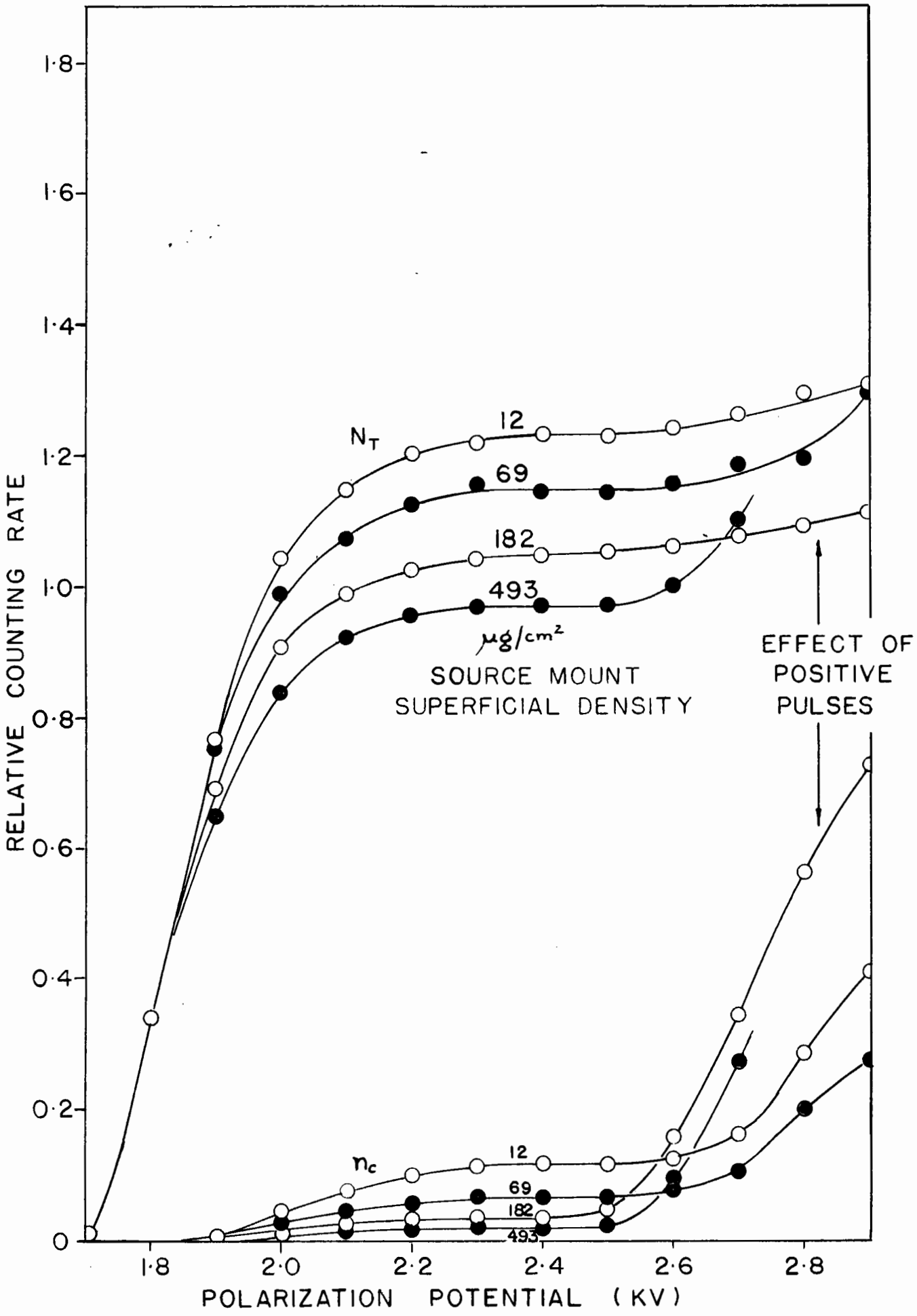
RELATIVE COUNTING RATE
1·8
1·6
1·4
1·2
1·0
0·8
0·6
0·4
0·2
0
N_T
12
69
182
493
μg/cm²
SOURCE MOUNT
SUPERFICIAL DENSITY
EFFECT OF
POSITIVE
PULSES
n_c
12
69
182
493
1·8
2·0
2·2
2·4
2·6
2·8
POLARIZATION POTENTIAL (KV)

3) DISCUSSION

(a) The Phenomena of Coincident Discharges

Of phenomena which can conceivably give rise to coincident discharges in a 4π-counter we may list the following.

(i) Nuclear γ-radiation accompanying beta-decay.

(ii) Conversion electrons accompanying beta-decay.

(iii) Inner bremsstrahlung accompanying beta-decay.

(iv) Inner bremsstrahlung electrons accompanying beta-decay.

(v) X-radiation accompanying beta-decay.

(vi) Secondary electrons from the source mounting film resulting from inelastic interaction by incident beta-radiation.

(vii) Bremsstrahlung from the mounting film produced by the incident beta-radiation.

(viii) X-radiation from the film produced by the incident beta-radiation.

(ix) Backscattering of beta-radiation from the counter gas.

(x) Backscattering of beta-radiation from the chamber walls.

(xi) Secondary electronic radiation from the counter gas.

(xii) Secondary electronic radiation from the counter walls.

(xiii) Secondary electromagnetic radiation from the counter gas.

(xiv) Secondary electromagnetic radiation from the counter walls.

In each case the coincidence event would be caused by one particle discharging one half counter, and the secondary particle or photon discharging the other. Or alternatively the scattering of a single particle from one half counter to the other would discharge both hemispheres. All the events described would succeed one another within a time interval very much shorter than the resolving time of the coinci-

dence apparatus.

Of these phenomena, we may eliminate several which, although possibly contributing a small effect, cannot be responsible to a significant degree for the effects we have observed, in which a coincidence follows up to 20 percent of the disintegration.

Thus since the five nuclides studied are known to decay by beta-transition to the ground state of the product nucleus, processes (i) and (ii) are ruled out. However the frequency of coincidence phenomena with nuclides whose decay mechanism does lead to gamma-emission, or to emission of annihilation radiation (with β^+ emitters), would not in fact be expected to be much different from that we observe owing to the low response probability of the counter to electromagnetic radiation. Most of the ionization produced in a counter by photons is not due to interaction of the photon with the counter gas, but to electrons produced by photo-electric and Compton scattering processes occurring in the counter walls. The calculation of the number of electrons which will emerge into the counter volume and cause discharges is liable to be subject to considerable uncertainty. There are however empirical data available due to Bradt et al. (21) of the response probability of Geiger counters of differing wall material to gamma radiation of varying energy. Their results are probably of the correct order of magnitude for our purposes, ie. less than 0.01 in the photon range 0-1.8 Mev.

On this basis then we may also eliminate any other processes involving photon production, unless this production occurs with high probability and either in the source or mount in a position of high

geometry with respect to both hemispheres, ie. we can eliminate processes (iii), (v), (vii), (viii), (xiii) and (xiv).

For instance, the phenomenon of inner bremsstrahlung (iii), in which the energy available from the disintegration is shared between a beta-particle, neutrino and a photon, has been described by several authors (17, 19, 81, 109, 147). The production probability of inner bremsstrahlung is of the order of 10^{-3} (19), and when this is multiplied by the low response probability to photons, its effects must be entirely negligible in our present consideration.

Similarly for external bremsstrahlung produced in the mounting film (vii). The probability that a quantum be emitted in the frequency range ν, $\nu + d\nu$ when an electron of energy E_o traverses a thickness, dx, of material is given (11, 123) by

$$I = N \Phi(E_o,\nu) d\nu dx \qquad .....(79)$$

where N is the number of atoms per cm^3 of material and $\Phi(E_o\nu)d\nu$ - the cross-section for production of a photon in the defined frequency range - is given by

$$\Phi(E_o,\nu)d\nu = \frac{Z^2}{137}\left(\frac{e^2}{mc^2}\right)^2 \frac{d\nu}{\nu} 4\left[1 + \left(\frac{E}{E_o}\right)^2 - \frac{2}{3}\frac{E}{E_o}\right]\left(\log \frac{2E_oE}{mc^2h\nu} - \frac{1}{2}\right) \qquad .....(80)$$

(neglecting screening) where $E = E_o - h\nu$ is the energy of the beta-particle after interaction, Z is the atomic number of the atom, e and m are the electronic charge and mass, and c is the velocity of light.

For polyvinyl chloride-acetate copolymer (85 percent chloride) of which the arithmetric mean atomic number $Z = 5.1$, and an incident beta energy of about 1 Mev, the value of Φ for the middle of the ν

spectrum is of the order of 10^{-26} cm^2. Substituting in equation (79) using $N = 10^{23}$ and $dx = 10^{-4}$ cm. (corresponding to a film thickness of the order of 100 μg./cm^2 we find that the probability of bremsstrahlung production per beta-particle incident on the source mount, $I = 10^{-7}$, which is again negligible for our present purposes.

Next we may consider electronic radiation arising from processes (iv), (vi), (xi) and (xii). The question of inner bremsstrahlung electron production (iv) was considered in the introduction to this section and will be neglected for the reasons stated. The process of inelastic interaction of electronic radiation with atomic electrons was described by Mott (104). If an interaction of an electron of initial energy E produces two (indistinguishable) product electrons of energies W and E-W, then the number of secondary electrons produced in a distance dx in the energy range W, W + dW is

$$I = ZN\, dx\, d\Phi\, (E,W) \qquad .....(81)$$

per incident primary electron, where the symbolism is as before and $d\Phi$, the differential cross-section for production of an electron in the defined energy range is

$$d\Phi(E,W) = \frac{\pi e^4}{E}\, dW \left[\frac{1}{W^2} + \frac{1}{(E-W)^2} - \frac{1}{W(E-W)} \cdot \cos\left(\frac{e^2}{h\nu} \log \frac{E-W}{W} \right) \right] \qquad .....(82)$$

or alternatively for relativistic electron energies (102)

$$d\Phi(E,W) = \frac{2\pi e^4}{mv^2}\, dW \left[\frac{1}{W} - \frac{1}{W(E-W)} \cdot \frac{mc^2(2E+mc^2)}{(E+mc^2)^2} + \frac{1}{(E-W)^2} + \frac{1}{(E+mc^2)^2} \right] \qquad .....(83)$$

The value of $d\Phi(E,W)$ for the scattering of β-radiation of energies between 0.6 and 1.7 Mev in collodion film (cellulose nitrate) has been determined experimentally by Page (110) to be in agreement with equation (83) and of the order of 10^{-24} cm^2 over most of the W spectrum. Substituting this value in equation (81) together with $\sim 10^{24}$ for the value of ZN and 10^{-4} cms. for the thickness of a film of superficial density about 100 $\mu g./cm^2$, a value of I of the order of 10^{-4} is obtained. Hence the probability of secondary electron production in the film is also below the order of magnitude we are considering.

Likewise for inelastic scattering in the counter gas (say methane with a superficial density of 700 $\mu g./cm^2$ per cm. of thickness), while the order of magnitude of scattering cross-section is increased by the greater thickness of scatterer, it will be decreased by the greater angle of scattering required to return an electron to the other half-counter (--> 180°). Also the further the scattering event occurs from the source, the worse is the geometry with respect to the other half-counter. Similar consideration apply to inelastic scattering processes occurring at the counter wall, where in addition a greater probability exists for the products of scattering to be absorbed in the scatterer.

Thus by elimination we are left only to consider

(1) backscattering of beta-radiation by counting-gas.

(2) backscattering of beta-radiation by chamber walls.

Backscattering effects have been shown by the experimental work discussed earlier in this section to be of the order of magnitude of the coincidence effects observed by us. In order to determine if either or both of processes (1) and (2) are contributing, let us examine the data of the

variation of coincidence-rate with aperture diameter, shown in Figure 44.

For a wall-scattered electron to cause a coincidence, it must first have penetrated the counter gas to the chamber wall, then have been backscattered into the gas space, have again penetrated the counter gas to the diaphragm, and finally have penetrated the source-mount to reach and discharge the second hemisphere. That is, the probability that a coincidence be produced by wall scattering per disintegration is

$$P = p_1 p_2 p_3 \qquad .....(84)$$

where

p_1 is the probability that the beta-radiation penetrate a path length of 3.5 cms. of counting gas to the wall, and the backscattering radiation penetrate a similar path length back to the diaphragm aperture.

p_2 is the probability that the beta-radiation will backscatter into the gas-space.

p_3 is the probability that the backscattered radiation penetrate the combination diaphragm + film. The probability that a particle emerging into the gas-space of the second hemisphere shall produce the necessary minimum number of ion-pairs to record is essentially unity.

We have computed the values of p_1 and the transmission of the aluminum of the diaphragm as a function of the beta end-point energy and these are seen in Figure 52. The calculations were performed by integration of the beta-spectra of Ni^{63}, S^{35} and P^{32} shown in Figures 59, 60 and 61 using the range-energy relation of Glendenin (56) (extended

Figure 52

Calculated Probability Functions p_1 and p_4 for Transmission of Counter Gas and Aluminum of Diaphragm to Beta- and Backscattered Radiation

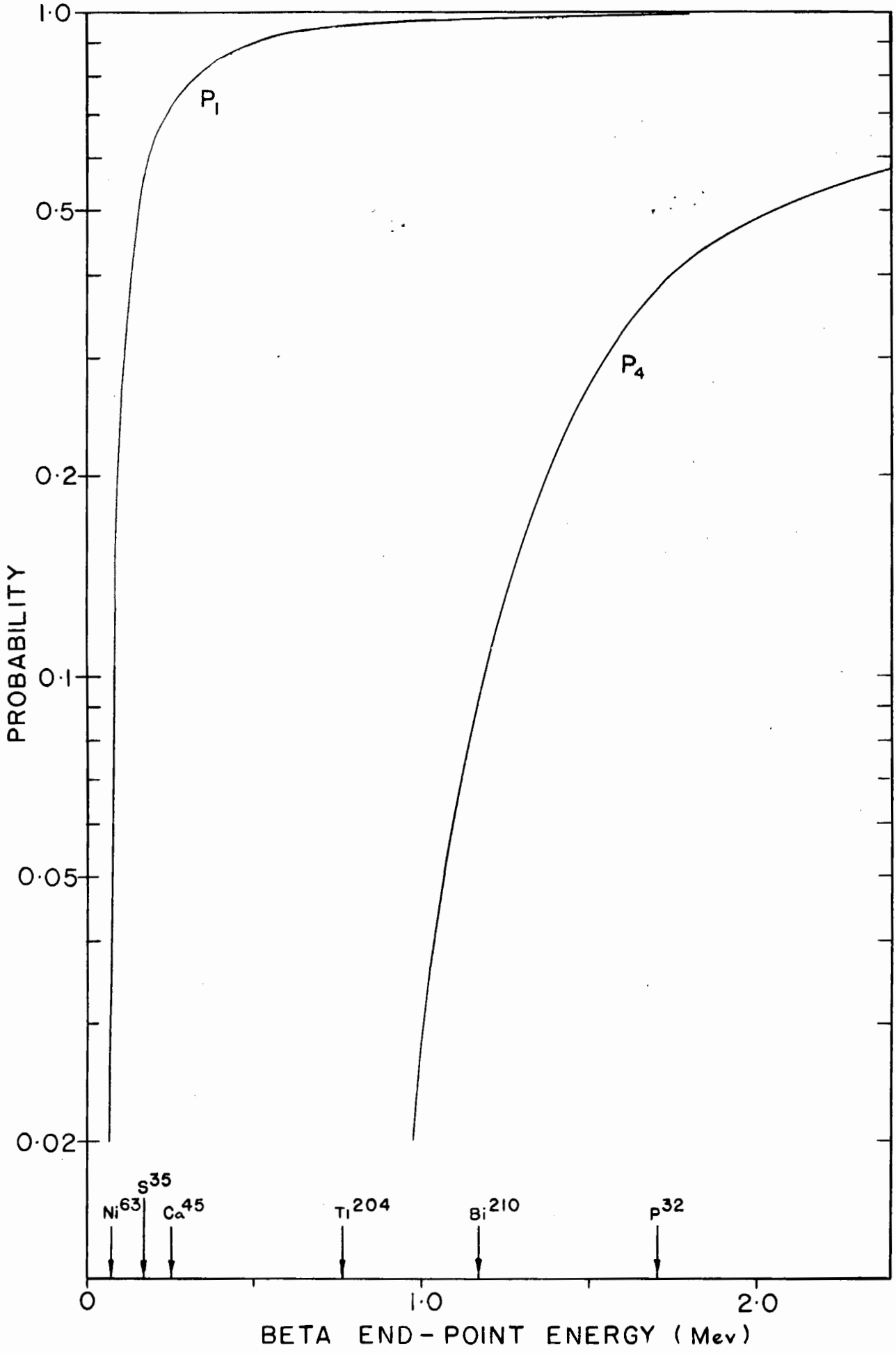
1·0
0·5
0·2
0·1
0·05
0·02
PROBABILITY
P1
P4
Ni63
S35
Ca45
Tl204
Bi210
P32
0
1·0
2·0
BETA END-POINT ENERGY (Mev)

to lower electron energies using data for the ranges of monoenergetic electrons in Rutherford, Chadwick and Ellis (121)) which is shown in Figure 58. For the purposes of these approximate calculations, we have assumed that the spectrum of Ca^{45} resembled that of S^{35}, and Tl^{204} that of P^{32}, apart from a translation of the energy, and that the back-scattered radiation had a similar energy spectrum to the incident radiation but that the end-point energy was reduced by one third (as above). We shall discuss calculation of the quoted beta energy spectra later.

If we are studying the variation of coincidence-rate with aperture size, p_1 and p_2 are constant. To compute the form of the variation of p_3, let us assume that the aluminum diaphragm of 230 mg/cm^2 superficial density will completely absorb the backscattered radiation. This is shown to be true at least for the first four nuclides of the series in Figure 52. Then the variation in p_3 will be equal to the variation of the solid angle subtended by the aperture at a point on the surface of the spherical chamber wall, averaged over all such points. This may be computed with the aid of Figure 53 (a). The integral arising from attempts to calculate the solid angle exactly is a very difficult one to evaluate. However the problem is much simplified if it is assumed that all points of the aperture are equidistant from P, which is true for small values of r (the aperture radius). Then the solid angle subtended by the aperture at P is

$$\Omega = \frac{\pi r^2 \cos \theta}{R^2} \qquad \ldots\ldots(85)$$

where R is the radius of the sphere and θ the angle made at the centre of the aperture O by the line OP with the normal ON.

Figure 53

Geometrical Arrangement of Source, Source-Mounting Film and Diaphragm Within the Counter Chamber

(a)

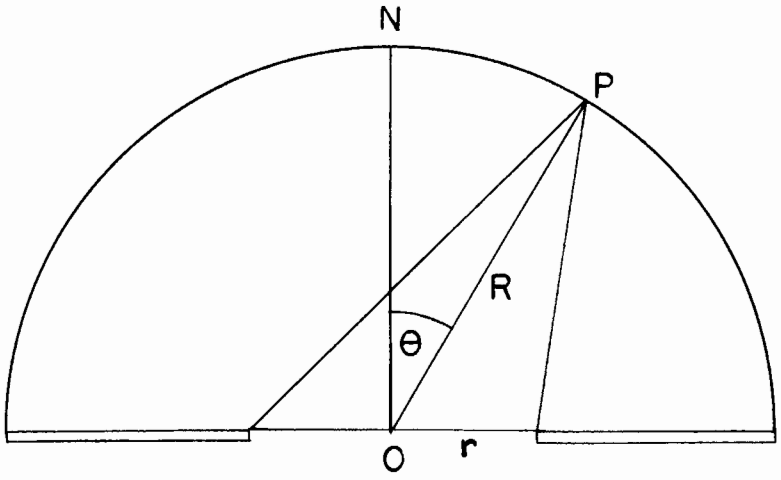

(b)

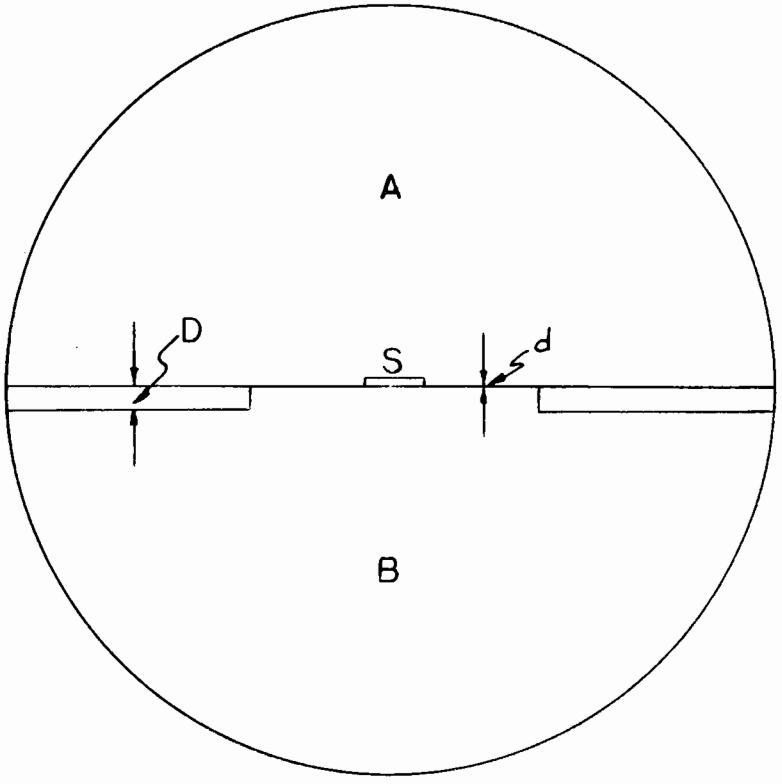

Then the mean of Ω over the whole spherical area is

$$\overline{\Omega} = \frac{1}{2\pi R^2} \int_0^{\frac{\pi}{2}} \pi r^2 \cos\theta \,.\, 2\pi \sin\theta \, d\theta \qquad .....(86)$$

where $2\pi \sin\theta.d\theta$ is the spherical area element.

Hence

$$\overline{\Omega} = \frac{\pi^2 r^2}{2\pi R^2} \left[\frac{\cos 2\theta}{2} \right]_0^{\pi}$$

$$= \frac{\pi r^2}{2R^2} \qquad .....(87)$$

Hence the variation of n_c is expected to be proportional to r^2. Figure 44 shows the result of fitting parabolas to the experimental data for n_c, and this is seen to be successful apart from the lowest values of r where the small aperture size might be expected, and was often found, to interfere with counter operation. Further it is seen that parabolas of essentially the same curvature satisfactorily fit all the sets of data except that of Ni^{63}; we shall discuss this fact at length later. Extrapolating the parabolic curves to $r = 0$ allows us to separate that part of the coincidence phenomenon independent of r. The values of n_c obtained at $r = 0$ are plotted against beta end-point energy in Figure 54, and are found to lie on two smooth curves, one each for the data obtained with methane and argon + 10 percent methane counting-gas.

The interpretation of the data, advanced by us, is as follows:-

That part of the coincidence phenomenon found to be independent of the aperture radius is due to the backscattering of beta-radiation by counting-gas in the neighbourhood of the source, while that part depen-

dent on r as r^2 is due to backscattering by gas nearer the chamber walls or more probably the chamber walls themselves.

Evidence for this assumption is as follows:

(1) Gas Backscattering

First, the coincidence rate with Ni^{63} with both methane and argon/methane is independent of r entirely. This is in accordance with the value of p_t given in Figure 52, which was found to be negligible, ie. that none of the beta radiation of Ni^{63} penetrates to the chamber wall, and back to the aperture after scattering. Hence wall scattering will not contribute to the coincidence rate and all the effect observed is due to gas-scattering. The complete invariance of n_c with r suggests moreover that the major part of the scattering occurs close to the source, despite the fact that a particle with the average energy of the Ni^{63} β-spectrum will have a range of about 1 cm. in for instance CH_4 gas.

Next the plot of the supposed gas-scattering contribution against energy (Figure 54) shows two significant features. Firstly the curve for argon/methane lies above that for methane alone, corresponding to the increased scattering resulting from the higher $\overline{Z}$ value for the gas mixture - 16 compared to 2.0 for methane. Secondly the curves show a similarity to those obtained by Yaffe and Justus (148) for the extent of backscattering from a constant thickness of backscatterer as a function of energy - neglecting however the fall at low energies they observed, which was probably due to preferential absorption of the backscattered radiation in the counter window (see earlier). Our curves may presumably be accounted for in a similar fashion. At low energies, the constant

Figure 54

Probability of Production of Coincidences in the

4π-counter by Gas Backscattering of β-radiation

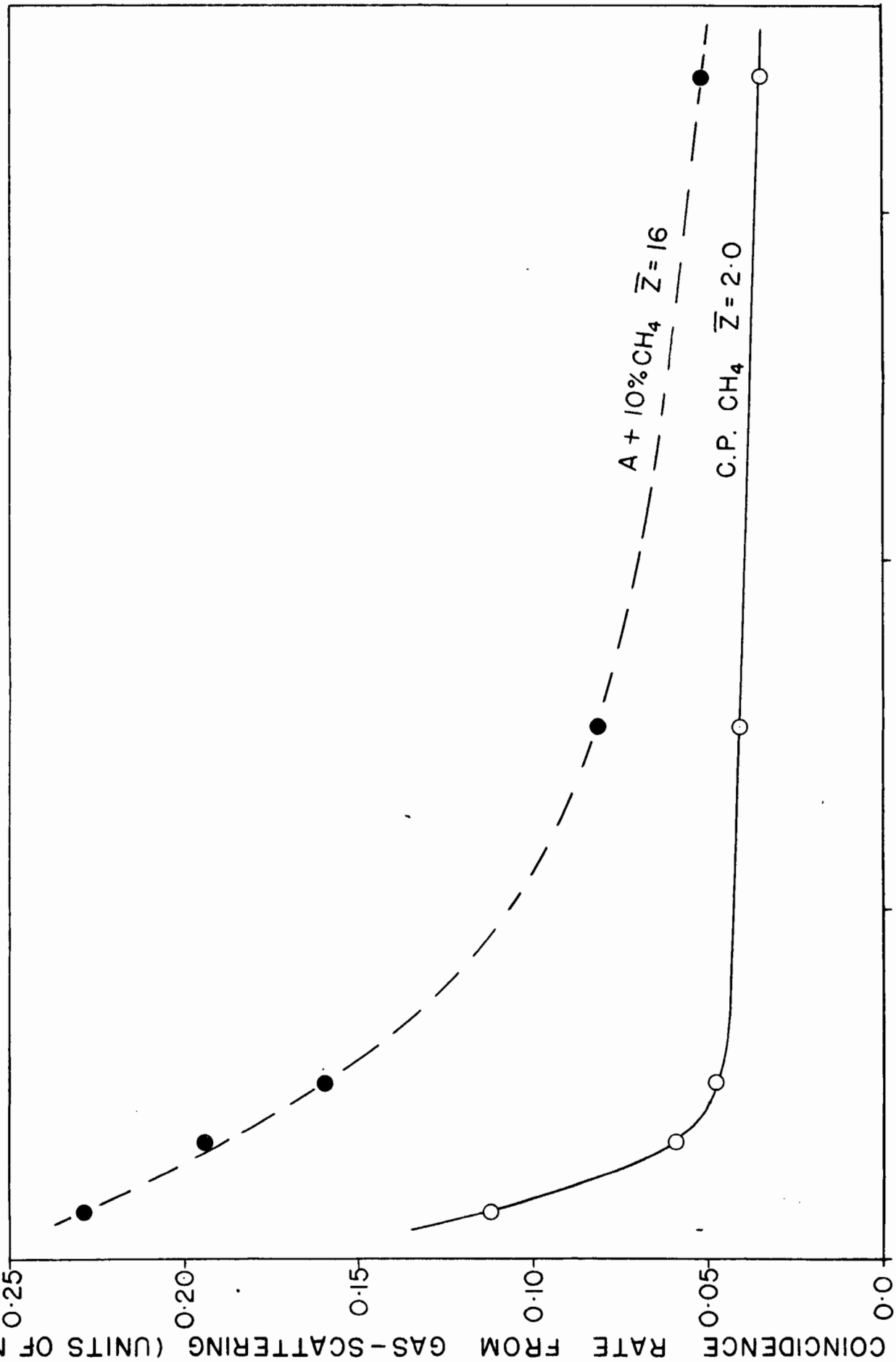
A + 10% CH_4 $\bar{Z}$ = 16
C.P. CH_4 $\bar{Z}$ = 2·0
COINCIDENCE RATE FROM GAS-SCATTERING (UNITS OF N_0)
0·0
0·05
0·10
0·15
0·20
0·25
0
0·5
1·0
1·5
BETA END-POINT ENERGY (Mev)

superficial density of scatterer available is a larger fraction of that required for saturation backscattering (which quantity is an increasing function of energy) than at higher energies, and thus a larger fraction of the saturation activity is obtained.

Thirdly we may cite data communicated to us by R. C. Hawkings of A.E.C.L. Chalk River, obtained with a counting-chamber similar to our own. These data were of the coincidence-rate obtained with S^{35} under variable gas pressure. They are plotted in Figure 55 after correction for film absorption. As the gas-pressure is increased the coincidence-rate, corresponding to gas-backscattering, increases, and at about 250 cms. of Hg is approaching a saturation backscattering value very much larger for argon/methane than for methane as expected. With diminishing pressure, the curves appear to extrapolate (as indicated with the dotted lines) to zero backscatter for zero gas pressure. However below about 150 cms. for methane, and 20 cms. for argon/methane, the gas layer ceases to be opaque to the S^{35} beta-radiation (cf. Figure 52) and wall scattering effects are observed. The curves in Figure 55 for the 5 cm. aperture and for the 2.5 cm. aperture are seen approximately to join at zero gas pressure in accordance with the behavior of the wall-scattered contribution (see below).

(2) Wall-backscattering

It was noted in the derivation of equation (87) that the simplifying assumption made was only true for small r, and thus the value of p_3 for larger r would be in error. Further by the nature of the assumptions made in the calculations of the value of p_1 in Figure 52, this too may well be in error. However, the apparent agreement of the data in

Figure 55

Variation of Coincidence-rate with Counting-gas Pressure

Using S^{35}

Data due to R. C. Hawkings of A.E.C.L. June 16th, 1954

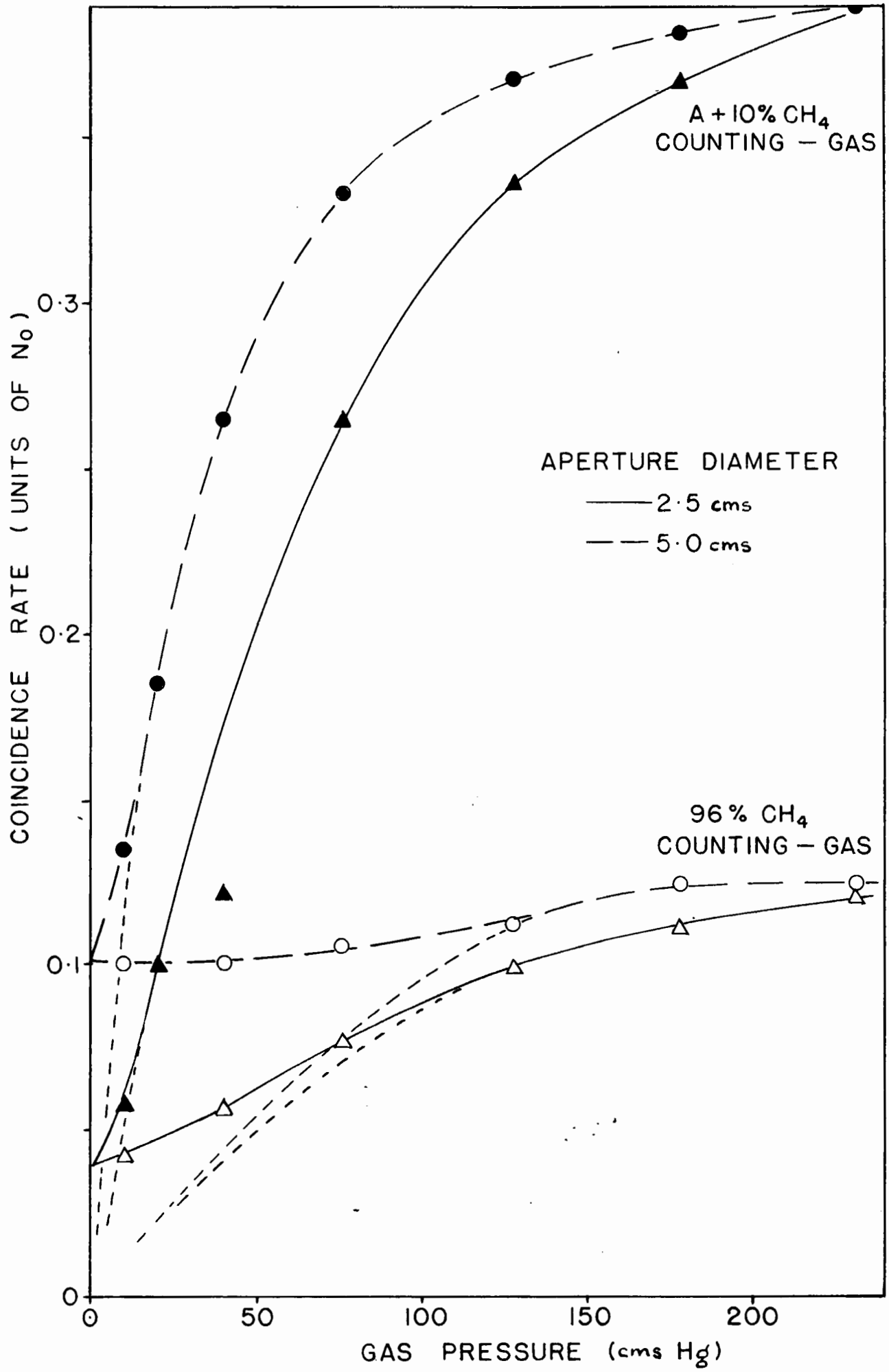
A + 10% CH4
COUNTING — GAS
APERTURE DIAMETER
2·5 cms
5·0 cms
96 % CH4
COUNTING — GAS
COINCIDENCE RATE (UNITS OF No)
0·3
0·2
0·1
0
0
50
100
150
200
GAS PRESSURE (cms Hg)

Figure 44 with a single parabola, displaced from case to case an amount along the coincidence-rate axis characteristic of the corresponding backscattering contribution, is consistent with the variable portion of the coincident phenomenon being due to wall scattering. The conditions at the wall will correspond to saturation-backscattering for all the energies of beta-radiation examined. Thus the value of p_2 will be independent of energy, since for a given Z the saturation backscattering value is energy independent, and hence by equation (84) with p_1 constant to an order of magnitude at least, n_c will vary with r only through p_3 as observed. In view of the uncertainties in the various calculations, an attempt at a more quantitative interpretation of the data does not appear profitable.

(b) Absorption and Scattering of Beta-Radiation by the Source-Mounting Film

In order to resolve the curves of Figures 45 to 50 into those for the component absorption and scattering effects, we shall adopt a method somewhat similar to those used previously in calculations of this kind (95, 135). However we shall treat all absorption and scattering factors as functions of energy and of film thickness, in the light of the discussion in the previous part of this section.

Thus the only processes we shall consider are absorption and elastic scattering of electrons in the mounting-film, and backscattering of electrons by the electron diffusion mechanism from the counter gas and chamber walls. We shall assume a counter response probability towards electrons of unity, and neglect all processes involving electromagnetic radiation and all processes involving the production of secondary elec-

tronic radiation by a simple inelastic scattering mechanism. We shall consider the chamber system to be essentially as shown in Figure 53 (b). Thus the chamber of radius 3.5 cms. is divided into two hemispheres, A and B, by the aluminum diaphragm of superficial density D (= 230 mg/cm^2), in which is an aperture of diameter 2.5 cms. (assumed constant at the value used for the experiments of Figures 45 to 50). The aperture is covered by a film of VYNS (Z= 5.1) of variable superficial density d, on the A face of which is a weightless point source S of an emitter of beta-radiation of variable end-point energy E.

Let us define the following probability coefficients: $p_1(E)$, $p_2(E)$, $p_3(E,d)$ refer to the wall scattering process and were defined earlier in connection with equation (6); however now p_3 is the probability that the wall-backscattered radiation will penetrate the combination of aluminum diaphragm + film, since the film absorption is no longer neglected. Thus, if $p_4(E)$ is the transmission of the aluminum diaphragm (which covers 86 percent of the area of the plane between the hemispheres) towards the backscattered radiation of original end-point energy E, and $p_5(E,d)$ the corresponding transmission of the film of thickness d (which covers the remaining 14 percent of the area) then approximately

$$p_3 = 0.86\ p_4 + 0.14\ p_5 \qquad .....(88)$$

for an aperture of 2.5 cms. diameter.

Further let us define

$p_6(E,d)$ as the transmission of the film to the incident beta-radiation from S.

$p_7(E,d)$ the probability per beta-particle originally emitted into the 2π steradian angle towards hemisphere B that the particle will be

scattered in the film so as to enter hemisphere A.

$p_8(E)$ the probability that the β-radiation incident into either hemisphere is backscattered by the counter gas so as to enter the other hemisphere. We shall neglect the small energy degradation attendant on passage of the β-radiation through the film to reach hemisphere B, and assume that the coefficient p_5 describes the transmission of the film to the radiation backscattered by the gas as well as the chamber walls.

Further simplification will be effected by neglecting second order processes. Thus for example, we will neglect the wall scattering of those β-particles which reach the counter walls after backscattering from the film. This is justified since (a) the process will have a total probability given by the product of two smaller component probabilities, (b) in this particular instance the majority of this backscattering effect is due to electrons scattering at small angles. These will arrive at parts of the chamber wall at which the angle subtended by the diaphragm aperture is vanishingly small, and hence from which the backscattering effects are also small.

By the same reasoning, the electrons effective in producing coincidences by the gas-scattering mechanism will principally be those emitted at larger angles to the film than those undergoing film scattering. We may therefore neglect the variation of the gas-scattering coincidence-rate due to variation in film scattering effects with d, and no dependence via p_7 will be introduced into the relevant terms of the expressions below.

Therefore bearing in mind these simplifications, without which the algebra involved in the analysis becomes very complex, we may by inspection of Figure 53 (b) write down the following expressions for the half-counter and coincidence counting-rates:-

$$n_a = \frac{N_o}{2}\left[(1 + p_7) + p_6p_8p_5 + p_6kp_5\right] \quad \text{.....(89)}$$

incident beta + film scattering; gas-backscattering from other hemisphere; wall scattering from other hemisphere

$$n_b = \frac{N_o}{2}\left[(1-p_7)p_6 + p_8p_5 + kp_5\right] \quad \text{.....(90)}$$

$$n_c = \frac{N_o}{2}\left[p_8p_5 + p_6p_8p_5 + p_6kp_5 + kp_5\right] \quad \text{.....(91)}$$

where N_o is the source beta-disintegration rate, and $k = \frac{p_1p_2p_3}{p_5}$ $= p_1p_2 \times 0.14$. Special cases of the foregoing are their values at $d = 0$, when $p_5 = p_6 = 1$ and $p_7 = 0$.

Then $$n_a = \frac{N_o}{2}(1 + p_8 + k) \quad \text{.....(92)}$$

$$n_b = \frac{N_o}{2}(1 + p_8 + k) \quad \text{.....(93)}$$

and $$n_c = \frac{N_o}{2} \cdot 2\,(p_8 + k) \quad \text{.....(94)}$$

Also it should be noted that

$$N_T = n_a + n_b - n_c$$

$$= \frac{N_o}{2}\left[1 + p_7 + (1 - p_7)p_6\right]$$

$$= \frac{N_o}{2}\left[2 - (1 - p_7)(1 - p_6)\right] \quad \text{.....(95)}$$

$$N_T(0) = N_o$$

This substantiates the expression used for calculating N_T earlier in this section, and agrees with the expectation that N_T will be independent of the factors governing the magnitude of the coincidence rate, and will differ from N_o only due to the absorption of radiation in the mounting film. (This absorption will be effective only for that fraction of the radiation originally emitted in the direction of hemisphere B which escapes backscattering by the film, ie. the fraction $(1 - p_7)$.

In equations (89) to (95), we already know the magnitude of many of the probability coefficients. For instance we already have available the value of p_8 from Figure 54, k from Figure 44, and n_a , n_b and n_c from Figures 45-49. The only unknown quantities are those we are attempting to separate, namely p_6, p_7 and p_5.

Thus equations (89), (90) and (91) form a set of three simultaneous equations from which the three unknowns can be computed for a series of values of E and d by simple algebraic means. The results of these calculations are shown in Figures 56 and 57.

Backscattering of Beta-Radiation from Thin Films

The curves of p_7, the film backscattering coefficient, as a function of d bear a superficial resemblance to the results of previous work on backscattering in conventional ($< 2\pi$) counter systems outlined earlier. There are, however, several important differences.

Firstly the magnitude of the effect is much larger at low film thicknesses in the 4π-counter. In the case of S^{35} for instance, a backscatter of > 30 percent is observed with 600 $\mu g./cm^2$ of polyvinyl chloride-

Figure 56

Backscattering of β-Radiation from Thin VYNS Films

in a 4π-counting Geometry

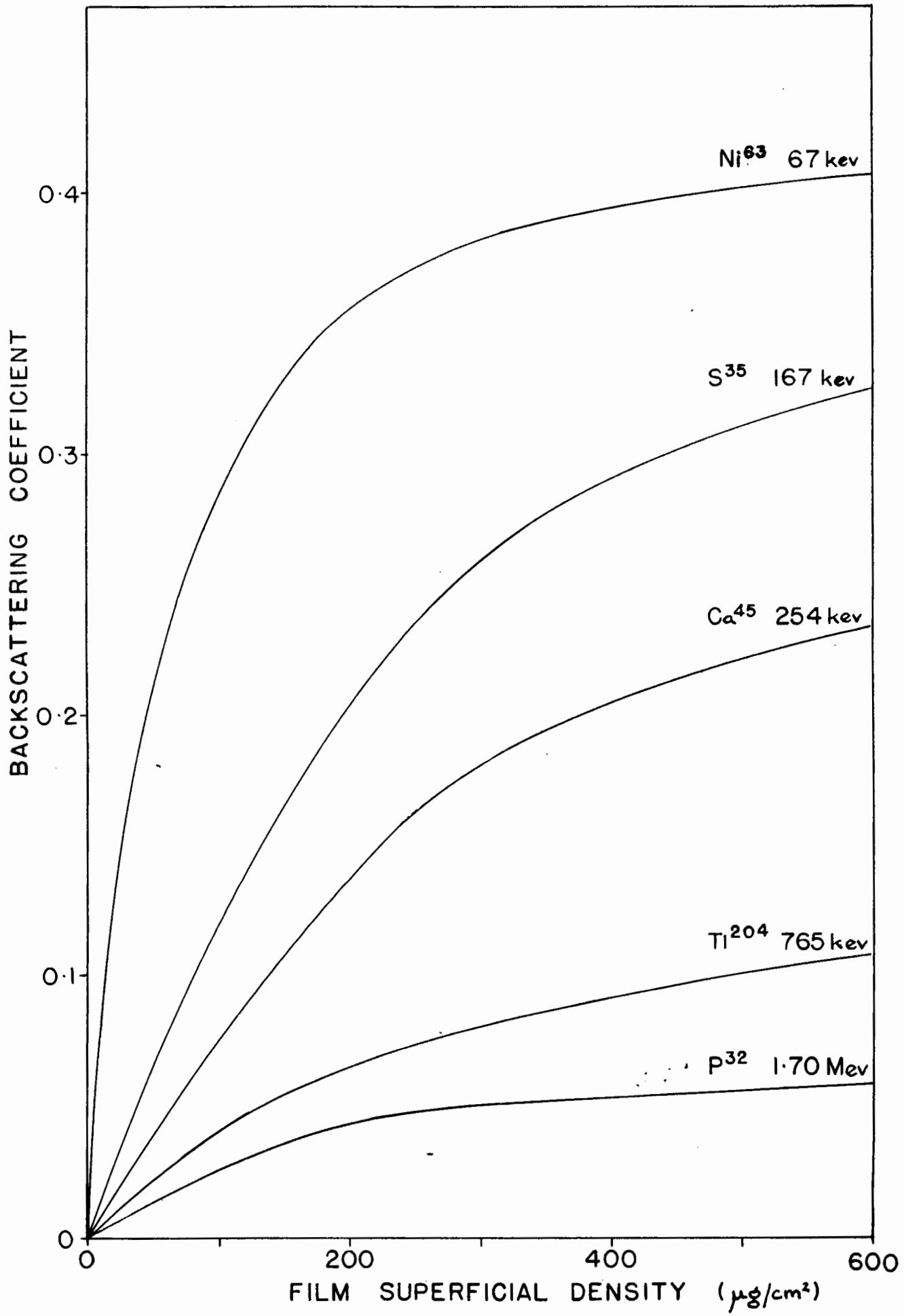
Ni63 67 kev
S35 167 kev
Ca45 254 kev
Tl204 765 kev
P32 1·70 Mev
BACKSCATTERING COEFFICIENT
0·4
0·3
0·2
0·1
0
0
200
400
600
FILM SUPERFICIAL DENSITY (μg/cm²)

Figure 57

Absorption of β-Radiation and Backscattered Radiation

in Thin VYNS Films in a 4π-counting Geometry

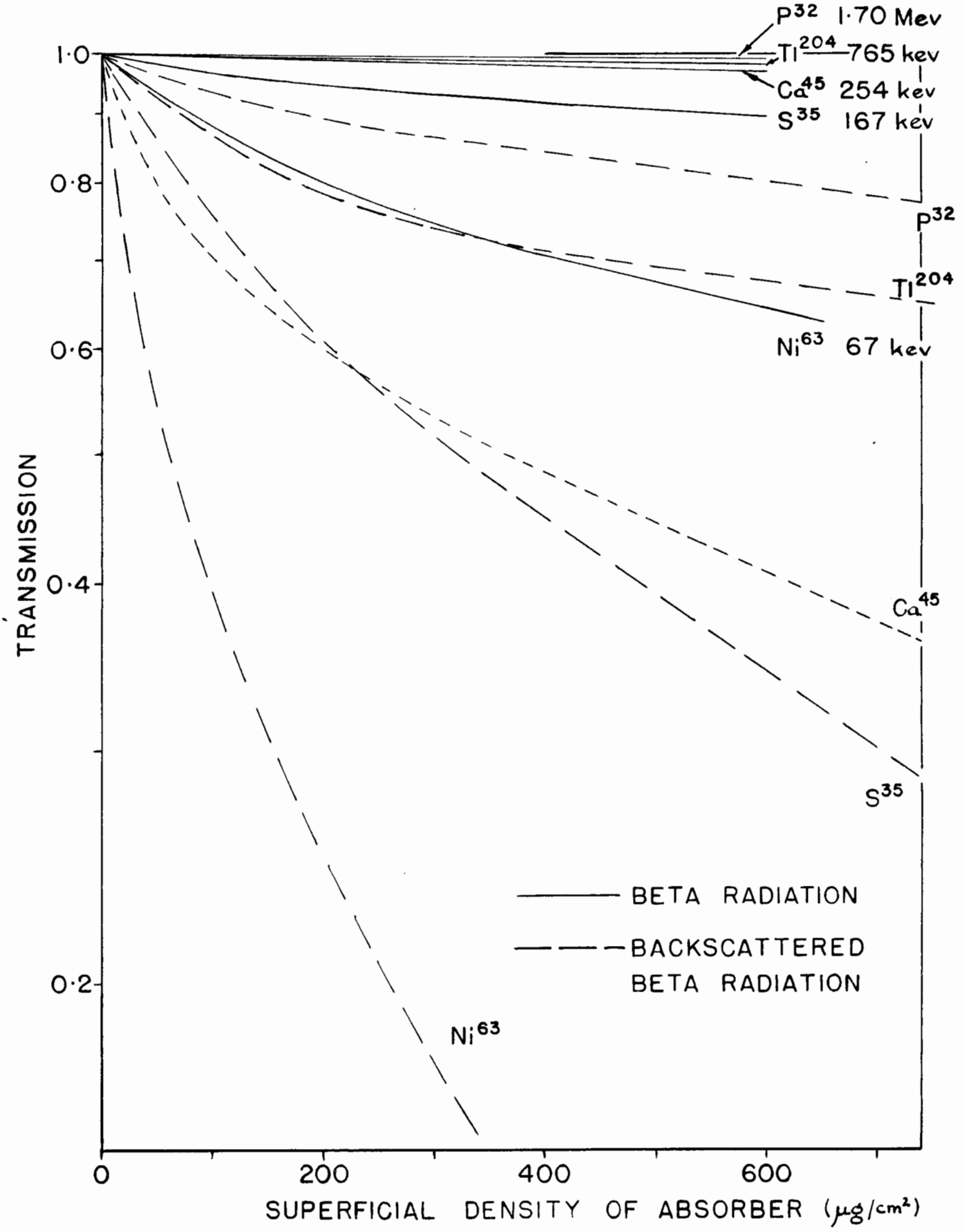
P32 1·70 Mev
Tl204 765 kev
Ca45 254 kev
S35 167 kev
P32
Tl204
Ni63 67 kev
Ca45
S35
Ni63
BETA RADIATION
BACKSCATTERED BETA RADIATION
TRANSMISSION
1·0
0·8
0·6
0·4
0·2
0
200
400
600
SUPERFICIAL DENSITY OF ABSORBER (μg/cm²)

acetate (Z = 5.1), whereas a saturation value of < 5 percent is reported (148) for aluminum (Z = 13) and this is only obtained after ~ 30 mg/cm^2 of backing. The greater magnitude of the effect we observe is in agreement with previous observations in the 4π-counter system as discussed earlier.

Secondly, it is observed that the greatest scattering occurs for the weakest beta-emitters at a given mount thickness. We have not been able to reach "saturation backscattering" in the range of source mount thicknesses studied, but if the magnitude of backscattering effects at larger mount thicknesses for various energies lie in the same order as in the range 0-700 μg./cm^2 then this is the reverse of the order observed for saturation backscattering in a < 2π system.

These facts are in agreement with the hypothesis discussed earlier, that the scattering effect observed is due to single scattering events involving electrons incident at small angles to the film surface, rather than the electron diffusion type of backscattering. The Rutherford-type scattering of relativistic electrons by atoms has been described by McKinley and Feshbach (99) among others. For the differential cross-section $d\Phi$ for scattering through an angle θ into an angle element dθ they give

$$d\Phi = \frac{2\pi e^4 Z^2}{4m^2 v^4} (1 - \beta^2) \frac{\sin \theta \, d\theta}{\sin^4(\theta/2)} \times$$

$$\left[1 - \beta^2 \sin^2 \frac{\theta}{2} + \frac{Z\pi\beta}{137} \left(\sin \frac{\theta}{2} - 1 \right) \right] \quad \ldots\ldots(96)$$

where the symbolism is as before and $\beta = v/c$. From this it will be seen that, firstly, scattering occurs predominantly at very small angles (θ) falling off rapidly as θ increases, and secondly, it is greatest for

small electron velocities.

Both these facts agree with our observations. In view, however, of the combination of a complex geometrical arrangement and a continuous distribution of particle energies in the beta-spectrum, any attempt at more quantitative correlation of theory and experiment is impracticable.

Absorption of Beta-Radiation in Thin Films

In the case of the data of the absorption of the original beta-radiation in the film (Figure 57), however, a simpler geometrical arrangement allows us to attempt a more quantitative comparison with theory.

Since in a 4π-steradian geometry, we expect to observe absorption effects relatively undisturbed by scattering phenomena, we may compare the absorption observed with that calculated from the distribution of energies in the beta-spectrum, and the Glendenin range-energy relationship (56) extended to lower electron energies by data from Rutherford, Chadwick and Ellis (121) which is shown in Figure 58.

For this purpose we need to calculate the relevant energy distribution from beta-spectral data in the literature. The superficial densities of source-mounting film employed by us will correspond to the range of the electrons of lowest energy in these beta spectra. Unfortunately, published spectral data become very unreliable in the energy region of interest (< 4 kev) owing to instrumental limitations, and modification of spectral distribution by self-scattering and absorption in the material of the source. In order to obtain an approximation to the correct electron energy distribution, we have assumed that the Fermi theory of beta-decay (48) correctly describes the energy distribution down to zero beta energy. Present indications are that this is certainly true down to 6 kev (64) and there is no evidence to the contrary

Figure 58

The Range-Energy Relationship for Electrons.

The curve of L. E. Glendenin (56) extended to lower energies using the data for monoenergetic electrons due to

Schonland
Wilson, Nuttall and Williams
} Rutherford, Chadwick and Ellis (121)

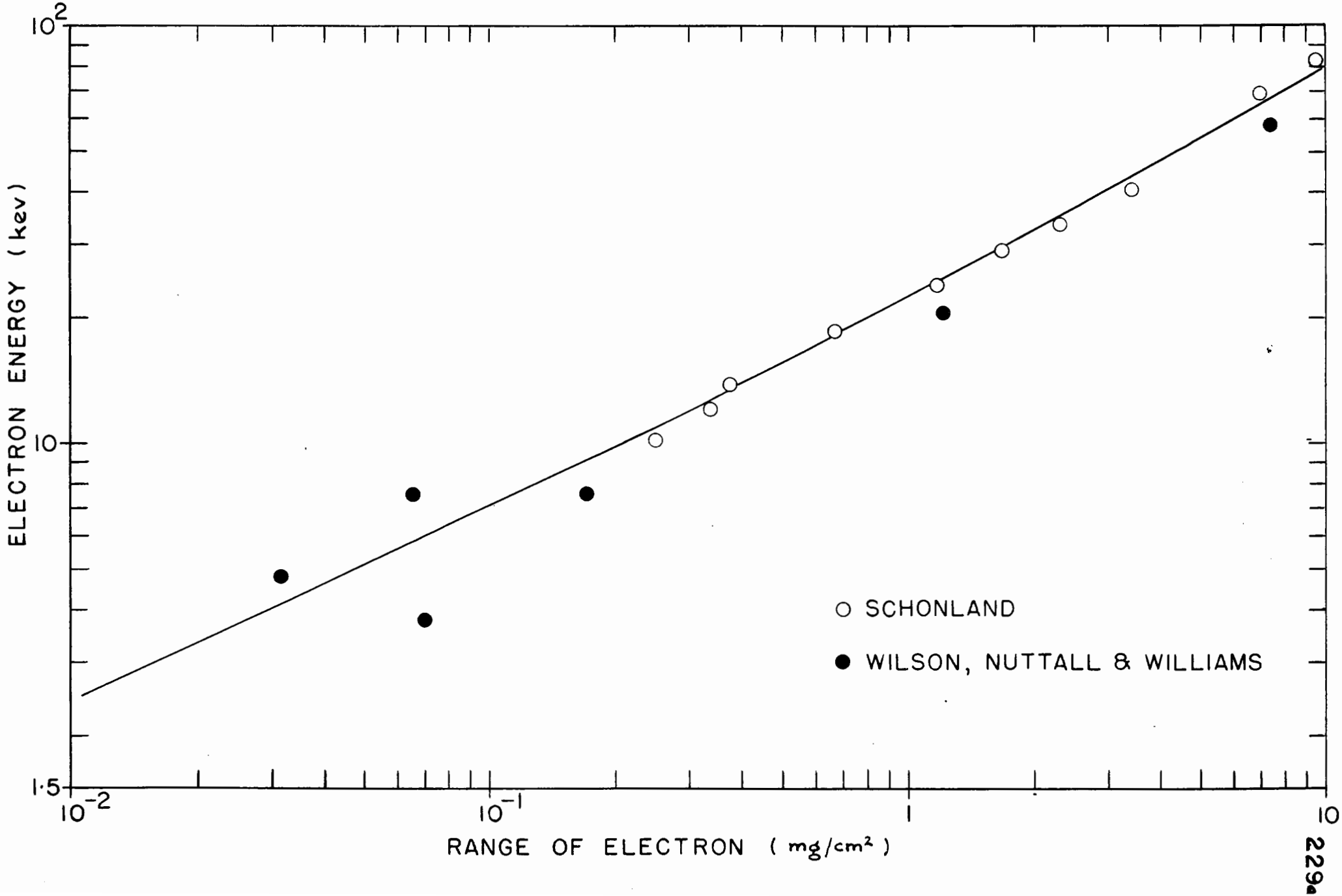
ELECTRON ENERGY (kev)
10^2
10
1·5
10^{-2}
10^{-1}
1
10
RANGE OF ELECTRON (mg/cm²)
○ SCHONLAND
● WILSON, NUTTALL & WILLIAMS

for lower energies (84).

The Fermi theory states that the probability of emission of a beta particle with an energy between E and E + dE during a nuclear transition of total energy release E_o is given by

$$N(E)dE = C\ E\ p\ (E_o - E)^2\ F(Z,E)dE \qquad .....(97)$$

where C is constant, p is the electron momentum, and F(Z,E) is given by

$$F(Z,E) = \frac{1+s}{2}\ (2pR)^{2s-2}\ \frac{e^{\pm\pi\eta}\ \left|\Gamma(s+i\eta)\right|^2}{\left|\Gamma(1+2s)\right|^2} \qquad .....(98)$$

where $s = \left[1 - \left(\frac{Z}{137}\right)^2\right]^{\frac{1}{2}}$ .....(99)

R = nuclear radius

and $\eta = \pm \frac{Z}{137}\ \frac{E}{pC}$ .....(100)

all other symbols having the meanings already defined.

The plot of $(N/EpF)^{\frac{1}{2}}$ against E (the "Kurie Plot") is linear, giving the value of E_o as the intercept of the curve with the energy axis, and beta-spectrometry data are most frequently reported in this form.

The original Fermi theory applied to allowed transitions. For the calculation of the energy distribution of beta-particles at the low energy end of the spectrum of S^{35} (allowed transition) and P^{32} (which exhibits a spectrum of allowed shape) we have assumed that a linear extrapolation of the Kurie plot given in the literature (90, 89) correctly describes the spectral form. The beta spectra obtained from the respective Kurie plots by means of the N.B.S. tables (45) are shown in Figures 60 and 61. As a further check we have first plotted the momentum-spectrum

$$P(p)dp = C\ F(Z,E)\ p^2\ (E_o - E)^2\ dp \qquad .....(101)$$

and ensured that the approach to the origin over the first small momentum range was linear with p as expected. The distribution-in-energy was then plotted from these results. Also in Figures 60 and 61, are shown the absorption curves obtained considering absorption, as described by the Glendenin curve (Figure 58), of the beta-spectra calculated.

The case of Ni^{63} beta-radiation is of particular interest, since the degree of beta-absorption in the film thickness range studied was much greater than with the other nuclides of the series. The most recent data for the Ni^{63} β-spectrum is due to Kobayashi et al. (82). Since these authors have assumed that the decay of Ni^{63} is a first forbidden transition ($\Delta J = 2$,yes), we have had to make a similar assumption in calculating the distribution in energy from their Kurie plot.

The original Fermi theory does not adequately describe forbidden transitions. However Konopinski and Uhlenbeck (83) have published a theoretical treatment of such transitions, which indicates that the energy distribution N(E)dE of the Fermi theory must be multiplied by a correction factor, which in the case of a $\Delta J = 2$,yes transition is given by

$$a = \frac{1 + S_o}{5}\left[p^2 + \Lambda q^2\right] \qquad .....(102)$$

where $$s_\nu = \left[(\nu + 1)^2 - \left(\frac{Z}{137}\right)^2\right]^{\frac{1}{2}} \qquad .....(103)$$

(Substitution of the value for the variable ν of $\nu = 0$ gives the s value quoted earlier.) p and q are the momenta of the beta-particle and neutrino respectively and

$$\Lambda = \frac{F_1}{F_o}\ (S_1 + 2 \,/\, 2 + 2S_o) \qquad .....(104)$$

where $$F_\nu(Z,E) = \left[\frac{(2\nu+2)!}{\nu!}\right]^2 (2pR)^{2(S_\nu - \nu - 1)} \cdot e^{\pi\eta} \frac{|\Gamma(s+i\eta)|^2}{|\Gamma(1+2S_\nu)|^2} \quad \text{.....(105)}$$

the remainder of the symbolism being as before.

It was necessary to evaluate the expression for α completely since none of the several approximations available were applicable in the energy range of interest. The energy spectrum for Ni^{63} calculated from the data of Kobayashi et al. (82) is shown in Figure 59 together with the theoretical absorption curve derived as before. (It should be noted that in these calculations the values of the gamma function for a complex argument, which are not yet extensively tabulated, were calculated as required from the relationship:

$$\left|\frac{\Gamma(x+iy)}{\Gamma(x)}\right|^2 = \prod_{n=0}^{\infty}\left[\frac{1}{1+\frac{y^2}{(x+n)^2}}\right] \quad (x,y \text{ real}, x > 0) \quad \text{.....(106)}$$

The absorption curves obtained in this way are those to be expected in a narrow angle geometry, ie. the absorption expected with a collimated beam of radiation since no allowance for oblique paths through the absorber was made. In our case however we are interested in the absorption effects observed with radiation emitted into a solid angle of 2π steradians, and it will be necessary to allow for increased absorption due to the fact that most particles will in fact follow an oblique path through the absorber and thus have a path length greater than the film thickness d. The extent of increase in absorption may be calculated in a fashion similar to that used for self-absorption in section D.

Figure 59

Beta-Spectral Data for Ni^{63}

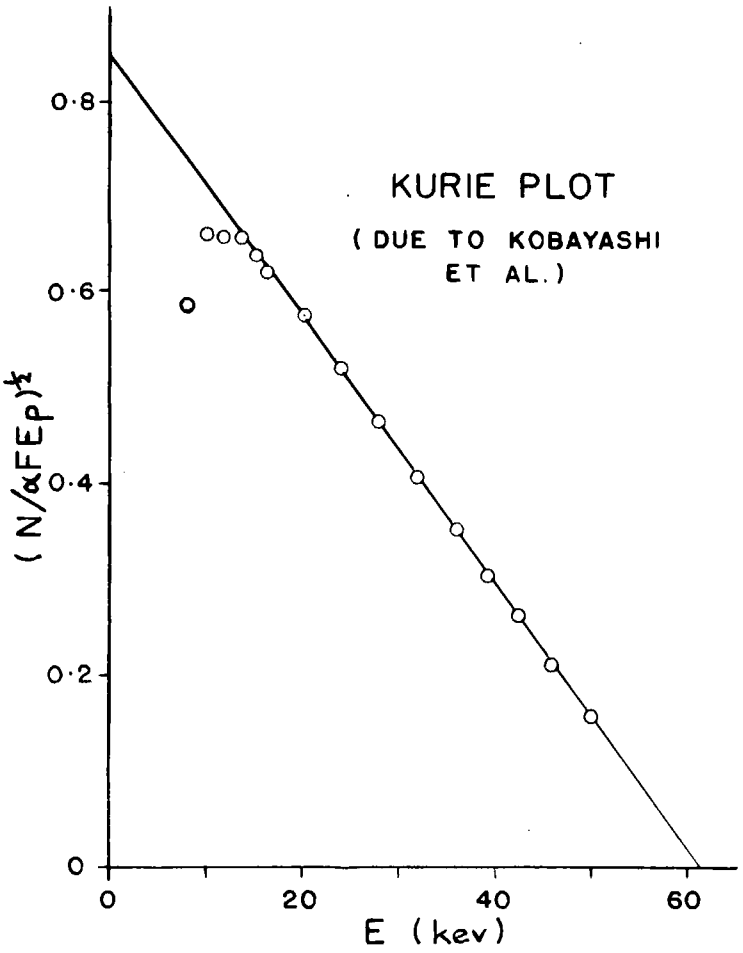
KURIE PLOT
(DUE TO KOBAYASHI ET AL.)
$(N/\alpha F E p)^{\frac{1}{2}}$
0·8
0·6
0·4
0·2
0
0
20
40
60
E (kev)

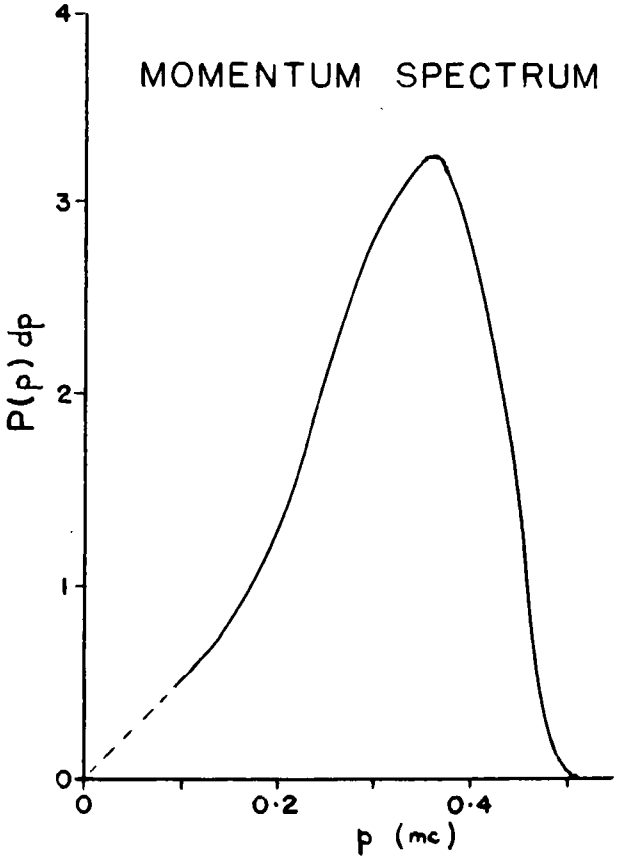
MOMENTUM SPECTRUM
P(p) dp
4
3
2
1
0
0
0·2
0·4
p (mc)

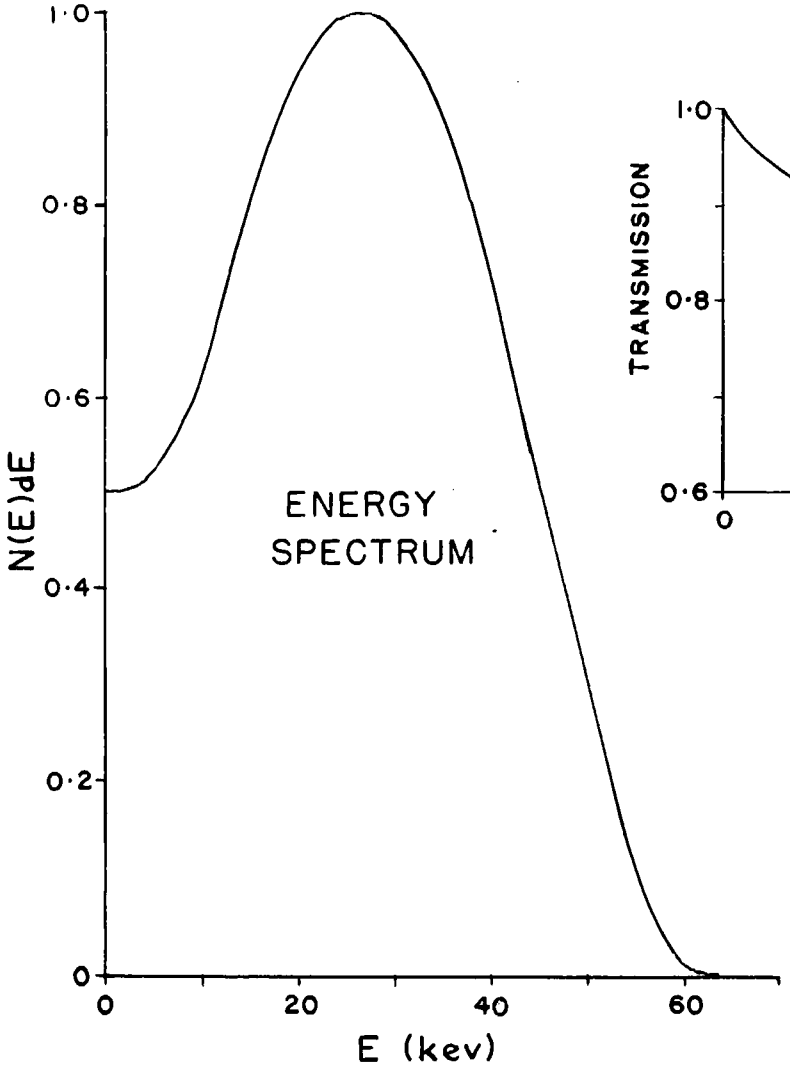
ENERGY SPECTRUM
N(E)dE
1·0
0·8
0·6
0·4
0·2
0
0
20
40
60
E (kev)

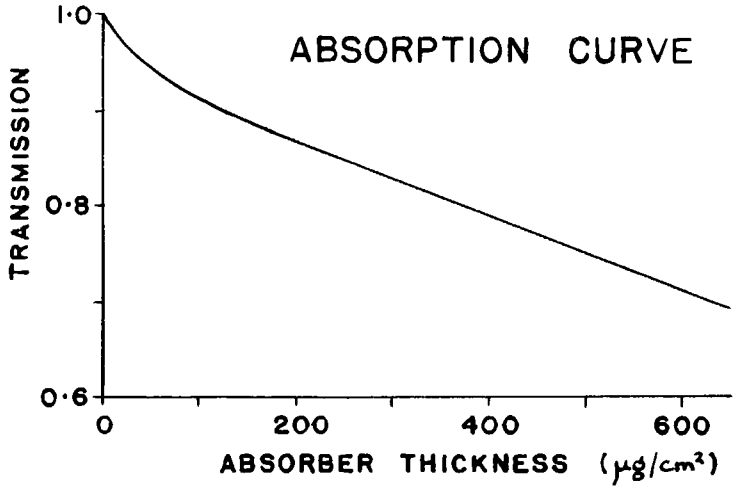
ABSORPTION CURVE
TRANSMISSION
1·0
0·8
0·6
0
200
400
600
ABSORBER THICKNESS (μg/cm²)

Ni^{63}

Figure 60

Beta-Spectral Data for S^{35}

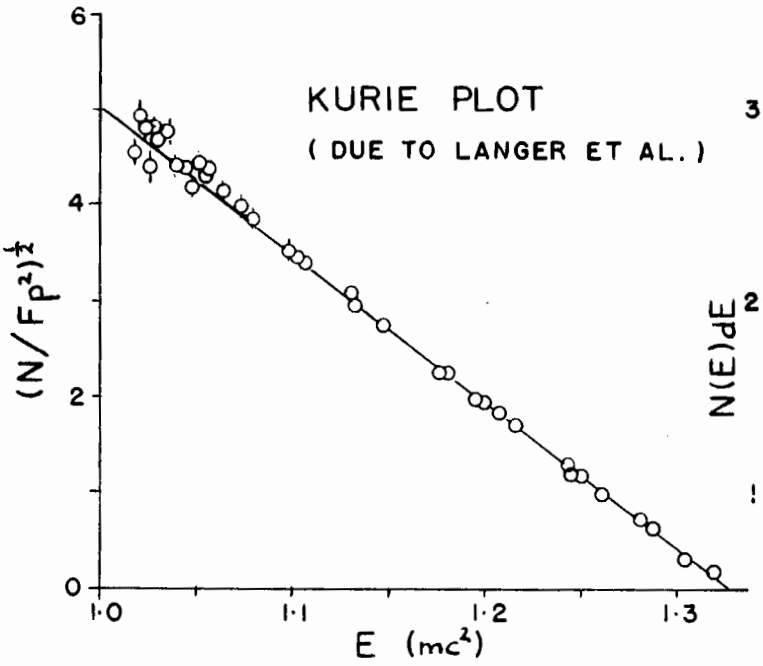
KURIE PLOT
(DUE TO LANGER ET AL.)
$(N/Fp^2)^{\frac{1}{2}}$
E (mc^2)
6
4
2
0
1·0
1·1
1·2
1·3

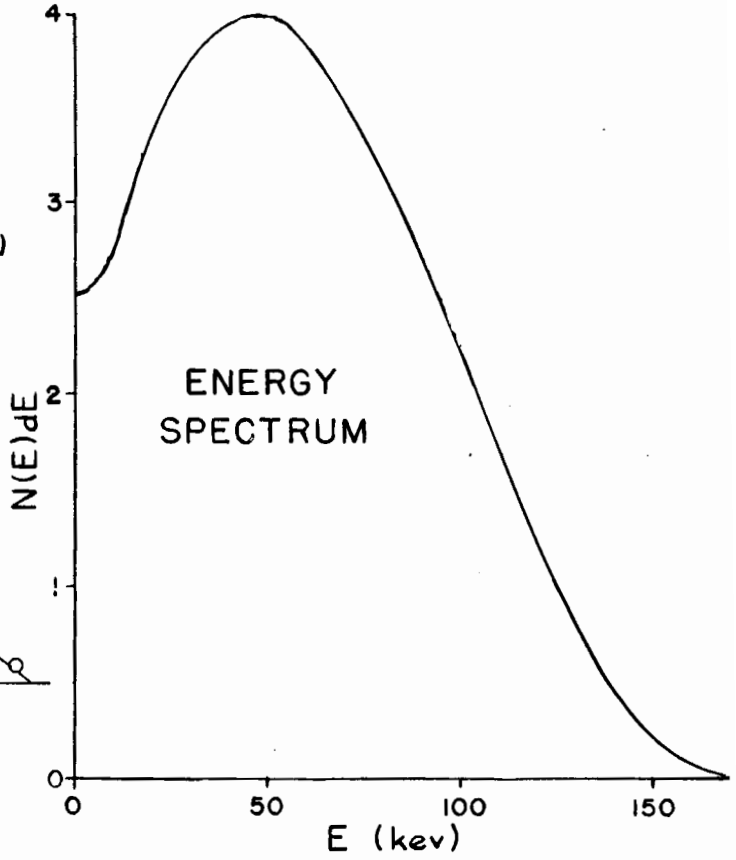
ENERGY
SPECTRUM
N(E)dE
E (kev)
4
3
2
1
0
0
50
100
150

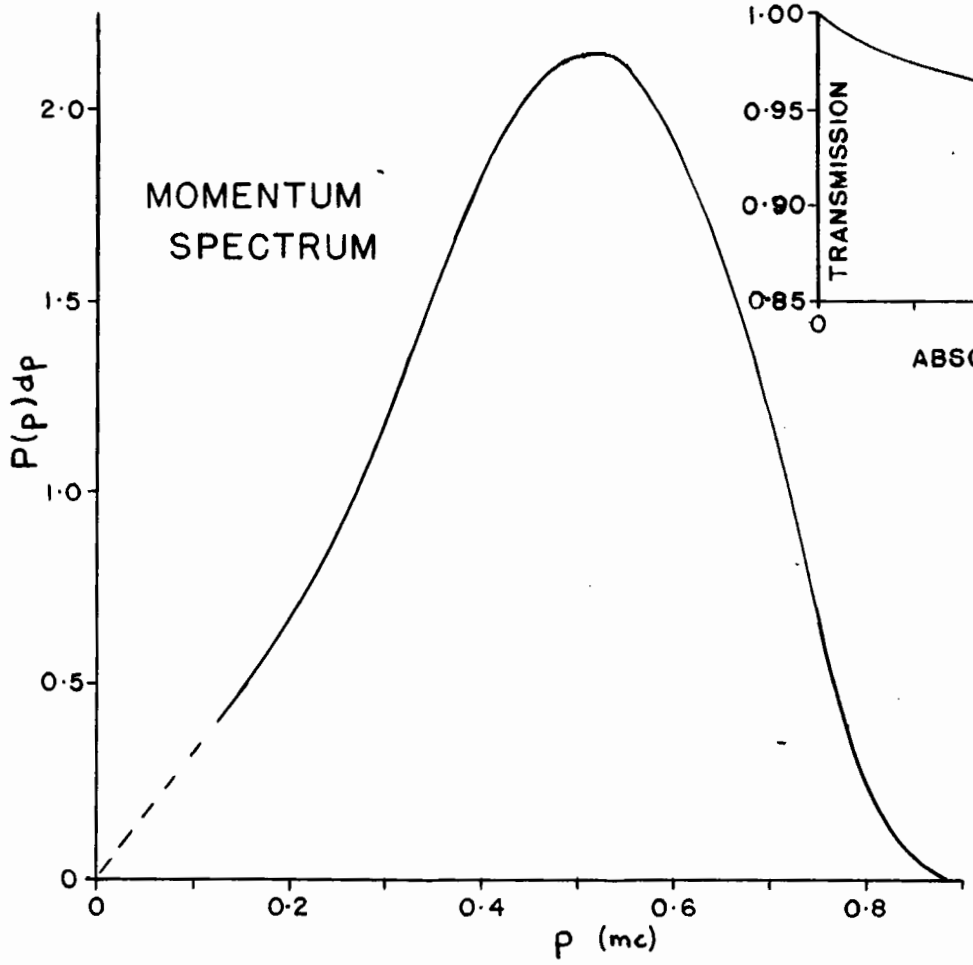
MOMENTUM
SPECTRUM
P(p)dp
p (mc)
2·0
1·5
1·0
0·5
0
0·2
0·4
0·6
0·8

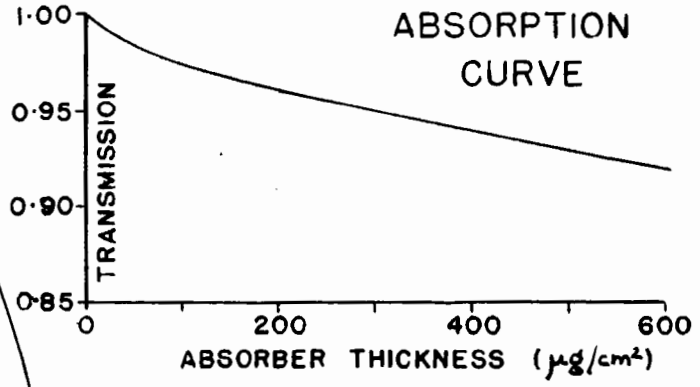
ABSORPTION
CURVE
TRANSMISSION
ABSORBER THICKNESS (μg/cm²)
1·00
0·95
0·90
0·85
0
200
400
600

S^{35}

Figure 61

Beta-Spectral Data for P^{32}

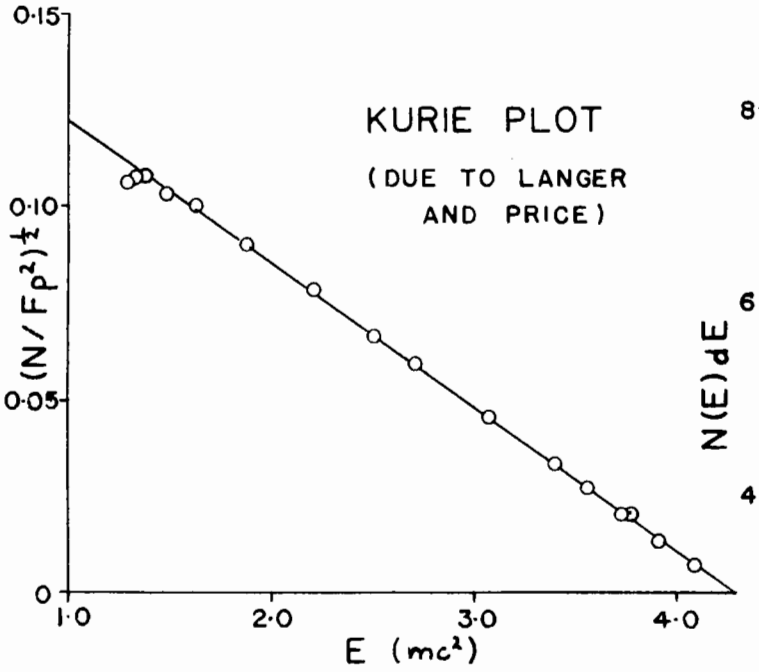
KURIE PLOT
(DUE TO LANGER AND PRICE)
0·15
0·10
0·05
0
(N/Fp²)½
1·0
2·0
3·0
4·0
E (mc²)

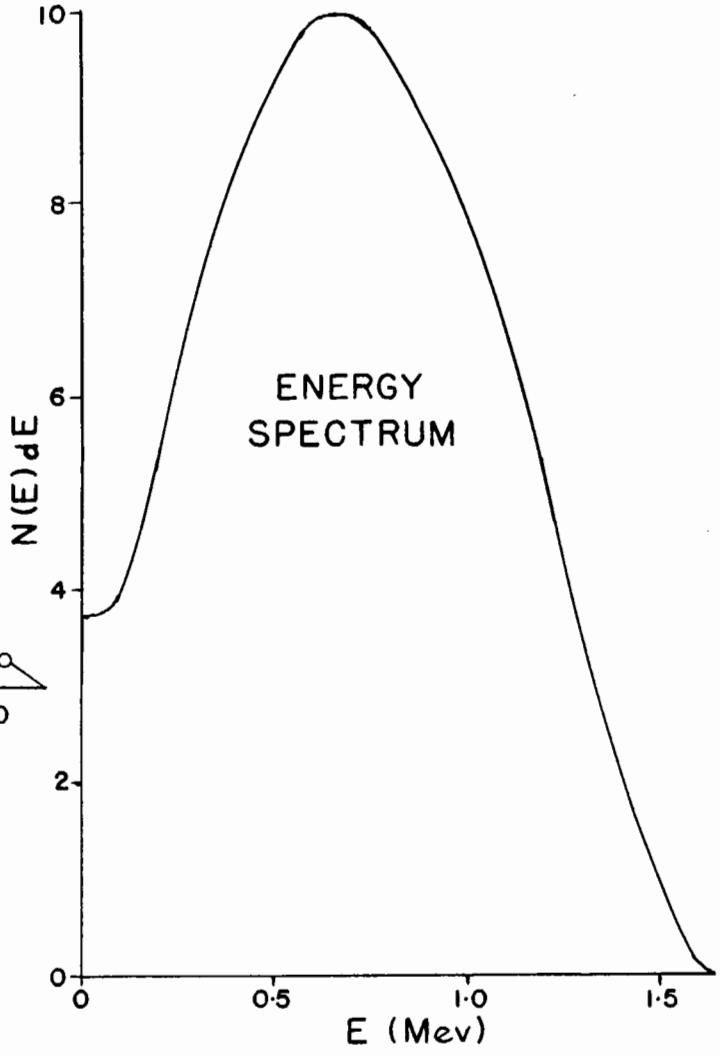
ENERGY SPECTRUM
10
8
6
4
2
0
N(E)dE
0
0·5
1·0
1·5
E (Mev)

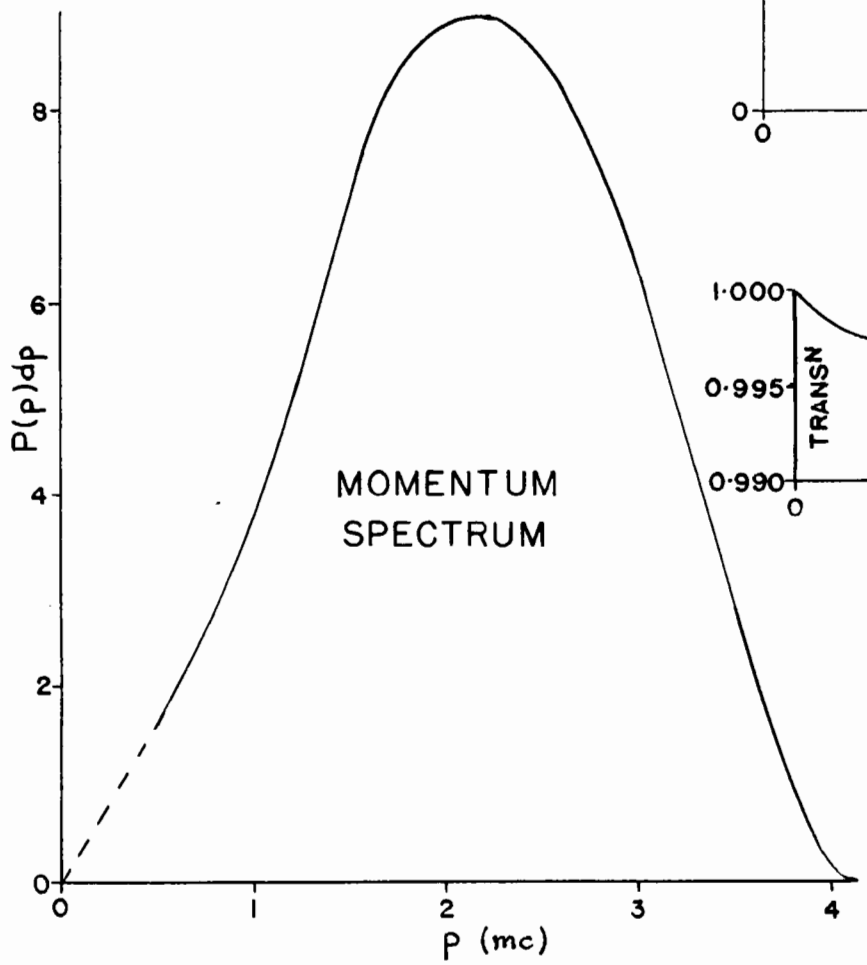
MOMENTUM SPECTRUM
8
6
4
2
0
P(p)dp
0
1
2
3
4
P (mc)

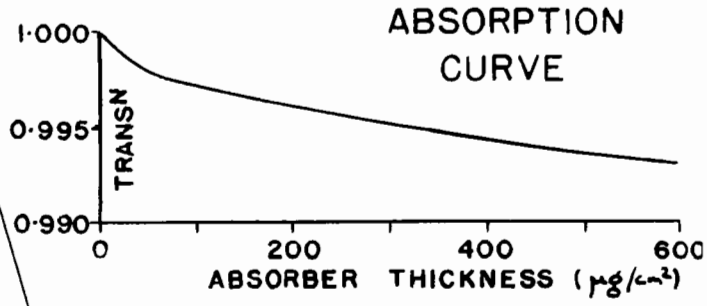
ABSORPTION CURVE
1·000
0·995
0·990
TRANSN
0
200
400
600
ABSORBER THICKNESS (μg/cm²)

P^{32}

First we need an analytical expression to describe the simple absorption relationships of Figures 59 and 60. The simplest with the necessary degree of accuracy is found to be

$$A_d = A_o \left[a\, e^{-\mu_1 d} + (1 - a)\, e^{-\mu_2 d} \right] \qquad .....(107)$$

ie. the absorption curve is treated as that obtained from two different beta emitters (assuming simple exponential absorption as earlier) of relative intensities a and (1 - a) and with external absorption coefficients μ_1 and μ_2. With Ni^{63} and S^{35}, the two cases we shall calculate, the values of a, μ_1 and μ_2 are as shown in table VII.

TABLE VII

	a	μ_1 $cm^2/\mu g$	μ_2 $cm^2/\mu g$
Ni^{63}	0.950	4.6×10^{-4}	3.2×10^{-2}
S^{35}	0.964	1.0×10^{-4}	2.4×10^{-2}

Then the activity observed at an angle θ through a film of thickness d, $A_{\theta,d}$, is given by

$$A_{(\theta,d)} = A_o \left[a\, e^{-\mu_1 d/\cos\theta} + (1 - a)\, e^{-\mu_2 d/\cos\theta} \right] \qquad .....(108)$$

Therefore the activity observed over a solid angle of 2π steradians is given by

$$A_{(\frac{\pi}{2},d)} = A_o \int_0^{\frac{\pi}{2}} \left[a\, e^{-\mu_1 d/\cos\theta} + (1 - a)\, e^{-\mu_2 d/\cos\theta} \right] 2\pi \sin\theta\, d\theta \qquad .....(109)$$

where A_o is suitably normalized.

Since α and $(1 - \alpha)$ are constant, this can be treated as two separate but identical integrals.

Let us make the following substitutions,

$$\lambda = \mu d$$

$$y = \frac{\lambda}{\cos \theta}$$

$$dy = \lambda \tan \theta \sec \theta \, d\theta$$

$$= \frac{y^2}{2\pi\lambda} \, d\Omega$$

where $d\Omega = 2\pi \sin \theta \, d\theta$, the solid angle element. Each term of equation (109) then reduces to

$$\lambda \int_{\lambda}^{\infty} \frac{e^{-y}}{y^2} \, dy = \lambda \left[- \frac{e^{-y}}{y} \right]_{\lambda}^{\infty} - \lambda \int_{\lambda}^{\infty} \frac{e^{-y}}{y} \, dy \qquad .....(110)$$

$$= e^{-\lambda} + \lambda \, Ei(-\lambda) \qquad .....(111)$$

where $Ei(-\lambda)$ is the exponential integral function. If we define

$$F = e^{-\lambda} + \lambda \, Ei(-\lambda) \qquad .....(112)$$

then equation (109) becomes

$$A_{(\frac{\pi}{2}, d)} = A_o(\alpha \, F_1 + (1 - \alpha) \, F_2) \qquad .....(113)$$

$$= A_o \, F \qquad .....(114)$$

The functions F_1, F_2 and hence F can be evaluated, by means of the values of the Ei function from the data of Jahnke and Emde (78). We have plotted function F against d for Ni^{63} and S^{35} in Figure 62, together with the absorption curve for narrow angle geometry from Figures 59 and 60, and the experimental values from Figure 57.

Figure 62

Comparison of Theoretical and Experimental Absorption Curves

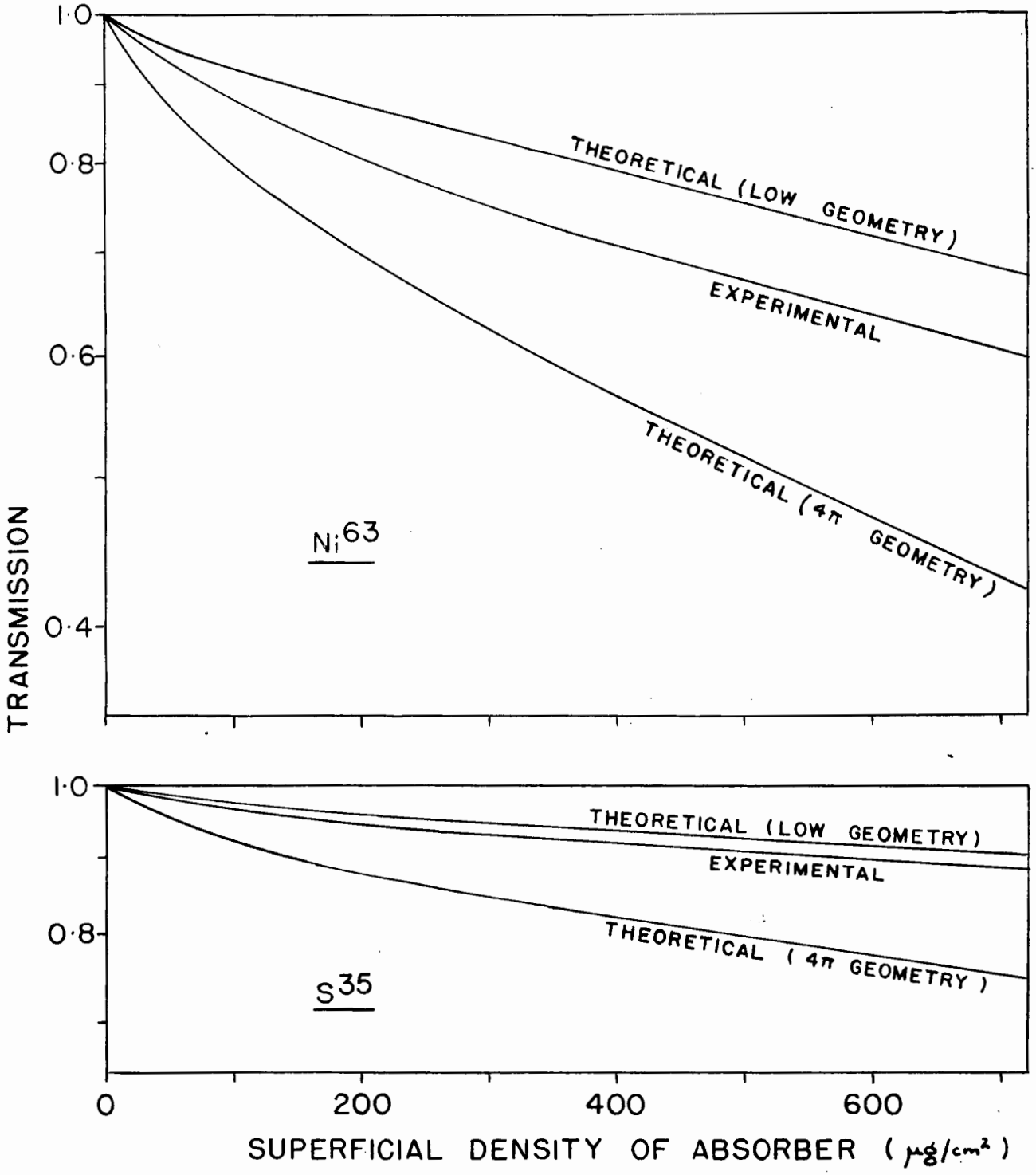
1·0
0·8
0·6
0·4
TRANSMISSION
THEORETICAL (LOW GEOMETRY)
EXPERIMENTAL
THEORETICAL (4π GEOMETRY)
Ni63
1·0
0·8
THEORETICAL (LOW GEOMETRY)
EXPERIMENTAL
THEORETICAL (4π GEOMETRY)
S35
0
200
400
600
SUPERFICIAL DENSITY OF ABSORBER (μg/cm²)

It is seen that the experimental curve lies between the theoretical curves for 4π and low geometries, being nearer to the latter than the former. The explanation for this may be as discussed earlier. The above calculations assume that the beta-particle follows a rectilinear path through the absorber, whereas changes in direction due to scattering are certainly known to occur. Thus a particle traversing the film at a small angle θ to the surface will have a high probability of being scattered out of the film before completing a path length $d/\cos\theta$, but after a path length of more than d alone. Thus the absorption effects will be between those corresponding to the extreme cases, as observed.

Absorption of Backscattered Radiation

In Figure 57 are compared the absorption curves for the back-scattered radiation and the original beta-radiation. It is seen that the energy degradation is very much more than observed by previous workers on backscattering in a $< 2\pi$ geometry. They found a ratio of half-thicknesses or ranges for the backscattered to the original radiation of about 0.4 to 0.8, whereas for example in the case of Ni^{63}, we find a half-thickness ratio of 0.05 or less.

This is doubtless due to the fact that we are using a windowless counter, whereas previous workers were not. Our results clearly point to the existence of a large proportion, in the energy spectrum of the backscattered radiation, of low energy particles, in agreement with the results of Balfour (6). These would to a large extent be absorbed in a counter window, and not be observed in the counter set-ups used previously.

(c) Sandwich Procedure for Correcting for Source-Mount Absorption Losses

It was shown in section C of this thesis that the mathematical relationships (95) proposed for the correction of source-mount absorption losses by means of "sandwich" measurements lead to erroneous (high) values for the source disintegration-rate. On the basis of the interpretation of the coincidence-rates and half-counter counting rates presented in this section, we may formulate expressions for the corresponding quantities in the case of a "sandwiched" source, in terms of the scattering and absorption coefficients obtained above, and compare them with those obtained previously (95).

The situation with a sandwiched source is illustrated schematically in Figure 63. The expressions for the half-counter and coincidence rates may be formulated by inspection in a similar way to that used earlier for a single mounting film. We shall again neglect the effect of film scattering (coefficient p_7) on the various contributions to the coincidence rate, as described earlier. In view of the magnitude of the film scattering coefficient p_7 (Figure 56) we shall however assume (as did Mann and Seliger) that continued scattering of electrons between the films (ie. from one film to another) is a significant effect, and hence the term for the total intensity of radiation after emerging from between the films will be of the form

$$\frac{N_o}{2}(1 - p_7)\, p_6\, (1 + p_7 + p_7^2 \ldots\ldots)$$

$$= \frac{N_o}{2} p_6 \qquad \ldots\ldots(115)$$

Then the complete expression for the half-counter rates and coincidence

Figure 63

Sandwich Arrangement of Source-Mounting Film

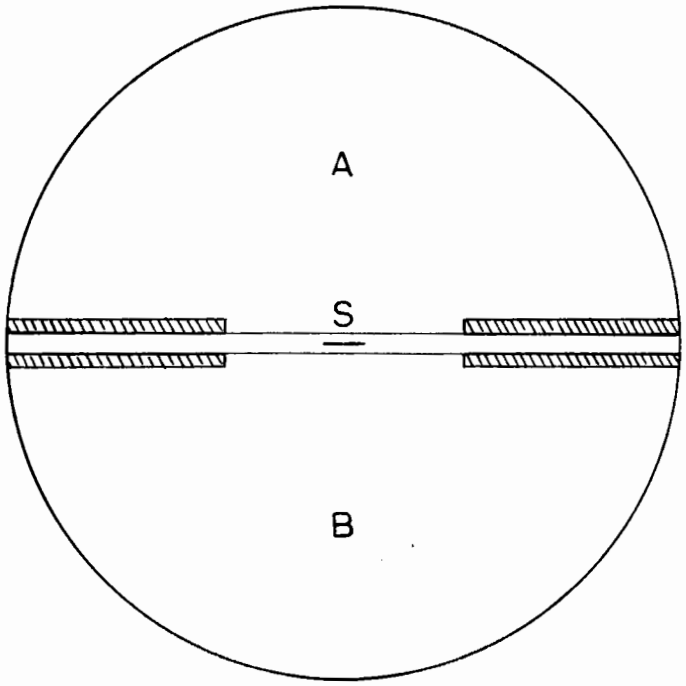
A
S
B

rates are as follows.

The half-counter counting-rates observed with sandwiched films (same for hemispheres A and B):

$$n_s = \frac{N_o}{2}\left[p_6 + (1 - p_7)\, p_6 p_5^2\, (p_8 + k)\right] \qquad .....(116)$$

Coincidence rate with sandwiched films

$$n_{sc} = N_o\, (1 - p_7)\, p_6 p_5^2\, (p_8 + k) \qquad .....(117)$$

and as before total counting rate with sandwiched films

$$N_S = 2n_s - n_c$$

$$= N_o\, p_6 \qquad .....(118)$$

This expression for N_S is similar to that obtained by Mann and Seliger but to compare the two calculations further, let us consider their formula for computing the value of t, equivalent to our $(1 - p_6)$, the absorption coefficient of the single film:

$$\frac{t}{2} = \frac{N_T - N_S}{2N_T - N_S} \qquad .....(119)$$

this from above

$$= \frac{1 + p_7 + p_6 - p_6 p_7 - 2p_6}{2 + 2p_7 + 2p_6 - 2p_6 p_7 - 2p_6}$$

$$= \frac{1 + p_7 - p_6 - p_6 p_7}{2 + 2p_7 - 2p_6 p_7} \qquad .....(120)$$

If p_7 is negligible this expression reduces to

$$\frac{1 - p_6}{2} = \frac{t}{2}$$

as assumed by Mann and Seliger.

However we find that p_7 is far from negligible. Take for example the value for Ni^{63} with a film of 100 $\mu g./cm^2$, when $p_7 = 0.3$ and $p_6 = 0.85$. Then from Figures 56 and 57.

$$\frac{N_T - N_S}{2N_T - N_S} = \frac{1.3 - 0.6}{2.6 - 0.5} = 0.35$$

That is $t = 0.7$ compared with a measured value of $(1 - p_6) = 0.15$. Hence the Mann and Seliger method (95) of determining film absorption is liable to be grossly in error, since the value of p_7 even at beta-energies of 1.7 Mev was found to be of the order of 5 percent except at very low film thicknesses.

These authors were however fortunate in as much as their neglect of film-scattering produced an error of opposite sign when the value of t was used to correct for absorption losses, although the cancellation of errors was still far from complete. This arose since they assumed that the disintegration rate was given by

$$N_T = N_o - \frac{N_o}{2} t \qquad \text{.....(121)}$$

ie. that exactly half the emitted radiation entered the film and was "available" for absorption. As was seen earlier, however, this amount of radiation was reduced by that fraction scattered from the film

$$N_T = N_o - \frac{N_o}{2} (1 - p_7)(1 - p_6) \qquad \text{....see equation (95)}$$

Clearly, despite the cancellation of error, calculations which treat the film-scattering process as being of negligible order of magnitude can only be considered as approximations in accurate disintegration-rate determinations.

Scattering and Absorption of Alpha Radiation

The data in Figure 50 for the source mount absorption characteristics for the α-radiation of Po^{210}, may briefly be compared with those for beta-radiation discussed above. The coincidence rate n_c for an α-emitter is observed to be less than 0.1 percent of the disintegration-rate, which substantiates the postulate, outlined above, that the coincidence rate with beta emitters is due to gas and counter-wall scattering. These processes would be expected to be unimportant for α-radiation. Similarly the counting-rate in the hemisphere A is observed to remain constant with increasing film thickness, indicating that small angle scattering from thin films is likewise unimportant, as expected. The fall in counting rate in hemisphere B with increasing film thickness has already been correlated with radiation absorption in the discussion of section C of this thesis.

F. SUMMARY AND CONTRIBUTIONS TO KNOWLEDGE

The various methods available for the determination of absolute disintegration rates have been reviewed, and the advantages of the most widely applicable and potentially most precise of these, 4π-counting, have been discussed. 4π-counting is subject to three sources of experimental error. Each has been examined, in order to reduce its effect on the final disintegration-rate value.

(1) The response probability of the counter is a function of the polarization potential, amplifier gain, and discriminator bias used with the chamber, of source position within the chamber, of the amount of conducting material applied to the source mounting film, of the purity of counting gas used, and of the source disintegration rate. The response probability has been examined as a function of all these variables, and the conditions determined under which departure from unity was at a minimum. It has been shown experimentally that this departure can be reduced to less than 0.1 percent.

Theoretical calculations indicate that at 2.9 kv polarization potential, the production of one ion-pair in the chamber will trigger the recorder. Calculationsof the fraction of beta-radiation with a very low end-point energy (Ni^{63} and S^{35}) which will fail to produce this minimum ionization, agree with the estimated error due to a low response probability.

(2) Absorption of radiation in the source mounting film has been reduced by the use of very thin gold-coated films of VYNS resin. Entirely new techniques for the fabrication and accurate measurement of the thick-

ness of very thin films have been described. These combined with the hitherto unreported employment of VYNS resin allow up to 100 cm^2 of tough, highly chemically resistant film, of superficial density down to less than 1 $\mu g./cm^2$, to be used as a source mount in both 4π-counting and β-spectrometry.

The radiation absorption still remaining due to the source-mount has been examined as a function of particle energy, and of the nature of the radiation, and a new procedure devised for correcting for it. The results are more accurate than those reported hitherto, and the error still arising from this source is estimated to be less than 0.2 percent.

(3) Self-absorption errors have been examined. Sources of radiation (Ni^{63}, S^{35} and Co^{60}), in which self-absorption effects were uniform and reproducible, have been prepared by a specially developed technique, which involves vacuum distillation of an organic derivative of the nuclide studied. The deposits arising from this technique were shown by electron microscopy to be micro-crystalline. Sources of superficial density down to 0.5 $\mu g./cm^2$ can readily be deposited on to a 5 $\mu g./cm^2$ VYNS film. Spectrophotometric techniques for the accurate measurement of deposit thickness have been described, and these indicate a potential application of this mounting method to absorption spectrophotometry generally.

The preparation of a source of Ni^{63} beta-radiation with 0.5 $\mu g./cm^2$ superficial density, and the preparation of a self-absorption curve for this material between 0 and 80 $\mu g./cm^2$ source superficial density, reported in this thesis are the first instances of work of this nature

in this thickness range to be published. Likewise the 4π-counter self-absorption curves for Ni^{63}, S^{35} and Co^{60} β-radiation obtained in the range 0-300 $\mu g./cm^2$ are also the first of their kind. These curves are shown to agree with the expected relationships derived by Gora and Hickey for a 2π-counting geometry.

The results thus far obtained in self-absorption studies indicate that accurate measurements of and correction for these effects in vacuum distilled sources, will be possible to within ± 0.5 percent. At present, the error is greater than this with very low-energy radiation emitters due to calibration difficulties.

Thus an overall accuracy of better than ± 0.5 percent is now possible in disintegration-rate determinations of emitters of β-radiation of end-point energy in excess of about 0.5 Mev, by 4π-counting. At present this error increases to about 1-2 percent at an end-point energy of 167 kev and to 3-4 percent at 67 kev, due to errors in the self-absorption determination. A general accuracy of ± 0.5 percent should eventually be possible.

In addition to the above experimental work, measurements on phenomena leading to coincident discharges in the two half-counters have been made. The coincidence phenomena have been positively identified as arising from backscattering of radiation from counting gas and the chamber walls. These measurements also allowed a separation of the various counting-rates into curves for the scattering and absorption of β-radiation in a 4π-steradian geometry, and the effects observed have been successfully correlated with existing theories.

BIBLIOGRAPHY

1. Anger, H.O. and Tobias, C.A., Conference on Absolute β Counting. (Preliminary Report No.8. Nuclear Science Series. N.R.C. Washington, D.C. 1950) p.8.

2. Armstrong, W.D. and Schubert, J., Anal. Chem., 20: 270 (1948)

3. Backus, J., Phys. Rev., 68: 59 (1945)

4. von Baeyer, H.J., Z. für Physik, 95: 417 (1935)

5. Baker, R.G. and Katz, L., Nucleonics 11, No.2: 14 (1953)

6. Balfour, J.G., J. Sci. Inst., 31: 395 (1954)

7. Bannerman, R.C., Lewis, G.M. and Curran, S.C., Phil. Mag., 42: 1097 (1951)

8. Barreau, P., Léger, P., Moreau, J. and Prugne, P., J. de Phys. et Rad., 15: Suppl. to No.1, 4A (1954)

9. Bethe, H., Ann. Physik, 5: 325 (1930)

10. Bethe, H.A., Handbuch der Physik, Julius Springer, Berlin, Vol.24 (1933)

11. Bethe, H. and Heitler, W., Proc. Roy. Soc. A 146: 83 (1934)

12. Bethe, H.A., Rose, M.E. and Smith, L.P., Proc. Am. Phil. Soc., 78: 573 (1938)

13. Bethe, H.A. and Ashkin, J. in Experimental Nuclear Physics, E. Segre (Ed)., Wiley, New York (1953) Vol.1, Section II

14. Beyster, J.R. and Wiedenbeck, M.L., Rev. Sci. Inst., 19: 819 (1948)

15. Birks, J.B., Scintillation Counters, McGraw-Hill, New York (1953)

16. Bleuler, E. and Zünti, W., Helv. Phys. Acta, 19: 375 (1946)

17. Bloch, F., Phys. Rev., 50: 272 (1936)

18. Blüh, O. and Terentiuk, F., Nucleonics 10, No.9: 48 (1952)

19. Bolgiano, P., Madansky, L. and Rasetti, F., Phys. Rev., 89: 679 (1953)

20. Borkowski, C.J., Conference on Absolute β Counting (Preliminary Report No.8, Nuclear Science Series, N.R.C. Washington, D.C. 1950) p.55.

21. Bradt, H., Gugelot, P.G., Huber, O., Medicus, H., Preiswerk, P. and Scherrer, P., Helv. Phys. Acta, 19: 77 (1946)

22. Broda, E., Grummitt, W.E., Guéron, J., Kowarski, L. and Wilkinson, G., Proc. Phys. Soc., 60: 460 (1948)

23. Brode, R.B., Rev. Mod. Phys., 11: 222 (1939)

24. Bruner, J.A., Phys. Rev., 84: 282 (1951)

25. Burtt, B.P., Conference on Absolute β Counting. (Preliminary Report No.8. Nuclear Science Series. N.R.C. Washington, D.C. 1950) p.1.

Nucleonics 5, No.2: 28 (1949)

26. Cannon, C.V., Conference on Absolute β Counting (Preliminary Report No.8. Nuclear Science Series. N.R.C. Washington, D.C. 1950) p.51.

27. Cannon, C.V. and Jenks, G.H., Rev. Sci. Inst., 21: 236 (1950)

28. Charpak, G. and Suzor, F., Comptes Rend., 231: 1471 (1950)

29. Charpak, G. and Suzor, F., Comptes Rend., 232: 322 (1951)

30. Cohen, R., Compt. Rend., 229: 356 (1949)

31. Cohen, R., Ann. Phys., 7: 185 (1952)

32. Collie, C.H., Shaw, P.F.D., and Gale, H.J., Proc. Phys. Soc. 63A: 282 (1950)

33. Conference on Absolute β Counting. Preliminary Report No.8. Nuclear Science Series, N.R.C. Washington, D.C. (1950)

34. Conway, D.C. and Rasmussen, J.O., UCRL-2075 (1953)

35. Curie, P. and Laborde, A., Compt. Rend., 136: 673 (1903)

36. Curran, S.C., Angus, J. and Cockroft, A.L., Phil. Mag., 40: 36 (1949)

37. Curran, S.C., Cockroft, A.L., and Angus, J., Phil. Mag., 40: 929 (1949)

38. Dunworth, J.V., Rev. Sci. Inst., 11: 167 (1940)

39. Elliott, N., Engelkemeir, D.W. and Rubinson, W., Natl. Nuclear Energy Series, McGraw-Hill (1949) Div. IV, Vol.9, Paper 1.

40. Elliott, N. and Shapiro, E., Natl. Nuclear Energy Series, McGraw-Hill (1949) Div. IV, Vol.9, Paper 2

41. Engelkemeir, A.G., Hamill, W.H., Inghram, M.G. and Libby, W.F., Phys. Rev., 75: 1825 (1949)

42. Engelkemeir, D.W., Seiler, J.A., Steinberg, E.P. and Winsberg, L., Natl. Nuclear Energy Series, McGraw-Hill (1949) Div.IV, Vol.9, Paper 4

43. Fano, U., Phys. Rev., 70: 44 (1946)

44. Fano, U., Phys. Rev., 72: 26 (1947)

45. Fano, U., U.S. Dept. of Commerce, National Bureau of Standards, Applied Mathematics Series - 13, (1952)

46. Feather, N., Proc. Camb. Phil. Soc., 34: 599 (1938)

47. Feather, N., British Atomic Energy Report B.R.504 (1944)

48. Fermi, E., Z. Physik, 88: 161 (1934)

49. Flammersfeld, A., Zeit. Naturforsch 2A: 370 (1947)

50. Freedman, M., Smaller, B. and May, J., Phys. Rev., 77: 759 (1950)

51. Frisch, O.R., (1948) Unpublished

52. Fry, L.M. and Overman, R.T., U.S. Atomic Energy Commission Report AECD 1800 (1948)

53. Geiger, H. and Müller, W., Phys. Z., 29: 839 (1928)

54. Germer, L.H., Phys. Rev., 56: 58 (1939)

55. Glendenin, L.E. and Coryell, C.D., U.S. Atomic Energy Commission Report M.D.D.C. 19 (1946)

56. Glendenin, L.E., Nucleonics 2, No.1: 12 (1948)

57. Glendenin, L.E., Conference on Absolute β-Counting (Preliminary Report No.8. Nuclear Science Series, N.R.C. Washington, D.C. 1950) p.20.

58. Glendenin, L.E. and Solomon, A.K., Science, 112: 623 (1950)

59. Glendenin, L.E., Natl. Nuclear Energy Series, McGraw-Hill, New York and London, Vol.9, Div.IV (1951) Paper 259

60. Gora, E.K. and Hickey, F.C., Anal. Chem., 26: 1159 (1954)

61. Gray, L.H., Proc. Roy. Soc. A156: 578 (1936)

62. Gray, L.H., Proc. Roy. Soc. A159: 263 (1937)

63. Gray, L.H., Brit. J. Radiol., 22: 677 (1949)

64. Gross, L. and Hamilton, D.R., Phys. Rev., 80: 484 (1950)

65. Hanna, G.C., Kirkwood, D.H.W. and Pontecorvo, B., Phys. Rev., 75: 985 (1949)

66. Hawkings, R.C., Hunter, R.F., Mann, W.B. and Stevens, W.H., Can. J. Res. B.27: 545 (1949)

67. Hawkings, R.C., Hunter, R.F. and Mann, W.B., Can. J. Res. B.27: 555 (1949)

68. Hawkings, R.C., Merritt, W.F. and Craven, J.H., Proc. of Symposium: Maintenance of Standards, May 1951, N.P.L. (H.M.S.O. 1952)

69. Haxel, O. and Houtermans, F.G., Z. Physik, 124: 705 (1948)

70. Hendricks, R.H., Bryner, L.C., Thomas, M.D. and Ivie, J.O., J. Phys. Chem., 47: 469 (1943)

71. Henriques, F.C. Jr., Kistiakowsky, G.B., Margnetti, C. and Schneider, W.G., Ind. Eng. Chem. Anal., 18: 349 (1946)

72. Henriques, F.C. Jr. and Margnetti, C., Ind. Eng. Chem. Anal., 18: 415 (1946)

73. Henriques, F.C. Jr. and Margnetti, C., Ind. Eng. Chem. Anal., 18: 417 (1946)

74. Henriques, F.C. Jr. and Margnetti, C., Ind. Eng. Chem. Anal., 18: 420 (1946)

75. Holland, L., Vacuum 1, No.1: 23 (1951)

76. Houtermans, F.G., Meyer-Schützmeister, L. and Vincent, D.H., Z. Physik, 134: 1 (1952)

77. Hurst, R. and Hall, G.R., Analyst, 77: 790 (1952)

78. Jahnke, E. and Emde, F., Tables of Functions, Dover Publications, New York (1943)

79. Jenks, G.H., Ghormley, J.A. and Sweeton, F.H., Phys. Rev., 75: 701 (1949)

80. Kirkwood, D.H.W., Pontecorvo, B. and Hanna, G.C., Phys. Rev., 74: 497 (1948)

81. Knipp, J.K. and Uhlenbeck, G.E., Physica, 3: 425 (1936)

82. Kobayashi, Y., Miyamoto, G. and Mori, S., J. Phys. Soc. Japan, 8: 684 (1953)

83. Konopinski, E.J. and Uhlenbeck, G.E., Phys. Rev., 60: 308 (1941)

84. Konopinski, E.J., Rev. Mod. Phys., 15: 209 (1943)

85. Korff, S.A., Electron and Nuclear Counters, Van Nostrand, New York (1946)

86. Kovarik, A.F., Phil. Mag. 20: 849 (1910)

87. Kulp, J.L., Nucleonics 12, No.12: 19 (1954)

88. Langer, L.M., Rev. Sci. Inst., 20: 216 (1949)

89. Langer, L.M. and Price, H.C. Jr., Phys. Rev., 76: 641 (1949)

90. Langer, L.M., Motz, J.W. and Price, H.C. Jr., Phys. Rev., 77: 798 (1950)

91. Langmuir, I. and Schaefer, V.J., Chem. Rev., 24: 181 (1939)

92. Lewis, G.M., Phil. Mag., 43: 1070 (1952)

93. Libby, W.F., Anal. Chem., 19: 2 (1947)

94. Mann, W.B. and Parkinson, G.B., Rev. Sci. Inst., 20: 41 (1949)

95. Mann, W.B. and Seliger, H.H., J. Res. Nat. Bur. Stand., 50: 197 (1953)

96. Marinelli, L.D., Conference on Absolute β-Counting (Preliminary Report No.8. Nuclear Science Series. N.R.C. Washington, D.C. 1950) p.54.

97. Marshall, J.S. and Ward, A.G., Can. J. Res., 15A: 29 (1937)

98. Mateosian, E. Der, and Smith, A., Phys. Rev., 88: 1186 (1952)

99. McKinley, W.A. Jr. and Feshbach, H., Phys. Rev., 74: 1759 (1948)

100. Meyer-Schützmeister, L. and Vincent, D.H., Z. Physik, 134: 9 (1952)

101. Miller, W.W., Science, 105: 123 (1947)

102. Møller, C., Ann. Physik, 14: 531 (1932)

103. Moseley, H.G.J. and Robinson, H., Phil. Mag., 28: 327 (1914)

104. Mott, N.F., Proc. Roy. Soc. A126: 259 (1930)

105. Myers, O.E., Nucleonics 5: 37 (Nov. 1949)

106. Nervik, W.E. and Stevenson, P.C., Nucleonics 10: No.3, 18 (1952)

107. Novey, T.B. and Elliott, N., Natl. Nuclear Energy Series, McGraw-Hill (1949) Div.IV, Vol.9, paper 3

108. Novey, T.B., Conference on Absolute β-Counting (Preliminary Report No.8. Nuclear Science Series. N.R.C. Washington, D.C. 1950) p.13.

Rev. Sci. Inst., 21: 280 (1950)

109. Novey, T.B., Phys. Rev., 89: 672 (1953)

110. Page, L.A., Phys. Rev., 81: 1062 (1951)

111. Perry, W.E., Proc. of Symposium: Maintenance of Standards, N.P.L. May 1951 (H.M.S.O. 1952)

112. Pohm, A.V., Waddell, R.C., Powers, J.P. and Jensen, E.N., Phys. Rev., 97: 432 (1955)

113. Putman, J.L., Brit. J. Radiol., 23: 46 (1950)

A.E.R.E. N/R 318 (1949)

114. Reid, A.F., Preparation and Measurement of Isotopic Tracers, Edwards Bros., New York (1946)

115. Reid, A.F., Weil, A.S. and Dunning, J.R., Anal. Chem., 19: 825 (1947)

116. Rose, M.E. and Korff, S.A., Phys. Rev., 59: 850 (1941)

117. Rossi, B.B. and Staub, H.H., Ionization Chambers and Counters, Natl. Nuclear Energy Series, McGraw-Hill New York and London, Vol.2, Div. V. (1949)

118. Rubinson, W., Private communication to L. Yaffe (1954)

119. Rutherford, E. and Barnes, H.T., Nature, 68: 622 (1903)

120. Rutherford, E. and Geiger, H., Proc. Roy. Soc. A81: 141 (1908)

121. Rutherford, E., Chadwick, J. and Ellis, C.D., Radiations from Radioactive Substances, Camb. Univ. Press, London (1930)

122. Sargent, B.W., Can. J. Res. A17: 82 (1939)

123. Sauter, F., Ann. Physik, 20: 404 (1934)

124. Sawyer, G.A. and Wiedenbeck, M.L., Phys. Rev., 79: 490 (1950)

125. Schaefer, V.J., J. Phys. Chem., 45: 681 (1941)

126. Schaefer, V.J. and Harker, D., J. Appl. Phys., 13: 427 (1942)

127. Schmieder, K., Ann. Physik, 35: 445 (1939)

128. Seliger, H.H. and Cavallo, L., J. Res. Nat. Bur. Stand., 47: 41 (1951)

129. Seliger, H.H., Phys. Rev., 88: 408 (1952)

130. Seliger, H.H. and Schwebel, A., Nucleonics 12, No.7: 54 (1954)

131. Sharpe, J. and Stafford, G.H., Proc. Phys. Soc. A64: 211 (1951)

132. Simon, F., Nature, 135: 763 (1935)

133. Simpson, J.A. Jr., Rev. Sci. Inst., 15: 119 (1944)

134. Smith, C.C. and Seliger, H.H., Rev. Sci. Inst., 24: 474 (1953)

135. Smith, D.B., British Atomic Energy Report A.E.R.E. I/R 1210 (1953)

136. Snyder, H.S., Phys. Rev., 72: 181 (1947)

137. Solomon, A.K., Gould, R.G. and Anfinsen, C.B., Phys. Rev., 72: 1097 (1947)

138. Staub, H.H. in Experimental Nuclear Physics, E. Segre (Ed), Wiley, New York (1953) Vol.1, Part 1.

139. Stout, J.W. and Jones, W.M., Phys. Rev., 71: 582 (1947)

140. Suzor, F. and Charpak, G., Compt. Rend., 232: 720 (1951)

141. Suzor, F. and Charpak, G., Compt. Rend., 234: 720 (1952)

142. Suzor, F. and Charpak, G., J. de Phys. et Radium, 13: 1 (1952)

143. Wick, A.N., Barnet, H.N. and Ackerman, N., Anal. Chem., 21: 1511 (1949)

144. Wiedenbeck, M.L. and Chu, K.Y., Phys. Rev., 72: 1164 (1947)

145. Wiedenbeck, M.L. and Chu, K.Y., Phys. Rev., 72: 1171 (1947)

146. Wilkinson, D.H., Ionization Chambers and Counters, Camb. Univ. Press, Camb. (1950)

147. Wu, C.S., Phys. Rev., 59: 481 (1941)

148. Yaffe, L. and Justus, K.M., J. Chem. Soc. Supplement S.341 (1949)

149. Yankwich, P.E., Rollefson, G.K. and Norris, T.H., J. Chem. Phys., 14: 131 (1946)

150. Yankwich, P.E., Norris, T.H. and Huston, J., Anal. Chem., 19: 439 (1947)

151. Yankwich, P.E. and Weigl, J.W., Science, 107: 651 (1948)

152. Zumwalt, L.R., Cannon, C.V., Jenks, G.H., Peacock, W.C., and Gunning, L.M., Science, 107: 47 (1948)

153. Zumwalt, L.R., U.S. Atomic Energy Commission Report M.D.D.C. 1346 (1949)

APPENDIX A

1) Circuit Diagram of AEP 1448 Amplifier

AMPLIFIER AEP 1448

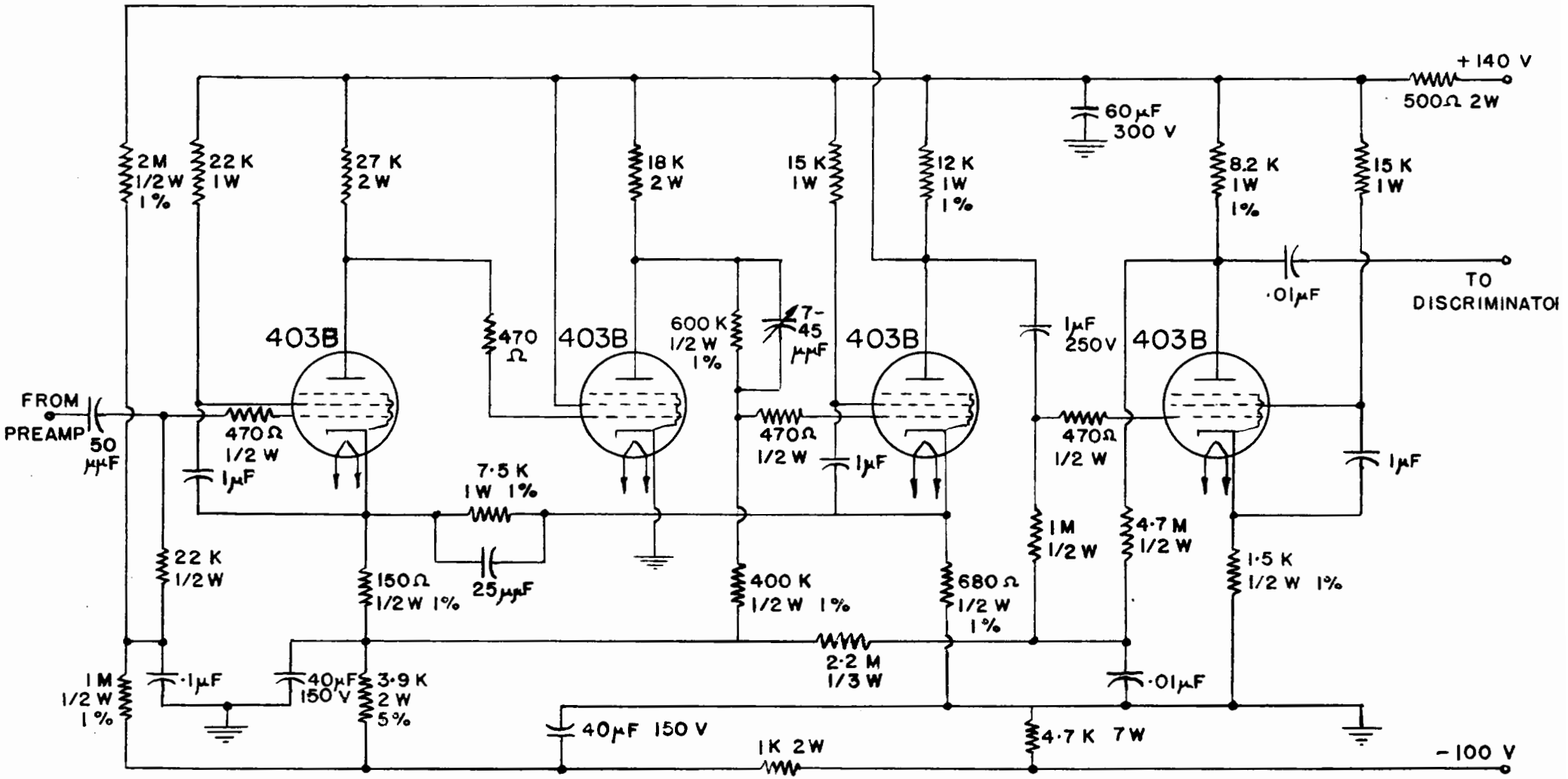

APPENDIX A

2) Circuit Diagram of AEP 1509 Coincidence Unit

COINCIDENCE UNIT AEP 1509

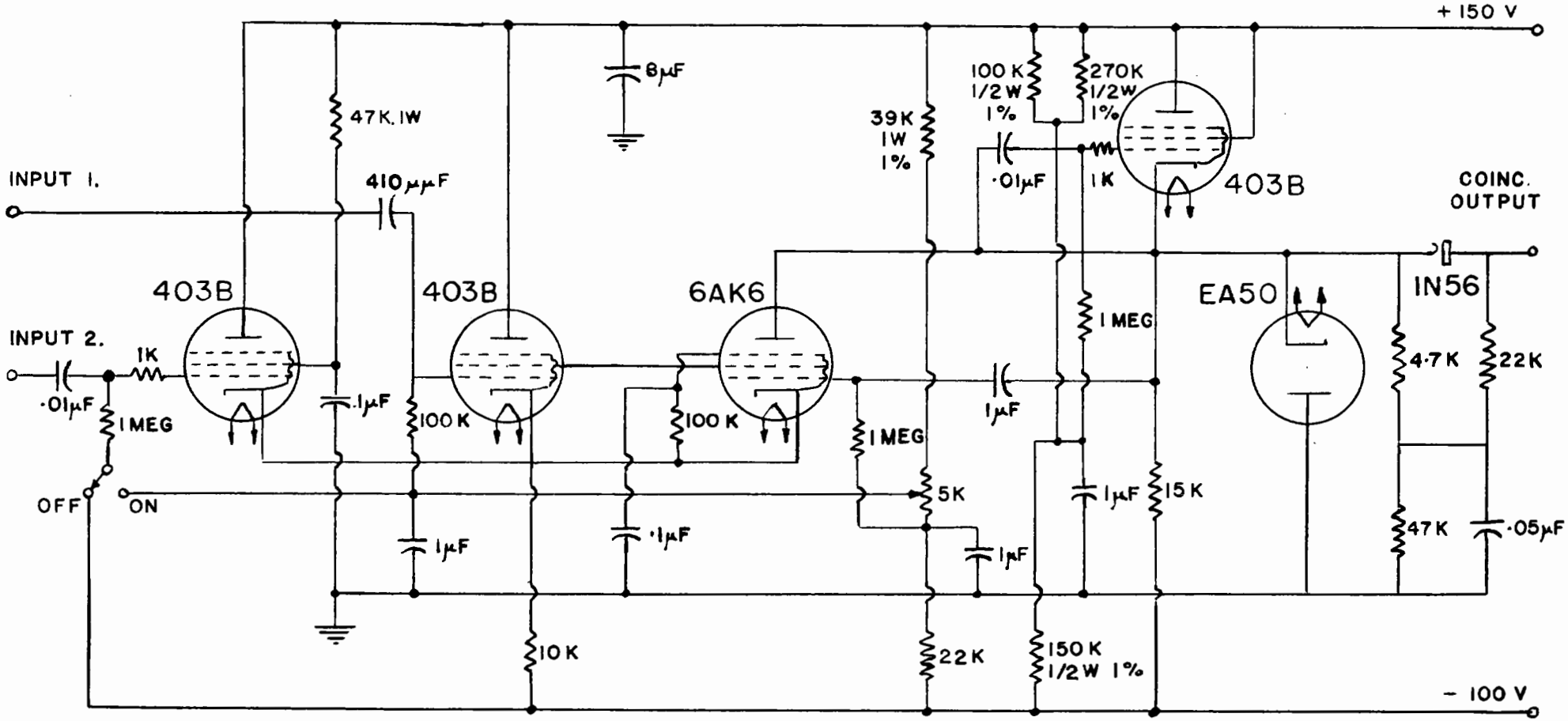

APPENDIX B

International Intercomparison of Standards

The following are the results of disintegration-rate determinations on solution standards distributed by the National Bureau of Standards, Washington, D.C., U.S.A.

1) Sample of Na^{24} distributed on October 4th, 1954. Values corrected to 08.00, October 7th, 1954.

Our value (result of 5 separate determinations by 4π β-counting):

$(1.407 \pm 0.005) \times 10^5$ dis/sec/ml.

N.B.S. values

R. W. Hayward (β-γ coincidence counting):

$(1.407 \pm 0.007) \times 10^5$ dis/sec/ml.

H. H. Seliger (β-γ coincidence counting):

$(1.410 \pm 0.03) \times 10^5$ dis/sec/ml.

(4π β-counting):

$1.417 \times 10^5 \pm 1$ percent dis/sec/ml.

2) Sample of Au^{198} distributed on November 10th, 1954. Values corrected to 08.00, November 4th, 1954.

Our value (result of 7 separate determinations by 4π β-counting):

$(3.796 \pm 0.014) \times 10^5$ dis/sec/ml.

N.B.S. value:

$(3.84 \pm 0.11) \times 10^5$ dis/sec/ml.

APPENDIX C

Papers published or prepared for publication during the two years in which this work was carried out.

Published:

1) A New Material and Techniques for the Fabrication and Measurement of Very Thin Films for Use in 4π-Counting

by B. D. Pate and L. Yaffe
Can. J. Chem., 33: 15 (1955)

2) Disintegration Rate Determination by 4π-Counting. Part I.

by B. D. Pate and L. Yaffe
Can. J. Chem., 33: 610 (1955)

Accepted for publication:

3) Disintegration Rate Determination by 4π-Counting. Part II. Source-Mount Absorption Correction

by B. D. Pate and L. Yaffe
Can. J. Chem., (May 1955)

To be published

4) Disintegration Rate Determination by 4π-Counting. Part III. Self Absorption Correction

by B. D. Pate and L. Yaffe

5) Absorption and Scattering of Radiation in a 4π-Counting Geometry

by B. D. Pate and L. Yaffe